HYDRODYNAMIC CONTROL OF A SUBMARINE CLOSE TO THE SEA SURFACE

Paul Crossland

A Thesis submitted for the degree of

Doctor of Philosophy

from

University College London

Department of Mechanical Engineering, University College London

May 2022

Supervisor: Professor Guo Xiong Wu

DECLARATION

I confirm that the work presented in this thesis is my own. Where I have used information derived from other sources, I confirm that this has been identified appropriately.

Signed:

Date: 27 May 2022

University College London

Department of Mechanical Engineering

Doctor of Philosophy

HYDRODYNAMIC CONTROL OF A SUBMARINE CLOSE TO THE SEA SURFACE

ABSTRACT

The submarines of today are generally described as one of the most complex system engineering design problems and this research covers one aspect of performance in this large design problem space. Manoeuvring and control performance is traditionally treated as at least two distinct problems, the performance of the deeply submerged submarine and the performance of the submarine operating close to a boundary such as the sea surface. The study of the manoeuvring and control performance of a submarine operating in deep water has been an active discipline for some years; the primary purpose of such studies has been to understand, to a high level of fidelity, the manoeuvring characteristics of a submarine to help ensure that the design is safe and operationally effective.

However, when a submarine is operating at depths typical of those required when using the periscope, when snorting during the period of recharging the batteries or, in the some cases, at slow to zero speed whilst hovering, the submarine can experience complex oscillatory motion due to higher order sea loads. The second order vertical plane loads can manifest themselves as a time varying suction force effectively that can cause the submarine to be drawn to the surface risking broaching and increasing the possibility of detection or the submarine may need to take on sea water ballast to counter the suction effects which may mean the submarine has a significant out-of-trim if is needs to rapidly break away from the surface. These unsteady effects are not modelled to a sufficient level of fidelity using the traditional quasi-steady state approaches that are employed so successfully for modelling the deeply submerged submarine.

Therefore, to understand the behaviour of a submarine under the influence of surface waves at the early stages of design, the impact on whole boat design, from the perspective of the hydrodynamic shape of the hull, internal arrangements, performance requirements of ballast

tanks and pumps and the requirements of control surfaces, a suitable design tool and analysis process is required.

The thesis includes outcomes from different engineering disciplines; principally, naval architecture (particularly the specialised areas of submarine hydrodynamics and ocean engineering) and control engineering. The thesis particularly draws upon research from the area of ocean engineering, specifically in the methods of quantifying second order effects, to bring insights into control system design for the problem of submarine control under waves. This is achieved by providing a potential approach for developing control system specifications in reflection of the available assessment methods.

RESEARCH IMPACT STATEMENT

This thesis has contributed to the understanding of the mechanisms behind the hydrodynamic forces and moments on a submarine when operating under the influence of surface waves, which is key to improving submarine safety and operational effectiveness. This research has developed processes aimed at generating the numerical techniques and experimental data that can be used to inform on the design of hydrodynamic and hydrostatic control systems in future submarines; the output of the research can be used to help define the key requirements, to inform on the design and to tune the control parameters of candidate control system in future submarines.

Future underwater capability requirements have identified potential roles for manned and unmanned off-board vehicles to achieve a cost effective solution to these requirements. The large submarines designed to accept these off-board vehicles, so called, SSHs (Ship Submersible Host) and SSHNs (Ship Submersible Host Nuclear), will be required to operate effectively at very low speeds close to the free surface. The outcomes from this research can be developed further to help understand, to a higher degree of fidelity, the complex issues associated with operating large submarines, in conjunction with the operation of small submersibles, manned or unmanned, in the presence of the free surface.

ACKNOWLEDGMENTS

First and foremost, I would like to express my sincere thanks to my supervisor, Professor Guo Xiong Wu for his guidance in helping me complete my research. It was particularly challenging for me to undertake this research on a part-time basis, whilst in full-time employment at QinetiQ, and I appreciate his patience throughout.

I would like to acknowledge QinetiQ Ltd and the UK Ministry of Defence for their continued support throughout my research and the members of the EUCLID10.17 Consortium for their agreement to include project data as part of my research.

Finally, I want to thank all those colleagues from QinetiQ, both past and present, who have guided me through a career that has led to me undertaking this research.

CONTENTS

LIST OF FIGURES

LIST OF TABLES

NOTATION

Roman

Parameter	Meaning	Unit
A	Cross section area	m^2
A_n	Coefficients in Glauert formula	
a_e	Effective aspect ratio	
a_i	Amplitude of i^{th} wave component	m
B	Buoyancy force and centre of buoyancy	N and m
B'	Non-dimensional buoyancy force	
$\bar{c}$	Mean chord	m
C_D	Drag coefficient	
C_L	Lift coefficient	
C_{LC}	Correct lift coefficient	
C_m	Inertia coefficient	
c_r	Appendage root chord	m
c_t	Appendage tip chord	m
C_{WD}	Wave force coefficient	
D	Body diameter	m
dF	Incremental force	N
dm	Mass of element	kg
ds	Element length	m
e	Taper ratio	
$\vec{F}$	Body force vector	N
F_r	Froude number	
g	Acceleration due to gravity	m/s^2
g_1	Impulse response function for first order wave forces	N
g_2	Impulse response function for second order wave forces	N
$\vec{G}$	Body moment vector	Nm
h	Depth of immersion from calm water free surface to axis	m
$\vec{h}$	Angular momentum	kgm^2rad/s

H_D	Depth of axis to calm water surface	m
H_W	Significant wave height	m
I_0	Moment of Inertia matrix	kgm^2
K	Roll moment	Nm
K′	$K' = \frac{K}{\frac{1}{2}\rho U^2 L^3}$	
k_{BL}	Correction factor for effects of the hull	
L	Length of body	m
M	Mass matrix	kg
m	Mass of body	kg
m′	Non-dimensional mass $m' = \frac{\nabla}{\frac{1}{2}L^3}$	
M	Pitch moment	Nm
M′	$M' = \frac{M}{\frac{1}{2}\rho U^2 L^3}$	
n′	Propulsor state	
N	Yaw moment	Nm
N′	$N' = \frac{N}{\frac{1}{2}\rho U^2 L^3}$	
p	Rotational velocity about x-axis	rad/s
Q(τ)	Smoothing function	
q	Rotational velocity about y-axis	rad/s
Q_∞	Free stream velocity = $(U_\infty, V_\infty, W_\infty)$	
r	Rotational velocity about z-axis	rad/s
$\overrightarrow{R_0}$	Position vector of origin of body axes	
S	Appendage surface area	m^2
S	Geometric appendage span	m
S_E	Effective appendage span	m
T_P	Spectral peak period	s
U	Velocity in x-axis (body axes)	m/s
$\vec{U}$	Velocity vector,$\vec{U} = U\hat{\imath} + V\hat{\jmath} + W\hat{k}$	
u	Small perturbation in axial velocity	m/s
u_f'	Axial fluid velocity in earth axes	m/s
V	Velocity in y-axis (body axes)	m/s
v	Small perturbation in sway velocity	m/s

$v_f^{'}$	Sway fluid velocity in earth axes	m/s
v'	$\mathrm{v}' = \frac{\mathrm{V}}{U}$	
w	Small perturbation in heave velocity	m/s
w	Velocity of water (perpendicular to local body surface)	m/s
$\dot{w}$	Acceleration of water (perpendicular to local body surface)	m/s^2
w_b	Velocity of body element	m/s
$\dot{w}_b$	Acceleration of body element	m/s^2
$w_f^{'}$	Vertical fluid velocity in earth axes	m/s
w	Velocity in z-axis (body axes)	m/s
(x_b, y_b, z_b)	Position of centre of buoyancy	m
(x_G, y_G, z_G)	Position of centre of gravity	m
(x_0, y_0, z_0)	Origin of body in fixed coordinate system	m
X	Axial force	N
X'	$X' = \frac{X}{\frac{1}{2}\rho U^2 L^2}$	
x_E	Coordinate in the direction of wave (Earth Axes)	m
x_{FP}	Longitudinal distance from the forward perpendicular	m
Y	Sway force	N
Y'	$Y' = \frac{Y}{\frac{1}{2}\rho U^2 L^2}$	
y_A	Normal distance from hull surface to geometric centre (Figure 12)	m
Z	Vertical force	N
Z'	$Z' = \frac{Z}{\frac{1}{2}\rho U^2 L^2}$	
z_E	vertical coordinate from the mean water surface	m
z^*	Submergence depth to body axis	m

Greek

Parameter	**Meaning**	**Unit**

α	Angle of attack	rad
$\dot{\alpha}$	Rate of change of angle of attack	rad/s
β_L	Local angle of incidence	rad
∇	Form volume	m^3
δ_b	Bow plane angle	rad
δ_{bl}	Extent of hull effects	m
δ_r	Rudder angle	rad
δ_s	Stern plane angle	rad
ε_i	Phase of the i^{th} wave	rad
ε_b	Bandwidth parameter	
Φ	Roll (Earth axes)	rad
ϕ	Velocity potential and roll angle	m^2/s and rad
ϕ_w	Velocity potential due to undisturbed wave	m^2/s
ϕ_d	Velocity potential due to wave diffraction	m^2/s
ϕ_{α_i}	Radiation potential due to i^{th} mode of motion	m^2/s
η	Non-dimensional spanwise distance	
η	Wave elevation	m
η_0	Wave amplitude	m
ζ	Appendage camber surface	
λ	Wave length	m
μ	Wave heading	deg
υ'	Cross flow velocity ($\upsilon' = \sqrt{w'^2 + v'^2}$)	m/s
υ	Kinematic viscosity	m^2/s
Θ	Pitch (Earth axes)	rad
θ_A	Spanwise coordinate of lifting surface	rad
ρ	Density	kg/m^3
w	Velocity of the water	m/s
ω_e	Wave encounter frequency	rad/s
ω	Wave frequency	rad/s
$\xi_j,\ j = 1,2,3$	Rigid body motion (surge, heave and pitch)	
Ψ	Azimuth (Yaw)	rad
Θ	Elevation (Pitch)	rad

Φ	Orientation (Roll)	rad
$\vec{\Omega}$	Rotation velocity vector	

1. INTRODUCTION

1.1 Introduction to submarine manoeuvring and control

World War I saw, for the first time, submarines having a significant impact on naval warfare; as described by [Clancy, 1993] "…Within a month of the outbreak of World War I, the German Unterseeboot fleet,…., were sinking British Naval units in the North Sea.". More like submersible ships than the submarines of today, they had to operate surfaced using their diesel engines, submerging under battery power only when operationally necessary. Germany used submarines to devastating effect during World War II [Sheffield, 2010] attempting to cut off Britain's supply routes by sinking merchant ships crossing the Atlantic from North America; supply lines that were crucial to Britain's war effort. It has been reported that Winston Churchill wrote that the U-boat threat was the only thing that ever gave him cause to doubt the Allies' eventual victory [Clancy, 1993]. During the Cold War, the United States and the Soviet Union maintained large submarine fleets patrolling areas under the Atlantic Ocean and beyond. Probably the most prominent of these submarines were the ballistic missile submarines capable of attacking strategic targets such as cities or missile silos anywhere in the world from an unknown, changing, position. These submarines played an important part in Cold War mutual deterrence, as both the superpowers had the credible ability to conduct a retaliatory strike against the other, [Hennessy and Jinks, 2015].

Submarines of today are even more complex particularly in the context of the changes in submarine operations since the end of the Cold War requiring submarines to be able to multi-task and have multiple roles; changes involving concepts and doctrine that is now targeted towards supporting national interests in regional crises and conflicts around the world, [Hennessy and Jinks, 2015].

Military submarines can typically operate in a very restricted portion of the world's ocean depths; according to [Gabler, 1986] the typical collapse depths of submarines from World War II was around 280m (representing a depth around 4 times the length) and the average depth of the Atlantic Ocean is around 3300 metres. Therefore, the means of ensuring that a submarine is capable of operating within these rather tight boundaries is by understanding the manoeuvring characteristics early on in the design process, [Burcher and Rydill, 1995]; this is crucial in reducing the risks of producing designs that are unsuitable for the environment in which they are expected to operate.

Manoeuvring and control (M&C) performance of a submarine is traditionally treated as two distinct problems; the performance of the deeply submerged submarine and the submarine operating close

to a boundary such as the sea surface. The problem of the submarine operating on the surface is also an M&C problem but studies tend to focus on the performance of surfaced submarines in waves, i.e. a seakeeping problem or even stability problem in extreme waves, [Crossland and Pope, 2017]

At some stage in the submarine design process, the designer will need to consider a number of design options and to be able to evaluate those designs against manoeuvring performance requirements; these designs are usually, at some point in the design process, evaluated using advanced experimental or numerical techniques, [Bayliss *et al,* 2005]. The study of the manoeuvring and control performance of a submarine operating in deep water away from any boundary has been an active discipline for decades, [Ray *et al,* 2008]. The primary purpose of such studies has been to understand, to a high level of fidelity, the manoeuvring characteristics of a submarine to help ensure that the product of the design, the submarine, meets it operational requirements and is able to fulfil its mission effectively. In particular, understanding the risk of excessive depth excursions, following the failure of a control surface, is the primary reason for undertaking detailed studies of the manoeuvring performance of a submarine in the vertical plane, [Haynes *et al*, 2002].

Whilst experimental and numerical techniques exist to help understand the particular aspect of a submarine operating close to the free surface, [Veillon et al, 1996] for example, it has not been the focus of research to the same extent of the manoeuvring and control performance of a deeply submerged submarine. However, when a submarine is operating at depths typical of those required when using the periscope or when snorting during the period of recharging the batteries, it can experience complex oscillatory motion due to higher order sea surface load effects that manifest themselves as a suction force [Musker *et al*, 1988]. In many cases, the forces can effectively cause the submarine to be drawn to the surface, risking broaching and increasing the possibility of detection. Furthermore, submarine operators will take on additional ballast to avoid broaching during PD operations; this can put the submarine in a heavy out-of-trim condition should it need to breakaway from the surface in an emergency. This may cause the submarine to experience a large depth excursion before the out-of-trim is managed effectively. Thus, it is important to understand the behaviour of a submarine under the influence of surface waves at the early stages of design, [Ray *et al,* 2008] because of the impact on whole boat design from the perspective of the hydrodynamic shape of the hull, internal arrangements, performance requirements of ballast tanks and pumps and the requirements of control systems.

The challenge to the Naval Architect is to design a submarine that is not influenced by waves to an extent that they become a problem, or to be able to develop a submarine design that can minimise the influences of waves effectively using a system of control to mitigate against the adverse effects of the free surface, for example.

The effect of the waves on a submarine are related to geometrical characteristics such as hull length and hull diameter and to physical characteristics such as depth of submergence, speed, sea state and heading to the waves; physical characteristics, like depth of submergence for operations such as snorting, are driven by the design and limitations of such systems. Speed and heading can be, to some extent, directed by operating procedures that aim to maximise the mission effectiveness. Environmental physical characteristics such as sea states are not controllable and the design requirement would be to, ostensibly, maximise the sea state at which periscope depthkeeping or snorting operations can take place.

Whilst geometrical characteristics of a particular design, such as overall hull length and diameter are usually dictated by other requirements, [Burcher and Rydill, 1995], and are therefore probably not negotiable for improving near surface performance. Instead, consideration of the use of hydrodynamic and hydrostatic control systems in the design of a submarine when operating close to the free surface should provide improvements in performance.

Consideration of the control surface design, including the size of appendages, their means of actuation and the control algorithms, provides the most immediate solution to the challenge of operating a submarine close to the free surface. However, since periscope depth-keeping is typically undertaken around the lower speeds, [Bayliss *et al,* 1998], the ability of any hydroplanes to control against these complex forces can be limited. An additional consideration could be to offset the suction force hydrostatically using internal compensation systems, rather than hydrodynamically using lift based control surfaces, but since space in a submarine is limited there will be severe constraints placed upon the size of any compensation tanks and associated pumps, [Burcher and Rydill, 1995]. Fundamentally, both approaches of control require a detailed understanding of the magnitude of the wave induced forces early in the design of the submarine to ensure that any control surfaces and compensation tanks are sufficiently large and that their respective means of "actuation" such as servos and pumps have sufficient capacity to meet the operational requirements of the submarine. Furthermore, the design of the control algorithm itself is fundamental in the overall design of the control system; if a control algorithm has been designed

inappropriately, then the effectiveness of that control system will be severely limited, [Grimble *et al,* 1993].

1.2 Aims of thesis

The manoeuvring characteristics of a deeply submerged submarine, where wave effects are considered negligible, can be readily determined from hydrodynamic derivative based non-linear models. Such models are based on the assumption that the motion of a deeply submerged submarine can be regarded as a quasi-steady state phenomenon whereby each component of the hydrodynamic force and moment is a function of the instantaneous values of the velocity and acceleration components of the body and the deflection of the control surfaces, [Lewis, 1989]. There is an additional, hydrostatic, contribution to the force on the body that is due that is due to roll and pitch. Equations used to characterise the submarine as a "system", for subsequent application to control system design, are typically based on the linearisation of these non-linear, derivative based, methods [Booth, 1983]. However, whilst this approach, to control system design is not without limitations[1],it is considered a straightforward design problem that can lead to satisfactory control performance in the absence of wave disturbances, [Liceaga-Castro and Van Der Molen, 1995]. The linearisation of this non-linear "system" is successful because deviation from the mean is usually small due to the way submarines are operated, particularly in the vertical plane, whereby large motions through extreme manoeuvres during a planned depth change (so excluding depth changes due to casualty scenarios such as plane jams and floods) are avoided; the autopilot will perform a depth change by imparting modest pitch angles in the submarine.

The most difficult depthkeeping control problem is when the submarine is at periscope depth in a high sea state, [Marshfield, 1991]. This is because as the submarine approaches the surface, there are a number of different hydrodynamic effects that significantly influence the manoeuvring characteristics of the submarine are ignored in the conventional model. This may result in a reduction in the effectiveness of the control system based on this model. There, for example, will be unsteady or non periodic accelerations imparted on the submarine, due to the waves, and so the method of using a time independent or frequency dependent added mass may no longer be valid; there are additional , inviscid, damping effects due to wave radiation generated by the motion of the body excited by the incoming surface waves: this means that the interaction between the free

[1] These limitations are in-part due to the fact that all combinations of velocity and acceleration cannot be considered in an experiment leading to derivatives being omitted. For example, maintaining depth during a turn can be particularly challenging for a submarine control system, possibly as a consequence of non-linear cross coupling effects not been accounted for adequately in the derivative based model, [Tolliver, 1986].

surface (including calm water free surface and incident wave) and the submarine will introduce additional forces and moments that are not present when the submarine is deeply submerged and therefore is absent in the conventional model, [Tolliver, 1986]. Carrica *et al*, 2016 provided an example of solving an unsteady Reynolds Average Navier Stokes equations to determine the instantaneous unsteady forces and moments on a deeply submerged manoeuvring submarine and for the case of a submarine close to the free surface. This work showed that, to understand the way a submarine operates near the free surface, the solution requires a variety of numerical capabilities; motions of the submarine and appendages, including the influence of surface waves, coupled with an autopilot. Whilst these techniques are capable of predicting the total forces on the submarine, rather than approximations from coefficients they are computationally intensive.

The current empirical approach of utilising a coefficient-based approach for quantifying the first and second order wave forces provides a readily applicable methodology, [Mandzuka, 1998] for example, but is low fidelity and does not capture the free surface effects sufficiently well. Therefore, there is a key requirement to understand to a higher fidelity the free surface effects on a submarine operating at periscope depth under the influence of surface waves through simulation and experimentation.

This thesis aims to provide an in-depth understanding of how the behaviour of a submarine under the influence of the free surface can be quantified to assist in the design of submarines and in the design of typical control systems that are used to mitigate against the adverse effects of surface waves. The outcome of the research described here is to develop a reliable and practicable methodology to assess the behaviour of a submarine when at depths where free surface wave may have a negative impact on its ability to operate safely and effectively. It is evident that by understanding the nature of the wave effects on a submarine, in detail, will help greatly in design to counter these adverse effects as well as to develop more effective methods for improved submarine motion control and hence increase the capability to operate submarines under waves.

The thesis includes outcomes from different engineering disciplines; principally, naval architecture (particularly the specialised areas of submarine hydrodynamics and ocean engineering) and control engineering. The thesis particularly draws upon research from the area of ocean engineering, specifically in the methods of quantifying second order effects, to bring insights into control system design for the problem of submarine control under waves. This is achieved by providing a potential approach for developing control system specifications in reflection of the available assessment methods. A time domain computational approach has been developed, based on the refinement of

existing theoretical methods that can be readily interfaced with the quasi-steady state empirical modelling approaches usually adopted for quantifying the manoeuvring performance of a deeply submerged submarine. This time domain capability can be applied to modelling the non-linear control phenomena where the control surface angle and actuator rate saturation occurs.

The rationale for including, in this thesis, a review of a number of technical areas was to draw upon the extensive research performed in quantifying the second order steady and slowly varying forces on offshore floating structures to advance the field of the hydrodynamics of a submarine under waves. Furthermore, knowledge of control system design in submarines then provides the technology exploitation route for this improved understanding of submarine hydrodynamics. By reviewing this range of technical areas, the rationality of quantifying the second order forces and moments on a submarine by using Quadratic Transfer Functions (QTFs) has been established. However, there is very little experimental data for validation, reported in open literature from a fully appended submarine model, particularly from tests in bichromatic waves at both zero and non-zero forward speed. Furthermore, whilst the use of a non-zero mean heave force and pitch moment on a submarine is readily recognised in control system design, the slowly varying second order force that is quantified by QTFs has not been incorporated into the control system design; these shortfalls have been systematically investigated throughout this research.

To meet the shortfall, this PhD study has conducted a series of benchmark tests using a lightly restrained EUCLID model in head seas; these tests included both regular waves and irregular waves. In fact, it is for the first time the tests have been conducted on a fully appended submarine model in bichromatic waves, to provide an in-depth understanding the second order effects on a submarine in realistic sea states. Further research gaps are identified and future work is proposed. In particular, a concept solution for a test rig is developed that can extend the tests to include the cases of a submarine in oblique seas.

1.3 Thesis overview

To address the particular subject area, described in this thesis, requires a blend of engineering disciplines (submarine hydrodynamics, control engineering and ocean engineering). This thesis begins by presenting some of the more fundamental aspects to introduce those subject areas.

Firstly, the thesis introduces how submarine manoeuvring and control influences submarine design, particularly from the perspective of the design of the hull and the control surfaces and the balance between agile control in the horizontal plane and safe control in the vertical plane. The methods

used for quantifying performance of a deeply submerged submarine are reviewed, highlighting the advantages and disadvantages in the context of their application to the problem of a submarine operating under the influence of surface waves. The thesis then focuses on a review of the research undertaken to address the specific problem of the submarine operating under the influence of surface waves and the problem of controlling the submarine to minimise the adverse effects of the waves. It will demonstrate that the existing approaches are largely based on using empirical simplifications to support the design of control systems for submarines and they do not entirely capture the second order wave effects that can been very significant on the submarine and can very much influence control system performance.

The thesis then draws on some of the technologies that are widely used in the ocean engineering discipline, particularly in the area of quantifying second order forces and moments that create the slowly varying drift motions of offshore floating structures. However, the application of these technologies, to the problem of a submarine hydrodynamic control under the influence of surface waves, has been rare or absent. Therefore, such an application in this thesis is one of the novel aspects of the present research.

The different techniques, which are currently used for submarine control, are introduced including both hydrodynamic and hydrostatic approaches for periscope depthkeeping; the physical systems in a submarine are described and a review of the control algorithms used in these systems is undertaken. We shall see that the approach, traditionally, used in designing control systems for depthkeeping in submarines utilises a simplified mathematical model obtained from the linearisation of the vertical plane components of the non-linear six degrees of freedom equations of motion derived for the deeply submerged submarine. In controller design, the effects of the waves on the submarine are considered as external disturbances, which are usually characterised by empirical relationships for the first and second order wave forces. Therefore, the key to control system design, for periscope depthkeeping, is in the accurate quantification of the external disturbance due to the waves. However, typically, only the vertical plane equivalent of the steady drift force component of the second order force is considered in control system design; the slowly varying second order effect tends to be ignored in the design. Therefore, this research shows how, by including the slowly varying second order vertical forces in the form of the QTFs as part of the control system design, improvements in control system performance are obtained.

Chapter 2 is in two parts, in Part 1, there is a detailed analysis of the fundamentals of predicting the hydrodynamic characteristics of a deeply submerged submarine is undertaken, which is then

expanded to include the problem of the submarine under the influence of surface waves, covering techniques ranging from the, simplistic, heavily empirically based, methods to the higher fidelity, computationally intensive, unsteady Reynolds-Averaged Navier Stokes Computational Fluid Dynamics (RANS CFD). These existing hydrodynamic theories are evaluated, leading to the development of a practicable time domain computational approach based on the extension and refinement of a rational combination of some of these existing theoretical methods; this time domain method is described fully in Part 2. Using a hybrid approach that provides a prediction capability, somewhat akin to those used to solve the problem of a surface ship manoeuvring in waves, this time domain computational approach has been interfaced with traditional quasi-steady state empirical modelling approaches, usually used for quantifying the manoeuvring performance of a deeply submerged submarine, which can then be used in the design and evaluation of control system performance of a submarine under waves.

This research has drawn upon the extensive work undertaken in the field of ocean engineering in the development of experimental and numerical techniques for evaluating the second order effects on large floating structures and considered these approaches to the current problem. These techniques give clear guidance on how to quantify second order effects both experimentally and numerically that can be applied to the problem of a submarine operating under waves. The role of first and second order potential flow methods are discussed and the thesis looks to the research from the offshore structure community for capturing the second orders forces on large volume submerged structures through the use of Quadratic Transfer Functions (QTFs).

In this research, the principal purpose is to establish a sufficiently accurate and efficient method which can be readily used to resolve the real engineering problems in submarine design and operation. By introducing this enhanced modelling approach, coupled with the use of QTFs in control system design, it has been shown, through case studies, that the desired control system performance can be obtained.

To ensure the reliability of the developed method, a series of comparisons are made through comparisons of the forces and moments obtained from time domain predictions and the analytic analysis of simple shapes and through comparisons of predictions of forces and moments on a fully captive model of the EUCLID 10.17 geometry and experimental data. Further studies have been conducted by comparing the QTFs from the time domain calculations of the EUCLID submarine in bichromatic waves with those predicted by the commercially available code WAMIT for the zero speed cases only.

The time domain code developed as part of this research was used to perform investigative studies alongside WAMIT. The studies were aimed at understanding the relative importance of the Froude-Krylov, diffraction and radiation components in the first order force and the contribution of the second order potential in the prediction of second order forces on a fully appended submerged submarine; additionally, the validity of Newman's approximation [1974] to the prediction of QTFs for a submarine is considered.

The numerical and experimental techniques developed in the ocean engineering community are exclusively for the case of a fixed or floating body at zero speed (in some cases incorporating the effects of current). In Chapter 3, the experiments conducted in this PhD study are presented. A series of tests were performed using a lightly restrained model of the same EUCLID 10.17 hull form; these tests included regular waves, irregular waves and bichromatic tests at zero speed and forward speed. To the author's knowledge, this is the first time that the second order slowly varying suction forces on a lightly restrained fully appended submarine model have been measured, systematically, in an experiment. The challenges faced in performing such an experiment was in the design of a towing arrangement that would allow the model to respond in heave and pitch motion to the first order wave effects; yet have the capability to withstand the expected vertical plane forces due to the second order wave effects. Analysis of these experiment data have allowed for a good understanding and quantitative assessment of the mean and slowly varying suction forces on a submarine under waves that can be used to support the design of depthkeeping control systems in submarines. It has confirmed that the second order forces, quantified through the RAO of the mean forces from regular wave tests and the QTFs from tests in bichromatic waves, can be used to predict the mean and slowly varying suction forces, respectively, in irregular waves. These tests also provide the data that can be used to validate the time domain approach developed in this thesis, and in a much broader context, be used as a benchmark, which enables prediction tools to be validated in general.

The predicted and measured second order forces and moments on a body, allowed to respond to first order excitation are compared, with those on the same body that is fully restrained and the implications of the findings for submarine design are discussed. These comparisons show that the predicted and measured mean heave forces, due to waves, on a restrained submerged body are greater than on the same body that is allowed to respond to first order excitation. This finding is important as it provides clear guidance on the type of simulations and/or experimental tests that

are required to provide a good understanding of the control system requirements for periscope depthkeeping at the early stages of submarine design.

Chapter 3 also provides a concept for the testing of a lightly restrained submarine model in oblique waves as a basis for future work. This concept is based upon a review of techniques adopted by the surface ship community. Whilst this concept may form the completed work of this thesis, this rig design has been developed, the model has been manufactured and has recently been successfully employed to measure the second order forces on a submarine model at periscope depth in oblique waves. The results from these tests have been used to derive first order motion transfer functions for all and second order forces and moments as means and as QTFs for all 6 degrees of freedom, which have then been compared with the numerical tool, WAMIT, that can be used to support the design of a depthkeeping control system in a submarine. The mean forces and moments in regular waves produced a robust set of measurements in the vertical plane, with a repeatability that is considered suitable for numerical validation. The use of bichromatic waves to derive QTF forces and moments proved successful for both the horizontal and vertical planes but further work is required to fully understand the influence of the design of the system used for lightly restraining the model in the vertical plane.

Chapter 4 provides a reflection on submarine control using both hydrodynamic and hydrostatic methods or compensation tanks respectively. By way of a series of case studies, time domain computational analysis of the EUCLID submarine has been performed for a number of control approaches culminating in the use of the QTF to support control system design; the improvements in depthkeeping performance are presented and discussed. The benefits of using a notch filter to remove the demands on the depth-autopilot due to the first order wave effects are confirmed; improvements in depth-keeping performance are demonstrated with significant reduction in the duty cycle of the control actuators leading to reduced wear and tear on the bearing arrangements. Moreover, the results from these case studies have shown that rather than considering an input disturbance filter designed to provide good performance against only the steady state second order force, a filter that is designed with knowledge of the low frequency QTF of the second order heave force can lead to further improvements in control system performance.

The final chapter, the outcomes are discussed, conclusions are made and recommendations for future work are provided. The achievements and contributions to the field can be summarised as follows:

- Developed a time domain computational approach, based on the extension and refinement of a rational combination of existing theoretical methods, to predict the first and second order forces on a fully appended submarine with forward speed.

- Drawn upon the extensive research in the field of ocean engineering in the development of experimental and numerical techniques for evaluating the second order effects on large floating structures and applied these techniques to understand the problem of a submarine under waves.

- Used improved understanding of the second order effects to demonstrate how an improvement can be made in controller design; by accounting for both the steady non-zero mean and the slowly varying suction force in the controller design, improvements in depthkeeping control could be achieved.

The output of this work can be used to help define the key requirements, to inform on the design of specific systems and to tune the control parameters of candidate control systems in future submarines.

2. SUBMARINE MANOEURVING AND CONTROL – Part 1

2.1 Scope of chapter

To understand the problem of a submarine operating under the influence of surface waves, it is pertinent to first understand the approaches used for predicting the performance of a deeply submerged submarine particularly in the context of submarine design and control system development. Therefore, this chapter provides some context to the problem of submarine manoeuvring and control by describing what submarine design for manoeuvring means and how manoeuvring performance is, typically, quantified for the deeply submerged problem. Through this it shows the justification for the requirement to develop high fidelity mathematical models for predicting submarine manoeuvring performance from the perspective of quantifying the hydrodynamics and the control system design; how these approaches are applied to the periscope depthkeeping problem is then discussed. We shall show that the understanding of behaviour of a submarine close to the free surface requires the development of mathematical models of the submarine in a representative environment, that will address hydrodynamic phenomena that are ignored in the deeply submerged case. Furthermore, existing depth control systems are traditionally designed using mathematical models based upon a linearisation of models of the deeply submerged submarine where first order wave filters are included to reduce the demands on the actuation systems when close to the free surface. It is perhaps not surprising that any control design strategy places the priority on manoeuvring performance when the submarine is deeply submerged rather than near surface control. This is due to the significant emphasis being placed on ensuring that the deeply submarine is manoeuvring safely compared to operational performance associated with PD activities. Furthermore, in the vertical plane, pitch and depth excursions are expected to be small when the submarine is operating near the free surface that in some way justifies the approach to linearising the models.

In this chapter, options for improvements in the approach to modelling are discussed, in Part 1, leading to the development of a hydrodynamic theory adopted in Part 2, which forms the basis for computations of the first and second order forces and moments on a submarine under the influence of waves. The chapter concludes by providing comparisons of the developed numerical model against previously generated experimental data.

2.2 Submarine design for manoeuvring and control

To put this thesis in context, it is prudent to discuss the wider impact of hydrodynamics and control systems on submarine design and operation. In the first instance, the design compromises are briefly discussed before highlighting why the ability to predict the manoeuvring performance of the deeply submerged submarine is important from a safety perspective. The choices for control system design are also covered in the context of the deeply submerged submarine and the case of the submarine under the influence of waves.

The shape of the outer envelope of the submarine (hull shape) influences the above hydrodynamic characteristics. However, the requirement for an efficient structural configuration for the pressure hull is not necessarily compatible with a hydrodynamically optimised hull form [Burcher and Rydill, 1995]. Furthermore, requirements for internal equipment and other constraints also mean that optimised hydrodynamic designs do not represent feasible design solutions for a submarine form, [Burcher and Rydill, 1995]. Thus, an important aspect of the design process is in the understanding of the impact of making such design compromises on the hydrodynamic performance of the submarine [Ray *et al,* 2008]. In terms of the requirements of design tools for predicting the manoeuvring performance of a deeply submerged submarine, this would include the capability to predict parameters such as turning circles, advance, transfer, tactical diameter, and overshoot (these terms are defined using Figure 1) at the early design stage, see [Comstock, 1967] for a detailed explanation of the parameters.

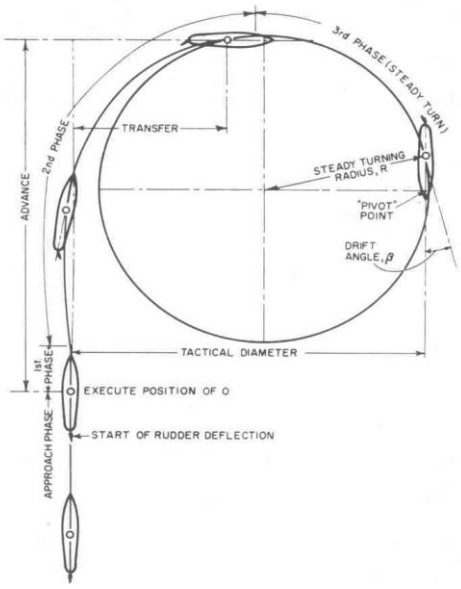

Figure 1: *Definition of manoeuvring performance parameters [Comstock, 1967]*

In some cases, a good understanding of the response of the submarine to casualty scenarios such as floods and hydroplane jams is required, [Haynes *et al*, 2002]. A key element of manoeuvring and control performance is the provision of operator guidance, or assurance, to the submarine operators that in the event of a failure the submarine will recover safely. The existence of these failure hazards requires that submarine operators are provided with appropriate advice in a form that ensures the submarine is never in a situation where recovery from these failure modes would not be possible. According to [Burcher and Rydill*,* 1995], the sort of guidance is produced in the manoeuvring limitation diagrams, Figure 2. As described by [Bayliss *et al,* 2005] there is a continuing need to understand the manoeuvring performance of a submarine throughout its operational life; requiring evaluation using model tests, trials and simulation.

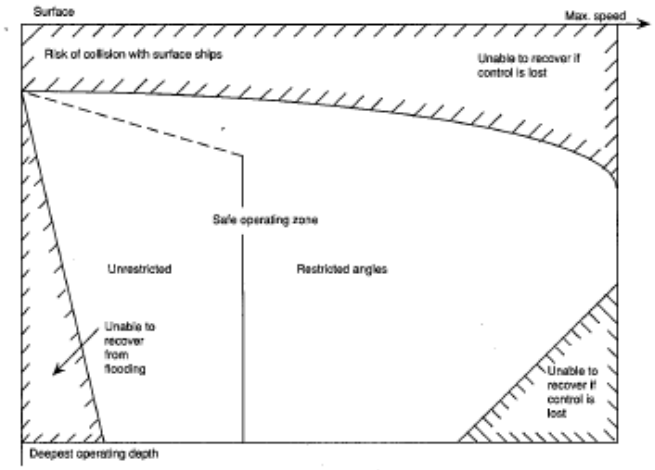

Figure 2: Submarine safety envelope [Burcher and Rydill, 1995]

The example in Figure 2 provides boundaries of safe operation in terms of speed and depth; the slow speed boundaries are present as a consequence of a flood and at higher speeds the restrictions are limited to mitigate against a plane jam. To generate such a robust set of curves, the response of the submarine following such emergency scenarios must be known; the only practicable means of doing that is to have a reliable mathematical model of a submarine's manoeuvring performance. Thus, the study of the manoeuvring and control performance of a deeply submerged submarine operating away from the effects of the free surface has been an active discipline for decades [see Ray *et al*, 2008]. The primary purpose of these studies has been to understand, to a high level of fidelity, the manoeuvring characteristics of a submarine. In the first instance, this would ensure that any submarine design would have sufficient directional stability and control ability, thus avoiding unsuitable designs early in the process. Subsequent higher fidelity methods would provide an understanding of the agility of the submarine in the horizontal plane, which informs on the

performance of the submarine against manoeuvring requirements. Ultimately, understanding the ability of the submarine to recover from emergency scenarios such as floods and control surface failures is required to define the boundaries in the safety envelope and compare against operational requirements.

The previous discussion has centred around the need for a robust prediction capability of the manoeuvring submarine. However, as described by [Burcher and Rydill, 1995], a streamlined bare hull form is usually directionally unstable in both the horizontal and vertical planes unless some form of stabiliser and/or control surfaces are provided. So, control surfaces form an integral part of the design of a submarine whether it is deeply submerged or near the free surface. Any control surfaces (appendages) or internal systems (tanks) are designed to allow a level of controllability in the vertical and horizontal planes (clearly, hydrostatic control, through buoyancy, is only effective in the vertical plane). See, Figure 3 for a schematic of the typical control systems onboard a submarine; the following describes some of the typical submarine control systems.

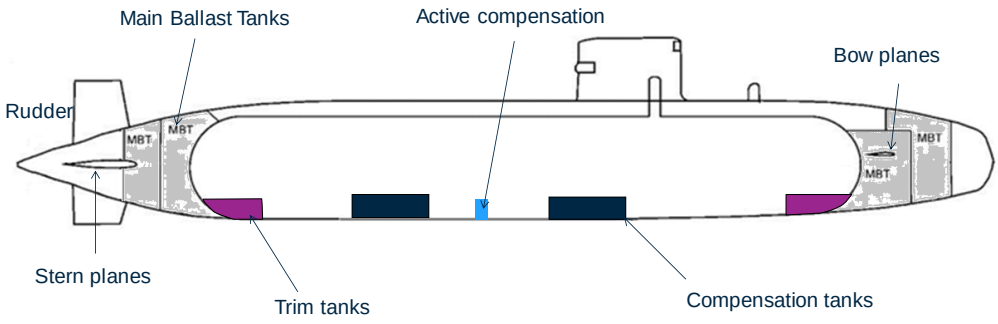

Figure 3: Hydrodynamic and hydrostatic control in submarines

Typically, in the horizontal plane, agility is usually desirable when higher rates of turn (defined, in this context, as the ratio of steady yaw velocity to the rudder angle, achieved during the turn) and lower tactical diameters can be achieved. However, from an operational and safety perspective, a reduced level of agility is typically required in the vertical plane, to mitigate the risk of large pitch and depth excursions occurring following a mechanical failure or damage leading to an unplanned angle of attack on the control surface. These large unplanned pitch and depth excursions may cause the submarine to broach or to dive too deep.

So, a submarine will usually have a set of appendages or control surfaces that provide the required horizontal plane turning performance yet ensuring safe manoeuvring in the vertical plane; these control surfaces can be controlled manually (helm) or by a suitable autopilot (for both the vertical and horizontal planes). In a traditional cruciform arrangement, control may be by means of bow

planes and stern planes for vertical plane control (depth keeping) and rudders for manoeuvring in the horizontal plane (course keeping). Control surfaces are usually fitted in pairs, port and starboard for the planes and upper and lower rudders. Bow planes are usually all moving (do not include a portion of the control surface that is fixed or flapped) low-aspect-ratio hydrofoils and can be linked by a single actuator or independently actuated. The stern planes are usually larger than bow planes, [Burcher and Rydill, 1995], and they tend to be flapped type designs, with a moving portion towards the trailing edge, incorporated into a fixed portion (or stabiliser); to balance vertical plane control authority against stabilisation. Again, stern planes can be moved by a single actuation system or split with independent actuators. The rudder tends to be all moving and the upper rudder is larger than the lower rudder, to ensure that the lower portion does not protrude below the keel; rudders in a cruciform arrangement tend to be linked with a single actuator, [Marshfield, 1991]. There are other control surface configurations such as X-plane aft arrangements and fore planes mounted on the bridge fin (or sail); the benefits of these alterative arrangements are discussed by [Renilson, 2014].

Hydrostatic control can come in the form of a number of systems. During routine operations, the Main Ballast Tanks (MBTs) would be used to generate significant changes in the weight and buoyancy of the submarine in order to dive or surface; trim and compensation tanks have the capacity to transfer water to and from the sea to manage weight and buoyancy fluctuations that may occur during periods of submerged, for example changes in sea water density or hull compressibility, the pumps for these systems are usually controlled manually, [Burcher and Rydill, 1995] and [Ying and Jian, 2010]. Hydrostatic control in the submerged condition comes in the form of tank compensation systems, used as a means of adjusting the balance of the submarine to account for changes in weight and buoyancy due to effects such as:

- changes in seawater density due to temperature, salinity and pressure due to depth;
- the weight, disposition and usage of consumables including fuel usage for example;
- compressibility of the hull (due to elasticity of the hull)

The above factors tend not to require large and rapid correction to the submarine condition and can be achieved by a simple trim and compensation system with manual control and modest pump rates. However, there may be specific operational needs where more demanding performance requirements mean that a more sophisticated system is required. A hover system in a submarine

provides the ability for the submarine to remain within a given depth envelope at zero or low forward speeds where hydrodynamic control becomes ineffective. Such a system would require the ability to pump and flood water more rapidly than a compensation system and would not be a manual system and so require some form of automatic control system.

Any system of control, hydrodynamic or hydrostatic, which is designed to regulate an output by keeping it at a desired value requires some type of mathematical algorithm or control system. This system is designed to regulate an output by keeping it at a desired value. In the context of a submarine this would be maintaining heading or depth; if the input changes, a heading or depth change is required for example, then the system would respond by demanding a rudder angle or hydroplane angle respectively. A submarine that is undergoing a manoeuvre with no regulation or control is referred to as an open loop manoeuvre, for example when a submarine is undertaking a turn with no depth control; the submarine would experience a depth change during the heading change, [Kimber and Crossland, 2008]. A closed loop system is essentially an open loop system with feedback and thereafter a control system that responds to that feedback.

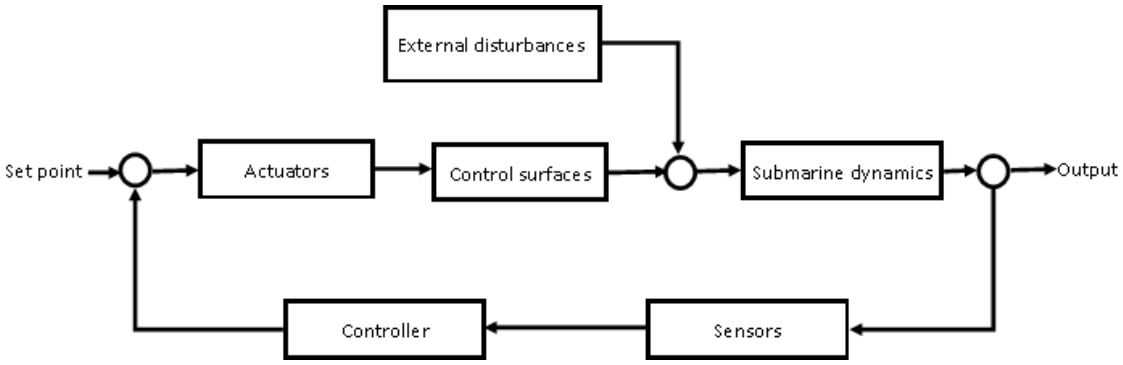

Figure 4: Schematic of the control system in a submarine

Figure 4 shows a schematic of a control system in a submarine; the model describing the submarine dynamics and the external disturbances (in the case of the submarine, the wave induced forces and moments for example) have been introduced and will be covered in more detail later in this thesis. The hydrodynamic characteristics of the control surfaces (in the case of a submarine, hydroplanes and rudders) and their hydraulic actuators form a key component of the entire system model in that they represent the one main source of design constraints that affect the performance of control surfaces, [Perez, 2003]. In the case of a submarine, the constraints will be the size of the control surfaces, the maximum angle and the maximum rate of change of angle that can be applied to the control surfaces. The sensors provide the mechanism for the feedback, in the horizontal plane this

would be a heading gyro and the vertical plane would be pressure sensors to measure depth, [Burcher and Rydill, 1995] and pitch through an inertial navigation system (INS).

The design of the controller, typically, requires an understanding of the performance limitations and any design objectives for the control system, [Perez, 2003]. In the context of an autopilot controlling a deeply submerged submarine, the performance limitations of such a system may be characterised by the limitations of the servo mechanism controlling the appendages and the design objectives characterised by the behaviour of the system, (Fossen, 1995). The design of a control system requires, in the first instance, an understanding on how the submarine behaves or so called "plant model"; as described, this is usually quantified using mathematical models. In most cases, these mathematical models will have been developed for detailed performance assessment at the design stage of a submarine and usually require simplification for use in control design, [Fossen, 1995].

The principal aim of any controller is to enable the actuator to respond to planned, or demanded commands, and to counteract any effects of the external disturbances (disturbance rejection). In the case of the deeply submerged submarine, the controller could be demanding control surface angles in response to a planned depth change or an unplanned depth change as a consequence of a change in buoyancy due to fluctuations in seawater density. In the case of a submarine close to the free surface the external disturbance due to the effect of the waves would cause the unplanned depth changes.

Autopilot design is normally focussed on the control of depth and heading of the submarine; under standard control design conditions, control in the horizontal plane (heading) and vertical plane (depth) are assumed to be decoupled, [Solberg,1992] which means that the control algorithms for vertical and horizontal plane control can be designed in isolation of each other. The depth controller is considered to be the more important part of the submarine control systems, [Grimble *et al,* 1993]. This is largely from a perspective of safety and the requirement to operate within tight constraints such as the avoidance of large unexpected depth excursions (overshoot) as a result of an autopilot-controlled depth change; conventional control schemes work with bow and stem planes geared together controlling depth, [Marshfield, 1991].

In summary, it is unusual for a submarine to be designed from a purely hydrodynamic perspective, but a hydrodynamically poorly designed submarine is unlikely to provide the desired operational capability. So, as far as understanding the impact of manoeuvring and control of a deeply submerged

submarine on design choices is concerned, the ability to accurately evaluate the performance of a particular hull and appendage configuration at the design stage enables the designer to:

- determine indices of directional stability
- determine whether standard manoeuvres meet international maritime regulations for ship manoeuvring (so exclusively for the case where the submarine is manoeuvring on the surface) and national design guidelines
- establish the size and power requirements of any control surfaces
- design suitable motion control systems (that includes the control surfaces, actuators and control algorithms)
- Ensure, early in the design process, that the submarine is safe to operate.

2.3 Axes system and equations of motion

Use is made of two coordinate axes systems; define as a body-fixed coordinate system Oxyz (with origin at x_0 , y_0 , z_0) and an earth-fixed coordinate system O'x'y'z' as shown in Figure 5 Here, z' is vertically downwards and z'=0 is the mean horizontal surface at the water surface.

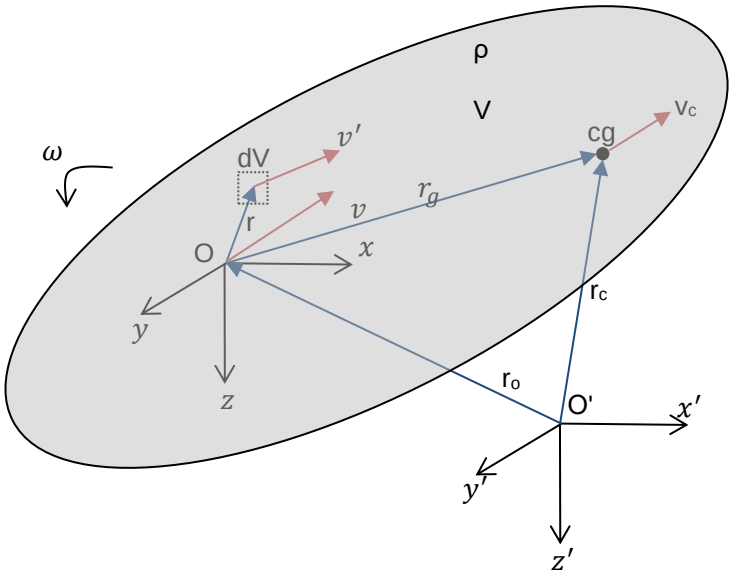

Figure 5: The inertial, earth-fixed axes, and the body-fixed axes both in translation and rotation (Fossen, 1995)

The motion of the body is described by Newton's Law in terms of the conservation of both linear and angular momentum, where the rate of change of momentum (or angular momentum) of a rigid body is equal to the total force (or moment) acting on the body.

We denote m as the mass of the body with rotational inertial matrix I_o given as:

$$I_o = \begin{bmatrix} I_{xx} & -I_{xy} & -I_{xz} \\ -I_{yx} & I_{yy} & -I_{yz} \\ -I_{zx} & -I_{zy} & I_{zz} \end{bmatrix}$$

1

We further define;

$F = [X, Y, Z]^T$ is the external force

$M = [K, M, N]^T$ is the external moment

where the components of the forces and moments are in the earth fixed system (x'y'z' directions respectively).

and

$v = [u, v, w]^T$ is the linear velocity

$\omega = [p, q, r]^T$ is the angular velocity

$r_g = \left[x_g, y_g, z_g\right]^T$ is the centre of gravity which is not necessarily at the origin

where the components of these variables are in the body-fixed system (xyz directions respectively).

Transformation of the unit vectors in the body axes system to an earth axes system is given by:

$$\begin{bmatrix} \hat{\imath}' \\ \hat{\jmath}' \\ \hat{k}' \end{bmatrix} = \underline{T} \begin{bmatrix} \hat{\imath} \\ \hat{\jmath} \\ \hat{k} \end{bmatrix}$$

2

where $\hat{\imath}, \hat{\jmath}, \hat{k}$ and $\hat{\imath}', \hat{\jmath}', \hat{k}'$ are the unit vectors in the body and Earth axes respectively and $\underline{T}$ is the transformation matrix given by [Gentle,2007]:

$$\underline{T} = \begin{bmatrix} \cos\Theta\cos\Psi & -\cos\Phi\sin\Psi + \sin\Theta\sin\Phi\cos\Psi & \sin\Phi\sin\Psi + \sin\Theta\cos\Phi\cos\Psi \\ \cos\Theta\sin\Psi & \cos\Phi\cos\Psi + \sin\Psi\sin\Theta\sin\Phi & -\sin\Phi\cos\Psi + \sin\Theta\cos\Phi\sin\Psi \\ -\sin\Theta & \cos\Theta\sin\Phi & \cos\Theta\cos\Phi \end{bmatrix}$$

where Φ, Θ and Ψ are Euler angles from x'y'z' to xyz, reflecting the body orientations.

The sign convention is given in Figure 6.

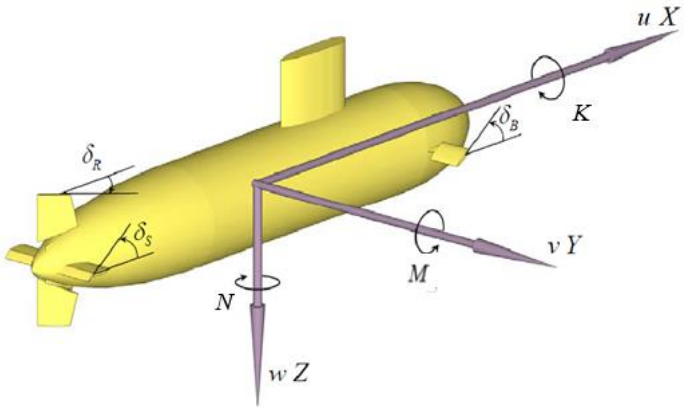

Figure 6: Submarine axis sign convention

The equations of motions are taken from [Fossen, 1995],

$$m\left[\dot{u} - vr + wq - x_g(q^2 + r^2) + y_g(pq - \dot{r}) + z_g(pr + \dot{q})\right] = X$$

$$m\left[\dot{v} - wp + ur - y_g(r^2 + p^2) + z_g(qr - \dot{p}) + x_g(qp + \dot{r})\right] = Y$$

$$m\left[\dot{w} - uq + vp - z_g(p^2 + q^2) + x_g(rp - \dot{q}) + y_g(rq + \dot{p})\right] = Z$$

$$I_{xx}\dot{p} + \left(I_{zz} - I_{yy}\right)qr - (\dot{r} + pq)I_{xz} + (r^2 - q^2)I_{yz} + (pr - \dot{q})I_{xy}$$
$$+m\left[y_g(\dot{w} - uq + vp) - z_g(\dot{r} - wp + ur)\right] = K$$

$$I_{yy}\dot{q} + (I_{xx} - I_{zz})rp - (\dot{p} + qr)I_{xy} + (p^2 - r^2)I_{xz} + (qp - \dot{r})I_{yz}$$
$$+m\left[z_g(\dot{u} - vr + wq) - x_g(\dot{w} - uq + vp)\right] = M$$

$$I_{zz}\dot{r} + \left(I_{yy} - I_{xx}\right)pq - (\dot{q} + rp)I_{yz} + (q^2 - p^2)I_{xy} + (rq - \dot{p})I_{zx}$$
$$+m\left[x_g(\dot{v} - wp + ur) - y_g(\dot{u} - vr + wq)\right] = N$$

3

The above equations are fully coupled and non-linear (as a consequence of the velocity products and the dependence of force on the motion) in which there have been no other assumptions other than the body is rigid and the mass is constant.

$[X\ Y\ Z\ K\ M\ N]^T$ represents all the forces on the submarine including hydrodynamic forces, restoring forces, forces due to control surfaces and external forces due to the waves.

As computational capabilities have increased more and more, Computational Fluid Dynamics (CFD) has been used to obtain predictions through free-running simulations where the hydrodynamic forces and moments on the manoeuvring surface ship or submarine are used directly in solving the equations of motion. These approaches can provide more reliable predictions of manoeuvring motions than theoretical methods because of the ability to include both viscous and rotational effects in the solution to the problem. One of the problems with these approaches still lie in the computational cost in directly calculating the free running trajectory of a manoeuvring ship or submarine is considerably high for many applications. This computational cost increases significantly when considered the additional problem of manoeuvring in waves, largely because of the long runs lengths required to obtain meaningful statistics.

It is likely that, a fully consistent theoretical or numerical model describing the hull hydrodynamic forces on a vessel manoeuvring in waves can only be obtained using computational fluid dynamics methods, i.e. problems formulated for the Reynolds-Averaged Navier–Stokes (RANS) equations, Sutulo and Guedes Soares, [2006]. Other less computationally intensive approaches must have simplifying assumptions, keeping a certain degree of representation of the problem, such as the fluid being considered inviscid and irrotational in the flow solution.

These simplified approaches generally require a means of solving the manoeuvring and seakeeping problems separately, see [Fossen, 1995] for example. There are two main approached for dealing with the coupled manoeuvring and seakeeping, manoeuvring in waves, problem: the first method, called the two time scales method, is based on a coupled but independent solution of the manoeuvring and seakeeping problems, in low and high frequency respectively. This method, introduced by Hirano et al. (1980), assumes that the motions from the manoeuvring and seakeeping problems can be linearly superimposed on each other. The second method is based on a unified description of the hydrodynamic problem, where the forces due to the manoeuvring and seakeeping behaviour are linearly superimposed in the same equations of motion, Bailey et al. [1997] for example.

Sutulo and Guedes Soares, [2006] considered the hydrodynamic manoeuvring forces and the wave induced, or seakeeping, forces by developing a simplified theoretical model to obtain the forces on a vessel manoeuvring in waves. However, they accounted for the limitations of this simplified theoretical model for the manoeuvring problem and replaced those predicted forces with the manoeuvring forces predicted by an experiments based manoeuvring model (typical of one described in section 2.4.1). So, the hydrodynamic forces on the vessel were decomposed as follows:

$$F(W,M) = F_{WM}(W,M) - F_{WM}(O,M) + F_M(M) \qquad 4$$

Where

F_{WM} are the forces predicted by the simplified model

W is a generalised set of parameters defining the waves; $W = 0$ means the still water condition

M is a generalised set of parameters defining the manoeuvre; $M = 0$ corresponds to the more typical seakeeping condition and not associated with any manoeuvring.

Sutulo and Guedes Soares, [2006] considered that $F_{WM}(O,M)$ would be less accurate than those manoeuvring forces predicted by an experiment-based mathematical model, represented by $F_M(M)$.

This decomposition of the hydrodynamic forces and moments is the approach adopted in this thesis. This is because of the known limitations of predicting the forces and moments on a manoeuvring submarine using inviscid, potential flow, theory (due to inability to predict flow separation on the body). Also, this decomposition has been consider because a full set of hydrodynamic derivatives is often available. This decomposition implies that the manoeuvring forces and wave forces do not interact with each other in which case the total force on the body can be represented as:

$$\begin{aligned}[X\ Y\ Z\ K\ M\ N]^T \\ &= [X_{man}\ \ Y_{man}\ \ Z_{man}\ \ K_{man}\ \ M_{man}\ \ N_{man}]^T \\ &+ [X_{wave}\ \ Y_{wave}\ \ Z_{wave}\ \ K_{wave}\ \ M_{wave}\ \ N_{wave}]^T\end{aligned} \qquad 5$$

When the forces and moments on the right-hand side of Eqn 5 are known, the accelerations can be found and through time integrations the translational and rotational velocities and, subsequently, the translational and rotational displacements can be found; the key challenge is the determination of the total forces and moments $[X\ Y\ Z\ K\ M\ N]^T$ on the submarine for each time step.

Traditionally, the manoeuvring problem and the problem of the submarine in waves are considered separately; the following sections describe the approaches that can be used to obtain the calm water manoeuvring forces and moments (for the deeply submerged submarine and close to the free surface) and the wave induced forces on a submarine.

2.4 Calm water manoeuvring forces and moments

2.4.1 Deeply submerged submarines

This section discusses the approaches used for modelling the hydrodynamic behaviour of a deeply submerged submarine in the context of the applicability of these techniques to the near surface problem. A general overview of the methods of predicting the manoeuvring performance of marine vehicles is shown in Figure 7 taken from [ITTC, 2005]. The remainder of this section describes methods in which the case of a deeply submerged submarine manoeuvring performance can be quantified in both the horizontal and vertical plane. The figure illustrates that there are a number of approaches to predict the manoeuvring performance parameters of a deeply submerged submarine.

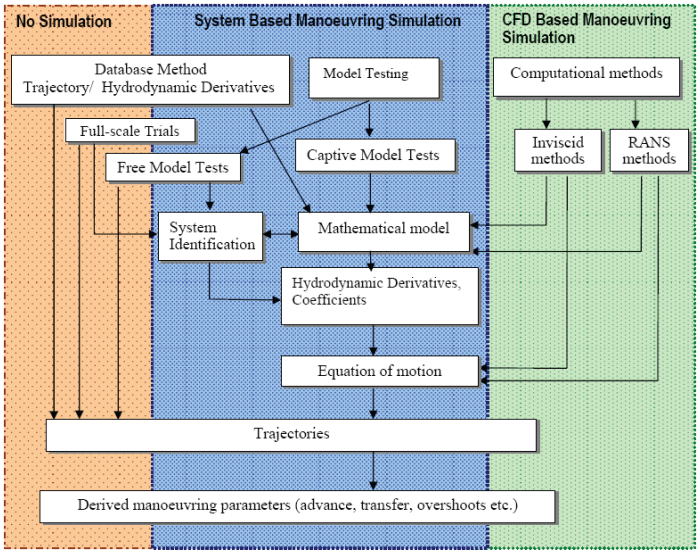

Figure 7: Manoeuvring prediction methods for marine vehicles (ITTC, 2005)

In the case of understanding the directional stability of the submarine, [Spencer, 1968] used small disturbance theory to derive stability and control indices as a measure of performance (MOP). This MOP was based on the evaluation of the directional stability of the submarine without the need to undertake simulations of trajectories; these indices are obtained from the hydrodynamic derivatives and coefficients (described later in this section). Hydrodynamic databases can be used to develop empirical or semi-empirical methods for predicting trajectories directly [Lloyd 1983], or by providing

hydrodynamic derivatives and coefficients for subsequent use in the equations of motion, see [Kormilitsin and Khalizev, 2001], for example in which empirical relationships for the key hydrodynamic coefficients have been derived from regression analysis.

Generally, to predict parameters such as advance, transfer overshoots, as defined in Figure 1 the fundamental trajectories of the submarine, undertaking specific manoeuvres, are required which in the absence of numerical based simulations methods can be obtained from free running model tests or even full-scale trials. Kimber and Crossland [2008] commented that free-manoeuvring model experiments can fulfil several purposes, including:

- confirmation of basic manoeuvring performance
- a measure of performance in waves
- confirmation of autopilot performance
- investigation into recovery from casualty scenarios

Scale effects can be significant in model tests of this nature, particularly in relation to the effects of the control surfaces; using as large a model as is practicable, and by including turbulence stimulation in the model, the scale effects can be reduced. However, the low Reynolds numbers that are typical of the flow over the model scale appendages means that the control surface lift curve slope and the stall angle may not be fully representative of the full-scale equivalent. In some cases, empirical corrections can be obtained by correlating model scale and full-scale performance once the submarine is at sea.

An alternative (or complimentary) approach to free running model tests is the “System Based Manoeuvring Simulation Method”, a term used by ITTC [2005], which describes a method that is widely used to predict manoeuvring trajectories, Figure 7. In this case, the components of the hydrodynamic forces and moments acting on a deeply submerged submarine are treated as a function of the motion state variables, [Ray, 2008]. The traditional approach used in this method, again, requires a physical model to be manufactured and tested in a series of experiments. However, these experiments use a captive model, which, in principle, is a simpler construction than a free running model, to obtain directly the hydrodynamic forces and moments acting on the appended submarine as a function of the motion state variables (see [Lewis, 1989] for example). This approach is based on the assumption that the motion of a deeply submerged submarine can be regarded as

quasi-steady state whereby each component of the hydrodynamic force and moment is a function of the instantaneous values of the velocity and acceleration components of the body and the deflection of the control surfaces.

This “slowly varying assumption”, coupled with the assumption of “small disturbance”, enables these forces and moments to be related to the motion state variables by a set of hydrodynamic derivatives. These derivatives are those in the Taylor series expansion of forces *X, Y, Z,* and moments *K, M, N* , shown in Figure 6, in terms of the displacement, velocity and acceleration of the submarine and control surfaces, as described by [Comstock, 1967] and derived by [Bishop and Parkinson, 1970a]. Taking vertical force for a deeply submerged submarine away from the free surface, Z_{deep}, for example, this force can be represented as a function of the following terms (or motion state variables):

$$Z_{deep} = f(\phi, \theta, u, v, w, p, q, r, \dot{u}, \dot{v}, \dot{w}, \dot{p}, \dot{q}, \dot{r}, \ddot{u}, \ddot{v}, \ddot{w}, \ddot{p}, \ddot{q}, \ddot{r}, \delta_b, \delta_s, \delta_r, \dot{\delta_b}, \dot{\delta_s}, \dot{\delta_r}, \ddot{\delta_b}, \ddot{\delta_s}, \dddot{\delta_r}) \quad 6$$

where $\delta_b, \delta_s, \delta_r$ are the angles of the control surfaces (bow plane, stern planes and rudders in this case) u,v,w and p,q,r are the components of translational and rotational velocities. The over dot in the equation indicates temporal derivative. The displacement has no affect as the weight or buoyancy of the submarine does not change. Eqn 6 can be used to obtain a Taylor series expansion across the state variables, based on the assumption that the motion state variables do not change rapidly with time. This slowly varying assumption is where $v \ll U$ and $w \ll U$ or alternatively the reference motion shall be considered “slow” if:

$$\frac{|w|}{|\dot{w}|}, \frac{|\dot{w}|}{|\ddot{w}|}, \frac{|\ddot{w}|}{|\dddot{w}|} \geq \frac{L}{U} \quad 7$$

where L is the length of the boat, U is the forward speed and $\frac{L}{U}$ is therefore the time taken to travel one boat length, [Bishop and Parkinson, 1970b].

A complete Taylor expansion of Eqn 6 to a high order would lead to a practically impossibly large number of derivative terms, as the value of each term needs to be found in some way. So, more practicable methods have been developed, whereby the infinite Taylor series has been truncated, such as that described by [Gertler and Hagen, 1967], (all symbols used in the equations are defined at the beginning of this thesis), in which the heave force can be represented as:

$$
\begin{aligned}
Z'_{deep} = {} & \left(Z'_{\mathrm{uu}}u'^2 + Z'_{uw}u'w' + Z'_{uv}u'v' + Z'_{vv}v'^2 + Z'_{\mathrm{uu}\,\delta\mathrm{b}}u'^2\delta\mathrm{b} + Z'_{\mathrm{uu}\,\delta\mathrm{s}}u'^2\delta\mathrm{s}\right) \\
& + \left(Z'_{wv}w'v' + Z'_{u|w|}u'|w'| + Z'_{|wv|}|w'v'|\right) \\
& + \left(Z'_{\dot{w}}\dot{w}' + Z'_{uq}u'q' + Z'_{vp}v'p' + Z'_{vr}v'r'\right) \\
& + \left(Z'_{wv|\frac{q}{w}|}w'v'\left|\frac{q'}{w'}\right| + Z'_{\mathrm{u}|q|\delta\mathrm{s}}u'|\mathrm{q}'|\delta\mathrm{s}\right) \\
& + \left(Z'_{\dot{q}}\dot{q}' + Z'_{pp}p'^2 + Z'_{rr}r'^2 + Z'_{rp}r'p'\right) + (\mathrm{m}'\mathrm{g}' - B')\,cos\phi cos\,\theta \\
& + \left(Z'_{uw\,n'}u'w' + Z'_{uq\,n'}u'q' + Z'_{w|w|n'}w'|w'| + + Z'_{\mathrm{uu}\,\delta\mathrm{s}n'}u'^2\delta\mathrm{s}\right)(n' - 1)
\end{aligned}
\qquad 8
$$

where $v = \sqrt{v^2 + w^2}$ and is known as the cross flow velocity. The above expansion is not a complete Taylor Series expansion, only some derivative terms have been retained and some derivatives are written in terms of the absolute value of w to account for asymmetry in the hull form. Indeed, the form of the equations derived by Gertler and Hagen is based on physical considerations based on experience gained from performing physical model tests. Also, for a submarine that is "in-trim" the term $(\mathrm{m}'\mathrm{g}' - B')$ is zero (where the weight is equal to the buoyancy). However, operationally, a submarine is unlikely to be always in-trim. For example, there will be occasions where the buoyancy will change due to hull compressibility effects as a result of a depth change. The other forces and moments can be given similarly as:

Surge force

$$
\begin{aligned}
X'_{deep} = {} & \left(X'_{uu}u'^2 + X'_{vv}v'^2 + X'_{ww}w'^2\right) + \left(X'_{\dot{u}}\dot{u}' + X'_{vr}v'r' + X'_{wq}w'q'\right) \\
& + \left(X'_{qq}q'^2 + X'_{rr}r'^2 + X'_{rp}r'p'\right) \\
& + \left(X'_{uu\delta b\delta b}\,u'^2\delta b^2 + X'_{uu\delta s\delta s}\,u'^2\delta s^2 + X'_{uu\delta r\delta r}\,u'^2\delta r^2\right) + (B' - m'g')\,sin\,\theta + X'_{n'} \\
& + \left(X'_{vvn'}v'^2 + X'_{ww\,n'}w'^2 + X'_{uu\delta s\delta s\,n'}u'^2\delta s^2 + X'_{uu\delta r\delta r\,n'}u'^2\delta r^2\right)(n' - 1)
\end{aligned}
\qquad 9
$$

Sway force

$$
\begin{aligned}
Y'_{deep} = {} & \left(Y'_{\mathrm{uu}}u'^2 + Y'_{uv}u'v' + Y'_{vw}v'w' + Y'_{vv}v'v' + Y'_{\mathrm{uu}\,\delta\mathrm{r}}u'^2\delta\mathrm{r}\right) \\
& + \left(Y'_{\dot{v}}\dot{v}' + Y'_{up}p' + Y'_{ur}r' + Y'_{vq}v'q' + Y'_{wp}w'p' + Y'_{wr}w'r'\right) \\
& + \left(Y'_{vv|\frac{r}{v}|}v'v'\left|\frac{r'}{v'}\right| + Y'_{\mathrm{u}|\mathrm{r}|\delta\mathrm{r}}|\mathrm{r}'|\delta\mathrm{r}\right) \\
& + \left(Y'_{\dot{p}}\dot{p}' + Y'_{\dot{r}}\dot{r}' + Y'_{p|p|}p'|p'| + Y'_{pq}p'q' + Y'_{qr}q'r'\right) + (\mathrm{m}'\mathrm{g}' - B')\,sin\phi cos\,\theta \\
& + \left(Y'_{\mathrm{ur}\,n'}u'\mathrm{r}' + Y'_{uv\,n'}u'v' + Y'_{v|v|n'}v'|v'| + Y'_{\mathrm{uu}\,\delta\mathrm{r}n'}u'^2\delta\mathrm{r}\right)(n' - 1)
\end{aligned}
\qquad 10
$$

Roll moment

$$K'_{deep} = \left(K'_{uu}u'^2 + K'_{uv}u'v' + K'_{vw}v'w' + K'_{vv}v'v' + K'_{uu\delta r}u'^2\delta r\right) + \left(K'_{\dot{v}}\dot{v}' + K'_{up}u'p' + K'_{ur}u'r' + K'_{vq}v'q' + K'_{wp}w'p' + K'_{wr}w'r'\right) + \left(K'_{\dot{p}}\dot{p}' + K'_{\dot{r}}\dot{r}' + K'_{p|p|}p'|p'| + K'_{pq}p'q' + K'_{qr}q'r'\right) + \left(\mathrm{m}'\mathrm{g}'y_g - \mathrm{B}'y_b\right)cos\phi cos\,\theta - \left(\mathrm{m}'\mathrm{g}'z_g - \mathrm{B}'z_b\right)sin\phi cos\,\theta + K'_{uu\,n'}u'^2(n' - 1) + K'_{n'}$$

11

Pitch moment

$$M'_{deep} = \left(M'_{\mathrm{uu}}u'^2 + M'_{uw}u'w' + M'_{vv}v'^2 + M'_{\mathrm{uu\,\delta b}}u'^2\delta\mathrm{b} + M'_{\mathrm{uu\,\delta s}}u'^2\delta\mathrm{s}\right) + \left(M'_{wv}w'v' + M'_{u|w|}u'|w'| + M'_{|wv|}|w'v'|\right) + \left(M'_{\dot{w}}\dot{w}' + M'_{uq}u'q' + M'_{vp}v'p' + M'_{vr}v'r'\right) + \left(M'_{qv}q'v' + M'_{\mathrm{u}|q|\delta\mathrm{s}}u'|\mathrm{q}'|\delta\mathrm{s}\right) + \left(M'_{\dot{q}}\dot{q}' + M'_{pp}p'^2 + M'_{rr}r'^2 + M'_{rp}r'p' + M'_{q|q|}q'|q'|\right) - \left(\mathrm{m}'\mathrm{g}'x_g - \mathrm{B}'x_b\right)cos\phi cos\,\theta - \left(\mathrm{m}'\mathrm{g}'z_g - \mathrm{B}'z_b\right)sin\,\theta + \left(M'_{\mathrm{uq}\,n'}u'q' + M'_{uw\,n'}u'w' + M'_{|wv|n'}|w'v'| + M'_{\mathrm{uu\,\delta s}n'}u'^2\delta\mathrm{s}\right)(n' - 1)$$

12

Yaw moment

$$N'_{deep} = \left(N'_{\mathrm{uu}}u'^2 + N'_{uv}u'v' + N'_{vw}v'w' + N'_{vv}v'v' + N'_{\mathrm{uu\,\delta r}}u'^2\delta\mathrm{r}\right) + \left(N'_{\dot{v}}\dot{v}' + N'_{up}u'p' + N'_{ur}u'r' + N'_{vq}v'q' + N'_{wp}w'p' + N'_{wr}w'r'\right) + \left(N'_{rv}r'v' + N'_{\mathrm{u}|\mathrm{r}|\delta\mathrm{r}}u'|\mathrm{r}'|\delta\mathrm{r}\right) + \left(N'_{\dot{p}}\dot{p}' + N'_{\dot{r}}\dot{r}' + N'_{r|r|}r'|r'| + N'_{pq}p'q' + N'_{qr}q'r'\right) + \left(\mathrm{m}'\mathrm{g}'x_g - \mathrm{B}'x_b\right)sin\phi cos\,\theta + \left(\mathrm{m}'\mathrm{g}'y_g - \mathrm{B}'y_b\right)sin\,\theta + \left(N'_{\mathrm{ur}\,n'}u'r' + N'_{uv\,n'}u'v' + N'_{vv\,n'}v'v' + N'_{\mathrm{uu\,\delta r}n'}u'^2\delta\mathrm{r}\right)(n' - 1)$$

13

where all the motion state variables are deviations from the initial values and their associated derivatives are assumed to be constant across the range of state variables. The symbol ' represents the parameters non-dimensionalised based on the combination of ρ, U and L by which the forces and moments can be written as, for example:

$$Z'_{deep} = \frac{Z_{deep}}{1/_2\,\rho U^2L^2}, M'_{deep} = \frac{M_{deep}}{1/_2\,\rho U^2L^3}$$

$[x_b, y_b, z_b]$ in the equation is the centre of buoyancy, δb, δs and δr are the bow plane, stern plane and rudder angles respectively and ϕ and θ are the roll and pitch angles of the submarine respectively.

$X'_{n'}, K'_{n'}$ are the axial force and roll moment due to the propeller which are treated as an external force.

$n' = \frac{u_c}{U}$ where u_c is the command speed (steady state ahead speed component for a given propeller rpm) when the submarine is in steady level flight; n' is termed the propulsor state by [Kimber and Crossland, 2008] although presented in terms of a ratio of rpm values rather than speeds.

As mentioned above, the terms in these formulations and their forms for the hydrodynamic loads on a deeply submerged submarine have been selected based on the physical considerations. For example, some of the product terms in the Taylor series expansion use the magnitude of the velocity to reflect the consideration that the force should be in the same direction as the velocity. Also, the series expansions may include up to third order terms in terms of temporal variation, based on the consideration that the force is mainly a function of displacement, velocity and acceleration, and those terms of related to variation of acceleration and beyond have been ignored. Also expansions include up to third derivatives of the functions, while not all terms up to third order are included in the expansion, partly because, in some cases the derivatives are zero due to symmetry in the xz-plane. Although, many of the terms that appear in the Gertler and Hagen model are rooted in empiricism rather than rigorous theory since some of the higher order terms were included to better represent the trends observed in captive-model tests at the time, [Feldmann, 1995]. This means that, if the hydrodynamic design of a submarine is sufficiently different to those from which the empiricism was derived, the mathematical model may be unable to predict the hydrodynamic forces and moments sufficiently well. For example, the construction of the Gertler and Hagen mathematical model is based upon a submarine design that has two sets of hydroplanes controlling the motions in the vertical plane and a single (probably linked upper and lower portion) rudder controlling motions in the horizontal plane. However, if the design arrangement for the aft control surfaces was an X-planes configuration, see [Renilson ,2015], the mathematical model would need to be expanded to account for the additional force and moment contributions of this configuration, see [Crossland *et al,* 2011, 2012].

Derivatives obtained from techniques such as those in [Gertler and Hagen, 1967] are traditionally extracted from an extensive range of physical captive model tests; see [Lewis, 1989]. The procedure for model tests is well established; internal instrumentation within a model consists of a strain-gauge balance capable of measuring the forces and moments acting on the body in all six degrees

of freedom. The design of the experiment (and run plan) is related to the hydrodynamic derivatives that are contained with the equations derived from the Taylor series expansion. That is, the experiment is designed so that the state variables can be controlled, as far as practicable, as independent variables.

In general, the model is towed in a Towing Tank at a range of body incidences in both the horizontal and vertical plane; thus providing the relationship between the forces and moments and the velocities (*u,w* for vertical plane and *u,v* for horizontal plane). Then, with the model at zero angle of incidence the various control surfaces are moved over their working range to measure forces and moments generated as a result of control surfaces deflections; Rotating Arm tests in a manoeuvring tank typically would follow a Towing Tank test to establish the relationship between the forces and moments and the rotation rates (*q,r*) in the horizontal plane. The approach to both experiments is to choose test conditions that produce force and moment data for only one of the motion variables at a time, which means that a captive model test campaign can be a lengthy process.

Finally, the experiment would also include oscillation tests or dynamic tests using a Planar Motion Mechanism (PMM), [Booth and Bishop, 1973] where the model is subjected to sinusoidal oscillations to obtain those coefficients related to the acceleration, of which the term proportional to the acceleration is the added mass.

In these particular tests, it is not a single parameter that is varying as the oscillation will induce components due to both velocity and acceleration, as well as their variation with time. Therefore, to determine the relationship between forces and moments and accelerations requires the components due to velocities to be removed (using the terms derived from the steady state tests). It is recognised that the scale effects on the hydrodynamic coefficients derived from model tests on a submerged body at an angle of attack are much smaller than the drag related coefficients obtained during a resistance test of a submerged body at zero angle of attack. However, to minimise the potential impact of these effects, a model as large as practicably possible tends to be used; at QinetiQ Haslar for example, the geometrical scales of the submarine models are typically between 1:19 and 1:22, and with the effective use of turbulence stimulators on the models the dynamic scaling errors associated with the differences between laminar and turbulent flow can be minimised. There are three reasons why turbulence stimulation is applied to a hydrodynamic model, [ITTC, 2017]: to ensure that the flow regime at model scale is equivalent to that at full scale, that the model scale flow is constant, and hence repeatable across the range of design conditions and between repeated tests, and that a known scaling approach can be applied.

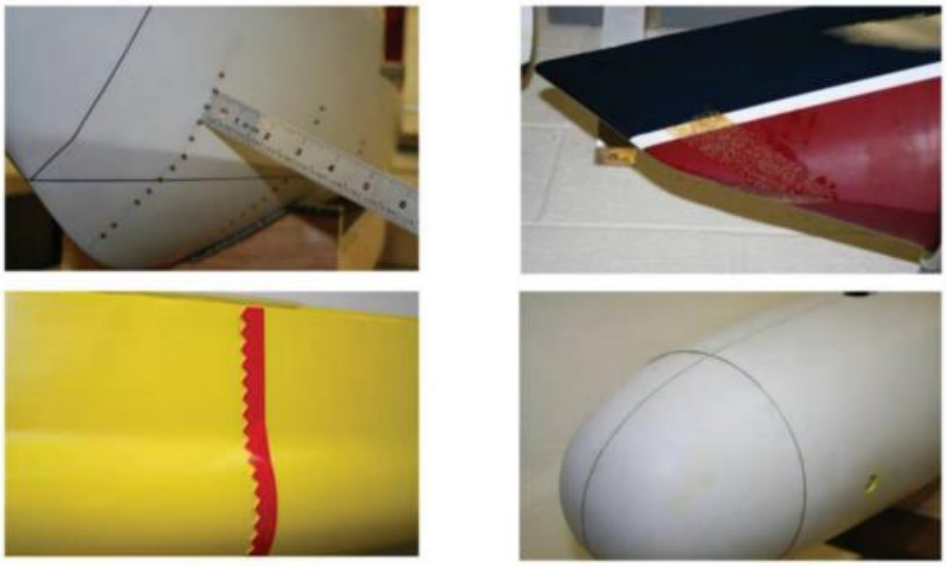

Figure 8: Types of turbulence stimulation devices, clockwise from top left: studs, sand strip, trip wire, hama strips [Murphy 2010].

Figure 8 shows the types of turbulence stimulation that can be used for both surface ships and submarines; according to [ITTC, 2017] the most common turbulence stimulators in use are studs, wires and sand strips. By way of an example, QinetiQ use cylindrical pins (approximately, 2.5 mm high and 3.2 mm in diameter) located on the bow at 5% of the length from the forward perpendicular and located on the leading edge of the bridge fine at 10% of the chord. QinetiQ then use wires (with diameter 0.8 mm located at 10% chord from the leading edge) on the remaining appendages.

As mentioned previously, the purpose of the turbulence stimulators is to create, at model scale, similarity in the flow regime expected at full scale. In most cases, the forces and moments measured on a model can then be scaled to full scale equivalence based on the geometric scale ratio. However, the resistance on the model will increase due to the parasitic form drag of the turbulence stimulators which needs to be corrected prior to extrapolation to full scale, [ITTC, 2017].

System Identification (SI) describes an approach to find a mathematical model of an unknown system, in the case of a deeply submerged submarine that would be the identification of the manoeuvring coefficients from free running model tests and/or full scale trials; see [Ray,2008] for more detail on SI techniques applied to submarine manoeuvring. [Kimber and Crossland, 2008] described how SI techniques can be used to improve the coefficient based mathematical model using data from captive model tests and a semi-autonomous free running model. This free running model test was capable of providing accurate motion results using a Doppler Velocity Log (DVL) that

provides accurate 3-dimensional velocity measurements, along with rotational measurements from the inertial navigation system and measurements of any control surface deflection, provides measurements of the state variables at any instance of time. These measurements provide the data to determine the trajectory of the model, to a high degree of accuracy, from which the forces and moments acting on the body at each instant in time can be reconstructed (see [Coxon, 1989], or [Tinker *et al,* 1979], for example). These forces and moments, derived from free-running model tests, can then be compared with the forces and moments on the body, derived using the hydrodynamic coefficients obtained from captive model tests. SI techniques can then be applied to correct the hydrodynamic coefficients to fit with the trajectory from the free running model test data.

An alternative, or in some cases complimentary, approach to model tests is to use Computational Fluid Dynamics (CFD) based simulation; including methods for both inviscid and fully viscous flows, such as Reynolds Average Navier Stokes (RANS) in the latter case.

CFD based simulation, in the context of submarine manoeuvring, can be broadly separated into two categories; the simulation for unsteady flow where the state variables, including forces and moments, vary with time and therefore a time stepping method is used; and the simulations of quasi-steady state flow where the temporal variation can be ignored. The following description covers the basic approaches, beginning with the most complex and computational demanding, methods, to the simplified and computationally more practical methods.

The time varying hydrodynamic forces and moments can be obtained from the solution of the Navier-Stokes equations for the unsteady problem associated with the submarine undergoing a manoeuvre. Currently, Direct Numerical Simulations (DNS) are only used for Reynolds numbers that are of many orders of magnitude smaller than that of a full submarine, see [Shan *et al*, 2005] for example, and are not considered to be practicable for this current problem. The advantage of DNS is that there is no requirement to simplify the way that turbulence in the flow region is modelled; DNS is able to simulate the flow down to the length scales where turbulence naturally dissipates. This makes DNS very accurate in predicting fluid flow, but requires excessive amounts of processing power (there is also a requirement to understand the nature of the turbulence length and time scales a prior) which limits the application of DNS to mostly research use, see He and Seddighi, [2013] for example.

A less computationally intensive, although still very demanding, approach would be based on using turbulence models such as Large-scale Eddy Simulations (LES) [Fureby, 2006]. This methodology revolves around the use of large-scale eddies that are associated with the geometry of the submarine. The benefit of this approach is the ability to describe the evolution of vortices and how they impact downstream on the submarine hull or appendages but the technique is still very computationally intensive. Whilst, these methods are considered to be computationally high for many applications including the current problem, this area of research continues to develop, Mofidi and Carrica [2014]; the development of supercomputing has led to increased application of LES methods for large scale geometries, Chen et al. [2015] used a LES model to investigate the wave forces on partially submerged circular and square cylinders. Kim et al, [2015] performed three-dimensional unsteady large-eddy simulations to evaluate the turbulent wake from a circular cylinder. The focus of the work was to investigate the large-scale near-wake structure and the small-scale shear-layer instability in the flow with increasing Reynolds numbers. This is typical of studies of this type whereby the interest is in predicting the detail in the flow structure as opposed to the overall forces and moments on a body.

Carrica *et al*, 2016 provided an example of solving an unsteady RANS equations (the difference between RANS and LES largely lies in the way turbulence is modelled) to determine the unsteady forces and moments on a deeply submerged submarine whereby the equations of motion are solved, implicitly, within the CFD software. Carrica *et al* [2016] also discussed the challenges for near surface manoeuvring simulations using unsteady CFD that includes the effects of waves on the submarine. The work shows that to understand the way a submarine operates near the free surface requires a variety of numerical capabilities; motions of the submarine and appendages, including the influence of surface waves, coupled with an autopilot.

However, the use of RANS based unsteady CFD simulations for predicting the behaviour of a deeply submerged manoeuvring submarine is perhaps considered a less mature technology when compared to steady CFD simulations. Steady CFD simulations can be used to determine the forces and moments on an appended submarine, using the same assumptions of slowly varying and small disturbance, whereby the hydrodynamic forces and moments acting on the submarine can be represented sufficiently well as a quasi-steady flow problem. These methods are, in effect, replicating, in steady CFD simulation, the experimental conditions in a towing tank, for example [Toxopeus, 2008] and [Cura-Hochbaum, 2006] or a rotating arm experiment, [Toxopeus *et al*, 2012] by using RANS methods. Toxopeus, [2008] and Toxopeus *et al*, [2012] reported on CFD predictions

on a bare hull in the steady drift condition or a steady turn, respectively. Similar predictions would need to be undertaken for a steady angle of attack, steady pitch rate and (assuming the design includes appendages) for control surface deflections. Cura-Hochbaum, [2006] considered only surface ships and therefore also limited the calculations to motions in the horizontal plane; as mentioned previously, for a submarine, CFD calculations would be required for motions in both the horizontal and vertical planes.

It is perhaps prudent to mention that results of CFD predictions can be greatly affected by the choice of turbulence model, see Nikushchenko and Zubova, [2015] for example. One choice of turbulence model may work well for some hydrodynamic applications but may not for others. Turbulence models are often chosen based on the knowledge and experience of the researcher in how well the same model has worked for similar applications; which are often supported by experimental validation.

In order to be able to use these CFD predictions of the quasi-steady state forces and moments in time domain simulations a set of hydrodynamic derivatives, that come from the Taylor series expansion such as the Gertler and Hagen method, need to be obtained using regression analysis in a similar way to those techniques applied to the model test data themselves. These CFD predictions of quasi steady state flows are less computationally intensive than time stepping based unsteady RANS for submarine in free manoeuvre and, by extracting the derivatives from the force and moment predictions, the output can be used in the coefficient based model to provide faster predictions of submarine trajectories than real-time simulations.

It should be noted that, the quasi-steady state CFD simulations do not provide the added mass and inertia terms. This is because these terms are related to the forces due to body acceleration (or by the variation of the speed); experimentally these are extracted from the oscillation tests using the PMM (as mentioned previously), in this case the model is subjected to sinusoidal oscillations. To emulate these sinusoidal oscillation tests, CFD would need to be able capture the unsteady forces and moments on the body that will be varying with time, i.e., using unsteady CFD simulations discussed earlier. These are principally the added mass terms. Since added mass contributions are mainly related to the acceleration of the body, these inertial forces are well predicted by potential flow theory.

Alternative approaches to the use of the unsteady and steady Navier Stokes based CFD methods described above are potential flow methods, see [Katz and Plotkin, 2001]. These approaches are a

simplification over the Navier Stokes equations in that the fluid is assumed to be inviscid and that the flow is irrotational. Here, the continuity equation can be simplified to the Laplace equation for an incompressible fluid. Ray *et al*, [2008] provides an overview of the types of inviscid methods used in the prediction of submarine manoeuvring performance.

As an example of combining viscous flow and potential flow theories is the application of the boundary layer theory, [Prandtl, 1904]. Katz and Plotkin, 2001, highlighted that, for a streamlined body at high Reynolds Number (which includes those appropriate to submarine modelling), there are two dominant regions in the flow field:

1. The outer region (away from the solid boundaries) where the viscous effects are assumed to be negligible. A solution for the potential flow provides information about pressures normal to the body surface and related forces.

2. Within the thin boundary layer (attached to solid boundaries) where the viscous effects cannot be neglected. Solution to the boundary layer equations provides information about the shear stress tangential to the body surface and related (friction) forces.

For a practical submarine design, viscous effects may be present along the length of the hull even when the body is not at an angle of attack. Flow separation may occur right after the bow (even for a streamlined shape, it may still occur at the forebody) of a submarine and since the boundary layer will grow along the length of the hull it is highly likely for flow separation to occur at some point along the length of the submarine.

Furthermore, in the case where the body is at an angle of attack, there is the increased likelihood for flow separation to occur even nearer to the bow and as a result a large part of the hull will be in the separated flow region. In these instances, the increase in moment, in particular, becomes strongly non-linear (with angle of attack), partly due to the centre of pressure moving aft as a result of the flow separation. Thus, the non-linearities, which are due to the viscous effect, present in the moment have different characteristics to the underlying force in the linear model.

[Mackay and Conway, 1991] described a panel method for the potential flow, that included the capability to model the cross flow separation vortices on a submarine at an angle of attack. The Neumann boundary condition was applied on the body surface and the Kutta conditions applied at the separation lines. Cross flow separation was modelled by shedding doublet sheets from user specified separation lines; the locations of these separation lines were identified from flow

visualisation experiments. As described by [MacKay and Conway, 1991], the out-of-plane-force, pitch moment at an angle of drift, was very sensitive to the location of the separation lines; the position of which is usually determined from experiments and thus, potential flow solutions with vortex sheet in this case do contain a certain amount of empirical data embedded within the formulation.

Alternative mathematical models, with even greater simplification than the lifting panel methods, described above,), are vortex line methods [Lloyd, 1983 for example]. This particular method assumes that the components of forces and moments on the hull and the forces and moments on the appendages can be determined in isolation and can be summed up to get their total effects, providing any interference effects due to upstream vortical flow on the downstream hull and appendages can be accounted for. In this method, there is no formal panelisation of the hull surface. Instead, the hull is represented by an equivalent body of revolution; the forces and moments on the hull are determined from expressions derived from systematic experiments on bodies of revolution with varying fineness ratios and prismatic coefficients. These empirical data therefore implicitly include the effects of the upstream flow on the downstream hull form. When a submarine is at an angle of attack (i.e. turning or changing depth) the flow around the hull is very complex as a consequence of the flow separating from the body and appendages. The flow around these separation points consists of flows generated by the hull and appendages and their interactions; these vortices, due to separation, can persist for some time, affecting the forces on the hull and appendages downstream of the separation point. [Lloyd, 1983] represented this complex flow pattern on the hull by 12 vortices located along curved arcs. The strength and location of these vortices were derived from experiments and implemented into the calculation using an empirical relationship. The appendage vortices and forces are generated using the method derived in [Glauert, 1947] with empirical corrections to account for the dynamic effects observed on an oscillating control surface and to account for the lift and drag during stall. Each appendage sheds trailing vortices that migrate around the hull under the influence of the cross flow velocities induced by the motion of the submarine and the velocities due to the presence of other vortices. Whilst these practical CFD methods are useful in evaluating the performance of submarines, the methods are heavily dependent upon empirical data; the obvious limitation of such methods is that any predictions of forces and moments on a submarine must be evaluated in the context of how similar the hull form is to those used in that empiricism.

The above methods only emulate the steady tests carried out during a towing tank or rotating arm tests. As mentioned previously, the added mass can be readily obtained from potential flow Newman [2018]. In the case of the deeply submerged submarine, the added mass can be obtained by assuming an instantaneous flow field associated with the body with unit constant speed in a given direction. Watt [1988] described a method for estimating the added mass and inertia terms of an appended deeply submerged submarine. The submarine may consist of a number of components, hull, bridge fin and control surfaces and each component is represented by an ellipsoid with three independently sized principal axes. By simplifying the fully appended submarine this way, the added masses to be determined analytically to enable a rapid solution. Watt justified the approximation of representing the appendages as ellipsoids because of the small contribution that the appendage makes to the coefficients dominated by the submarine hull. According to Watt, appendages have only a small effect on the principal added masses associated with translation and rotation in the transverse directions, but can have a significant effects on the coefficients associated with surge and roll, because of their distance to the rotational centre. Appendages are also important to the "off-diagonal" added masses (i.e., those coefficients of one mode due to the acceleration in another mode).

The above provides only an insight into the numerical approaches that are available for predicting the hydrodynamic performance of a deeply submerged submarine. These example techniques range from the most complex, entirely numerical, approaches to the much simplified classical approaches that are enhanced with empirical data. The purpose of this insight is to enable the following discussion on the problem of the submarine close to the free surface to be put into context.

2.4.2 Manoeuvring close to the calm water free surface

When a submarine is operating, with forward speed, close to a calm water free surface (in this context calm means a flat sea with no waves at all, perhaps apart from those waves that are generated by the submarine itself), there are vertical forces imparted on the hull by the free surface that are not present when the submarine is deeply submerged. This is due to the flow characteristics across the submarine being modified by the presence of the free surface. For modest Froude numbers, which are typical of periscope depthkeeping, this force manifests as a suction force drawing the submarine to the surface, the force is dependent upon the forward speed, depth of immersion and hull form.

As with the case for a deeply submerged submarine, the assumption that the motion can be regarded as quasi-steady state (or slowly varying), coupled with the assumption of small

disturbance, means that the forces and moments on a submarine close to the free surface can be related to the motion state variables by a set of hydrodynamic derivatives, Bishop *et al* [1978]. These derivatives are obtained from the Taylor series expansion of the 6 degrees of freedom forces and moments (*X, Y, Z, K, M* and *N*), for this case, in terms of the displacement, velocity and acceleration of the submarine and control surfaces in the same way as the case of the deeply submerged submarine.

For a submarine near the free surface, these perturbations in the forces and moment can be represented as Bishop *et al* [1978]:

$$\delta X, \delta Z, \delta M = f(z^*, \phi, \theta, u, w, q, \dot{u}, \dot{w}, \dot{q}, \delta_b, \delta_s, \dot{\delta}_b, \dot{\delta}_s, \ddot{\delta}_b, \ddot{\delta}_s)$$

$$\delta Y, \delta K, \delta N = f(\phi, \theta, u, v, p, r, \dot{u}, \dot{v}, \dot{p}, \dot{r}, \dot{\delta}_r, \ddot{\delta}_r) \qquad 14$$

where z^* is the submergence depth, is measured from the centre of mass of the body to the water surface, and ϕ and θ are the roll and pitch angles respectively. Actually, [Bishop *et al,* 1978] focused on the vertical plane (or symmetric motions) assuming that the forces and moments on a submarine in the horizontal plane would not change with submergence depth.

In the case of a submarine travelling close to the calm water free surface at constant forward velocity, the heave force and pitch moment on the body is a function of depth of submergence and Froude number, [Renilson, 2015]. For a body undergoing small disturbed motion, as in the case of a deeply submerged submarine, a Taylor series expansion of Eqn 14 will lead to a coefficient-based model for the hydrodynamic loads on a submarine close to the free surface. The form of Eqn.14 differs from the deeply submerged version (Eqn.6) in that there are terms included that are due to the proximity to the free surface (z^*, θ) and hence additional coefficients were identified compared to those for a deeply submerged submarine, Eqns.9 to 13.

As with the deeply submerged case, one means of determining these additional terms is through undertaking specific captive model tests, [Bishop *et al*, 1978]. For example, the means of determining the coefficients in z^*, for the case where the submarine is close to the calm water free surface, would be to tow a model at a suitably scaled forward speed *U* and a range of submergence depths, z^*. In the case of near surface testing, the model will be generating wave disturbances on the surface, which means that any tests should be conducted at the correct Froude number scale speeds.

However, performing model tests at the correct Froude number may mean that the test speeds are lower than the speeds that are usually used for tests for the deeply submerged model. For deeply submerged tests, it is typical to choose the highest model speeds that are possible within the constraints of the facility. However, when performing tests that include the effects of the free surface, then there is no choice other than to test at the correct Froude number. This means that scaling effects, as a consequence of testing at lower Reynolds numbers when close to the free surface (to achieve the correct Froude number), may need to assessed. [Hirom, 1977] suggested that Reynolds number effects should be examined by initially testing the model at the deepest possible submergence (where the effects of the free surface can be considered to be negligible). For the deeply submerged case, the model would be tested across a range of speeds that include those typical of periscope depthkeeping and higher speeds where the Reynolds number effects may be considered to be insignificant. Once the Reynolds number effects for the deeply submerged case have been quantified, approximate correction methods can then be applied to the near surface results.

The $_{\theta}$and $_{w}$coefficients are found from vertically inclined tow tests, where the model is towed, at a constant speed, at a number of pitch angles – the analysis for deeply submerged tests is straight forward but for tests near the free surface this is not the case. When the model is deeply submerged, a heave velocity is imposed by inclining the body at an angle of pitch; when deeply submerged there are no additional dynamic forces by the pitch angle itself, apart from hydrostatic restoring moment which can be easily subtracted. When the model is towed close to the free surface, there will be a wavemaking component of force on the body that is a function of pitch angle. As a result , the inclined tow test, once the body is close to the surface, the force cannot be interpreted due to heave velocity, $_{w}$,only , as it includes orientation (pitch) effect to too. This makes it less straightforward to reliably uncouple their effects for determining the associated derivatives. To circumvent this problem, [Bishop *et al*, 1978] introduced the “equilibrium axes”. The equilibrium axes system corresponds to a body axes system that continues to move at the steady speed *U* along the initial path. The use of the equilibrium axes changes the way the forces and moments due to a pitch disturbance are interpreted in that for pure pitch the heave velocity is considered to be zero for non-zero pitch angle and for pure heave the pitch angle is considered to be zero for non-zero heave velocity.

As mentioned earlier, Bishop *et al* [1978] acknowledged that the unsteady forces due to the action of surface waves were significant compared to the steady forces due to the submarine being in

proximity of the calm water surface itself. The forces on the body that are accounted for by the hydrodynamic derivatives are related to the motion of the body and the wave radiation force – it does not include the force on the body due to wave diffraction. So, the convenient approach for including the additional forces on the body due to the free surface tends to be by adding the respective wave-induced body force components into the right hand side of the force equations for a deeply submerged submarine (Eqns 9 to 13), or treating them as external forces. The terms in the equations existed for a deeply submerged submarine get no special treatment to account for the submarine being close to the free surface. Therefore, there is an implicit assumption that the form of the Taylor series expansion that provides the hydrodynamic derivatives do not change as the submarine approaches the free surface.

For the case where z^* does not change significantly (or remains constant), then the derivatives ($Z'_{uw}(z^*)$ for example) will not change significantly during the motion. However, where the submarine changes depth, then z^* is not constant during the motion, which means that some of the derivatives will change.

In the case where the depth varies significantly during the motion, then these depth varying derivatives would be derived from tests similar to the traditional captive model test or through CFD simulations, [Renilson, 2014]. However, in the case when the submarine is close to the free surface, the physical or numerical model would need to include conditions where the model is at a range of depths from the free surface to obtain those derivatives that change as a consequence of a change in depth of submergence. In the event of depth of submergence dependency being considered as part of the hydrodynamic derivatives then the effects of the calm water free surface should be excluded from the depth variation effects.

2.5 Wave induced forces and moment

2.5.1 Explanation of the free surface phenomena

Whilst a submarine generally operates deeply submerged, there are operational requirements for which the submarine operates close to the sea surface, for example when using the periscope or, in the case of a diesel–electric boat, when snorting during the period of recharging the batteries. In this case, the submarine can experience so called free surface effects (that includes the calm water free surface effect in section 2.4.2), such as suction force which pulls the submarine towards the free surface, that are not there when deeply submerged. In extreme cases, the submarine maybe drawn to the surface and to pitch whereby the submarine may broach the surface, [Bhattacharyya,

1978], increasing the possibility of detection. It is also possible, that in the event of a temporary loss of the suction force (or if the suction force becomes negative), the submarine may sink below depths where periscope and snorting operations can no longer be undertaken.

When a submarine is operating under an incoming wave, it can experience wave-induced forces that create a complex oscillatory motion [Musker *et al*, 1988]. The resultant complex motion can include oscillatory components at frequencies that are typical of those contained within a wave spectrum (so called first order responses that are linearly proportional to the individual wave amplitudes, [Pinkster, 1980]). The motion responses may also contain sum (high) and difference (low) frequencies that are beyond the dominant frequency region of the wave spectrum (called second order responses that are proportional to the square of the wave amplitudes, [Pinkster, 1980]). There are some problems, like hull structure vibrations, where the high frequency components are of interest. However, for the motion of a submarine near the surface and its control, the second order effects of the low frequency and non-zero mean components are the major concerns. The scale of these phenomena and their importance are dependent upon depth, speed, sea state, relative heading and hull form [Musker *et al,* 1988].

To explain the phenomena further , Figure 9 shows a submarine at forward speed in a regular wave of wave length approximately equal to the length of the submarine and wave amplitude approximately equal to a quarter of the hull diameter. The figure includes an illustration of the flow regime around the submarine when under the influence of the free surface.

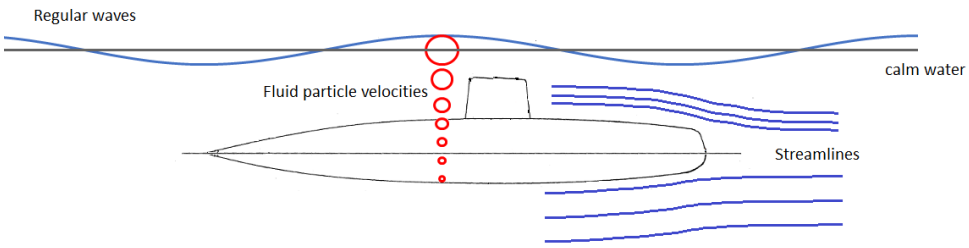

Figure 9: Flow features around a submarine under the influence of surface waves

In the first instance of steady flow, when the submarine is moving through calm water (no incoming waves) at constant speed, the presence of the free surface will mean that the streamlines (shown in Figure 5) over the upper surface of the submarine are closer together when compared to its lower surface thus creating a pressure differential between these two surfaces. This difference in

pressure would create a force that will draw the submarine to the surface, a suction force. Actually, [Renilson, 2015] noted that the suction force is upwards for low Froude number (based on submarine length) but becomes downwards at higher Froude numbers. If the problem is solved numerically where the free surface is treated as rigid and flat, the vertical force is always upwards for all speeds; it is only when the wave generated by the submarine is taken into account, the direction of the force will be affected by the speed. An example, of a submarine geometry with only a bridge fin [Griffin, 2002], shows the vertical force coefficients plotted against Froude numbers from 0.1 to 1.0. This change in direction of the suction force is attributed to the complex wave pattern forming on the free surface above the submarine, [Renilson, 2015]. However, it should be noted that typical maximum speeds, when a submarine is close to the free surface, correspond to Froude number around 0.25, [Bayliss *et al,* 2005]. Therefore at these low Froude numbers, the free surface can be treated as 'rigid' and therefore the force is almost always upwards.

When a submarine is close to a free surface, in the presence of waves, the flow effects are modified by the incident wave; for linear Stokes waves, the fluid particle trajectory is circular in nature (in deep water) and the amplitude (the radius of the circle) decreases exponentially with depth; this rate of reduction is related to wave length. This means that, in the first instance, the effect on the flow due to the wave is smaller when the submergence of the submarine becomes larger and it also means that the orbital velocities of the incoming wave on the upper surface of the submarine are greater than those on the lower surface. Furthermore, the calm water streamlines due to forward speed (shown in Figure 5) will be influenced by the wave diffraction due to the presence of the body and wave radiation effects as the body oscillates in response to the waves; based on linear theory the combined effects are obtained through superposition.

Therefore, in a natural sea condition, the suction force consists of a calm water steady component due to the forward speed of the submarine, first order wave components varying around the main wave frequencies and second order components consisting of a non-zero mean and a slowly varying component. The calm water steady component is usually drawing the submarine towards the water surface (suction force) because of the typical speed of the submarine, and the direction of the second order wave force depends on the wave direction, frequency, submergence depth and hull shape.

If the slowly varying force in waves (which can vary in sign) becomes a sufficiently large suction force that cannot be countered timely by the control system in the submarine, the force can draw the submarine to the surface causing it to broach and thus increasing the possibility of detection.

Moreover, submarines operators tend to take on additional ballast to reduce the possibility of broaching that can leave the submarine in a “heavy trim” state, which means, if the slowly varying force becomes positive (downwards), it could lead to excessive depth excursions before recovering depth control.

To put the suction force problem into context, the discussion included in the paper by [Crepel and Bovis, 1991] suggested that 5 tonnes of compensation would be required for a 2000 tonne submarine in a sea state 5 at typical snorting depths. Hirom [1974] suggested that in waves the fluctuating forces at the wave frequency, or 1st order forces, on a submarine can be of the order of 1,000’s of kN with the suction component around 10’s of kN (the reference does not differentiate between the wave induced suction forces and those due only to forward speed). However, the only practicable solution to mitigate against the undesirable free surface effects is by providing sufficient control authority, through the hydroplanes or internal compensation systems, to counter the suction effects. The design of hydrodynamic control surfaces or any compensation system, internal to the submarine, is largely focussed on the case where the submarine is deeply submerged which, as discussed, is a different operating regime to that associated with the submarine is responding to ocean waves. So, it is important to understand the behaviour of a submarine under the influence of surface waves at early stages of design because of the specific impact on whole boat design. This is from the perspective of the hydrodynamic form itself, the internal arrangements and performance requirements of ballast tanks and pumps and the requirements of hydroplane control surfaces, their actuators and control algorithms due to operating in this wave environment.

2.5.2 Second order forces on offshore and floating structures in the context of forces on the submarine

It is postulated that the submarine surface suction phenomenon due to waves is somewhat similar to the second order wave loads experienced on offshore floating structures, Pinkster [1980]. This section introduces some of the work aimed at understanding the problem of the forces and moments on large volume structures in waves and its link with the forces on the submarine.

Offshore structures are subject to a number of second order effects, due to the waves, that have different implications dependent on the type of offshore structure. The drift force, or low frequency force, is important when the stiffness in the structure is low; the high frequency force is important when the stiffness is high since it may lead to springing or ringing. Therefore, in the case of a submarine at periscope depth, there will be no stiffness in heave and only the restoring moment in pitch due to the BG in contrast to a surface ship that has additional stiffness modes associated with

variation in buoyancy due to the waterplane area. This results in the low frequency loads having a greater impact on the submarine at periscope depths than the high frequency loads.

The low frequency loads associated with the second order wave effects can cause slow drift motions and slowly varying heave, pitch and roll oscillations in large-volume structures with small waterplanes, such as semi-submersibles, that, as a consequence of these design features, have zero or low stiffness [Faltinsen and Løken, 1979] in heave and pitch; large volume structures here mean where the incident wave length is not sufficiently larger than the characteristic length of the body.

These second order effects acting on structures moored in waves are usually of interest from the point of view of quantifying mooring loads and motions. It is known that the low frequency component of the horizontal wave drift forces in irregular waves can excite low frequency horizontal motions of a large amplitude in moored floating structures, [Pinkster, 1979].

Attention is focussed mainly on the horizontal drift problem, however, Pinkster [1980] discussed how the influence of the second order wave drifting forces is not restricted to the horizontal plane, [Numata *et al.* ,1976], for example with the steady tilt of semi-submersible vessels in regular waves. Furthermore, the presence of low frequency components in the vertical motions of large volume structures with small water plane infers that non-linear hydrodynamic effects are significant in the vertical plane also.

To provide expressions for the second order force that would be more amenable to practical application, [Pinkster, 1976] showed that the second order wave exciting forces may be expressed in terms of the quadratic transfer function (or QTF) .

What follows is a brief explanation of the second order transfer function. According to Langley [1987], the total wave force F(t) in particular degree of freedom , correct to second order, can be expressed as a two-term Volterra series in the form:

$$F(t) = \int_{-\infty}^{\infty} g_1(\tau)\eta(t-\tau)d\tau + \int_{-\infty}^{\infty}\int_{-\infty}^{\infty} g_2(\tau_1,\tau_2)\eta(t-\tau_1)\eta(t-\tau_2)d\tau_1 d\tau_2 \quad 15$$

where

$\eta(t)$ is the incident wave at the centre of gravity of the body. $g_1(\tau)$ and $g_2(\tau_1, \tau_2)$ correspond to the impulse response functions of the first and second order wave forces respectively. The choice of location for the incident wave does not affect the fundamental result.

The first term in Eqn 15 represents the linear wave force and the second term represents the second order wave force, Pinkster, [1976]. Eqn 15 can also be written in the frequency domain, Langley, [1987] as:

$$F(t) = \int_{-\infty}^{\infty} G_1(\omega) H(\omega) e^{i\omega t}\, d\omega + \int_{-\infty}^{\infty}\int_{-\infty}^{\infty} G_2(\omega_1, \omega_2) H(\omega_1, \omega_2)\, e^{i(\omega_1+\omega_2)t} d\omega_1 d\omega_2 \qquad 16$$

where

$G_1(\omega)$, $G_2(\omega_1, \omega_2)$ and $H(\omega)$ are the Fourier transformations of $g_1(\tau)$, $g_2(\tau_1, \tau_2)$ and $\eta(t)$ respectively and given by:

$$G_1(\omega) = \int_{-\infty}^{\infty} g_1(\tau)\, e^{-i\omega\tau}\, d\tau$$

$$G_2(\omega_1, \omega_2) = \int_{-\infty}^{\infty}\int_{-\infty}^{\infty} g_2(\tau_1, \tau_2) e^{-(i\omega_1\tau_1 + i\omega_2\tau_2)} d\tau_1 d\tau_2$$

$$H(\omega) = \frac{1}{2\pi}\int_{-\infty}^{\infty} \eta(\tau)\, e^{-i\omega\tau}\, d\tau \qquad 17$$

The properties of the QTF, $G_2(\omega_1, \omega_2)$, are provided by [Dalzell and Kim, 1979] and summarised as:

$$G_2(\omega_1, \omega_2) = G_2(\omega_2, \omega_1)$$

$$G_2{}^*(\omega_1, \omega_2) = G_2(-\omega_1, -\omega_2)$$

where $G_2{}^*$ is the conjugate of G_2.

An alternative way of expressing the main characteristics of the low frequency component of the second order forces in relation to the waves is as follows.

By the principle of linear superposition, a free surface (to first order) in an irregular wave can be described as N_W discrete sinusoidal waves at equally spaced frequencies $\omega_i$with amplitudes a_i and phase components ε_i:

$$\eta(t) = \sum_{i=1}^{N_W} a_i cos(\omega_i t + \varepsilon_i)$$

18

The square of the wave elevation is therefore:

$$\eta^2(t) = \sum_{i=1}^{N_W}\sum_{j=1}^{N_W} a_i a_j cos(\omega_i t + \varepsilon_i)cos\left(\omega_j t + \varepsilon_j\right)$$

19

Pinkster [1979] presented the difference frequency component of the square of the wave elevation as:

$$\eta_L^2(t) = \frac{1}{2}\sum_{i=1}^{N_W}\sum_{j=1}^{N_W} a_i a_j cos\left(\left(\omega_i - \omega_j\right)t + \left(\varepsilon_i - \varepsilon_j\right)\right)$$

20

Each component of the square of the wave elevation has amplitude $\frac{1}{2}a_i a_j$, frequency$\left(\omega_i - \omega_j\right)$and phase$\left(\varepsilon_i - \varepsilon_j\right)$. By assuming that the wave spectrum, defining the irregular waves, can be considered to be narrow-banded, Pinkster [1979] considered the difference frequency components to be also low frequency (hence the use of the subscript L in the equations).

The low frequency component of the second order force can then be represented as:

$$F_L^2(t) = \sum_{i=1}^{N_W}\sum_{j=1}^{N_W} a_i a_j P_{ij} cos\left(\left(\omega_i - \omega_j\right)t + \left(\varepsilon_i - \varepsilon_j\right)\right) + \sum_{i=1}^{N_W}\sum_{j=1}^{N_W} a_i a_j Q_{ij} sin\left(\left(\omega_i - \omega_j\right)t + \left(\varepsilon_i - \varepsilon_j\right)\right)$$

21

where P_{ij} is the QTF of the part of the force, which is in-phase with the low frequency part of the wave height, and $Q_{ij}$is the out-of-phase part of the QTF. Eqn 21 is essentially a discretised form of Eqn 16 but only including terms associated with the difference frequencies.

The slowly varying components of the second order force is for the case where $\omega_i - \omega_j$ is small; the special case of $\omega_i = \omega_j$ (and $\varepsilon_i = \varepsilon_j$) Pinkster [1979] accounted for the mean drift force as:

$$\bar{F}^H = \sum_{i=1}^{N_W} a_i^2 P_{ii}$$

22

where $P_{ii}$is the mean drift force in regular sinusoidal waves with unit amplitude and frequency ω_i.

According to [Chakrabarti, 2005], it is difficult to establish QTFs through the spectral analysis of tests in irregular waves and an alternative approach was suggested. This approach involved by choosing pairs of frequencies from the wave spectrum that give rise to a symmetric matrix of runs. Waves from a frequency pair (or bichromatic waves) are generated during a test and the responses are measured; the low frequency components are used to derive the QTFs. Considering the specific case of bichromatic waves (where $N_W = 2$), once Eqn 19 has been expanded, it can be seen that $\eta^2(t)$will have a non-zero mean component and frequency components at $2\omega_1, 2\omega_2, \omega_1 + \omega_2, \omega_1 - \omega_2$. Since, the second order forces and moments are proportional to the square of the wave amplitude, the second order forces will consist of number of components at each of these different frequencies. Incidentally, the equations developed by [Mandzuka, 1998] and [Hirom,1977] used a single coefficient for the second order wave forces based on a function of $\eta^2(t)$; this is an oversimplification of the second order problem, since in this case, the contributions of the individual components to the second order force are quantified by a single coefficient.

However, tests in bichromatic waves, to extract the QTFs, can be time consuming since a number of pairs of wave frequencies are required. [Newman, 1974] produced an approximation for the QTF that has been adopted for modelling the slow-drift problem of moored floating vessels.

The approximation is based on the assumption that the irregular wave spectrum is considered to be narrow banded.

The bandwidth parameter is defined by Lloyd, [1989a] as

$$\varepsilon_b = \sqrt{1 - \frac{m_2^2}{m_0 m_4}}$$

where m_0, $m_2$and $m_4$are the variances of the wave amplitude time history, wave velocity time history and wave acceleration time history respectively. A narrow-banded wave spectrum is when $\varepsilon_b \approx 0$; for narrow banded spectra $a_i a_j$ is only significant when $(\omega_i - \omega_j)$ is small, [Marthinsen, 1983]. Therefore, the difference frequency contributions, corresponding to the off-diagonal elements are small compared to the mean.

So, considering Eqn 21 for a bichromatic wave.

$$F_L^2(t) = \sum_{i=1}^{2}\sum_{j=1}^{2} a_i a_j P_{ij} cos\left(\left(\omega_i - \omega_j\right)t + \left(\varepsilon_i - \varepsilon_j\right)\right) + \sum_{i=1}^{2}\sum_{j=1}^{2} a_i a_j Q_{ij} sin\left(\left(\omega_i - \omega_j\right)t + \left(\varepsilon_i - \varepsilon_j\right)\right)$$

$$F_L^2(t) = {a_1}^2 P_{11} + {a_2}^2 P_{22} + a_1 a_2 T_{12} cos\left((\omega_1 - \omega_2)t + (\varepsilon_1 - \varepsilon_2) + \varepsilon_{12}\right)$$

The first two terms on the right hand side are the mean forces due to the wave frequencies ω_1 and ω_2 respectively and T_{12} is the amplitude of the quadratic transfer function given as:

$$T_{12} = T(\omega_1, \omega_2) = \sqrt{(P_{12} + P_{21})^2 + (Q_{12} - Q_{21})^2} \qquad 23$$

$$\varepsilon_{12} = tan^{-1}\frac{-(Q_{12} - Q_{21})}{(P_{12} + P_{21})}$$

According to Pinkster [1979],

$$P_{12} = P(\omega_1, \omega_2) = P_{21} \quad \text{and} \quad Q_{12} = Q(\omega_1, \omega_2) = -Q_{21}$$

So, Eqn.22 becomes:

$$T_{12} = T(\omega_1, \omega_2) = 2\sqrt{P_{12}^2 + Q_{12}^2}$$

For the case where $\omega_1 - \omega_2 \approx 0$, $Q_{12} = 0$ and $T(\omega_1, \omega_2) \approx T(\omega_1, \omega_1)$. This can be approximated by:

$$T_{12} = \sqrt{\frac{P_{11}^2 + P_{22}^2}{2}}$$

Which for the general case becomes:

$$T_{ij} = \frac{1}{\sqrt{2}}\sqrt{P_{ii}^2 + P_{jj}^2} \qquad 24$$

The implication of the narrow-band assumption is that the low frequency second order drift forces on offshore structures can be obtained from either physical model tests or numerical calculations in regular singular frequency waves. Whether this assumption is valid or not is not only dependent

upon the bandwidth of the wave spectrum but also the equivalent bandwidth of the motion response of the platform under consideration. Pinkster confirmed that the Newman approximation could be used for determining the slowly varying excitation force on offshore structures (which means that the second order transfer function for the slowly varying drift force can be derived from steady second order force in regular waves). However, to confirm whether this approximation can be applied to the surface suction problem of a submarine under waves would require a series of experiments. similar to those described in Chapter 3 whereby the second order transfer functions obtained from tests in bichromatic waves are compared to the same transfer functions derived from tests in regular waves to be undertaken and compared with the results from tests in regular waves.

Whilst the focus of research at the time was aimed at the mean and low frequency wave drifting force in the horizontal plane, [Pinkster, 1979] extended the numerical method, for calculating the mean and low frequency wave drift forces, to all six degrees of freedom. Using perturbation expansion techniques, [Pinkster, 1979], derived the following for the first and second order potentials from the free surface boundary condition (the superscript in () represents the order of the potential).

$$g\frac{\partial \phi^{(1)}}{\partial t} + \frac{\partial^2 \phi^{(1)}}{\partial t^2} = 0$$

$$\frac{\partial^2 \phi^{(2)}}{\partial t^2} + g\frac{\partial \phi^{(2)}}{\partial z} = -\frac{\partial}{\partial z}\left|\nabla \phi^{(1)}\right|^2 + \frac{1}{g}\frac{\partial \phi^{(1)}}{\partial t}\frac{\partial}{\partial z}\left(\frac{\partial^2 \phi^{(1)}}{\partial t^2} + g\frac{\partial \phi^{(1)}}{\partial z}\right) \quad 25$$

It should be noted that if body motion is included, then the condition on the body surface also requires expansion, see Wu [1995] for example. Pinkster [1979] included the second order potential in the body boundary condition, at the mean position of the body, as:

$$\nabla \phi^{(2)}.n = -(X^{(1)}.\nabla)\nabla \phi^{(1)}).n + (v^{(1)} - \nabla \phi^{(1)}).N^{(1)}$$

where,

$\bar{n}$ - unit normal of the body surface relative to a body axes coordinate system

$\bar{X}^{(1)}$ – motion vector of a point on the hull

$\phi^{(1)}$ – first order velocity potential, given by Eqn 26 .

$v^{(1)}$ – first order velocity of a point on the mean wetted surface relative to the fixed system of co-ordinate axes.

$N^{(1)}$ - first order oscillatory component of the normal vector N of a surface element of the mean wetted surface relative to the fixed system of co-ordinate axes.

It is evident from the Eqn.25 that the second order problem is dependent upon the first order solution; also the numerical solution to the problem with this kind of free surface boundary condition requires the free surface to be discretized, which increases computational effort, [Matos *et al,* 2011].

The simple superposition approach, which has been widely accepted throughout, was used by [Pinkster, 1979] to consider the first order potential to be the linear summation of three elements:

$$\phi^{(1)} = \phi_w^{(1)} + \phi_d^{(1)} + \phi_{\alpha_i}^{(1)} \qquad 26$$

where the first order potentials $\phi_w^{(1)}$, $\phi_d^{(1)}$, $\phi_{\alpha_i}^{(1)}$ are the undisturbed incoming wave potential, the diffraction potential and the motion potential (or radiation potential for the i^{th} mode of motion where $i = 1,..,6$) respectively.

And $\phi^{(2)}$is the second order total velocity potential that consists of contributions from the incoming waves, diffraction and body motions. Pinkster developed an approximation for this second order potential largely due to the limitations of computing power at the time. The method was based on the transformation of the first order wave excitation force into a long wave corresponding to the length of the wave group to the second order excitation force as described by [Hsu and Blenkarn, 1970]. This approximation for the second order potential was shown to give the best results when the contribution to the second order potential was only due to the first order Froude-Krylov force, due to $\phi_w^{(1)}$, and that $\phi_d^{(1)}$, $\phi_{\alpha_i}^{(1)}$ are considered negligible. According to Pinkster, this approximation is probably more appropriate for vessels such as semi-submersibles than by typical displacement ships; whether this same approximation can be applied to the case of the surface suction problem will be discussed further in Chapter 3.

Pinkster [1980] divided the second order force into five components, as shown through five terms below, respectively:

$$\bar{F}_1^{(2)} = \int_{WL} -\frac{1}{2}\rho g {\zeta^{(1)}}^2 . \bar{n} . dl + \bar{\alpha}^{(1)} \times \left(M . \ddot{\bar{X}}_g^{(1)} \right) -$$

$$\iint_{S_0} \left[-\frac{1}{2}\rho \left| \bar{\nabla}\phi^{(1)} \right|^2 - \rho \left(\frac{\partial \phi_w^{(2)}}{\partial t} + \frac{\partial \phi_d^{(2)}}{\partial t} \right) - \rho \left(\bar{X}^{(1)} . \bar{\nabla} \frac{\partial \phi^{(1)}}{\partial t} \right) \right] \bar{n} . dS$$

27

where

$\zeta^{(1)}$ - first order relative wave height at a point along the waterline including effect of undisturbed waves, diffraction and body motions

$\bar{n}$ - unit normal of the body surface relative to a body axes coordinate system

dl - length element measured along the mean waterline

dS – area element across the surface area of the mean body S_0

$\bar{\alpha}^{(1)}$ - angular motion vector

$\bar{X}_g^{(1)}$ - motion vector of the centre of gravity

$\bar{X}^{(1)}$ – motion vector of a point on the hull

M - matrix containing the mass of the body

$\phi^{(1)}$ – first order velocity potential, given by Eqn. 26.

$\phi_w^{(2)}, \phi_d^{(2)}$ – second order velocity potential due to incoming wave and second order velocity potential due to diffraction respectively, which are proportional to the square of the wave amplitude.

The integral in Eqn.27 was broken down into the terms by Pinkster as:

I. First order relative wave elevation

$$-\int_{WL} -\frac{1}{2}\rho g {\zeta^{(1)}}^2 . \bar{n} . dl$$

28

II. Pressure reduction due to first order velocity

$$-\iint_{S_0}\left[-\frac{1}{2}\rho\left|\bar{\nabla}\phi^{(1)}\right|^2\right]\bar{n}.dS \qquad 29$$

III. Pressure due to product of gradient of first order pressure and first order motion

$$-\iint_{S_0}\left[-\rho\left(\bar{X}^{(1)}.\bar{\nabla}\frac{\partial\phi^{(1)}}{\partial t}\right)\right]\bar{n}.dS \qquad 30$$

IV. Contributions due to products of first order angular motions and inertia forces

$$\bar{\alpha}^{(1)}\times\left(M.\ddot{\bar{X}}_g^{(1)}\right) \qquad 31$$

V. Contribution due to second order potential

$$-\iint_{S_0}\left[-\rho\left(\frac{\partial\phi_w^{(2)}}{\partial t}+\frac{\partial\phi_d^{(2)}}{\partial t}\right)\right]\bar{n}.dS \qquad 32$$

Pinkster, [1981] illustrated the importance of these components in the mean vertical force on a 3D horizontal cylinder in head and beam waves and made the following points. Since the cylinder is fully submerged no contribution arises from the relative wave elevations around a waterline which means contribution I, (Eqn. 28), is identically equal to zero; since the cylinder is circular with the centre of gravity located on the axis no roll motions occur and so, in beams seas, contribution IV, (Eqn. 31), is also zero. Pinkster showed that the different contributions to the total force on a horizontal cylinder can vary significantly with heading; in head waves, contribution II is dominant and contributions III and IV have only a minor effect. In beam seas, contributions II and III are of the same order but opposite in sign. In both cases, the total mean force, second order effect, consists of contributions due to the product of first order terms. Only contribution V, Eqn.32 , involves the second order wave and diffraction potentials which require significant numerical effort to solve.

The results of computations were compared with model tests in regular and irregular waves. In two separate tests, forces and moments on a semi-submersible and a totally submerged horizontal cylinder were obtained. Pinkster concluded, on the basis of his comparisons, that the mean and slowly varying second order wave drift forces can be predicted using the method of direct integration of the pressures on the instantaneous wetted surface of the hull. According to Pinkster, the accuracy of the prediction

Lee *et al* [1991] used the so-called direct method for calculating contribution V for each mode of motion in irregular waves:

$$\vec{F}_{V,\alpha}^{(2)} = -i\rho(\omega_i - \omega_j) \iint_{S_0} \left(\phi_w^{(2)} + \phi_d^{(2)}\right) n_\alpha dS \qquad 33$$

where

(ω_i, ω_j) is any pair of wave frequencies considered in the discrete wave spectrum.

$\phi_w^{(2)}, \phi_d^{(2)}$ are the second order velocity potentials due to respectively the incoming wave and second order diffraction component at $(\omega_i - \omega_j)$.

Alternatively, Faltinsen and Loken [1978], Lighthill [1979] and Molin [1979] introduced a method, in which the contribution from the second order potential to the second order force can be obtained without the need to solve the second order diffraction problem as follows, Matos, *et al,* [2011]:

$$\vec{F}_{V,\alpha}^{(2)} = -i\rho(\omega_i - \omega_j) \left[\iint_{S_0} \left(\phi_w^{(2)} n_\alpha + \phi_\alpha^{(L)} Q_B^{(L)}\right) dS + \frac{1}{g} \iint_{S_{FS}} \left(Q_{WB}^{(L)} + Q_{BB}^{(L)}\right) \phi_\alpha^{(L)} dS \right] \qquad 34$$

where

$Q_B^{(L)}$ is the difference frequency forcing function on the body.

$Q_{WB}^{(L)} + Q_{BB}^{(L)}$ is a component of the free surface difference frequency forcing function computed from the first order solution.

$\phi_{\alpha}^{(L)}$ is the first order radiation potential for the α mode of motion computed in the difference frequency domain.

Kim and Yue [1989] considered the direct solution of the second order diffraction potential on bottom mounted vertical cylinders in regular waves involving a so-called wave or Havelock source Green function. This direct solution not only provides the overall force but also provides other detailed results such as local pressures, velocities and surface elevations. Kim and Yue [1989] found that, from comparing computations of the second order horizontal force and overturning moment from direct pressure integration on the body with semi-analytic results, the contribution of the second-order potential was larger than the quadratic products of the respective first order quantities; however, for this application these effects tended to be out-of-phase with each other so that the net second order effect was small compared with the linear (or first order) effect (depending on the wave amplitude). Kim and Yue [1989] concluded that the second order diffraction potential cannot be neglected in favour of the quadratic contributions from the linear potential when determining the slowly varying drift forces. This was attributed by Kim and Yue to be due to the different rates at which the pressures components associated with the potentials are attenuated with depth. The pressures due to the quadratic products of the first order potential (as well as the pressure due to the second order wave potential) attenuate with depth at a rate of approximately $2\frac{\omega^2}{g}$ (the pressure associated with the second order bichromatic waves attenuate with a rate of $4\frac{\omega^2}{g}$). However, the pressure associated with the second order potential itself attenuates with depth at a slower rate, [Kim and Yue ,1989]. [Kim and Yue ,1989] found that the depth-dependence of the second order potential can vary from being a constant to 0 = R) to $\cosh(\frac{2\omega^2(z+h)}{g})$ (here z is the depth of immersion and h is the depth of water).

Kim and Yue [1990] extended their earlier work to a second order diffraction solution for an axisymmetric body in bichromatic waves. The theory allowed for the estimation of sum and difference frequency wave excitation and responses in irregular seas; again, for their application, the second order potentials can be significant in the total wave load.

By performing this review, the potential of quantifying the second order forces and moments on a submarine by using QTFs has been identified but there is very little validation data reported in open literature from a fully appended submarine, particularly from tests in bichromatic waves at both zero and non-zero forward speed.

As mentioned previously the Euclid 10.17 captive model tests reported by Martinussen [2006] did not include tests in bichromatic waves, preventing the derivation of QTFs from experiments; regular (monochromatic) wave tests allowed for the measurement of the second order non-zero mean RAOs of forces and moments. Faltinsen and Løken, [1979] described the methodology by which QTFs can be obtained from model tests to measure the slow drift oscillations of a moored ship using tests in bichromatic waves, measuring the response and extracting the forces at the frequency $(\omega_i - \omega_j)$. In this case, where a model was kept at a mean position by a system of soft springs (to allow for first order motions), difficulties can arise when $(\omega_i - \omega_j)$ is close to the natural frequency of the system since damping can then become significant, [Faltinsen and Løken, 1979].

To avoid these difficulties, Pinkster, [1980] used a mooring system that was tuned for the specific tests – sufficiently soft to have an insignificant effect on the first order motions but stiff enough to measure the slowly varying drift forces without appreciable dynamic magnification effects.

Pinkster, [1980] considered a mooring system to be a simple passive system, consisting of linear springs, to restrain a surface vessel in the longitudinal direction. Assuming that the mass and damping of the system is constant, the restraining system can be modelled as shown in Figure 10.

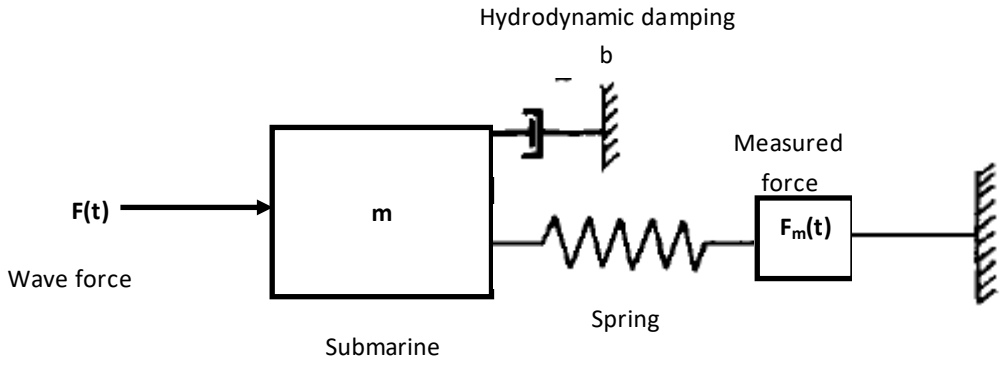

Figure 10: Representation of a passive restraining system (adapted from Pinkster [1980])

In Figure 10, the waves exert first and second order forces on the submarine which induces a motion response. The wave force is donated by F(t) in the figure, the restraining system has a force transducer mounted that measures the restraining force $F_m(t)$. If the submarine-restraining-system is assumed to be linear, the amplitude response function of the measured force in ratio to the wave force was shown by Pinkster, [1980] to be:

$$\frac{F_{ma}}{F_a} = \frac{1}{\sqrt{(1-\Omega^2)^2 + \eta^2\Omega^2}}$$

Where

$$\Omega = \frac{\omega}{\omega_d}$$

ω is the excitation frequency in rads/s

ω_d is the damped natural frequency of the submarine-restraining-system.

$\eta = \frac{b}{2\sqrt{cm}}$ is the non-dimensional damping factor and b,c and m are the damping coefficient, the stiffness of the restraining system and the mass of the submarine respectively. This amplitude response function will be revisited in chapter 3.

Lopez-Pavon et al. [2015] conducted a numerical and experimental investigation to estimate and verify second-order wave induced forces on a semisubmersible platform. An experimental investigation involved conducting fully captive model tests in bichromatic waves to directly measure the low-frequency loads. The numerical investigation included using the WAMIT [Lee, 1995] second-order module to reproduce the conditions of the model tests and the slow-drift forces expressed as QTFs. To provide further comparison, numerical results were compared with the captive model tests. The results showed that although the trends in the second-order forces were captured well by the numerical model, the measured loads were under predicted to some extent even when using the full second order capability in WAMIT.

Fonseca *et al,* [2011] provided a review of experimental work aimed at obtaining the second order drift forces on marine structures. The review highlighted how little data there were in open literature. Fonseca *et al*, therefore, performed experiments to obtain the mean and slowly varying wave exciting drift forces on a body of simple geometry. The aim of the tests was to provide insight into the physics of the second order forces and to obtain experimental data suitable for use in validation studies; tests on a fully restrained body were undertaken in regular and bichromatic waves.

However, fully restrained experiments may not capture the complete second order effects correctly, and free running model tests are extremely complex and difficult to control the independent variables to an extent that is required for validation studies, [Crossland et al, 2012].

For the regular wave tests undertaken by [Pinkster, 1981], the submerged cylindrical model was

restrained by soft linear spring mooring lines which themselves included forces gauges to measure the mean drift forces. The spring constants for these soft mooring lines were chosen such that the natural frequency of the entire "system" was sufficiently far away from the range of wave frequencies tested that the linear wave was unlikely to excite resonance.

Aranha *et al* [2001] performed a series of experiments on a model weathervane ship to measure the second order wave drift forces. The model was towed at a constant speed to represent the current; the displacements in the horizontal plane were restricted by three springs where the collective stiffness of these springs was designed to ensure that the natural frequency of the restraining system was well outside the wave frequency range. The maximum natural frequency was chosen based on $K_N T \cong \frac{RT}{\rho g \Delta}$, where $K_N = \frac{{\omega_N}^2}{g}$, ω_N is the natural frequency, T is the draught, $R$is the stiffness of the restraining system and Δ is the volume displacement. In the case of Aranha *et al* [2001], the rig was designed so that its natural frequency was such that $K_N T = 0.0005$ and the tests were done in the range $KT \geq 0.2$, suggesting that the resonance of the restraining system is unlikely , which means that its effect on the first order motion may be small and be ignored.

For the problem of a submarine under the influence of surface waves, the design of an experimental rig to measure the second order vertical forces on a submerged body at forward speed could adopt the same principle, by which the natural frequency of the designed system is significantly less than those expected at the wave encounter frequencies.

Pinkster [1979] considered it useful to be able to construct time histories of the low frequency second order force, but it is demonstrated, in this thesis, that the QTFs can be used as shaping functions for the development and evaluation of control algorithms for depthkeeping in submarines. In Chapter 4, a number of different approaches are described for designing and evaluating the performance of control systems to reduce the effects of surface waves on the submarine. The more advanced techniques design a control system that removes the first order effects of the waves by introducing filters into the control system algorithm. However, these control systems are designed on the assumption that the second order effects consist only of the vertical plane equivalent of the steady drift force. These approaches ignore the slowly varying second order effect. This thesis will demonstrate the potential role that QTFs have in control system design with the aim of improving the effectiveness of such a control system. Chapter 4 provides a series of example case studies illustrating the potential improvement in depthkeeping performance that can

be gained from considering the slowly varying component of the second order wave force in control design.

2.5.3 Empirical methods

The main focus of the work in modelling the response of a submarine under waves has been related to autopilot design and understanding submarine autopilot performance in this environment; these methods are also usually empirical in nature that look to quantify free surface effects in a practicable way.

[Veillon *et al,* 1996] developed a method based on the use of a physical model in a towing tank; in this case there was a need to develop a dynamic control system that could compensate for the reduced effectiveness of the hydroplanes at low to zero speeds. The main aim was to assist in sizing the stabilisation system and deriving specific control algorithms. In order to help size the actuators approximations to the first and second order forces where based on coefficients derived from numerical techniques, in the first instance, then physical model tests. Physical model tests were used to perform more detailed analysis of the verification of the stability of the autopilot and the identification of the performance of the stabilisation system.

[Mandzuka,1998] modelled the motion of a submarine under the free surface as 2 equations in the following form with constant coefficients; in this case, the centre of rotation of the submarine is assumed to be at the centre of gravity.

$$(m - Z_{\dot{w}})\dot{w}(\mathrm{t}) = Z_w w(t) + \big(Z_q + m\big)Uq(t) + Z_{uu\,\delta\mathrm{b}}U^2\delta\mathrm{b}(\mathrm{t}) + Z_{uu\,\delta\mathrm{s}}U^2\delta\mathrm{s}(\mathrm{t}) + Z_{wave}\,(t)$$

$$\big(I_y - M_{\dot{q}}\big)\dot{q}(\mathrm{t}) = M_w Uw(t) + M_q Uq(t) + M_{uu\,\delta\mathrm{b}}U^2\delta\mathrm{b}(\mathrm{t}) + M_{uu\,\delta\mathrm{s}}U^2\delta\mathrm{s}(\mathrm{t}) + Z_{bg}\,\theta(t) + M_{wave}\,(t)$$

36

where Z_{bg} is the vertical distance between the centre of buoyancy and centre of gravity.

The terms on the RHS of the first two equations in Eqn36 are obtained in the same way as those in Eqns. 8 to 13, i.e., by Taylor series expansion (but only considering vertical plane), but only the first order terms. Mackay, [2003] suggested that the range of linearity (in terms of the body forces) for a deeply submerged axisymmetric body at an angle of pitch is ±6 degrees ($w' = \pm 0.1$). Eqn. 36 also includes the force and moment (Z_{wave} and M_{wave} respectively) due to the wave diffraction. When the depth of submergence is large Z_{wave} and M_{wave} will become zero and the terms on the RHS of Eqn. 36 will be the same as the first order terms in Eqns. 8 to 13.

According to Mandzuka, the total force and moment on the submarine when under waves (given by the terms on the RHS of Eqn. 36) consist of quasi-steady and high frequency components. The quasi-steady components are those obtained from the same process of Taylor series expansion and are hence a reduced set of the standard derivative based model in Gertler and Hagen [1967]. The effects of the waves Z_{wave} and M_{wave} are considered by Mandzuka as being high frequency responses that include the first and second order vertical forces and moments on a submarine in an irregular unidirectional wave; the effects of the waves are modelled as a further set of equations with empirically derived coefficients.

$$Z_{wave}(t) = Z_1(t) + Z_2(t)\,,\; M_{wave}(t) = M_1(t) + M_2(t)$$

$$Z_1(t) = \sum_{i=1}^{N_w} C_{Z1}\nabla\rho(1.5sin^2\mu + 1)\,(1 - 0.02Ucos\mu)F_{1i}sin\omega_{ei}t$$

$$Z_2(t) = -\sum_{i=1}^{N_w}\sum_{j=1}^{N_w} F_{1i}sin\omega_{ei}t.F_{1j}sin\omega_{ej}t\frac{\nabla\rho}{g}\frac{(sin^2\mu + 3)}{10^{|sin\mu|}}C_{Z2}(1 - 0.04Ucos\mu)$$

$$M_1(t) = -\sum_{i=1}^{N_w} C_{M1}\mathrm{L}\nabla\rho\,(1 - 0.02Ucos\mu)Sgn(cos\mu)F_{1i}sin\omega_e t$$

$$M_2(t) = -C_{M2}L\theta(t)Z_2(t)$$

37

The term F_{1i} is the first order force due to the ith wave component), attenuated to account for the depth of the submarine.

$$F_{1i} = a_i\omega_i^2 e^{-\frac{\omega_i^2 H}{g}}$$

$$a_i = \sqrt{2S(\omega_i)\delta\omega_i}$$

$\omega_{ei} = \omega_i - \frac{\omega_i^2 U}{g} cos\mu$ (with the deep water approximation).

Z_1,Z_2,M_1,M_2 are the first and second order heave force and pitch moment respectively.

C_{Z1},C_{Z2},C_{M1},C_{M2} are the coefficients of the first and second order heave force and pitch moment respectively.

L, ∇ and θ are the length, volume displacement and pitch angle of the submarine respectively. H is the depth of submergence (to the submarine axis) and U is the forward speed.

g is the acceleration due to gravity, ρ is the fluid density, μ is the wave direction (0 degrees – following seas, 180 degrees head seas), ω_i is the wave frequency (in rads/s),

The amplitude a_i of each sine wave is obtained from a spectral formulation such as the ITTC, or Bretschneider, wave spectrum [Bretschneider, 1959], typical for deep water, open ocean environments.

$$S(\omega) = \frac{A}{\omega^5} e^{-\frac{B}{\omega^4}}$$

38

where $A = \frac{487.3 H_{1/3}^2}{T_0^4}$ and $B = \frac{1949}{T_0^4}$

for an irregular wave with significant wave height $H_{1/3}$ and modal period T_0 .

The focus of the work by [Mandzuka, 1998] was to define a mathematical model with sufficient accuracy to support depthkeeping autopilot control design (the approach was limited to the vertical plane). The instantaneous heave force and pitch moment equations consisted of first and second order contributions, again with constant coefficients. Both the first and second order expressions are functions of a force described as that due to the attenuated static head at the vehicle depth produced by the wave components. In the [Mandzuka, 1998] paper, Eqn 36 was modified to account for a phase difference between the heave force and pitch moment; the approach was empirical in nature relying on motion response data to derive the time constants in the transfer function.

Hirom [1977] developed a similar set of equations for estimating the effects of the waves on a submarine but considered first order forces and moments for the full six degrees of freedom; and second order terms for the heave force and pitch moment.

As the body approaches the free surface, the flow field around the submarine is modified by presence of the free surface itself and by the effect of the wave on the particle velocities, changing the pressure distribution across the body and hence the forces and moments, which are important in the case of the submarine close to the free surface. These empirical methods do not accurately capture these effects.

2.5.4 Numerical methods

In the case of the problem of a body subjected to the influence of waves, there is a large body of literature related to analytical and numerical tools for predicting the hydrodynamic forces and moments and the resultant response of a surface ship to waves, so called seakeeping. The majority of these techniques focussing on panel methods for the linear problem but volume based CFD methods for unsteady viscous flow are becoming more prevalent, particularly in for the non-linear free surface problem, [Sadat-Hosseini *et al,* 2011].

Therefore, it is prudent to consider some of the techniques applied to seakeeping of a surface ship and its relationship to the problem of the submarine under waves. According to the ITTC Seakeeping Committee report [ITTC, 2008a], the development of seakeeping codes is moved from frequency domain to time domain; from 2D to 3D schemes; from linear to non-linear and also from potential flow (panel or surface mesh methods) to viscous flow (not panel) or volume mesh methods in this case.

Based on linear theory, problems are solved in the frequency domain because a small amplitude irregular wave can be decomposed into components of sinusoidal waves. The forces and moments will excite the ship into sinusoidal motion at the same frequencies as those contained within the irregular wave; the problem for irregular and transient waves can also be solved in the time domain and, in the case of the linear problem, the results from a frequency domain and time domain can be related through the Fourier transform. One method to solve the linear problem is to use the strip theory in which the assumption is made that the transverse dimensions of the body geometry are small compared to its length; also, the cross section of the body should change gradually along its length, [Odabasi and Hearn, 1977]. The problem is then solved by the 2D method for each cross section through the body; thereby simplifying the determination of the hydrodynamic coefficients

[Salvesen et al, 1970]. The two dimensional problem is solved to ensure the boundary conditions are satisfied to a good degree of accuracy. According to [Westlake and Wilson, 2000], the form of the multipole expansion (Ursell 1949) together with conformal mapping is selected to satisfy the boundary condition on the arbitrary shape. The multipole solution to unit circles being known can then be transformed back into the arbitrary shape quite readily. [Westlake and Wilson, 2000] developed a multi-parameter conformal mapping technique to allow accurate representation of realistic ship sections; indeed 2D BEM methods can be readily used for any 2D shapes. However, strip theory is not widely applied to the problem of the submarine under waves; it is inherently 2D and not accurate when 3D effects cannot always be ignored. In 3D methods, the body geometry is discretised into many small panels. The body surface boundary conditions are satisfied at each panel, either at its centre or through a weighted average.

For the particular unsteady problem of a fully submerged body under the influence of surface waves, there are broadly two approaches which can be categorised as analytical and numerical, [Ursell,1999]. Ogilvie [1963], adopted the multipole method, first used by [Ursell,1949], as an analytic solution for the first and second order drift forces on a submerged 2D horizontal circular cylinder under the influence of surface waves at zero speed in infinite water depth. The coefficients in the multipole expansion are obtained through the body surface boundary condition; the first order oscillatory force and the second order steady state force are determined for the following cases (which again reflects the principal of superposition as discussed above);

i) The cylinder restrained under the effect of sinusoidal waves (wave diffraction)

ii) The cylinder undergoing forced sinusoidal oscillations (wave radiation)

iii) The submerged cylinder, neutrally buoyant, responding to the first order force. (cylinder in free motion)

[Wu, 1993] considered the second order wave radiation problem for an oscillating submerged cylinder which was regarded as an extension to [Ogilvie, 1963] by not only deriving the drift force, the second order harmonics force and the second order radiated wave amplitudes but also included finite water depth.

For 3D cases, the work in multipole expansion techniques is applied deriving analytic solutions for simple geometries, as in 2D. [Wang, 1986] considered the problem of a neutrally buoyant submerged sphere (at zero speed). In this case the pressure acting on the body was determined

from the linearised form of the Bernoulli equation. [Wu, *et al,* 1994] presented an analytical procedure for calculating the second order force (referred to as wave drift force) on a submerged sphere. The linear velocity potential was found by using multipole expansion techniques which are then used to derive new expressions for the wave induced drift forces by direct integration of the non-linear pressure over the body surface. This paper only considered the diffraction component of drift force but assumed that similar methods could be used for the radiation term. Since the focus of a great deal of development in this area is primarily targeted at the offshore industry, the paper also considered zero forward speed.

[Wu and Eatock-Taylor, 1987] suggested that it would be difficult to extend the method of multipole expansion to include free surface piercing bodies with forward speed. They looked to develop an alternative approach by solving the body boundary condition through expanding the source distributions into a series of Legendre functions (and solved analytically) rather than by discretization and solving numerically. This reference considered the zero-speed problem of a spheroid in the first instance as a step towards the more complex forward speed problem; with a view to developing an analytic solution as a means of checking numerical methods. [Wu and Eatock-Taylor, 1988] extended this work to obtain an analytic solution for a submerged spheroid travelling in waves where the source distribution is written as a series of Legendre functions. These analytic approaches cannot be applied to problems involving a typical fully appended submarine hull form but they do provide exact solutions (within the limits of their assumptions) which provide a means for the validation of numerical techniques such as boundary integral methods.

The application of numerical techniques for the potential flow allows investigation of arbitrary and more realistic geometries. For linearised potential flow problem, the panel method is widely used. Therefore, the following discussion is limited to Boundary Element Methods (BEM) only. It is well known that, for an arbitrary body, a general solution to the continuity equation can be found by a sum of source and doublet distributions on the body boundary, see Katz and Plotkin , [2001], for example, with special consideration for the wake of the body and of the appendages. Katz and Plotkin, [2001] describes several approaches to solving the boundary value problem numerically which are based on the premise that as the number of the panel increases and all the panel sizes decrease, the result will tend the exact solution. These approaches can be describes as:

- Point singularity solutions – The body surface is divided into N panels. A point source of strength σ_i located on each panel, which is usually positioned at the centre. The body surface boundary condition is imposed at each panel and N equations are established for the

strengths of N sources. (zeroth order)

- Constant strength singularity solution – In this case, the source strength on each panel is uniformly distributed across the panel, or $\sigma_i' = \frac{\sigma_i}{S_i}$ where S_i is the area of panel i. (first order)

- Linearly or bi-linearly varying singularity strength solution – In this refinement, σ_i', above, is no longer a constant within the panel. It varies linearly or by-linearly in each panel. (note linear: a+bx+cy for triangle, by-linear a+bx+cy+dxy for quadrilateral) (1.5th order)

When the body has sharp trailing edges, the velocity there can be infinitely large, which is non-physical. . Application of the, so called, 3D Kutta condition – the flow leaves the sharp trailing edge of the body smoothly and then the velocity there is finite – determines the circulation. Whilst submarine hulls usually do not tend to have sharp trailing edges, the control surfaces do have such trailing edges.

For the 3D case, Hess and Smith [1962] represented the potential for a body S in a steady uniform flow with source distribution. This is an example of the constant source distribution procedure. Through a source distribution σ over the body surface, the potential ϕ_b due to the body (without the free surface effect) and is written as:

$$\phi_b(x', y', z') = \iint_S \frac{\sigma(q)}{r(p,q)} ds$$

39

where $r(p,q)$ is the distance from the source point *q* on the surface to the field point *p* (x', y', z') (see Figure 11 from Hess and Smith [1962]) and $\frac{-1}{4\pi r}$ is the velocity potential due to a source of unit strength.

The form of ϕ_b in Eqn.39 satisfies, implicitly the mass continuity in the fluid domain, or the Laplace equation, and the far field condition; the function σ, which is the source strength distribution, must be determined to satisfy the boundary condition on the body, that requires the normal derivative of $\phi_b$to satisfy the impermeable condition. The normal derivative of Eqn.39 is singular when q and p meet on the surface, and so Hess and Smith, [1962] resolved the problem by extracting a principal value corresponding to the contribution of the local source to the local normal velocity and the contribution of the source to the remainder of the surface.

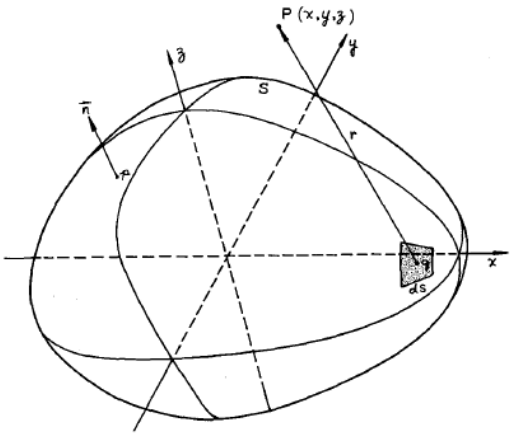

Figure 11: *An illustration of a surface source density distribution [Hess and Smith, 1962].*

This method is valid for arbitrary bodies, the only requirement is that the unit normal $\bar{n}$ is continuous across the body surface, [Hess and Smith, 1962] – this means, for practical purposes, that the body should not have sharp corners i.e., infinite curvature. This is not expected to be an issue for typical unappended submarine hull forms where sharp corners tend to be avoided. This, of course, is not the case for the appendages which need to be treated differently; an updated method was presented by [Hess, 1972] that represented lifting surfaces by finite-strength vorticity distributions.

Any numerical approach requires a representation of the body surface which could be by means of a single analytic expression approximating the surface or a large number of analytic expressions approximating the body surface from a series of surface data points, [Hess and Smith, 1962]. The first approach restricts the types of bodies that can be dealt with and would not represent a practicable approach for real submarine geometries; the second approximation is usually used for the integral equation, Eqn 39. It is then solved either through iteration or by a set of simultaneous linear algebraic equations, [Hess and Smith, 1962]. The numerical scheme adopted by [Hess and Smith, 1962] was to approximate the body surface by a number of small quadrilaterals (planar elements) where the source density is assumed constant over each of these elements, or a constant strength singularity solution; a first order approximation panel and zero-order approximation of the source to determine the potential flow around arbitrary 3D non-lifting bodies. This represented the first numerical solution of the flow around an arbitrary body that forms the basis of most numerical techniques for potential flow problems in earlier days, [Sahin et al, 1997]. Whilst this method of discretization was applicable for any plane element, [Hess and Smith, 1962] chose to use quadrilateral elements since the input points can be provided at constant chordwise and spanwise locations which provided a level of convenience, at the time, for subsequent data handling.

However, fitting quadrilateral planar elements to a curved surface means that the corners of the planar element no longer lie on the body surface. This can create the problem where adjacent elements may not have coincident edges leading to a phenomenon called “leakage” between panels, which can weaken the zero flow condition normal to the boundary, [Katz and Plotkin, 2001]. However this was not deemed a problem by Hess and Smith; providing the gaps are small, the resulting errors are negligible compared to other sources of errors as a result of the assumptions of constant strength, constant pressure and constant normal across the panel, [Bertram, 2000]. However, whilst triangular elements were indeed considered by Hess and Smith this approach did not allow for convenient data handling at the time; this is not an issue with modern CAD software.

As mentioned previously, the numerical scheme adopted by [Hess and Smith, 1962] was considered to be a first order approximation of the body geometry and a zeroth-order approximation of the source strength. Higher order methods have been developed that provide improvements in the discretisation of the body geometry and the definition of the source distribution across the panel.

The principles behind higher-order panel methods (also called Higher Order Boundary Element Methods or HOBEM) are similar to the approaches used to develop first-order solutions. However, higher order methods increase the complexity in which the surface geometry is discretised and how the singularities are represented and distributed across the discretised geometry, [Katz and Plotkin, 2001]. For example, higher-order panel methods, which used parabolic panels in describing the body geometry have been developed, see [Hughes and Bertram, 1995] (panels need to be at least quadratic in shape (second order approximation of the body geometry) and the source distribution be linear (1.5^{th} order approximation of the source distribution) to be considered higher-order, [Bertram, 2000]).

Hess, [1979] described a higher-order 3D panel method that represented the body by four-sided curved (quadratic) surface panels consisting of linearly varying source and vorticity distributions; this method was later updated to account for lift for body with sharp edges, [Hess, 1991]. Hess, [1979] compared the results from this higher-order method with the first-order method, [Hess, 1972], and found that the higher-order method achieved greater accuracy for a given number of panels, which has the potential to reduce computing time for a given level of accuracy, and to calculate flow about more complicated configurations.

According to [Datta and Sen, 2006], higher order methods can suffer from some drawbacks, for example, in [Hess, 1979], the use of curved panels and quadratic sources resulted in increases in

computational time. More recent higher order methods such as B-spline based methods being developed for wave–structure interaction and free-surface flow problems, [Datta and Sen, 2006]. The aims of these approaches are to provide a more accurate description of the geometry, compared to discretisation using panels (with the advantage that B-spline-based geometry techniques are used in CAD applications which can be directly used for the hydrodynamic computations, [Datta and Sen, 2006]), and to provide a reduction in computational resource (processing time and required memory) compared to lower order methods, for the same level of accuracy. For real ship geometries, first order panels are considered sufficient by [Bertram, 2000], however, in some applications where second derivatives of the potential are required, then second order panels lend themselves to this more easily than lower order methods.

[Shao,2010] developed a 3D cubic HOBEM to model the nonlinear wave-body interactions and applied the HOBEM to solve the third-order wave diffraction problem of a stationary three-dimensional body. Because Shao adopted a cubic HOBEM approach, the first-order and second-order derivatives were calculated directly by using the higher-order shape functions rather than requiring dealing with them numerically or by making simplifying assumptions.

In the development of the numerical scheme, choices can be made on the type of singularities used (sources, doublets or both) and the variation of the strength of the singularity (or order) across each panel (constant strength, linear or quadratic variation in strength). The type of source used is dependent upon the problem under consideration. Katz and Plotkin [2001] highlighted that for non-lifting configurations source-only methods are sufficient, but for a body with zero thickness, such as plate, these methods would not be applicable. Instead, it is appropriate to use the dipole to represent the discontinuity in the potential across the plate, or to use the derivative of the dipole (vorticity) along the surface to represent the discontinuity in the tangential velocity; the choice of the order of the singularity is related to convenience and the available computation resource.

Sahin *et al,* [1997] applied this approach to solving the problem of an underwater vehicle and found that the method with constant singularity strength across the panel provided a good balance between convenience, computational cost and accuracy for predicting flow around complex geometries. The authors chose this low order formulation involving both sources and doublets as singularities to model the hydrodynamic characteristics of underwater vehicles (in this case deeply submerged). The work described how the wakes were modelled through constant strength doublet panels (where the doublet strength is constant within each panel) behind the trailing edge of a lifting body, such as a fin, and considering the wake as aligned with the lifting body axis (unslanted) or

wake aligned with the free stream (slanted). Whilst modelling the wake is important, Sahin et al showed that modelling the wake as slanted or unslanted had little influence on the overall results. It was also shown that it is possible to truncate the wake at some distance astern of the body, about five body lengths was suggested by Sahin et al, without affecting the desired accuracy of the results. The paper considered two approaches to modelling the position from which the wakes were shed, positions determined from empirical results and wakes from the trailing edge of lifting bodies. In the example in the paper, the authors assumed no significant separation due to the low angles of attack considered (±4 degrees) so they only modelled wakes from the fins, dealing with the problems associated with wake panel interaction with body surface panels. Whilst turbulent flow will always separate from a streamlined hull at some point along its length, at 4 degrees, it is unlikely that any significant separation will be present as a consequence of the angle of attack. However, interaction of the wakes from upstream appendages on the downstream hull form and the interaction of wakes from the upstream hull on downstream appendages could be significant in determining the forces and moments on a fully appended submarine.

Usually, the form of the potential would automatically satisfy the far field boundary condition given by:

$$\nabla\phi \to 0 \; for \; r \to \infty$$

40

with $r^2 = x^2 + y^2 + z^2$

However, with Rankine source methods for example, the source does not satisfy the free surface boundary condition automatically and distribution of sources on free surface is required and integrals need to be evaluated. For the linearised problem an alternative is to use the Green function which satisfies the free surface boundary condition. Gourlay and Dawson [2015] used such a panel method, or the Havelock sources on the body surface, for solving the flow around near-surface submarines. The rationale of linearisation is that for a fully submerged submarine the disturbance on the free surface may be small and. The approach was developed to solve the steady state problem of the submarine under a calm water free surface, to provide predictions of the steady state pressure field, wave resistance and vertical force and moment. The method was not extended to the unsteady problem of a submarine under the influence of surface waves, which can be done by adopting an alternative Green's function formulation, [Wehausen and Laitone, 1960] that includes a convolution term in the integral equation if the problem is transient.

However, purely potential flow approaches are limited in that they are unable to capture significant flow features due to viscosity such as flow separation on the hull. Lloyd, [1989] represented the separated flow around the hull of a deeply submerged submarine by 12 discrete vortices arranged symmetrically about the plane of the incident flow at the stern of the hull. The position and strength of these vortices were determined through empirical relationships derived from experimental data and effectively become part of the system of equations used to solve for the kinematic body boundary condition. The hull wake was then represented by projecting the longitudinal locations of each of these vortices, from the plane that defines the incident angle, downstream of the body.

Musker *et al* [1998] introduced some corrections due to viscous effects into the potential solution by the panel method. The approach was to undertake a series of inviscid calculations that emulated the model tests, from which a set of inviscid hydrodynamic derivatives are obtained; Musker *et al* [1998] then assumed that the difference between the inviscid derivative set and the derivatives obtained from the model tests are the additional forces and moments due to purely viscous effects. This difference is obtained in the code prior to full unsteady calculation; a pre-processor undertakes a series of calculations varying the state variables from which the forces and moments are determined; from which the derivatives are then obtained. The viscous contribution to the forces and moments is then assumed to be calculated from those viscous derivatives and subsequently added to the forces and moment derived from the inviscid velocity potential. In the case of the submarine under waves, the control surfaces are actively moving to maintain depth; therefore re-calculating the influence that each source on the appendage has on the elements of the body surface would be required at each time step which would impact on the calculation time. An approach used by [Musker, 1988] was to undertake this “influence” calculation once by only considering the unappended body geometry; the contributions of the appendages were then defined separately to those of the unappended body. Through private communication, with Prof. Musker, it is known that subsequent updates led to the appendages been modelled using an empirical database containing lift and drag coefficients of various NACA sections [Abbot and Von Doenhoff, 1949]. Clearly, this heavily empirical approach is limited and it would enhance the design tool if a more analytic approach was used, such as that proposed by Glauert [1947].

A classical approach to determining the velocity distribution on a lifting surface is to use the knowledge of the spanwise circulation, Γ along the appendage. Glauert [1947] approximated Γ by a trigonometric expansion; Lloyd [1989b] applied this approach to modelling submarine appendages, which can be summarized below.

For a lifting, thin, finite hydrofoil moving at a constant speed with the free stream speed U_∞ at a small angle of attack relative to a coordinate system attached to the aerofoil, the velocity field for the potential flow problem is obtained by solving the Laplace equation for the disturbed potential $\nabla^2\phi = 0$ subject to the boundary condition requiring no flow across the solid boundary of the appendage (approximated as a thin plate on z=0).

$$\frac{\partial \phi}{\partial z}(x, y, \pm 0) = U_\infty \left(\frac{\partial \varsigma}{\partial x} - \alpha\right)$$

41

where

$\varsigma = \varsigma(x, y)$ is the camber surface.

α is the angle of attack.

The notation ± 0 in this context means the evaluation of the function as z approaches z=0 from above and as z approaches z=0 from below, respectively.

The simplest means of solving this 3D problem is to assume that the chordwise circulation, at any spanwise station, is replaced by a single concentrated vortex with circulation $\Gamma = \Gamma(\mathrm{y})$ placed along a single spanwise line, [Katz and Plotkin, 2001] which is usually along the quarter chord. The lifting line theory developed by Prandtl can be given as:

$$\frac{-\Gamma(\mathrm{y})}{\pi c(y) U_\infty} - \frac{1}{4\pi U_\infty} \int_{-b/2}^{b/2} \frac{1}{y - y_0} \frac{\mathrm{d}\Gamma(y_0)}{dy} dy_0 + \alpha = 0$$

42

where, $c(y)$ is the spanwise local chord, b is the span.

A solution to the spanwise circulation $\Gamma = \Gamma(y)$ can be obtained by describing the unknown distribution in terms of a trigonometric expansion. In the context of appendages on submarines [Lloyd, 1989] used a Fourier expansion with only odd powers, as a result of an assumption that submarine appendages would have symmetric chordwise cross sections. Lloyd [1989] also used an approximation for the variation of chord length across the span for appendages that are typical of

those used for submarines. To account for the effect of the hull on the appendage [Lloyd, 1989] used an empirical function k_{BL} that reduced the circulation close to the hull itself.

Whilst at periscope depth under the effects of surface waves, the control surfaces of a submarine will be continually changing to counter the effects of the waves, i.e. there is not just an angle of attack on the appendage but also an angle variation rate. [Klose and Acosta, 1968] derived an empirical formula to account for the effect of rate of change of angle of incidence $\dot{\alpha}$

$$C_{LC} = \frac{dC_L}{d\alpha}\left(\alpha + \frac{\bar{c}}{2U_\infty}\dot{\alpha}\right)$$

43

where $\bar{c}$ is the mean chord of the appendage

It should be noted that approximations used by [Lloyd, 1989] and [Klose and Acosta, 1968*]* are empirical in nature and therefore their use should be limited.

As mentioned earlier, [Hess, 1972] updated earlier work on non-lifting bodies by representing lifting surfaces using finite-strength vorticity distributions rather than lift line methods; in this case the Kutta condition, for the sharp edge of the body in the potential flow theory, was a practical means of approximating the real flow, as it is essentially a viscous flow phenomena. Therefore, the formulation of the potential flow model is based upon an understanding of the key characteristics that are required to be represented, particularly in the treatment of trailing edges. Hess [1972] approximated the lifting body and its trailing vortex wake by surface panels; the form of the integrand is the same but the treatment of the singularity on each panel is different depending on whether the surface is considered to be non-lifting or lifting

Hess [1972] represented a generic configuration, such as an aircraft, as consisting of portions of the geometry that are considered as non-lifting; with quadrilateral panels of constant source strength used to represent these portions of the geometry and portions of the configuration that consist of well-defined trailing edges, such as the wings, that are considered to be lifting bodies. The geometry of the lifting portions are represented as plane trapezoids with dipoles distributed on the surface and on the wake extending from the trailing edge downstream. [Hess, 1972] terminated the wake at a point aft of the trailing edge at which the wake effect on the flow can be considered insignificant; the Kutta condition is applied at the trailing edge of the lifting body.

In conclusion, this review has highlighted the approaches to modelling the problem of manoeuvring in waves applied to a submarine operating at periscope depth. The approach of combining the high frequency response of a vessel , due to the presence of surface waves, with the slowly varying assumption of a manoeuvring vessel has been used extensively in the predictions of the motion response of a surface ship in waves during a manoeuvre (so called manoeuvring in waves) [Hutchison, 1990]. Consequently, in the following sections a time domain computational approach is described that is based on a rational combination of existing theoretical methods, to predict the first and second order wave induced forces on a fully appended submarine with forward speed, that is then combined with a non-linear empirical manoeuvring model that uses hydrodynamic manoeuvring derivatives obtained from model tests.

This approach utilises the assumption that the total forces and moments on a manoeuvring submarine under the influence of surface waves is a linear combination of the calm water effects and the wave induced effects. The problem of determining the response of the submarine due to the presence of surface waves is solved by using a panel method, based on Hess and Smith, [1962], for sources distributed uniformly across the triangular panels (to reflect the triangular panels obtained from modern CAD software) on the body. Appendage lift and drag are obtained from lifting line theory , Glauert [1947], modified to include empirical equations to accommodate some viscous effects, [Lloyd, 1989].

During this review, it has become clear that, by far, most of the research undertaken to solve the problem of second order wave induced forces on large submerged bodies has been performed within the field of ocean engineering. This extensive research will be drawn upon later in this thesis in the development of experimental techniques for evaluating the second order effects on a submerged submarine under waves and compared with numerical analysis tools including the numerical methods developed as part of this current research.

2. SUBMARINE MANOEURVING AND CONTROL – Part 2

2.6 Fluid motion and boundary conditions

The theory is developed based on the assumption that the fluid surrounding the totally submerged body is inviscid, incompressible and constant density and the flow around the body is irrotational. It is assumed that the body is moving with constant forward speed at a mean depth beneath the

free surface. The fluid velocity components, in Earth axes, can then be described by a scalar velocity potential ϕ such that:

$$\begin{bmatrix} u'_f \\ v'_f \\ w'_f \end{bmatrix} = \begin{bmatrix} -\partial\phi/\partial x' \\ -\partial\phi/\partial y' \\ -\partial\phi/\partial z' \end{bmatrix}$$

44

The problem is defined with respect to Earth axes by equations associated with mass continuity, body kinematics, free surface dynamics and free surface kinematics

Mass continuity equation: $\nabla^2\phi(x', y', z', t) = 0$ everywhere in the fluid

45

Body impermeable condition means that at any point on the body-fluid boundary there is no relative normal fluid velocity component. Hence, the fluid velocity component in the direction of the local normal vector must equal the corresponding velocity component associated with the same point on the body given by:

Kinematic body boundary condition: $\frac{\partial\phi}{\partial n} = -\bar{V}'.\bar{n}$ on the surface of the body

46

where $\bar{n} = (n_x, n_y, n_z)$ is the local normal vector of the body surface and $\bar{V}' = (u', v', w')$ is its corresponding velocity vector of the body. The convention adopted for $\bar{n}$ is that it should be in a direction pointing into the fluid, away from the interior of the body.

The far field condition is given by:

$$\nabla\phi \to 0 \quad \text{as } r \to \infty$$

47

with $r^2 = x^2 + y^2 + z^2$

The elevation of the free surface η in the vertical direction in functional form referred to the O'x'y' plane is $\eta(x', y', t)$. The free surface is assumed to be a single value function of the two horizontal coordinates x' and y' in the earth fixed coordinate system

Kinematic free surface condition:

$$u_f' \frac{\partial \eta}{\partial x'} + v_f' \frac{\partial \eta}{\partial y'} = w_f' \; on \; z' = 0$$

48

The dynamic free surface condition follows from the application of the Bernoulli equation with the pressure being assumed to equal to the constant atmospheric pressure.

Dynamic free surface condition:

$$\frac{\partial \phi}{\partial t} - \frac{1}{2} \nabla \phi . \nabla \phi = 0 \; on \; z' = 0$$

49

The pressure on the body can be obtained from the unsteady form of the Bernoulli pressure equation:

$$\frac{p}{\rho} = \frac{\partial \phi}{\partial t} + g z' - \frac{1}{2} \nabla \phi . \nabla \phi$$

50

2.7 Solving the equations of flow and motion

Based on perturbation theory, the instantaneous wave elevation, velocity potential and the pressure can be approximated using the following perturbation expansion:

$$\eta = \eta^{(0)} + \varepsilon \eta^{(1)} + \varepsilon^2 \eta^{(2)}$$

$$\phi = \phi^{(0)} + \varepsilon \phi^{(1)} + \varepsilon^2 \phi^{(2)}$$

$$p = p^{(0)} + \varepsilon p^{(1)} + \varepsilon^2 p^{(2)}$$

51

where ε is a small parameter reflecting the perturbation of wave elevation or body motion from its mean position and may be defined as $\varepsilon \sim o\left(\frac{a}{\lambda}\right)$. $\eta^{(0)}$, $\eta^{(1)}$, $\eta^{(2)}$, $\phi^{(0)}$, $\phi^{(1)}$, $\phi^{(2)}$, are the steady, first and second order wave elevation and velocity potentials respectively; $p^{(0)}$, $p^{(1)}$, $p^{(2)}$ are the steady, first and second order pressures respectively. Here the steady component refers to the time independent forward speed problem in calm water.

The steady state problem can be solved based on the exact or simplified free surface boundary condition. The result can be used to help determine pressure signatures from submarines, [Sahin et al, 1994] for example. For the limiting case of low Froude number and submergence depths typical of PD operations, treating the free surface as rigid is considered sufficient for understanding the surface suction on a submarine and its impact on submarine control, [Musker, 1984]. At higher Froude numbers or in cases where the submarine is very close to the free surface this approach may be less accurate, but it would be sufficient to determine $\phi^{(0)}$ from the solution of the "double body" problem with a rigid free surface, [Shao, 2010].

For the linear or the first order unsteady problem, the velocity potential ϕ can be defined in terms of a known incident wave potential ϕ_I and an unknown body potential ϕ_B due to wave diffraction and radiation, such that

$$\phi = \phi_I + \phi_B$$

52

Consider an incident wave of amplitude a and wavelength λ propagating with a heading angle μ with respect to the x'-axis of the Earth-fixed coordinate system. The incident velocity potential ϕ_I of a regular wave, first order, in deep water takes the form:

$$\phi_I(x', y', z', t) = \frac{ag}{\omega}\cos(kx'\cos\mu + ky'\sin\mu - \omega t)e^{-kz'}$$

53

where

ω is the wave frequency

$k = \frac{\omega^2}{g} = \frac{2\pi}{\lambda}$ is the deep water wave number

Then, the wave induced particle velocities on the body will be:

$$u_I^{'} = -\frac{\partial \phi_I}{\partial x^{'}} = \frac{ag}{\omega} k\cos\mu \sin(kx^{'}\cos\mu + ky^{'}\sin\mu - \omega t)e^{-kz^{'}}$$

$$v_I^{'} = -\frac{\partial \phi_I}{\partial y^{'}} = \frac{ag}{\omega} k\sin\mu \sin(kx^{'}\cos\mu + ky^{'}\sin\mu - \omega t)e^{-kz^{'}}$$

$$w_I^{'} = -\frac{\partial \phi_I}{\partial z^{'}} = \frac{ag}{\omega} k \cos(kx^{'}\cos\mu + ky^{'}\sin\mu - \omega t +)e^{-kz^{'}}$$

So,

$$\frac{\partial \phi}{\partial n} = -V_f n$$

54

where

$$V_f = (u_f', v_f', w_f') = (u' + u_I', v' + v_I', w' + w_I')$$

and (u', v', w') are the components of the velocity vector of the body.

To determine the potential flow around a submerged body a singularity distribution over the body surface may be used, each of which is associated with a panel on the body surface. In this case at a point on the body surface a line normal to the local surface of the body point is constructed. The strengths of these singularities are chosen such that the total potential satisfies the impermeable kinematic boundary condition given by Eqn.46. The flat and rigid free surface condition is satisfied using an image of the body above the free surface, or the double body theory, which leaves the mass continuity equation Eqn.45 satisfied automatically by the nature of the singularities used. The source distribution approach used here is that first developed by Hess and Smith [1962] as discussed in section 2.5.4 in which the body surface (the hull and the bridge fin) is discretized. The Hess and Smith approach is described in more detail in Appendix A. Also, included in Appendix A is the method used to account for the effects of flow separation on the body of the submarine.

Eqn. 47 can be re-written in the following form for the jth body point.

$$n_{x'_j}\left[\frac{\partial\phi}{\partial x'}\right]_j + n_{y'_j}\left[\frac{\partial\phi}{\partial y'}\right]_j + n_{z'_j}\left[\frac{\partial\phi}{\partial z'}\right]_j = -\left(n_{x'_j}u'_j + n_{y'_j}v'_j + n_{z'_j}w'_j\right)$$

55

where $\left(n_{x'_j}, n_{y'_j}, n_{z'_j}\right)$ is the direction cosine of the outward normal and $\left(u'_j, v'_j, w'_j\right)$ is the velocity of the j[th] body point; all values refer to earth axes and are dependent upon the instantaneous orientation and motion of the body and the position of the body point with respect to the body itself.

Transformation of the unit vectors in the body axes system to an earth axes system is given by:

$$\begin{bmatrix}\hat{\imath}'\\ \hat{\jmath}'\\ \hat{k}'\end{bmatrix} = \underline{T}\begin{bmatrix}\hat{\imath}\\ \hat{\jmath}\\ \hat{k}\end{bmatrix}$$

56

where $\hat{\imath}, \hat{\jmath}, \hat{k}$ and $\hat{\imath}', \hat{\jmath}', \hat{k}'$ are the unit vectors in the body and Earth axes respectively and $\underline{T}$ is the transformation matrix given by [Gentle,2007]:

$$\underline{T} = \begin{bmatrix}\cos\Theta\cos\Psi & -\cos\Phi\sin\Psi + \sin\Theta\sin\Phi\cos\Psi & \sin\Phi\sin\Psi + \sin\Theta\cos\Phi\cos\Psi\\ \cos\Theta\sin\Psi & \cos\Phi\cos\Psi + \sin\Psi\sin\Theta\sin\Phi & -\sin\Phi\cos\Psi + \sin\Theta\cos\Phi\sin\Psi\\ -\sin\Theta & \cos\Theta\sin\Phi & \cos\Theta\cos\Phi\end{bmatrix}$$

where Φ, Θ and Ψ are Euler angles from x'y'z' to xyz, reflecting the body orientations.

These transformations are necessary to account for the change in panel location, relative to the free surface, due to the time dependent motions of the submarine.

The direction cosines in the body axes are constant for a particular body point and when referred to the earth axes become:

$$\begin{bmatrix}l'\\ m'\\ n'\end{bmatrix} = \underline{T}\begin{bmatrix}l\\ m\\ n\end{bmatrix}$$

Likewise, the coordinates of the j[th] body point in earth axes becomes:

$$\begin{bmatrix} x_j' \\ y_j' \\ z_j' \end{bmatrix} = \begin{bmatrix} x_0 \\ y_0 \\ z_0 \end{bmatrix} + \underline{T} \begin{bmatrix} x_j \\ y_j \\ z_j \end{bmatrix}$$

57

with $(x_0\ , y_0\ , z_0\ )$ the coordinates of the origin of the body axes in earth axes.

From Eqn. 57 the body point velocity components in earth axes can be determined as:

$$\begin{bmatrix} u_j' \\ v_j' \\ w_j' \end{bmatrix} = \frac{d}{dt} \begin{bmatrix} x_j' \\ y_j' \\ z_j' \end{bmatrix} = \frac{d}{dt} \begin{bmatrix} x_0 \\ y_0 \\ z_0 \end{bmatrix} + \frac{d\underline{T}}{dt} \begin{bmatrix} x_j \\ y_j \\ z_j \end{bmatrix}$$

or

$$\begin{bmatrix} u_j' \\ v_j' \\ w_j' \end{bmatrix} = \underline{T} \begin{bmatrix} u \\ v \\ w \end{bmatrix} + \frac{d\underline{T}}{dt} \begin{bmatrix} \begin{bmatrix} x_j \\ y_j \\ z_j \end{bmatrix} \end{bmatrix}$$

58

where

(u, v, w) is the velocity of the origin in body axes.

$\frac{d\underline{T}}{dt}$ gives rise to rates of change of Φ, Θ and Ψ which need to be related to the known angular rates p_b, q_b and r_b in body axes using the following:

$$\dot{\Phi}\left(\hat{\imath}'\, cos\,\Theta cos\Psi + \hat{\jmath}'\, cos\,\Theta sin\Psi - \hat{k}'\, sin\,\Theta\right) + \dot{\Theta}(-\hat{\imath}' sin\Psi + \hat{\jmath}'\, cos\Psi) + \dot{\Psi}\hat{k}' = p_b\hat{\imath} + q_b\hat{\jmath} + r_b\hat{k}$$

which, combined with Eqn. 56, leads to the following and the determination of $\frac{d\underline{T}}{dt}$.

$$\begin{bmatrix} \dot{\Phi} \\ \dot{\Theta} \\ \dot{\Psi} \end{bmatrix} = \begin{bmatrix} 1 & \sin\Phi\tan\Theta & \cos\Phi\tan\Theta \\ 0 & \cos\Phi & -\sin\Phi \\ 0 & \sin\Phi\sec\Theta & \cos\Phi\sec\Theta \end{bmatrix} \begin{bmatrix} p_b \\ q_b \\ r_b \end{bmatrix} \text{ for } \Theta \neq \pm\frac{\pi}{2}$$

59

The restriction of $\Theta \neq \frac{\pi}{2}$ needs to be imposed to ensure that the above matrix remains consistent by avoiding the case of $sec\Theta = \infty$. Whilst it may be physically possible for a submarine to pitch to 90 degrees, this is unlikely particularly in the context of operating at periscope depth.

To solve the potential when the body is under the effect of incident waves Eqns.57,54 and 40 are combined to provide the total velocity potential, ϕ, which is then substituted into Eqn 55 to give:

$$\frac{\partial \phi_b(x_j', y_j', z_j', t)}{\partial n} \equiv -\sum_{i=1}^{N} \sigma_i A_{ij}$$

and using the total derivative, due to using a moving frame of reference, to expand Eq. 54 to obtain

$$\sum_{i=1}^{N} \sigma_i A_{ij} = \left(n_{x_j'} u_j' + n_{y_j'} v_j' + n_{z_j'} w_j' + n_{x_j'} \frac{\partial \phi_I(x_j', y_j', z_j', t)}{\partial \mathrm{x}'} + n_{y_j'} \frac{\partial \phi_I(x_j', y_j', z_j', t)}{\partial \mathrm{y}'} + n_{z_j'} \frac{\partial \phi_I(x_j', y_j', z_j', t)}{\partial \mathrm{z}'} \right) \quad (60)$$

j=1,2,…N

where A_{ij} is known and is referred as the matrix of influence coefficients; the first term in the RHS includes the components of the instantaneous velocity of the body at the jth panel (u_j', v_j', w_j').

Eqn.60 represents a system of *N* simultaneous linear equations, for *N* unknown source strengths σ_j, uniformly distributed across the jth panel, and that is solved by direct matrix inversion or iteration. Once the source strengths are known the body potential can be determined from the equations shown in Appendix A.

The pressure at the jth body point is then found from the Bernoulli equation (Eqn.51). The terms involving the grad operator ∇ are found from Eqns. 53, 54 and 40 $\left[\frac{\partial \phi_I}{\partial \mathrm{t}}\right]_j$ can be determined as follows.

Eqn. 60 can be re-written as:

$$\sum_{i=1}^{N} \sigma_i A_{ij} = b_j \qquad \mathrm{j} = 1, \ldots \mathrm{N}$$

Applying time derivative to each of these equations, the j[th] equation yields

$$\sum_{i=1}^{N} \frac{\partial \sigma_i}{\partial \mathrm{t}} A_{ij} = \frac{\partial b_j}{\partial \mathrm{t}} - \sum_{i=1}^{N} \frac{\partial A_{ij}}{\partial \mathrm{t}} \sigma_i, \qquad \mathrm{j} = 1, \dots \mathrm{N}$$

or

$$\left[\sum_{i=1}^{N} \frac{\partial \sigma_i}{\partial t} A_{ij}\right]_j = n_{x_j}\left(\dot{u} - y_j \dot{\mathrm{r}} + z_j \dot{\mathrm{p}}\right) + n_{y_j}\left(\dot{v} - z_j \dot{\mathrm{q}} + x_j \dot{\mathrm{r}}\right) + + n_{z_j}\left(\dot{w} - x_j \dot{\mathrm{p}} + y_j \dot{\mathrm{q}}\right) +$$

$$\left[\frac{Dn_{x_j'}}{Dt}\right]\left(u_j' + \left[\frac{\partial \phi_I}{\partial \mathrm{x}'}\right]_j\right) + \left[\frac{Dn_{y_j'}}{Dt}\right]\left(v_j' + \left[\frac{\partial \phi_I}{\partial \mathrm{y}'}\right]_j\right) + \left[\frac{Dn_{z_j'}}{Dt}\right]\left(w_j' + \left[\frac{\partial \phi_I}{\partial \mathrm{z}'}\right]_j\right) +$$

$$n_{x_j'}\left[\frac{\mathrm{D}u_j'}{Dt}\right] + n_{y_j'}\left[\frac{\mathrm{D}v_j'}{Dt}\right] + + n_{z_j'}\left[\frac{\mathrm{D}w_j'}{Dt}\right] \qquad \mathrm{j} = 1, \dots \mathrm{N}$$

61

where the functions in the square brackets are to be evaluated at the j[th] body point.

Now, for the function $u_j' = u_j'\left(x_j', y_j', z_j', t\right)$, using the Chain Rule, the total derivative is:

$$\frac{\mathrm{D}u_j'}{Dt} = \frac{\partial u_j'}{\partial x_j'}\frac{\partial x_j'}{\partial t} + \frac{\partial u_j'}{\partial y_j'}\frac{\partial y_j'}{\partial t} + \frac{\partial u_j'}{\partial z_j'}\frac{\partial z_j'}{\partial t} + \frac{\partial u_j'}{\partial t}$$

62

and,

$(u_j', v_j', w_j') = (-\frac{\partial \phi_I}{\partial x_j'}, -\frac{\partial \phi_I}{\partial y_j'}, -\frac{\partial \phi_I}{\partial z_j'})$ and $(\frac{\partial x_j'}{\partial t}, \frac{\partial y_j'}{\partial t}, \frac{\partial z_j'}{\partial t}) = (u_j', v_j', w_j')$

Which means that Eqn. 62 can be re-written as;

$$\frac{\mathrm{D}u_j'}{Dt} = u_j'\left[\frac{\partial^2 \phi_I}{\partial \mathrm{x}^2}\right]_j + v_j'\left[\frac{\partial^2 \phi_I}{\partial \mathrm{x}\partial \mathrm{y}}\right]_j + w_j'\left[\frac{\partial^2 \phi_I}{\partial \mathrm{x}\partial z}\right]_j + \left[\frac{\partial^2 \phi_I}{\partial \mathrm{x}\partial t}\right]_j$$

Likewise, it follows that:

$$\frac{\mathrm{D}v_j^{'}}{Dt} = u_j^{'}\left[\frac{\partial^2\phi_I}{\partial \mathrm{x}\partial \mathrm{y}}\right]_j + v_j^{'}\left[\frac{\partial^2\phi_I}{\partial \mathrm{y}^2}\right]_j + w_j^{'}\left[\frac{\partial^2\phi_I}{\partial \mathrm{y}\partial z}\right]_j + \left[\frac{\partial^2\phi_I}{\partial \mathrm{y}\partial t}\right]_j$$

$$\frac{\mathrm{D}w_j^{'}}{Dt} = u_j^{'}\left[\frac{\partial^2\phi_I}{\partial \mathrm{x}\partial z}\right]_j + v_j^{'}\left[\frac{\partial^2\phi_I}{\partial \mathrm{x}\partial z}\right]_j + w_j^{'}\left[\frac{\partial^2\phi_I}{\partial \mathrm{z}^2}\right]_j + \left[\frac{\partial^2\phi_I}{\partial \mathrm{z}\partial t}\right]_j$$

and

$$\frac{Dn_{x_j^{'}}}{Dt} = -a_1\dot{\Psi} - a_2\dot{\Theta} + a_3\dot{\Phi}$$

$$\frac{Dn_{y_j^{'}}}{Dt} = a_4\dot{\Psi} + a_5\dot{\Theta} + a_6\dot{\Phi}$$

$$\frac{Dn_{z_j^{'}}}{Dt} = -a_7\dot{\Theta} + a_8\dot{\Phi}$$

63

where

$$a_1 = n_{x_j^{'}}\sin\Psi\cos\Theta + n_{y_j^{'}}(\sin\Phi\sin\Psi\sin\Theta + \cos\Phi\cos\Psi) + n_{z_j^{'}}(\sin\Theta\sin\Psi\cos\Phi - \sin\Phi\cos\Psi)$$

$$a_2 = n_{x_j^{'}}\sin\Theta\cos\Psi - n_{y_j^{'}}\sin\Phi\cos\Psi\cos\Theta - n_{z_j^{'}}\cos\Phi\cos\Theta\cos\Psi$$

$$a_3 = n_{y_j^{'}}(\cos\Phi\cos\Psi\sin\Theta + \sin\Phi\sin\Psi) + n_{z_j^{'}}(\cos\Theta\sin\Psi - \sin\Phi\sin\Theta\cos\Psi)$$

$$a_4 = n_{x_j^{'}}\cos\Psi\cos\Theta + n_{y_j^{'}}(\sin\Phi\cos\Psi\sin\Theta - \cos\Phi\sin\Psi) + n_{z_j^{'}}(\cos\Phi\sin\Theta\cos\Psi + \sin\Phi\sin\Psi)$$

$$a_5 = -n_{x_j^{'}}\sin\Theta\sin\Psi + n_{y_j^{'}}\sin\Phi\sin\Psi\cos\Theta + n_{z_j^{'}}\cos\Phi\cos\Theta\sin\Psi$$

$$a_6 = n_{y_j}(\cos\Phi\sin\Psi\sin\Theta - \sin\Phi\cos\Psi) + n_{z_j^{'}}(\sin\Phi\sin\Theta\sin\Psi + \cos\Phi\cos\Psi)$$

$$a_7 = n_{x_j^{'}}\cos\Theta + n_{y_j}\sin\Phi\sin\Theta + n_{z_j^{'}}\cos\Phi\sin\Theta$$

$$a_8 = n_{y_j^{'}}\cos\Phi\cos\Theta - n_{z_j^{'}}\sin\Phi\cos\Theta$$

In the above case, for known body accelerations, Eqn.61 represents a system of *N* simultaneous linear equations, with *N* unknowns $\frac{d\sigma_i}{dt}$, that is solved by the same method as that used for σ_i. The known rate of change of source strengths are used to obtain $\frac{\partial \phi_b}{\partial t}$ from the same equations used to define the body potential itself. Thus, accounting for the body motion in the pressure equation, Eqn. 51.

For a time stepping solution, an explicit method is used. In this case, the known body accelerations are used to determine the body potential which in turn is used to derive the pressures on the body. The forces and moments on the body due to the waves are found by numerical integration of these pressures which are then used in the non-linear equations of motion (Eqn 3) to determine the body acceleration for the next time step.

$$\vec{F} = \iint_{SB_0} p\bar{n}ds$$

$$\vec{M} = \iint_{SB_0} p(\bar{r} \times \bar{n})ds$$

64

The submarine appendages are treated separately to account for the fact that, in the unsteady case of the submarine under waves, the control surfaces maybe actively moving to maintain depth; therefore re-calculating the influence that each source has on the elements of the body surface (that include the appendages) would be required at each time step which would impact on the calculation time. The approach used by [Musker, 1988] was to perform two sets of independent calculations; firstly calculate the steady calm water forces on the body, for a constant depth, using the double-hull theory; but use Rankine sources, on the body surface only, to determine the unsteady forces in waves. For the unsteady case, this meant that the influence coefficients only needed to be determined once, as the relative distance between any two sources do not change. As a further simplification Musker only determined the influence calculation for the unappended body geometry; the contributions of the appendages were then defined separately to those of the unappended body. Through private communication, with Prof. Musker, it is known that subsequent updates led to the appendages been modelled using an empirical database containing lift and drag coefficients of various NACA sections [Abbot and Von Doenhoff, 1949]. Clearly, this heavily empirical

approach is limited and it would enhance the design tool if a more analytic approach was used, such as that proposed by Glauert [1947].

A classical approach to determining the velocity distribution on a lifting surface has been used here, based on the spanwise circulation, Γ along the appendage. Glauert [1947] approximated Γ by a trigonometric expansion; Lloyd [1989b] applied this approach to modelling submarine appendages which is the basis of the method adopted here and detailed in Appendix A.

To extend the time domain computation to irregular, long crested, waves, the assumption of the linear superposition of sinewaves is used to determine the wave induced flow velocities on the submarine hull (hence solve for the body boundary condition) and over the appendages. In this case, an irregular wave can be decomposed into a large number of regular waves travelling in the same direction:

$$\eta(t) = \sum_{i=1}^{N_W} a_i \sin(k_i x' \cos\mu + k_i y' \sin\mu - \omega_i t + \varepsilon_i)$$

Through linear superposition, the total potential of the incident wave will be

$$\phi_I(x', y', z', t) = \sum_{i=1}^{N_W} \frac{a_i g}{\omega_i} \cos(k_i x' \cos\mu + k_i y' \sin\mu - \omega_i t + \varepsilon_i) e^{-k_i z}$$

where $k_i = \frac{\omega_i^2}{g}$ is the deep water wave number and the wave induced particle velocities on the body will be:

$$u_I = \sum_{i=1}^{N_W} \frac{a_i g}{\omega_i} k_i \cos\mu \sin(k_i x' \cos\mu + k_i y' \sin\mu - \omega_i t + \varepsilon_i) e^{-k_i z'}$$

$$v_I = \sum_{i=1}^{N_W} \frac{a_i g}{\omega_i} k_i \sin\mu \sin(k_i x' \cos\mu + k_i y' \sin\mu - \omega_i t + \varepsilon_i) e^{-k_i z'}$$

$$w_I = \sum_{i=1}^{N_W} \frac{a_i g}{\omega_i} k_i \cos(k_i x' \cos\mu + k_i y' \sin\mu - \omega_i t + \varepsilon_i) e^{-k_i z'}$$

The amplitude a_i of each sine wave is obtained from a spectral formulation such as the ITTC, or Bretschneider, wave spectrum, [Bretschneider, 1959], typical for deep water, open ocean environments see Eqn 39.

2.8 Comparison with analytic solutions and experiments

A theoretical formulation of the hydrodynamic forces and moments acting on a submerged body has been presented that is based on a rational combination of existing theoretical methods. This section provides comparisons between the results of predictions using the time domain computations and other approaches. Musker et al [1988] focused on three typical scenarios for comparison, analytical solutions for a 2:1 prolate spheroid, restrained body in regular waves and a lightly restrained body in regular waves. In the latter case, the second order vertical force due to the waves was resisted by two low stiffness springs and the associated first order displacements were measured; this approach to testing is covered in more detail in Chapter 3. In Musker et al [1988], both the restrained and lightly restrained model tests were undertaken using a simplified, unappended, submarine geometry.

This thesis includes comparison of computations of hydrodynamic loads acting on various affine bodies with analytic solution and hydrodynamic loads on a real submarine geometry with model test data. Numerical computations have been performed using the distributed source technique described above. In these calculations, an approach to solving the three-dimensional unsteady problem has been developed and compared with analytic solutions, other frequency domain numerical computations using WAMIT (for zero speed case only) and, where available, model test data.

2.8.1 Affine forms

Chatjigeorgiou, [2012] provided the analytic solutions for the excitation forces on stationary submerged oblate spheroidal bodies, of varying aspect ratio, subjected to harmonic incident waves in deep water. By means of understanding the limitations of the time domain simulation developed as part of this thesis, numerical simulations were undertaken for the case of a sphere of radius *r* at zero speed and two submergence depths (to the axis of the sphere) of *2r* and 1.25*r,* in harmonic waves of amplitude ζ and compared with the analytic solution presented by [Chatjigeorgiou, 2012]; the heave exciting force, non-dimensionalised by $\rho g r^2 \zeta$ plotted against $K\zeta$ as shown in Figure 12 and Figure 13.

Also shown is the analytical wave exciting forces acting on the sphere assuming that the pressure field created by the incoming wave is not disturbed by the presence of the body – the so called Froude-Krylov assumption. The magnitude of the vertical wave exciting force on a sphere is given by the expression, [Wang, 1986].

$$F_z = \frac{4}{3}\rho\pi r^3\omega^2\zeta e^{-k(2r)}$$

It can be seen that in the case of this submergence depth that the Froude-Krylov forces account for around 60 - 70% of the total force. The total force includes both the Froude-Krylov force and the diffraction force; the diffraction component results from the disturbance due to the presence of the sphere on the incoming wave field. There are no contributions from the radiation forces since in this example the body is fixed.

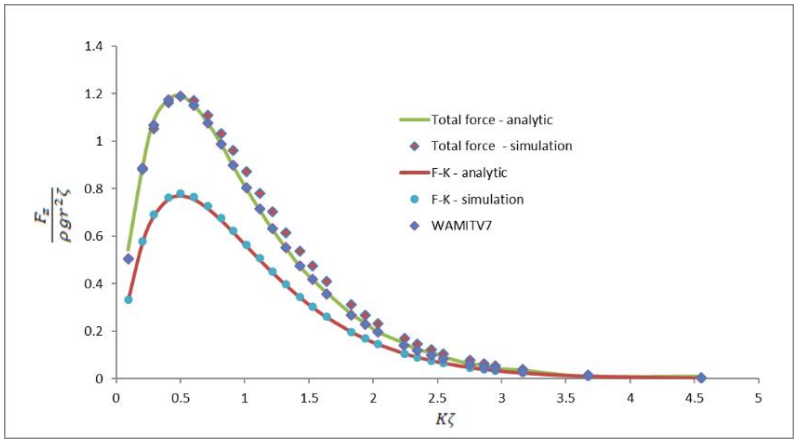

Figure 12: Magnitude of the heave exciting force on a sphere of radius r and depth of submergence of 2r in regular head waves; simulation compared with [Wang, 1986].

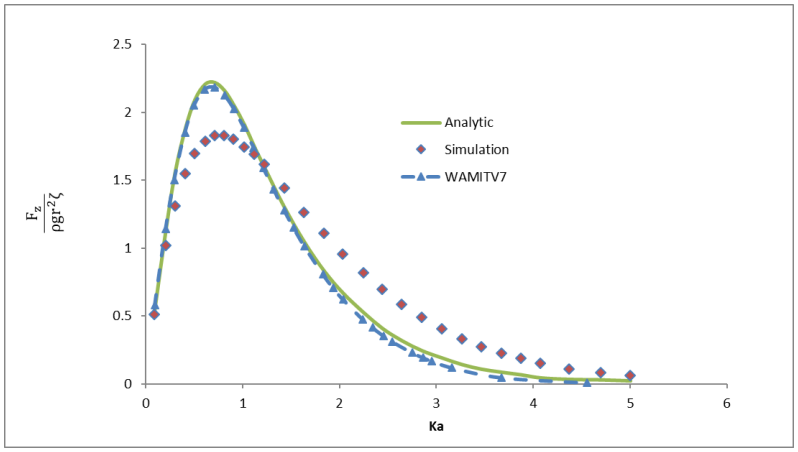

Figure 13: Magnitude of the heave exciting force on a sphere of radius r and depth of submergence of 1.25r in regular head waves; simulation compared with [Chatjigeorgiou, 2012].

The force obtained from the simulation (including the double hull assumption) appears to agree very well with the analytic expression for this depth of submergence. The depth of submergence reduces the numerical predictions are different to the analytic solution, largely as a consequence of treating the free surface as a solid boundary in the time domain simulation compared to WAMIT predictions which includes the linear free surface boundary condition.

However, a depth of submergence, to the axis, equivalent to one hull diameter is quite typical of submarine depths when the periscope is being used; Daum *et al* [2018] considered depth of submergence ranging from 1.0D to 1.75D, for example, where D is a representative diameter of the submarine.

Chatjigeorgiou, [2014] extended the analytic solutions to include the excitation forces on submerged prolate spheroidal bodies at zero speed and advancing in waves; each at a range of headings. The case of a prolate spheroid, with semi-major axis *a*, semi-minor axis *b* and $\frac{a}{b} = 4$, at Froude numbers of 0 and 0.15 in head waves was considered. Numerical simulations were undertaken for at a depth of submergence (to the axis of the sphere) of *f=2b* in harmonic waves of amplitude ζ and compared with the analytic solutions presented by [Chatjigeorgiou, 2014] and, in the zero speed case only, with WAMITV7; the first order heave exciting force, is in this case non-dimensionalised as $\frac{F_z}{\rho g a b \varsigma}$ and plotted against $K\zeta$, in Figure 14.

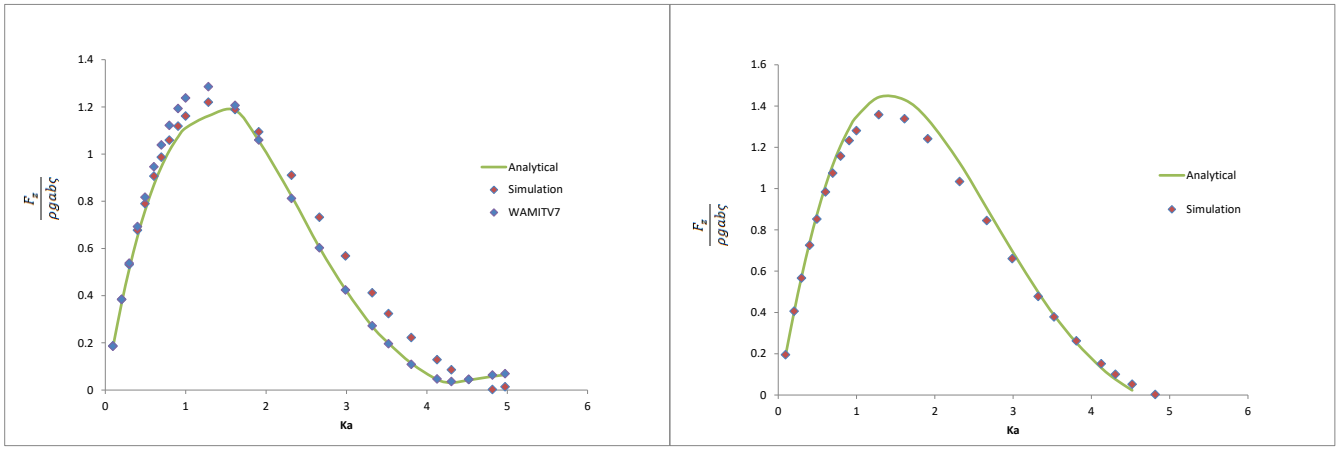

(a) Fn = 0.0 (b) Fn = 0.15

Figure 14: Magnitude of the first order heave exciting force on a prolate spheroid with semi-major axis a and semi-minor axis b at a depth of submergence of 2b in regular head waves; simulation compared with [Chatjigeorgiou, 2014].

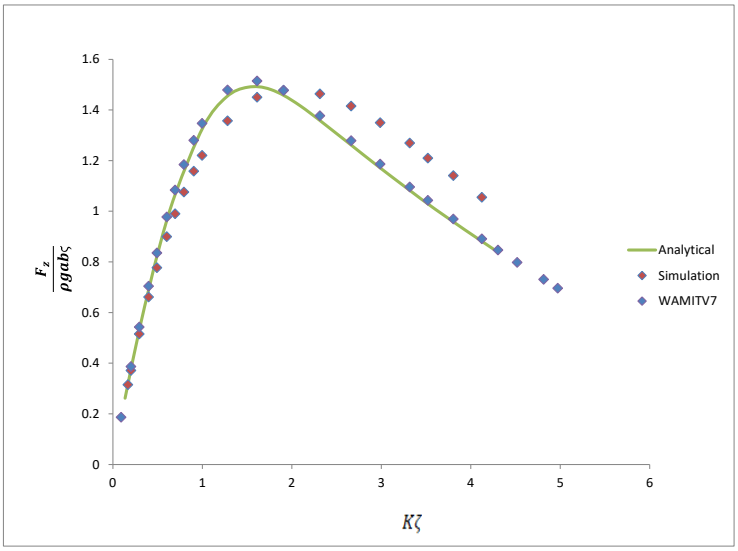

Figure 15: Magnitude of the first order heave exciting force on a prolate spheroid with semi-major axis a and semi-minor axis b at a depth of submergence of 2b in regular beam waves; simulation compared with [Chatjigeorgiou, 2014].

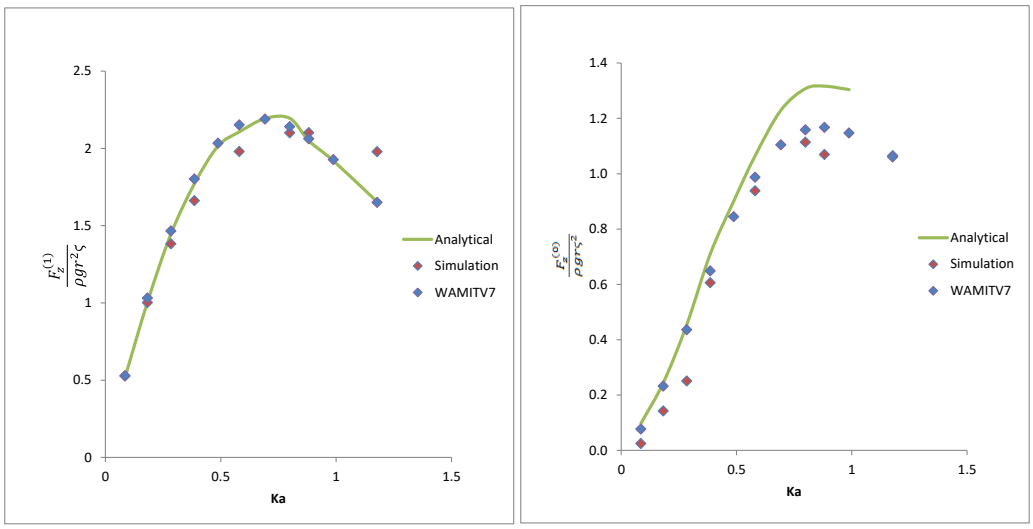

(a) First order (b) Mean force

Figure 16: Magnitude of the first order and mean heave exciting force on a sphere of radius r with a depth of submergence of 1.25r in regular head waves; simulation compared with [Wu et al, 1994].

Wu *et al,* [1994] presented analytic expressions for the first and mean wave induced drift forces acting on a submerged sphere in a finite water depth at zero speed. Figure 16 shows the first order and mean heave forces predicted from simulation and compared with those derived from the analytic expressions and with WAMITV7. The example in shows the forces derived for the deepest depth of water considered by [Wu *et al,* 1994], a depth of 11r where r is the radius of the sphere; Wu *et al,* found that the second order heave force was relatively insensitive to changes in water

depth (from 25r to 11r) for all but the lowest frequencies which is to be expected because of the exponential decay of the wave induced flow velocities (and hence the force on the body) with depth. The mean force predicted from simulation compares well with WAMITV7 but both predictions lie below the analytic solution from [Wu et al, 1994], particularly for the higher values of Ka.

2.8.2 Fully restrained appended submarine in regular waves

EUCLID 10.17 [Cooper, 2007] was a European collaborative project to develop validation techniques for predicting submarine performance close to boundaries – either the seabed or water surface. In the context of the behaviour of a submarine under waves, a series of experiments were undertaken, and reported by Martinussen [2006], to measure the forces and moments on a captive submarine model in close proximity to the free surface. A purposely designed generic submarine hull form, known as the EUCLID geometry, was fully appended but not fitted with a propeller. The reason for not including the propeller is not explained. It is known that a propeller can modify the flow especially over the aft part of the manoeuvring submarine influencing the total forces on the body. First and second order forces and moments were calculated from the mean and amplitude, respectively, of the measured force and moment time histories throughout a series of test conditions in regular waves.

Numerical simulations of the same conditions tested in the captive model tests were undertaken using the time domain approach based on the theory outlined in section 2.3; the first and second order forces and moments were extracted from the measured force time histories using the least squares method described in Appendix C. The first order forces are equal to the amplitude of the measured force and the second order force is the mean measured force.

There is a subtle difference in the approach for the non-zero forward speed since the frequency response is now the encounter frequency ω_e , which is given by $\omega_e = \omega^2 - \frac{2U\omega \cos\mu}{g}$ in deep water.

For the simulation, the distribution of the triangular facet elements on the surface of the submarine hull (at full scale) and the bridge fin is shown in Figure 17. The bridge fin is considered as a diffraction surface as well as generating lift; the other appendages are only considered as lifting surfaces (which does include accounting for the change of incoming flow due to the influence of the hull). The computations were carried out in the same wave conditions as the model tests.

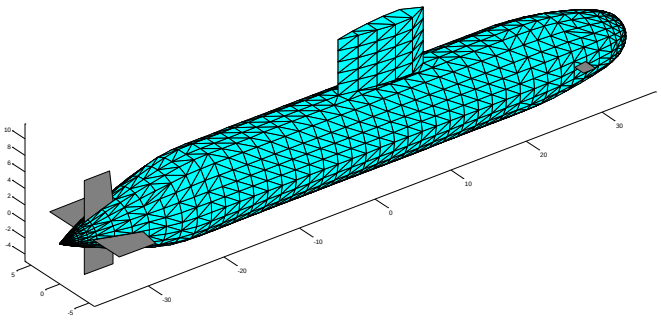

Figure 17: Faceting of the appended EUCLID geometry.

The results of the computations and the measurements with respect to the first order forces and moments and mean forces and moments in regular waves are shown in Figure 20 to Figure 31. Figure 20 shows the results of predictions from the time domain method compared with the MARINTEK experiments in head waves at zero speed and with predictions from the frequency domain software WAMIT.

WAMIT is commercially available software that provides a frequency domain method used to evaluate the unsteady hydrodynamic pressure, loads and motions of bodies at zero speed. The fluid flow is assumed to be potential and the effects of flow separation or lifting effects are neglected. It is possible to include aspects of the geometry, in WAMIT, that are considered to be thin, such as strakes, these elements can be represented using panels and sources or by considering it as a zero-thickness plate to be represented as a series of dipoles, Kerwin and Lee, [1978]. In the latter case, the Kutta condition is applied to the trailing edge of the element. WAMIT uses the linearized free surface boundary condition while the present simulations are based on the flat and rigid free surface. So, in WAMIT the free surface boundary condition is given as:

$$\left(-\omega^2 + g\,\frac{\partial}{\partial z}\right)\phi = 0\ on\ z = 0$$

Where as in the time domain simulation the free surface boundary condition is:

$$\frac{\partial \phi}{\partial z} = 0\ on\ z = 0$$

Which means the body potential will not be correct especially when the body is close to the free surface.

Figure 20 shows the first order forces and moments, taken as the amplitude of the fundamental frequency from the analysis and the second order forces and moments taken as the mean values. The first and second order forces and moments have been non-dimensionalised in as shown in Table 1 and plotted against non-dimensional wavelength.

Force or moment	Non-dimensional term for first order	Non-dimensional term for second order
X	$\rho g D^2 \zeta$	$\rho g D \zeta^2$
Y	$\rho g L^2 \zeta$	$\rho g L \zeta^2$
Z	$\rho g L^2 \zeta$	$\rho g L \zeta^2$
K	$\rho g D L^2 \zeta$	$\rho g D L \zeta^2$
M	$\rho g D L^2 \zeta$	$\rho g D L \zeta^2$
M	$\rho g D L^2 \zeta$	$\rho g D L \zeta^2$

Table 1: Non-dimensional terms used for the first and second order forces and moments

where D is the diameter of the submarine and ζ is the wave amplitude. The sign convention adopted in WAMIT is more typical of that used for studies of the motions of floating platforms, Figure 18, rather than the more traditional sign convention used for submarine manoeuvring. This means that whilst direct comparisons of amplitude of the first order forces is possible, the signs of some of the mean forces from WAMIT need to be modified to be consistent with those derived according to a more traditional submarine axis system, Figure 6, in the following way.

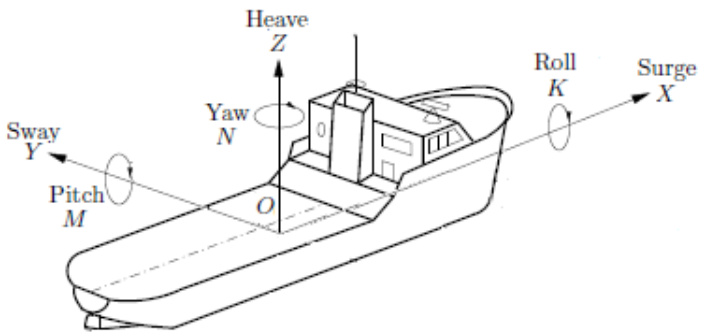

Figure 18: Sign convention used in WAMIT (SNAME, 1950)

Comparisons of ship axes system with a submarine axes system is therefore:

$$X_{ship} = X_{sub} \qquad K_{ship} = K_{sub}$$

$$Y_{ship} = -Y_{sub} \qquad M_{ship} = -M_{sub}$$

$$Z_{ship} = -Z_{sub} \qquad N_{ship} = -N_{sub}$$

65

Before going onto comparisons of computations with experimental data, it is prudent to investigate the wave force contributions for the Euclid design. The components of wave induced heave force are considered. Figure 19 provides a comparison between the time domain computations of the total non-dimensional heave force (Froude-Krylov and diffraction components) and Froude-Krylov component along with a comparison with the combined effect of the Froude-Krylov and diffraction forces from WAMIT.; all forces have been non-dimensionalised by $\rho g L^2 \zeta$. For this case of zero speed in head waves, the Froude-Krylov force accounts for around 45% of the total force (for most of the ranges of wavelengths).

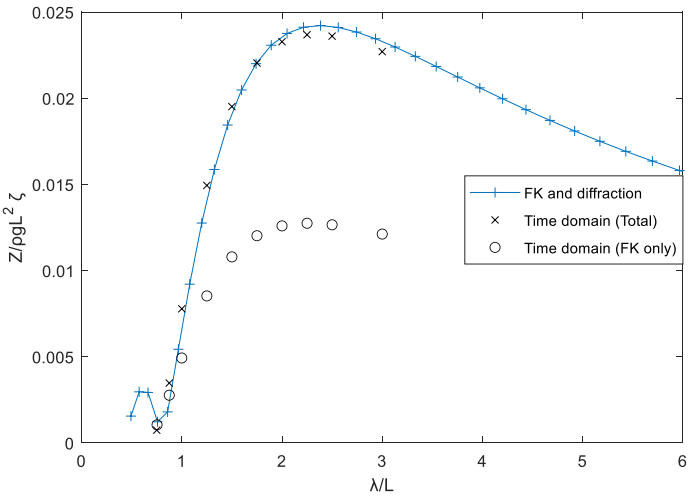

Figure 19: Components of wave force, zero speed head waves

Given below is comparison between results from computations and experimental data, from Martinussen, [2006], of the first order forces and moments at zero and forward speed. For the zero speed case, computations have been performed using the time domain code developed as part of this thesis and WAMIT. The comparison between computations and experiments in Figure 20 to Figure 31 shows that the first order vertical plane forces are generally well predicted by the time domain and the WAMIT computations. First order sway force and yaw moment are also predicted

quite well by both the time domain approach and WAMIT but there are significant differences in the measured roll moment and that predicted by both methods across the frequency range. These differences could be due to both computational methods omitting any viscous contribution from the bridge fin and the hull to the roll moment, see similar example in [Dev and Pinkster, 1995]. There will also be an impact on the sway force as a consequence of not predicting the forces on the bridge fin correctly.

For the case of zero speed, the results of time domain and WAMIT predictions of the mean second order forces and moments indicate that, in general, the mean heave force and pitch moment are reasonably well-predicted for all headings. Although there are some differences, which demonstrate the limitations in the assumptions used in the time domain approach; particularly in the assuming that the flow is inviscid and the free surface boundary condition. For the mean forces in the lateral plane, the quality of the predictions vary with heading; in some cases the predictions are very good in others the prediction quality is poor. This variation in the quality of the prediction, particularly in the lateral plane (in contrast to the typical comparisons seen for the vertical plane) will be mainly due to not capturing the effects of the bridge fin correctly. The discretisation of the bridge fins means that the diffraction forces due to the appendage will be calculated correctly; the lift based forces, determined using Glauert's theory enhanced with empirical data may not be correct, possibly due to the high angle of flow velocities experienced by the bridge fin at zero speed in oblique waves.

However, the main focus of this current research is on the suction forces on the submarine, i.e., those forces that are acting in the vertical plane. It is expected, therefore, that the low prediction quality of the mean forces in the lateral plane will have little impact on the development of control algorithms for periscope depthkeeping.

For the case with forward speed, the comparisons between the time domain computations (no WAMIT predictions since this code is zero speed only) and the experiments are similar to those found for the zero speed case, in that first order forces and moments are predicted quite well, including the roll moment on this occasion. With the exception of the mean heave force, the second order forces with forward speed are not as well predicted by the time domain as with the zero speed case. Again, this is probably due to the application of the free surface boundary condition, assuming it is a rigid flat plate. However, in the practical cases of understanding the surface suction problem, an accurate prediction of the second order heave force and pitch moment is only required.

The comparisons between the time domain predictions and measurements made from fully-captive model tests, have shown that the time domain code developed as part of this research is suitable for evaluating the first and second order vertical plane forces and moments on a submarine body in the context of further understanding the surface suction problem.

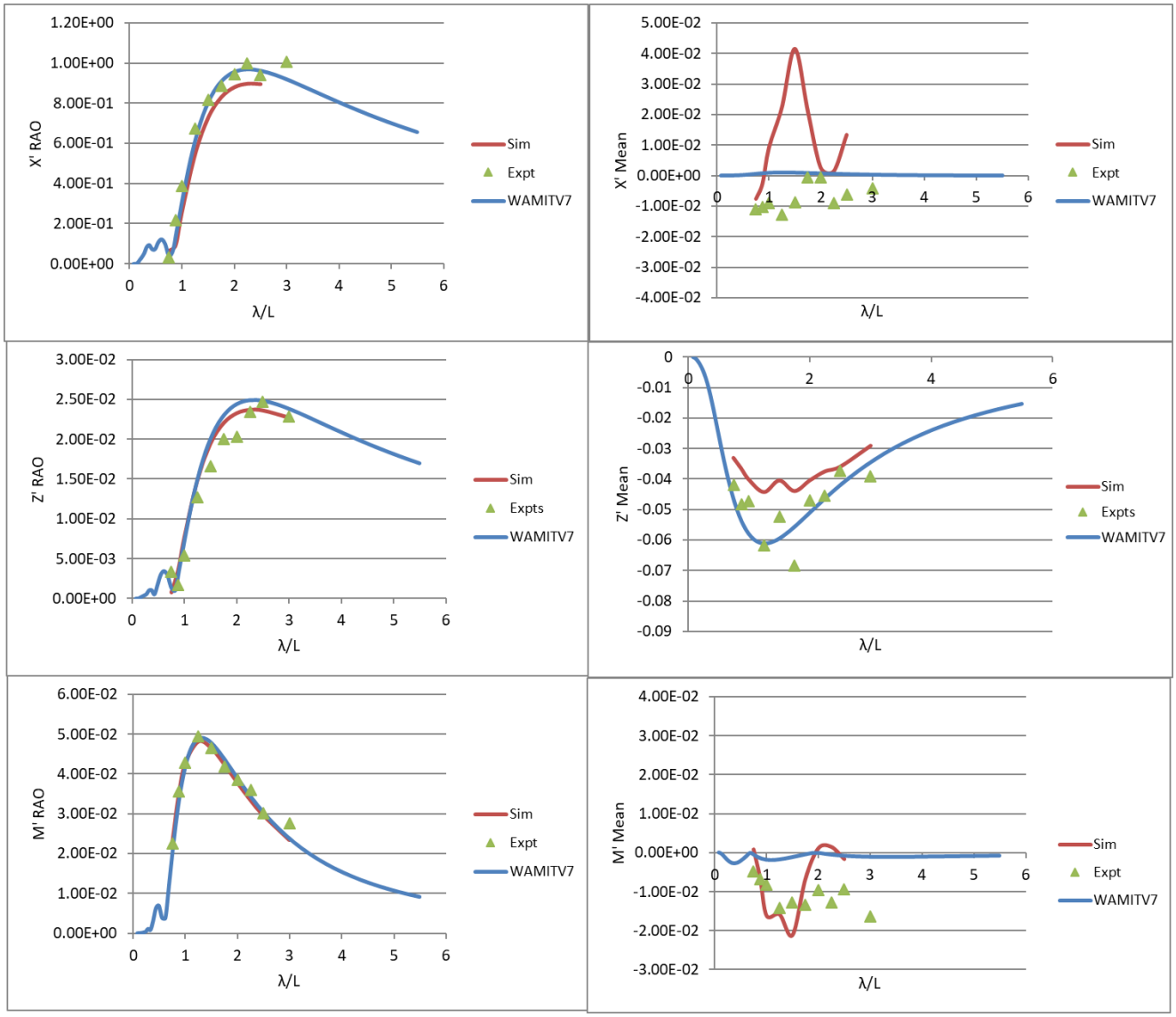

(a) First order (b) Mean force

Figure 20: First order and mean forces in regular head waves (F_r=0.0)

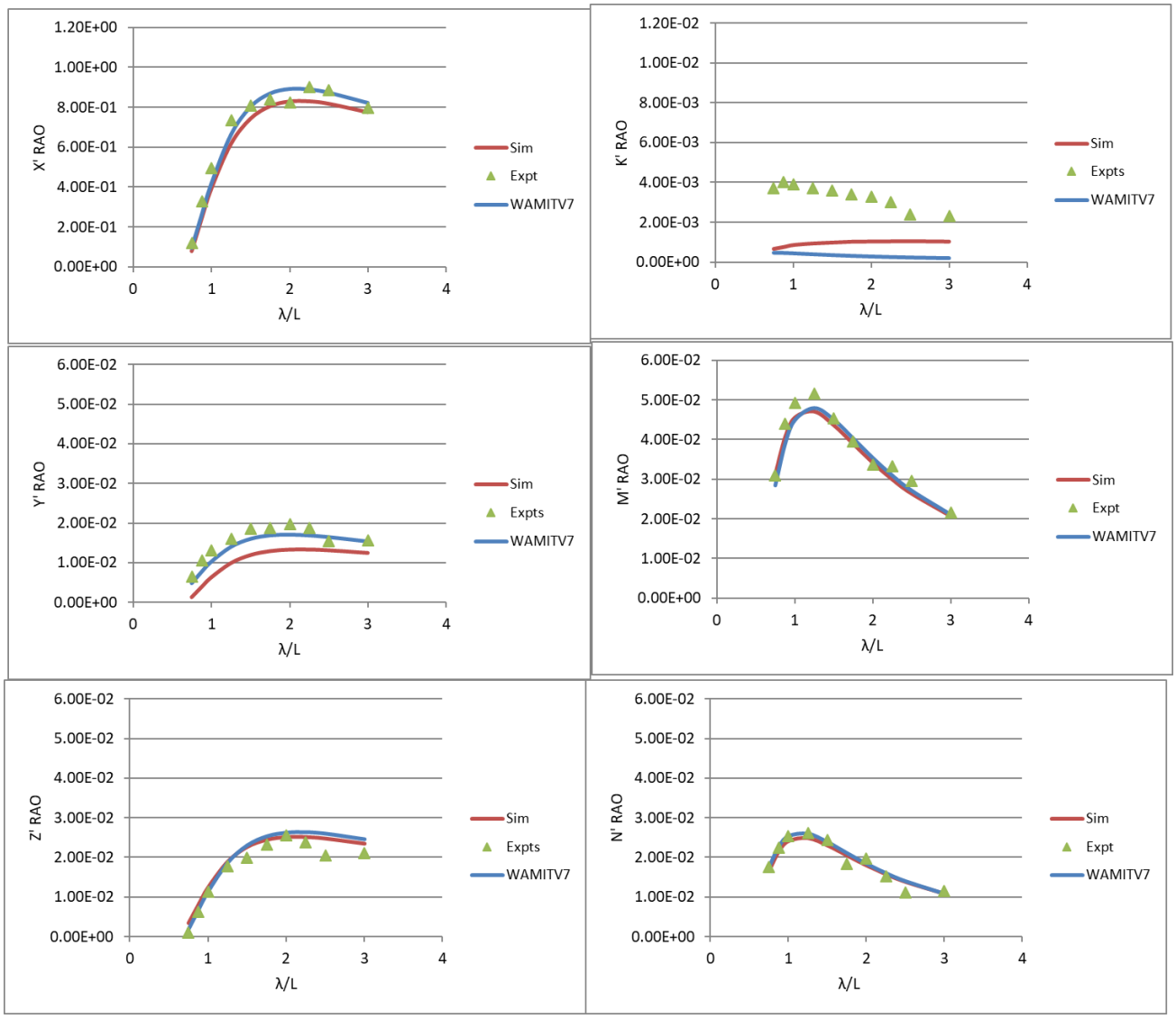

Figure 21: First order forces in regular waves, 150 degrees heading (F_r=0.0)

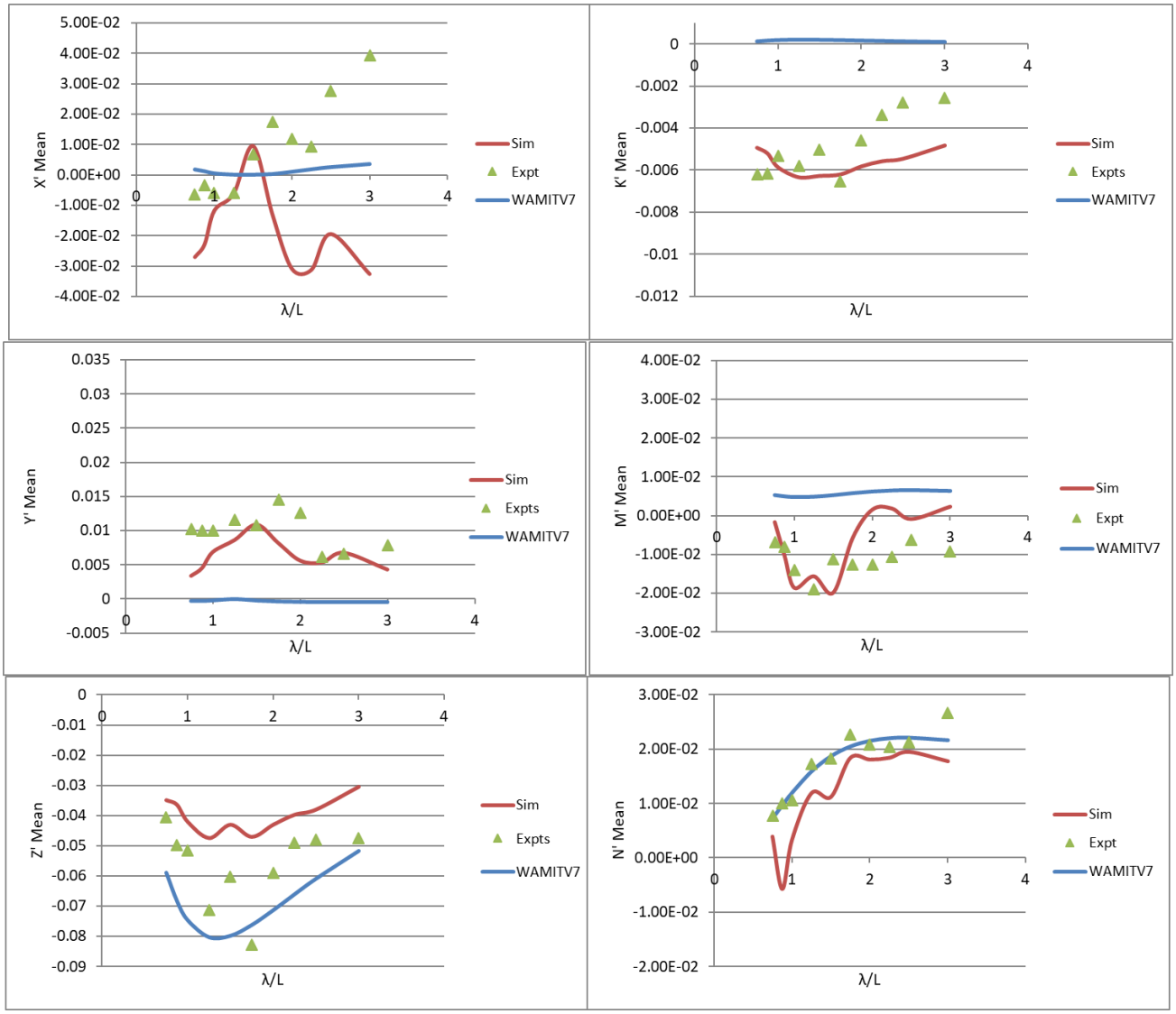

Figure 22: Mean forces in regular waves, 150 degrees heading (F_r=0.0)

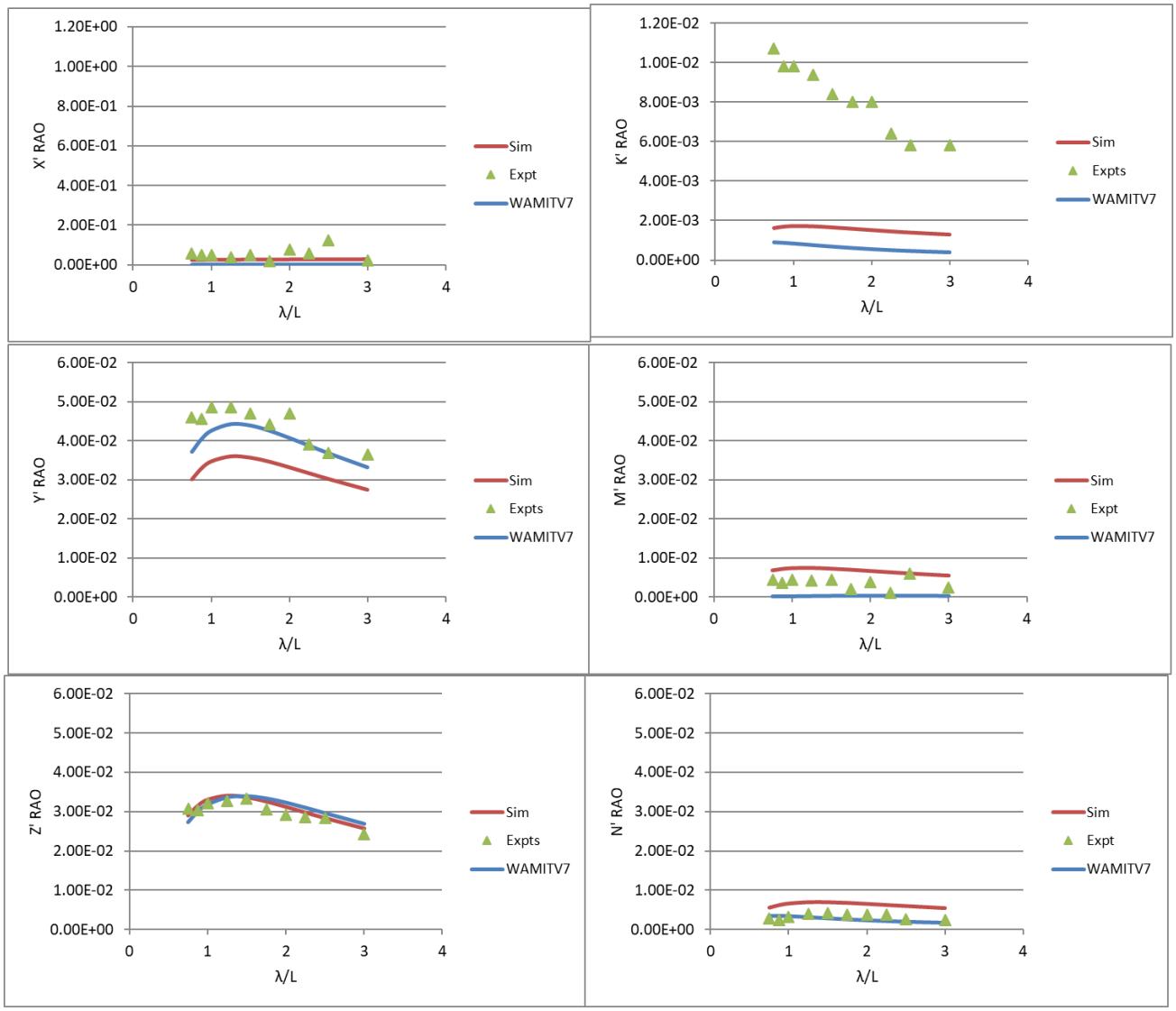

Figure 23: First order forces in regular beam waves (F_r=0.0)

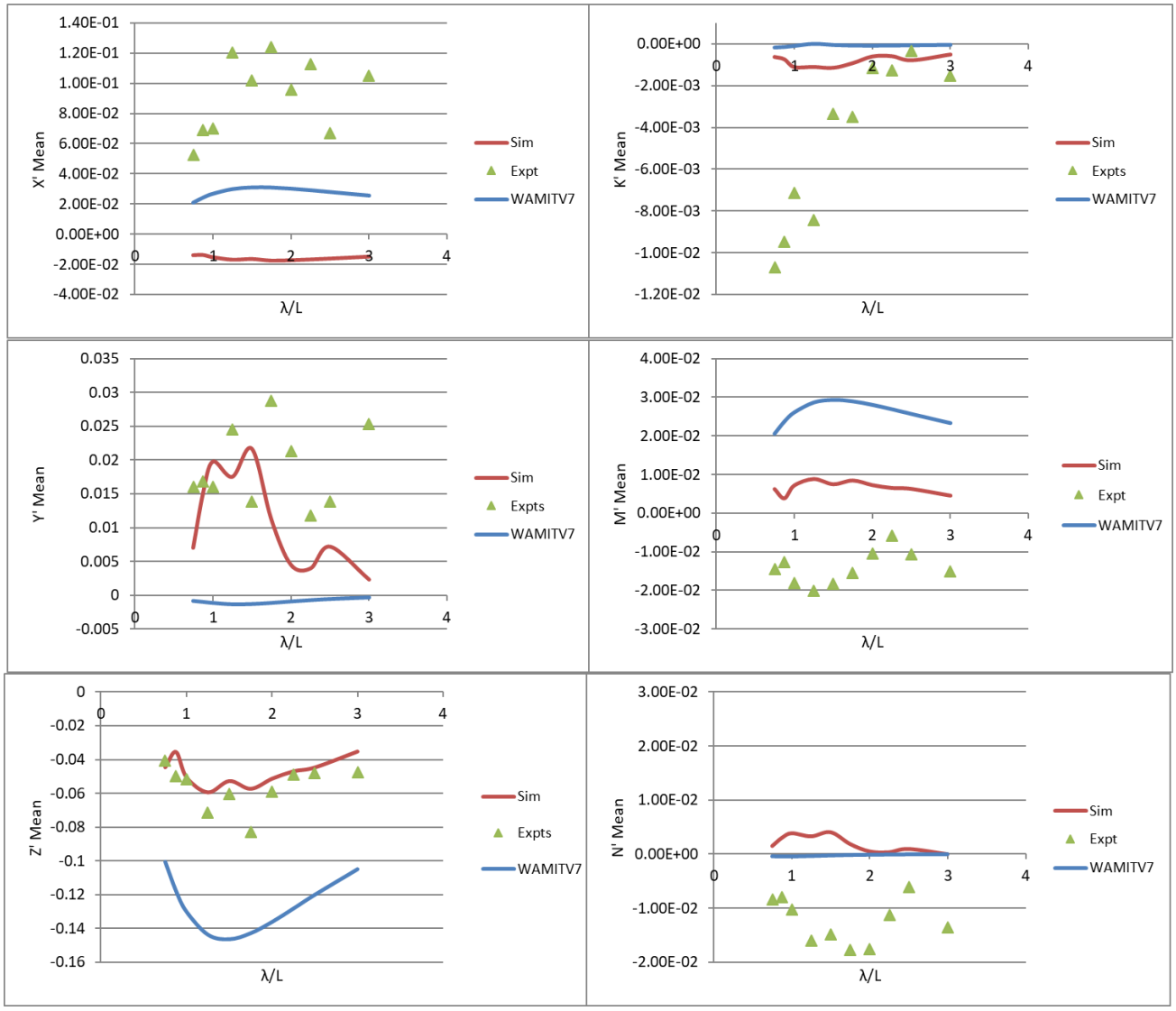

Figure 24: Mean forces in regular beam waves (F_r=0.0)

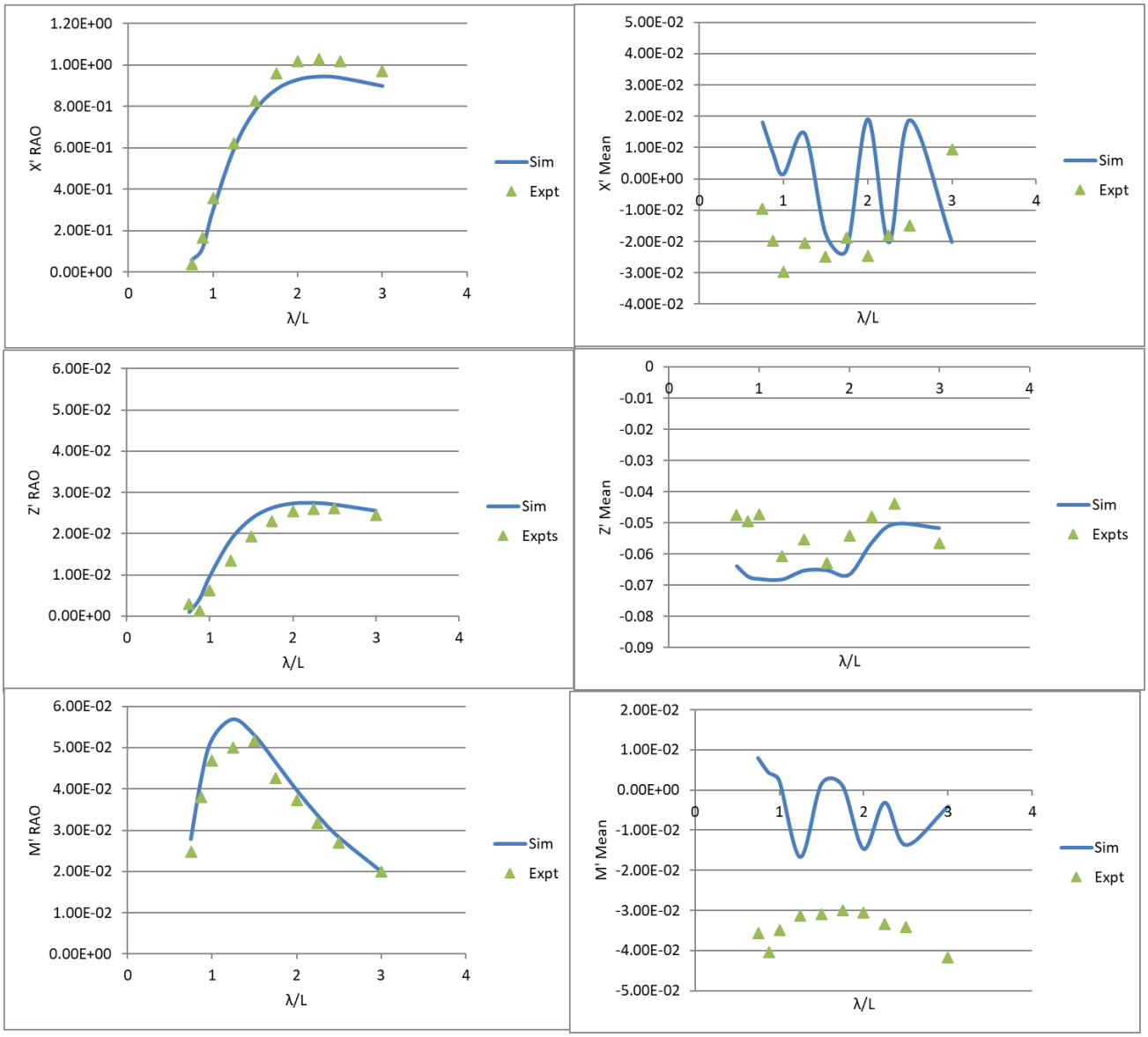

(a) First order (b) Mean force

Figure 25: First order and mean forces in regular head waves (F_r=0.2)

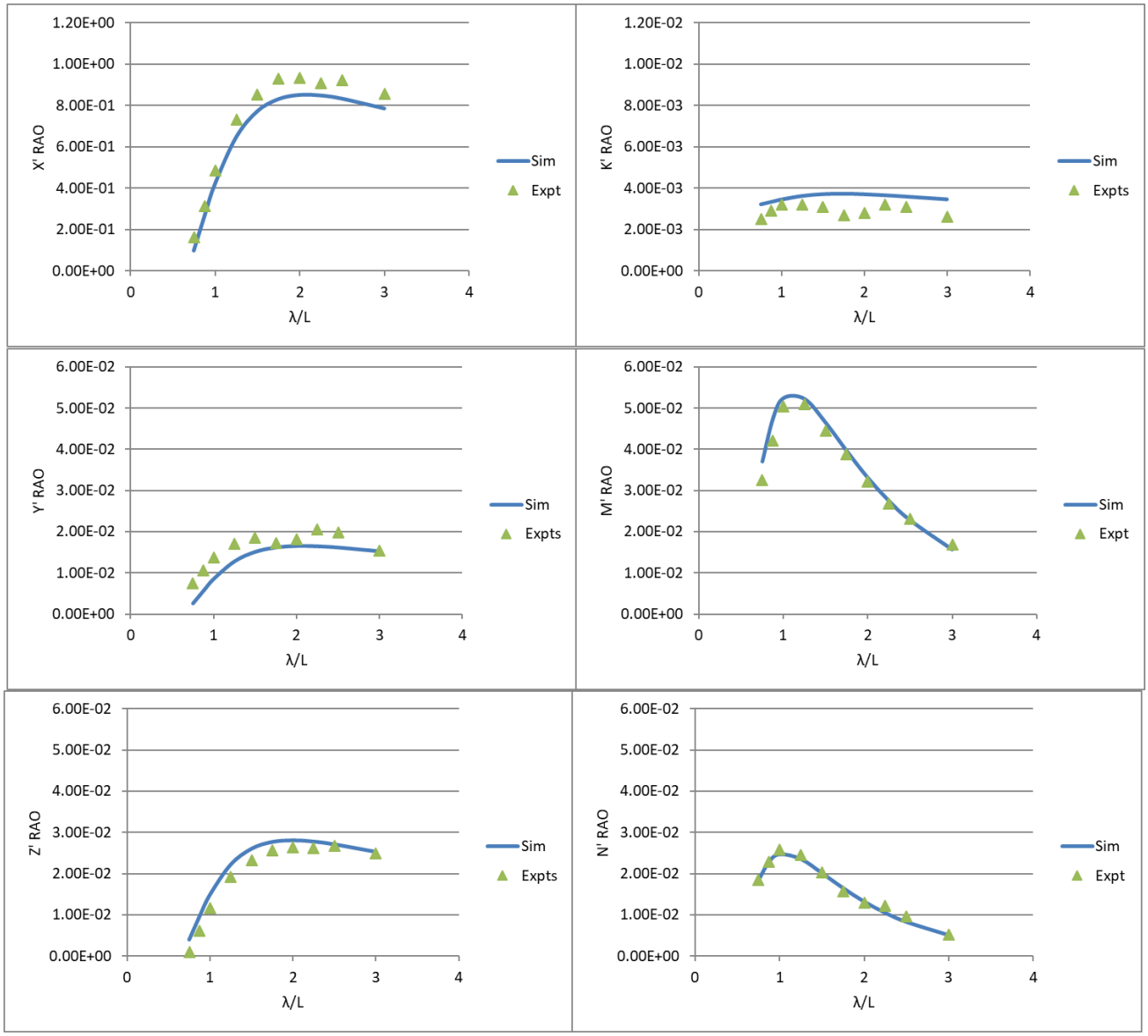

Figure 26: First order forces in regular waves, 150 degrees heading (F_r=0.2)

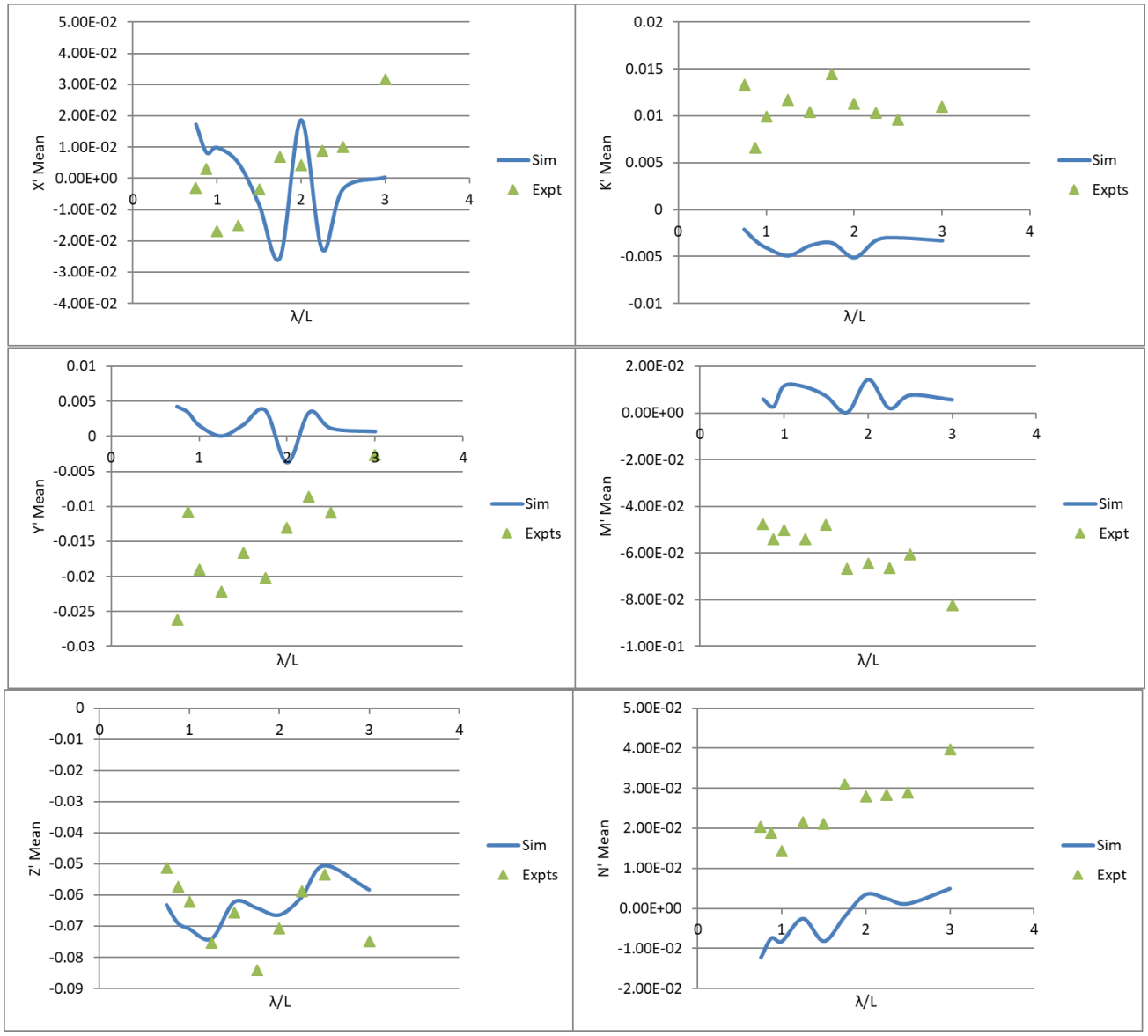

Figure 27: Mean forces in regular waves, 150 degrees heading (F_r=0.2)

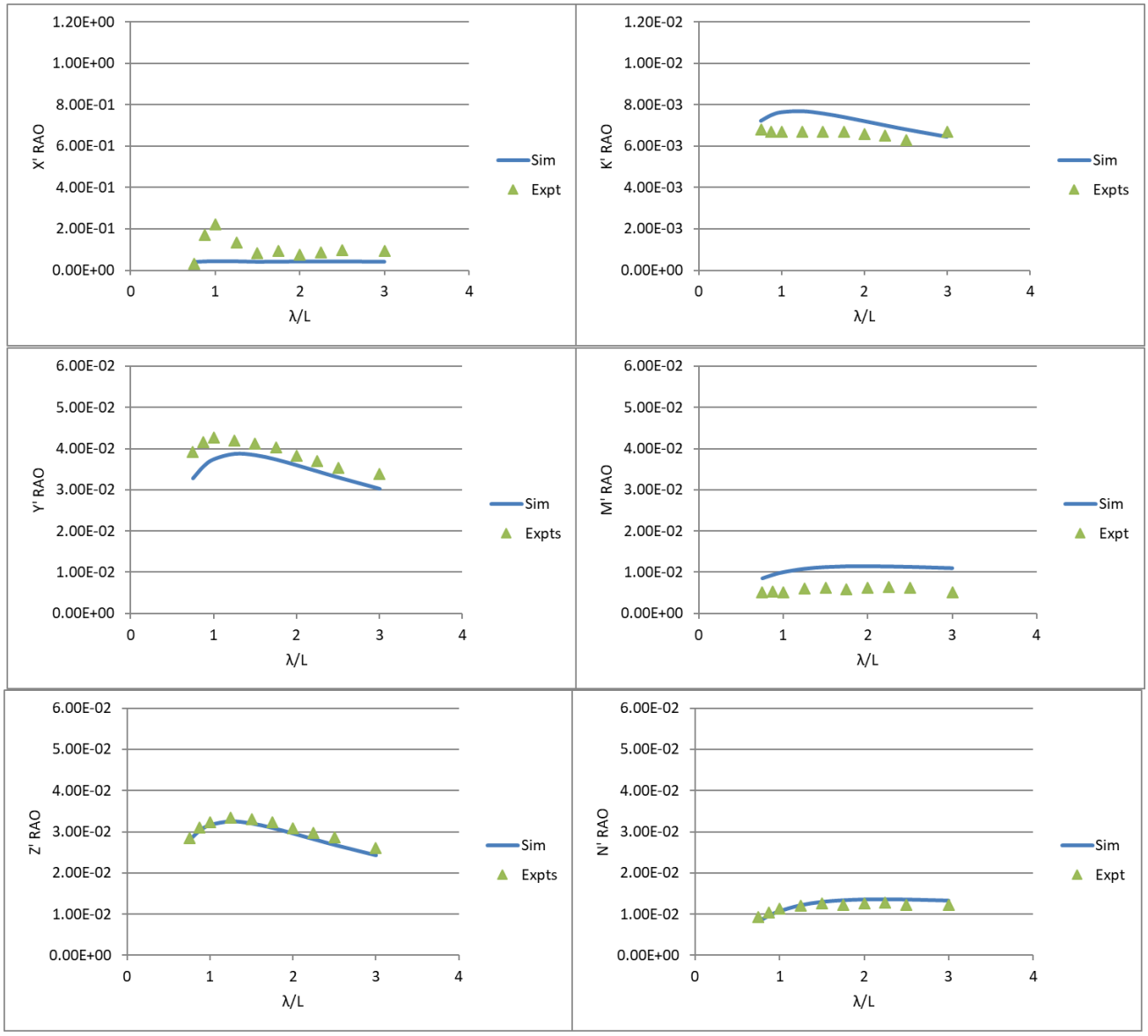

Figure 28: First order forces in regular waves, 90 degrees heading (F_r=0.2)

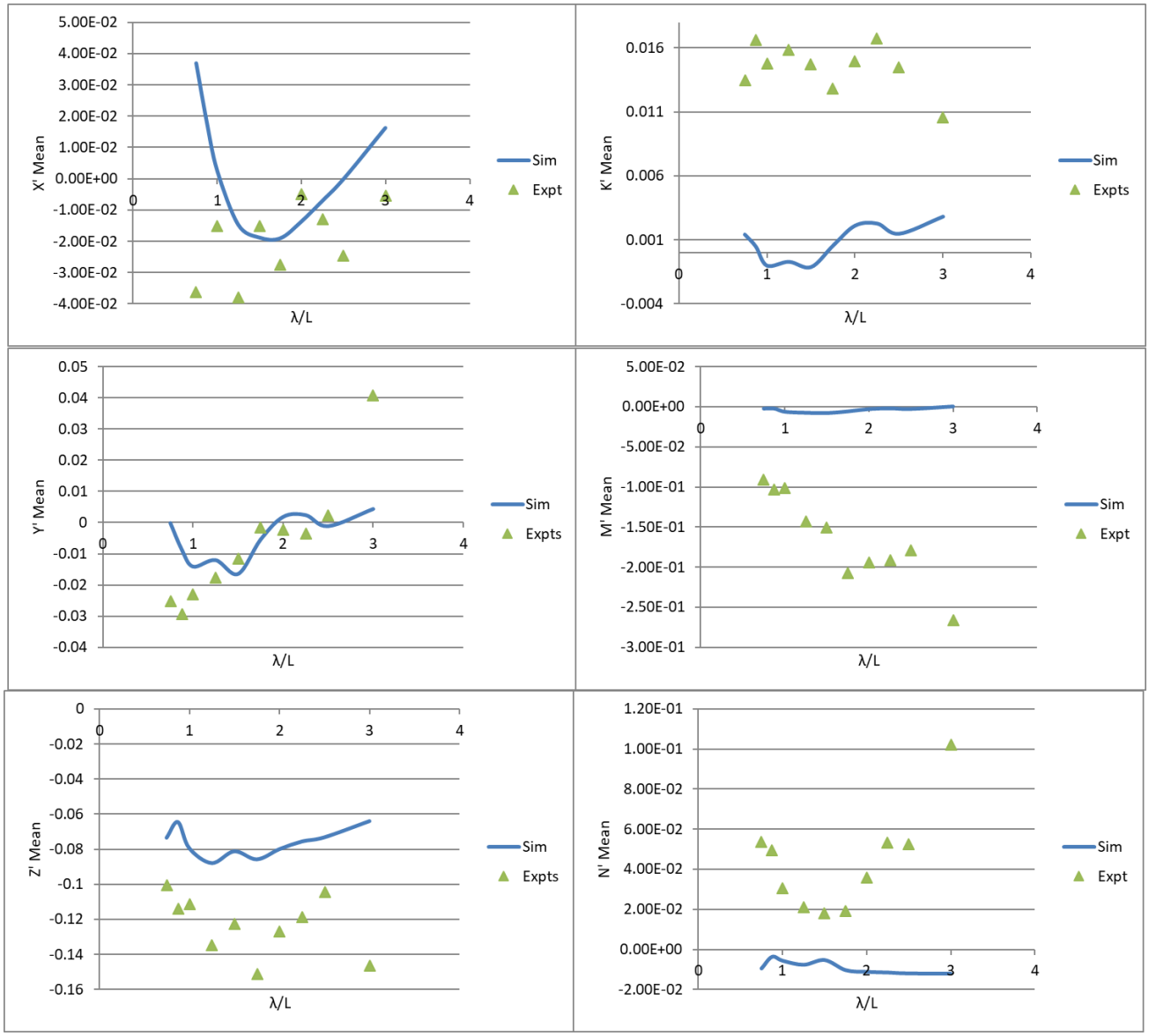

Figure 29: Mean forces in regular waves, 90 degrees heading (F_r=0.2)

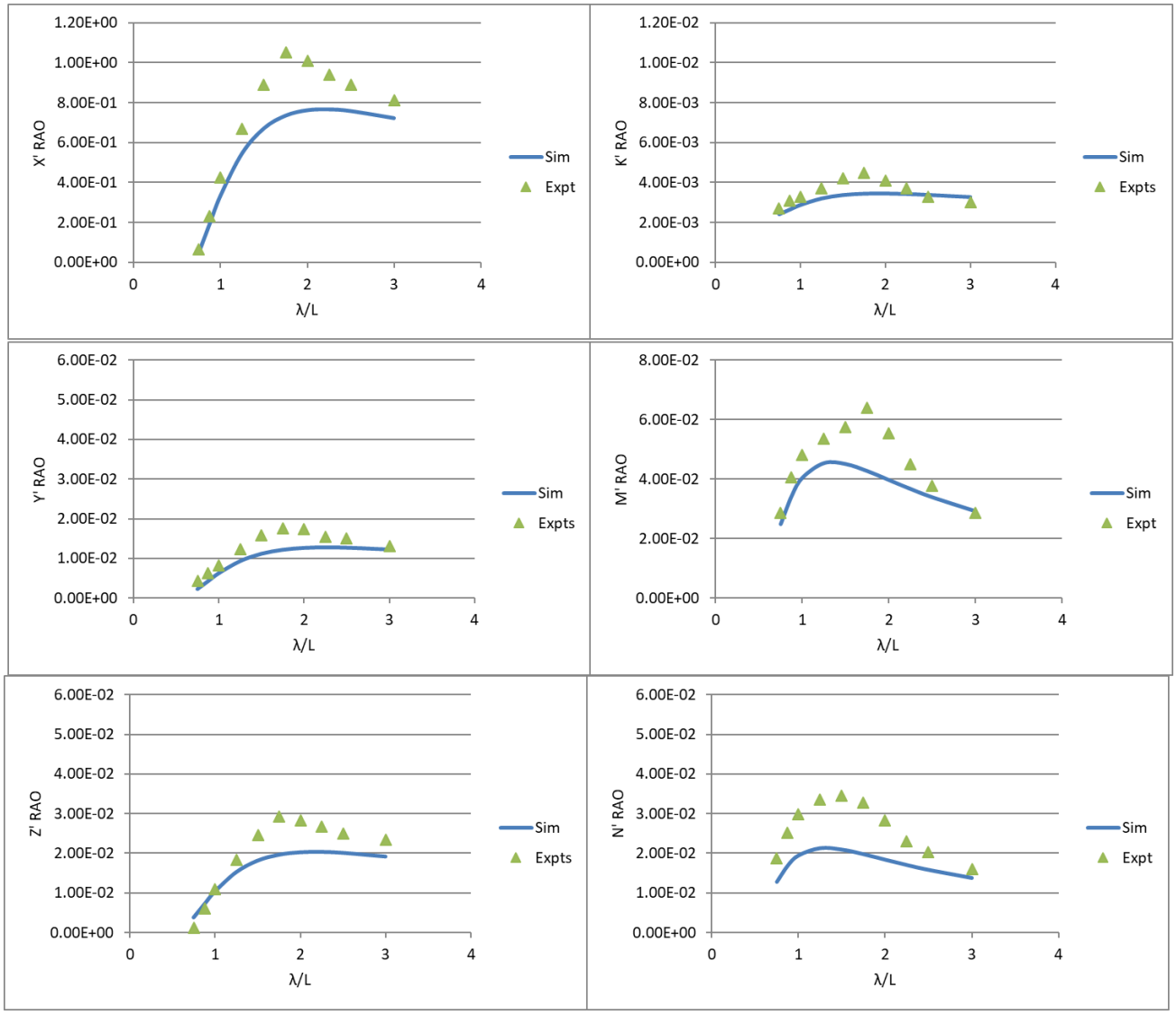

Figure 30: First order forces in regular waves, 30 degrees heading (F_r=0.2)

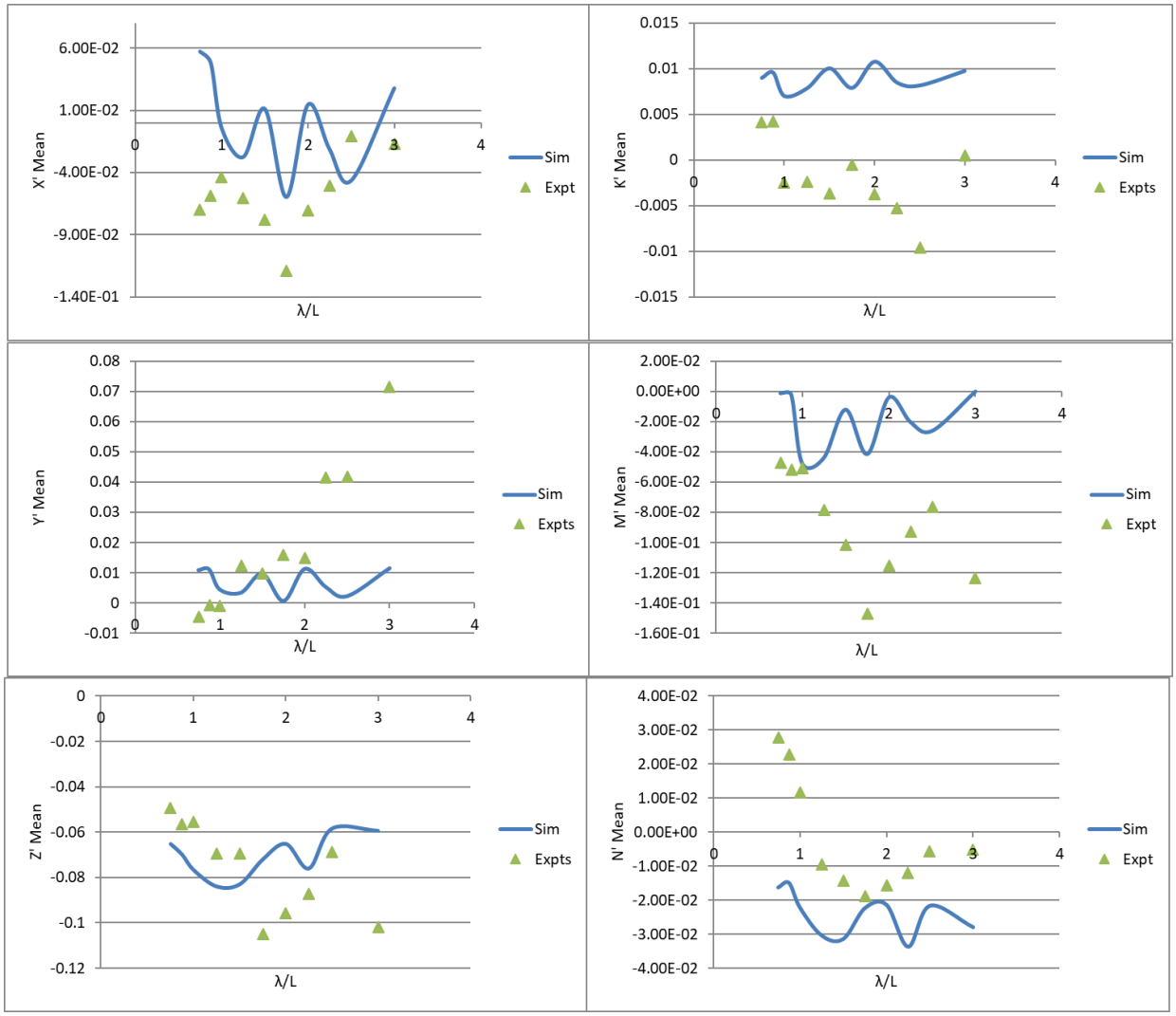

Figure 31: Mean forces in regular waves, 30 degrees heading (F_r=0.2)

2.8.3 Forces due to body motion

As mentioned in section 2.3, the approach adopted in this thesis, is to assume that the wave forces can be considered separately from the slowly varying manoeuvring forces. In such a case, the whole problem can be quantified as a linear combination of the forces and moments due to calm water manoeuvring and the forces and moments due to the waves. One of the issues with this assumption is how to separate the forces and moments due to body motion at the frequency of the waves, considered as the added mass and damping of the body, and the forces and moments due to the slowly varying motion quantified as part of the hydrodynamic derivatives that also includes added mass and damping contributions in Eqns.8 to 12. The following provides a comparison between the heave force due to body motion obtain from extrapolating the slowly varying derivatives to typical wave frequencies and added mass and damping coefficients obtained using WAMIT.

For only heave motion, the heave force (at zero speed) is a simplified form of Eqn 8 and presented in dimensional form as:

$$Z_{heave} = \frac{1}{2}\rho l^2\left(Z'_{wv} w \quad v \quad + Z'_{|wv|}\left|w \quad v \quad\right|\right) + \frac{1}{2}\rho l^3 (m' - Z'_{\dot{w}})\dot{w}$$

66

where m' is the non-dimensional mass of the body (this term has been included in the context of the following discussion).

and $v = \sqrt{(v^2 + w^2)}$

For the simplified case of motion only in the vertical plane, then $v = \sqrt{(w^2)} = |w|$ and Eqn 66 can be simplified to

$$Z_{heave} = \frac{1}{2}\rho l^2 \left(Z'_{w|w|} w|w| + Z'_{|w|w||}\left|w|w|\right|\right) + \frac{1}{2}\rho l^3 (m' - Z'_{\dot{w}})\dot{w}$$

67

If the heave motion in waves is given as $\xi_3 = \xi_{30}\sin\omega t$, then

$$w = \xi_{30}\omega cos\omega t$$

And

$$\dot{w} = -\xi_{30}\omega^2 sin\omega t$$

which can be substituted into Eqn 67 to obtain:

$$Z_{heave} = \frac{1}{2}\rho l^2 \left((\xi_{30}\omega)^{\,2} Z'_{w|w|} cos\omega t|cos\omega t| + (\xi_{30}\omega)^{\,2} Z'_{|w|w||}\left|cos\omega t|cos\omega t|\right|\right) - \left(\frac{1}{2}\rho l^3\omega^2 (m' - Z'_{\dot{w}})\xi_{30} sin\omega t\right)$$

which, to first order in w, in heave amplitude, can be approximated to:

$$Z_{heave} \approx -\left(\frac{1}{2}\rho l^3\omega^2 (m' - Z'_{\dot{w}})\xi_{30} sin\omega t\right)$$

68

Alternatively, from frequency domain analysis, the complex amplitudes of the heave motion ξ_3 can be obtained from the solution of the following, obtained by applying Newton's Law. The frequency dependent heave force due to body motion, in dimensional form, is:

$$F_3 = \left(-\omega^2\left(m + A_{33}(\omega)\right) + i\omega B_{33}(\omega)\right)\xi_3$$

69

where A and B are the frequency dependent, dimensionalised, added mass and damping coefficients respectively. So, Eqn 69 is the heave force on the submarine obtained from the first order approximation, in w of the hydrodynamic derivatives and Eqn 70 is the heave force on the body derived from linear frequency domain analysis.

Figure 32 shows the forces calculated in accordance with Eqns 69 and 70 for the EUCLID geometry. The heave force in Eqn 69 is obtained from the use of the relevant derivative in Appendix C2; the heave force in Eqn70 is derived using WAMIT predictions of A_{33} and B_{33}. For both methods, the amplitude of the sinusoidal heave force, in response to a sinusoidal input, has been non dimensionalised in a common way as follows:

$$F'_{30} = \frac{|F_{30}|}{\frac{1}{2}\rho l^3 \omega^2 \xi_{30}}$$

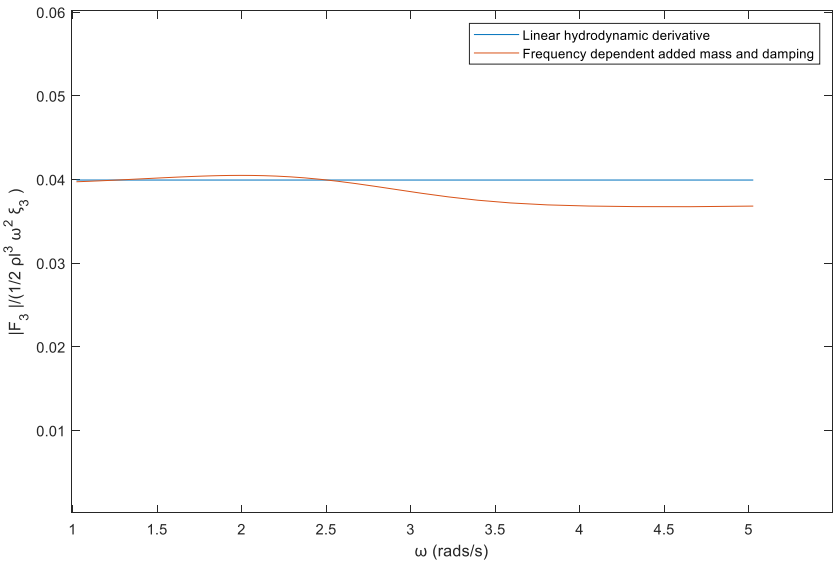

Figure 32: Magnitude of the non-dimensional heave force amplitude on the EUCLID geometry.

Figure 32 shows that the non-dimensional heave force does exhibit some frequency dependency at frequencies above 2.5 rad/s, this is clearly not captured by a single derivative. The differences in the two approaches are around 8% at the highest frequencies. The heave force due to body motion is at the lower frequencies are similar in both approaches suggesting the force is dominated by the mass of the body at these frequencies .

This suggests that for the problem of a submarine under waves, the added mass and damping contributions to the heave force can be considered to be frequency independent. Furthermore, through linear superposition , the Froude-Krylov and diffraction forces can be calculated separately from the body induced forces that are obtained from the hydrodynamic derivatives.

2.9 Fully restrained appended submarine in bichromatic head waves

As discussed in section 2.5.2, the second order wave forces induce low frequency drift oscillations and slowly varying heave, pitch and roll oscillations in large-volume structures such as semi-submersible offshore platforms. In order to determine a cost-effective solution for design evaluation, Matos *et al,* [2011] presented a number of different options for modelling the second order forces and induced motions on a large volume semi-submersible using WAMIT®, Lee, [1995]. In the case of Matos *et al,* [2011), different hydrodynamic approximations were considered by directly comparing the predicted responses with measured data.

In the case of the EUCLID 10.17 hull form, there are no experimental data available from fully captive model tests in bichromatic waves. So, in first instance, for the zero speed case, QTF predictions are made of the force responses for the case of the EUCLID 10.17, [Cooper, 2007], submarine (fully restrained) at PD under the influence of regular and bichromatic head waves using the commercially available frequency domain software WAMIT®, Lee, [1995]. The aim, of performing this comparison, is to repeat the work of the Matos *et al,* [2011], to help understand the validity of a number of simplifications that can be made to the calculations when applied to the problem of a submarine operating under waves.

WAMIT is a radiation/diffraction program developed for the analysis of the interaction of surface waves with offshore structures. It is a zero speed three-dimensional panel method following the theory summarized by [Lee and Newman, 2004]. The bodies may be located on the free surface, submerged, or mounted on the sea bottom. In WAMITV7, the free-surface condition is linearised, however, there is a derivative of WAMIT (WAMITV6.4S) that was developed for the extended analysis of the second order potential theory for bichromatic and bi-directional waves, including the

sum and difference components. It is these second-order effects that may be significant in predicting the behaviour of a submarine under waves.

WAMITV6.4S computes the Quadratic Transfer Functions based on solving the boundary integral equations using free surface Green functions, Lee and Newman [2004]. However, this could require significant computational effort; Matos *et al,* [2011], looked at a number of approximations based on simplifications in the calculation of the QTFs and simplifications based on the dynamics of the platform under consideration.

For the purpose of understanding the validity of the simplifications made by Matos *et al,* [2011] when applied to the problem of a submarine operating under waves, QTFs are presented as contour plots. In this case, the first frequency (ω_1 – converted to wavelength and non-dimensionalised as λ_1/L) on the x-axis and the second frequency (ω_2 – converted to wavelength and non-dimensionalised as λ_2/L) on the y-axis. The colour of the contour represents the non-dimensional heave force or pitch moment, respectively as:

$$X' = \frac{X}{\rho g L \zeta_1 \zeta_2} \; Z' = \frac{Z}{\rho g L \zeta_1 \zeta_2} \text{ and } \; M' = \frac{M}{\rho g L^2 \zeta_1 \zeta_2}$$

70

Where ζ_1 and ζ_2 are the amplitudes of the first and second regular wave respectively.

The following approximations made by Matos *et al*, [2011] applied to the problem of the fixed submarine body under waves were considered:

QTF without the contribution of the second order total velocity potential

WAMIT permits the user to calculate the QTFs without including Contribution V, Eqn 32, in the breakdown by Pinkster, [1981]; thus neglecting the contribution of the second order total velocity potential; this approximation means that only the first order potentials need to be determined.

Figure 33 shows the second order forces on the EUCLID 10.17 hull form (non-dimensionalised according to Eqn 71 in bichromatic waves computed using WAMIT by solving for the second-order potential including the second order free surface integral (Figure 33b) compared with the second order forces neglecting the contribution of the second order potential (Figure 33a). The QTFs are symmetrical about the $\lambda_1 = \lambda_2$ line which corresponds to the mean forces obtained from regular waves and whose values are the same for both methods. This symmetry property (since $P_{ij} = P_{ji}$

and $Q_{ij} = Q_{ji}$ for $\neq j$) allows for a convenient way of comparing the results from two different methods on the same plot.

Figure 34 shows the (a) non-dimensional heave force and (b) non-dimensional pitch moment computed using WAMIT by solving the full second-order problem including the second order free surface (section of the contour plot below $\lambda_1 = \lambda_2$ line) compared with the second order force neglecting the contribution of the second order potential (section above $\lambda_1 = \lambda_2$ line).

A 2D slice through the QTF has been taken, in Figure 34, by constructing a line where $\omega_1 - \omega_2$ is constant, that intersects the peak in the predicted second order forces (for the case where the 2nd order potential is included). The heave force and pitch moment along this line (and the equivalent where the 2nd order potential is not included) can be plotted on a Cartesian coordinate system (also in Figure 34) which clearly shows that the peaks in both heave force and pitch moment are lower when excluding the 2nd order potential in the overall determination of the second order forces. This suggests that, for the case of a submarine under waves, the contribution of the second order potential to the second order force cannot be neglected.

QTF without free surface forcing terms

This simplification involved solving the second order problem without evaluating the free surface integral, which means that the second order potential in Eqn 25 was simplified to:

$$\frac{\partial^2 \phi^{(2)}}{\partial t^2} + g \frac{\partial \phi^{(2)}}{\partial z} = 0 \text{ for z=0}$$

If the free surface approximation is valid then there would be no requirement to discretise the free surface making the calculation of the second order potential faster . Matos *et al,* [2011] concluded that, for their particular application, the effect of excluding the free surface forcing term, defined by the free surface integral, was insignificant . Figure 35 shows Z' computed using WAMIT by solving the full second-order problem including the second order free surface forcing term (below $\lambda_1 = \lambda_2$ line) compared with neglecting the free surface forcing term (above $\lambda_1 = \lambda_2$ line); in this case the frequency range has been chosen around the peaks in the second order forces. It appeared that, in this case, the inclusion of the second order free surface boundary condition has little influence on the overall results for heave force over this frequency range.

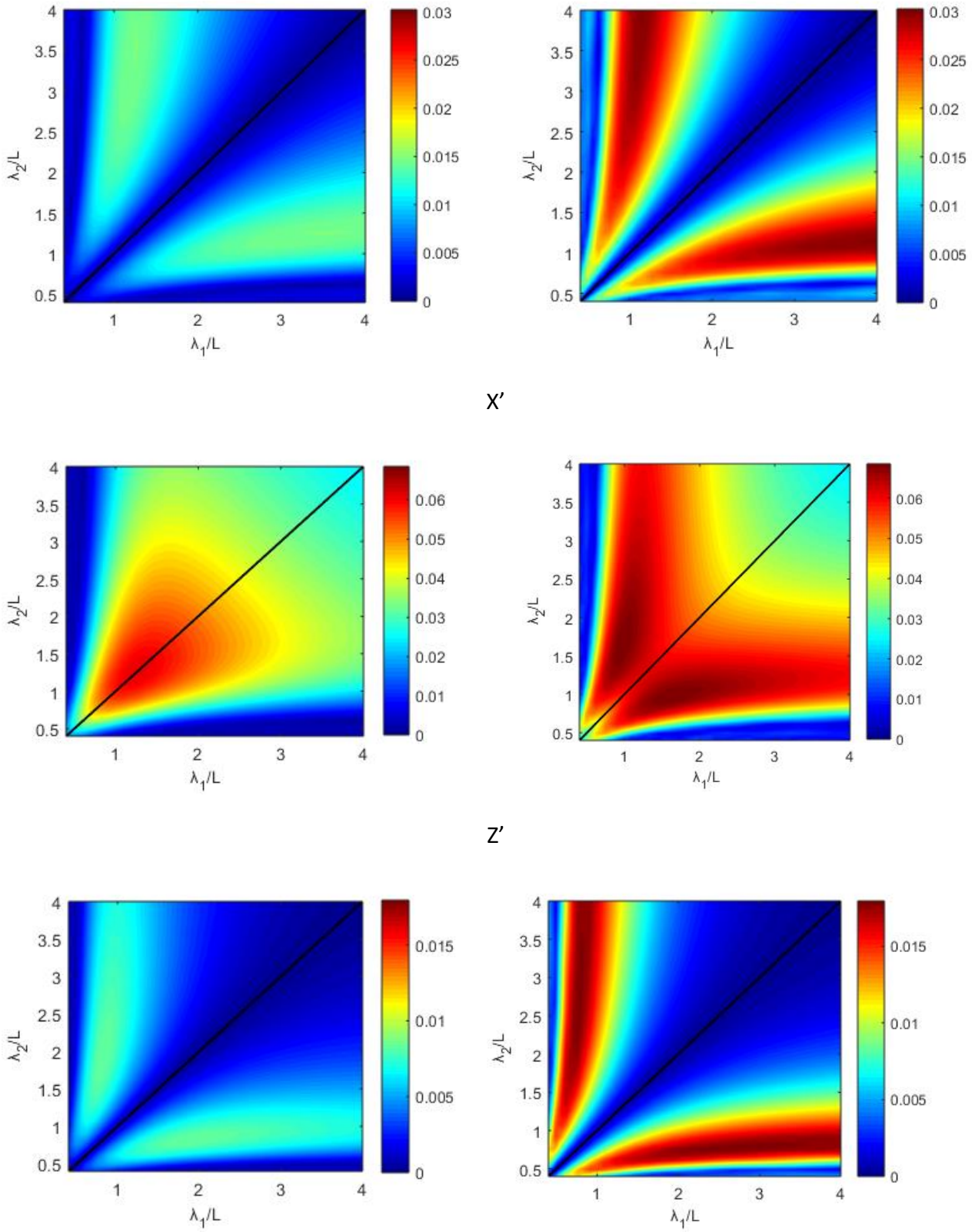

(a) Excluding Second order potential (b) Including second order potential

Figure 33: WAMIT predictions of second order forces on Euclid 10.17 hull in head waves

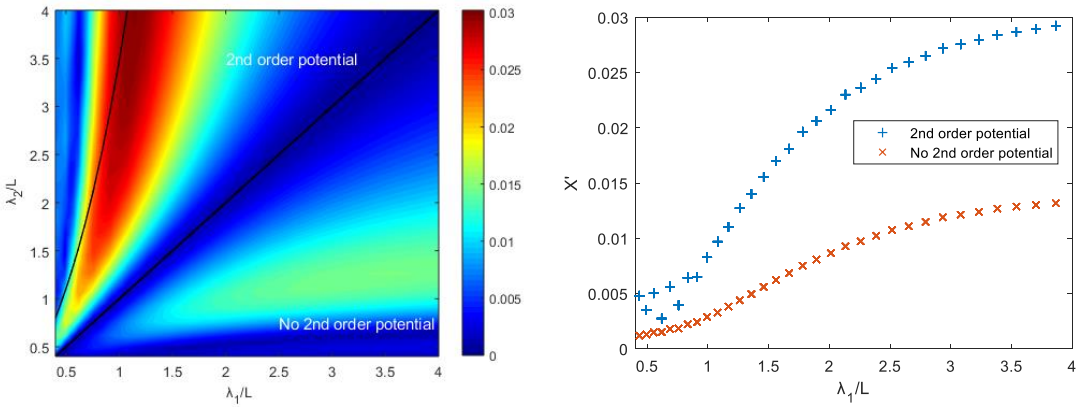

X’

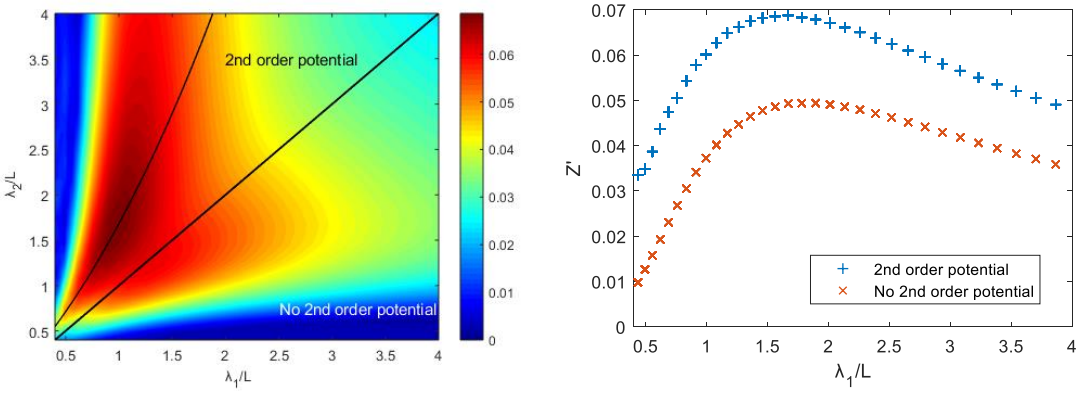

Z’

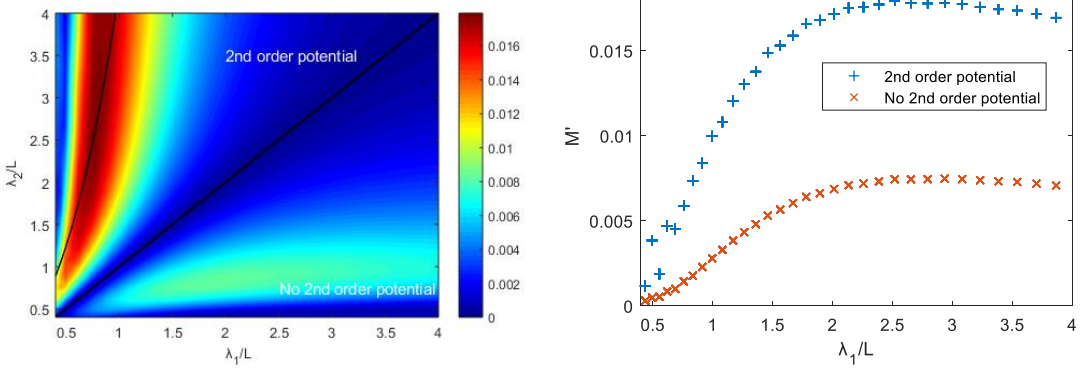

M’

Figure 34: Effect of second order total velocity potential on forces on Euclid 10.17 hull in head waves

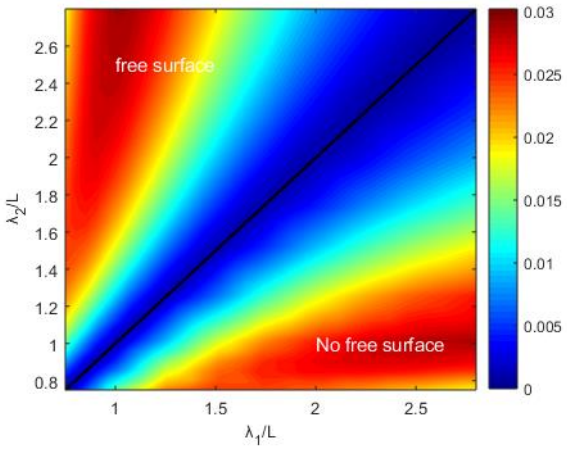

X’

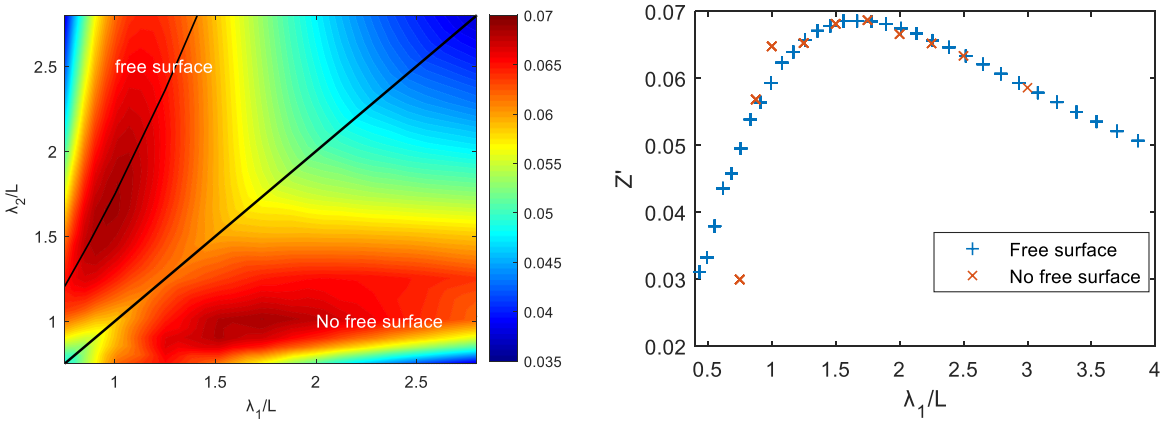

Z’

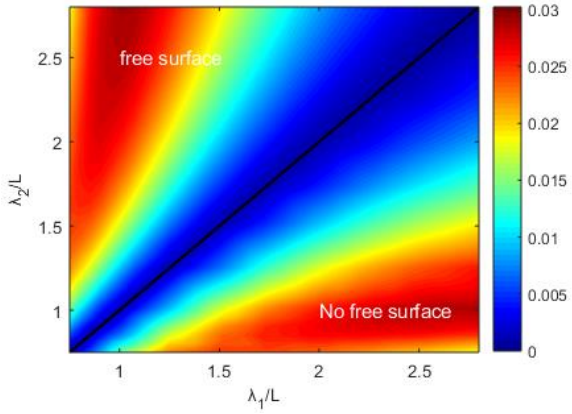

M’

Figure 35: Effect of including free surface forcing term boundary condition on second order forces on Euclid 10.17 hull in head waves

Newman's approximation

The approximation developed by [Newman, 1974], and given in Eqn 24, is used for modelling the slow drift problem for floating vessels, [Faltinsen and Loken, 1979] for example. In this case, this approximation was shown to be a practicable way of calculating the slowly varying drift forces on a surface ship. As a consequence of this finding the slowly varying drift forces can be calculated from results of numerical simulations, or model tests, in regular waves, which avoids the need to calculate, and/or perform model tests, for a great number of pairs of frequency combinations; the mean drift force coming from computations or model tests in regular waves. Matos *et al*, [2011] cautioned using Newman's approximation for vertical plane motions of the semi-submersible, largely due to the considerably lower natural periods of heave, roll and pitch (typically 20 – 80s) compared to the natural periods of drift (generally above 100s). There is no explicit assumption in Newman's approximation that is related to the natural period of the vessel. However, for the approximation to be valid the exact quadratic transfer function must have be "flat" over the difference frequency range of interest, [Aranha and Fernandes, 1995]; flat in this context means that: $\frac{\partial S_F}{\partial \Omega} = 0 \; for \quad \Omega = 0$).

where

S_F is the low-frequency force spectrum

Ω is the difference between two frequency pairs

This condition of the exact quadratic transfer function is based on the assumption that the difference in the two wave frequencies is small which is the case for the practical applications in offshore floating bodies described by [Aranha and Fernandes, 1995].

For the current application, it is clear from Figure 35 that $\frac{\partial S_F}{\partial \Omega} \neq 0 \; for \quad \Omega = 0$ and in this case, applying the Newman approximation would result in under predicting the second order slowly varying drift forces. It is conjectured that since there is no restoring force, due to buoyancy, for the submarine at periscope depth (unlike the buoyancy in offshore floating bodies), the submarine is more sensitive to the slowly varying drift force over a wider range of frequency differences.

[Aranha and Fernandes, 1995], $\mu \cong 0.1$ or smaller in their application, which confirms the observation made by [Matos *et al*, 2011].Figure 36 compares the WAMIT predictions of second order Z' (including 2nd order potential and inhomogeneous free surface boundary condition) with

that derived using the Newman approximation (Eqn 24) – the figure shows the contour plot (along the same lines as previous examples) and the same data plotted for the case where $\omega_1 - \omega_2$ is constant. It can be seen from the combined contour plot that Newman's approximation to the exact QTF is valid when the frequency difference is close to zero ($\omega_1 \cong \omega_2$) . However, once the frequency difference increases (see the example of the slice through the contour plot where $\omega_1 - \omega_2$ is constant), there is a peak in the force response that is predicted at frequencies away from $\omega_1 = \omega_2$, then Newman's approximation leads to an under prediction of the quadratic transfer functions. Hence, since for the case of the submarine under waves there are more significant resonant frequencies away from where $\omega_1 = \omega_2$, Newman's approximation can only be considered to be an approximation without sufficient accuracy.

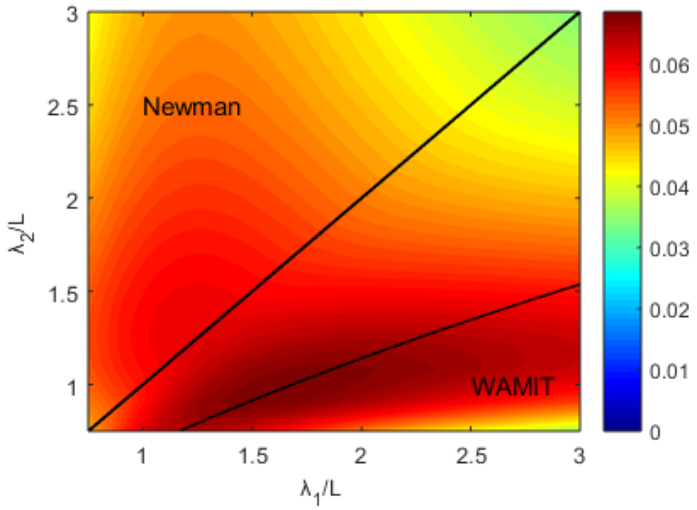

Combined contour

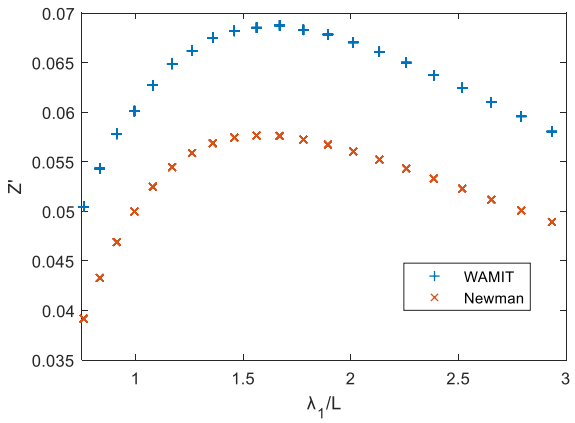

$\omega_1 - \omega_2 = const$

Figure 36: Combined second order Z' from WAMIT and Newman's approximation on Euclid 10.17

Figure 37 shows the same WAMIT calculation, including the second order potential, of the non-dimensional heave force Z' for zero speed in head waves shown in Figure 33; Figure 37 shows the WAMIT calculations over a smaller frequency range. However, in the case of Figure 37, the WAMIT calculations are now compared to the time domain calculations for the same conditions. There are multiple values for each location on the x-axis due to there being multiple values for λ_2/L for a single λ_1/L.

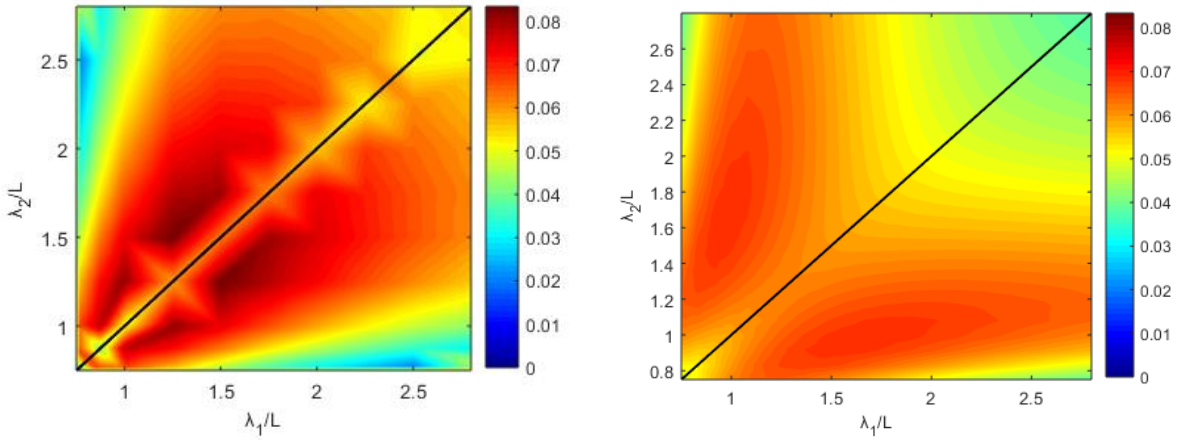

(a) Time domain simulation (b) WAMIT

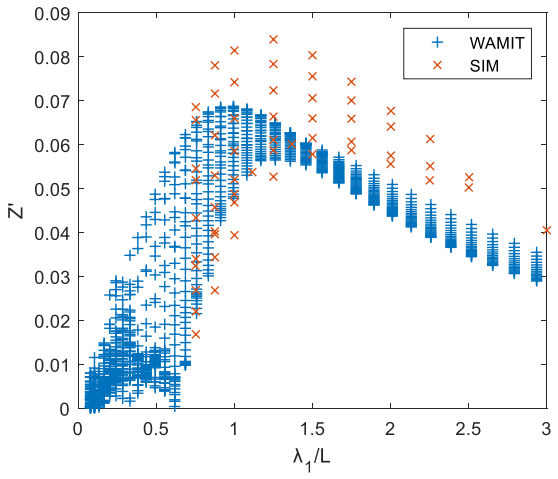

(c) Cartesian axes plot

Figure 37: Comparison of second order Z' on Euclid 10.17 hull in head waves (F_r=0.0)

The contour and Cartesian plots show that the peak Z' obtained from the time domain simulations can be up to 28% higher than those from WAMIT – although the frequency around which the peak Z' occurs, in the time domain simulations, is similar to WAMIT. The impact of an over-prediction of the second order transfer functions would lead to estimates of the second order forces on the submarine to be also over-estimated which could lead to over designing the compensation system to counter the suction effects.

As a consequence of the assumptions in the method developed in this thesis, the time domain approach is considered to be an approximation to the theory used in WAMIT. However, Chapter 3 describes a series of experiments, including tests in bichromatic waves, that will provide an insight into the quality of the time domain predictions.

2.10 Chapter summary

In this chapter, existing hydrodynamic theories are evaluated; a time domain computational approach is described and developed in this thesis, which is based on the extension and refinement of a rational combination of these existing theoretical methods, to predict the first and second order forces on a fully appended submarine with forward speed. The extension and refinements made to develop the time domain approach is to include semi-empirical components to account for viscous effects due to flow separation on the submarine body and to include non-linear effects, such as stall, on the submarine appendages. The Hess and Smith approach was re-cast to determine the pressure on a body discretised using triangular elements in an attempt to minimise leakage between non-coincident adjacent panels. Finally, this time domain code of the wave induced forces and moments on a submarine body can be readily interfaced with a coefficient based non-linear manoeuvring simulation.

The result of the theory has been compared against analytic solutions for simple affine forms and against existing data from experiments using a restrained fully appended model of a generic SSK type submarine design.

As part of the contribution to the field, the candidate has drawn upon the extensive work undertaken in the field of ocean engineering in the development of experimental and numerical techniques for evaluating the second order effects on large floating structures and considered these approaches to the current problem. These techniques give clear guidance on how to quantify second order effects both experimentally and numerically that can be applied to the problem of a submarine operating under waves.

For the zero speed case, frequency domain predictions using the commercial-off-the-shelf software WAMIT have been included as a comparison with the time domain code. For the zero speed case, frequency domain predictions have demonstrated that consideration of the second order potential when including the body boundary condition is significant in the determination of the QTFs of the vertical plane second order force and moment. However, for the submergence depth and frequency range considered in this thesis, it does not seem necessary to include the inhomogeneous terms in the free surface boundary condition of the second order potential for determining the QTFs. For the case considered in this chapter, as expected, Newman's approximation does not replicate, accurately, the QTFs for large frequency differences. However, numerical predictions of QTFs show that there are peaks in the 2^{nd} order force that occur at large frequency differences (away from mean values or the case where the frequency difference is zero); The approximation may be sufficient for use in early system design studies in establishing sizes of hover tanks and pump capacities for example. However, there is a possibility using such an approach could lead to such systems having insufficient capacity to deal with the slowly varying forces entirely.

Previously generated data, Martinussen, [2006], obtained from regular wave tests on the EUCLID 10.17 design were used for comparison with the time domain and frequency domain predictions (zero speed only). In general first order forces and moments were predicted well by both time domain and frequency domain methods with the exception of roll moment which appears to be under predicted in both cases which is possibly due to the inviscid approaches neglecting friction effects and the effects of vortices shedding from the hull and appendages. The accuracy of the predictions of mean forces and moments vary considerably with heading in some cases the agreement is good and in other poor. For the forward speed case, the time domain approach appears to capture the first order forces and moments well, including the roll moment. Again, the quality of prediction for the mean forces and moments is mixed. There is probably no single reason why the quality of the results is variable, but it could be attributed to neglecting a number of viscous effects in the numerical model.

For zero speed, time domain prediction of the Quadratic Transfer Functions (QTFs) compare very well with the same calculations from WAMIT; there were no captive model test data available for the EUCLID geometry in bichromatic waves for comparison with predictions.

3. WAVE INDUCED MOTION ON A LIGHTLY RESTRAINED SUBMARINE MODEL AT PERISCOPE DEPTH

3.1 Introduction

The key to understanding the response of a submarine, whilst operating at submergence depths typical of those required undertaking periscope operations, is to be able to reliably predict the wave induced forces and moments on that submarine. The main concern to the designer is to understand how best to accommodate the effects of the suction force (present when a submarine operates near the free surface), which could mean that if the hydroplanes and compensation systems are poorly designed they may be unable to control the submarine in certain wave conditions. A key source of information available to the designer are data from model tests – these data provide the validation evidence for any simulation tool but can also be used to aid in making design choices. In this Chapter, we shall see that whilst the available datasets identified as part of this research form an important part of understanding the problem of the behaviour of the submarine under waves, the data are not entirely suitable for use in making design decisions for a submarine near the free surface. Therefore, to meet this shortfall in publically available data, this chapter describes a series of tests using a lightly restrained model of the EUCLID model in head seas; these tests included regular waves, irregular waves and, for the first time on a fully appended submarine model, bichromatic waves to have in-depth understanding the second order effects on a submarine. The tests are described in a great level of detail to allow the tests to be repeated as an experiment or in simulation.

The review of the literature, undertaken as part of this research, identified some examples of existing data that have then been used to compare with the forces and moments predicted using the simulation capability developed as part of this research. These datasets included analytical solutions, problems with simple parametric shapes, calculations using the frequency domain software WAMIT, or measurements from model tests on the EUCLID hull form. All these datasets considered the case where the body was fully restrained. However, as mentioned, the forces and moments obtained from these types of experiments may not be representative of the complete second order forces and moments on a body that is free to move, Fonseca *et al,* [2011]. This highlights the issue that, whilst data from fully captive tests form an important part of the process for understanding the physics based phenomena that can be used to inform on the development of a new simulation capability, these data can't really be used for design purposes since the measured

forces and moments on a captive body will be different to those forces and moments when a body is free to move.

In order to provide more robust data (that can be used for design purposes or used for comparison with simulations), experiments using lightly restrained models are routinely undertaken to understand second order wave interaction problems, on floating bodies. These include wave drift; these tests usually investigate the horizontal loads on offshore structures rather than the vertical loads on a submerged body. The approaches used for these kinds of tests will be described, in more detail, in Section 3.2 but for example, Aranha et al [2001] performed a series of experiments on a model weathervane ship to measure the second order wave drift forces. The model was towed at a constant speed to represent the current; the oscillatory displacements in the horizontal plane were restrained by three springs where the collective stiffness of these springs was designed to ensure that the natural frequency of the system was well outside the main frequency range of the wave, to which the ship responds.

However, the design of an experimental rig to measure the second order vertical forces on a submerged body at forward speed would adopt the same principle as the approach adopted for surface platforms, by which the restraining system is designed to ensure that the natural frequency is far less than those expected at the wave encounter frequencies.

The research in this thesis adapted the experimental approach used by Driscoll and Musker, [1988], to perform tests on a model of the Euclid hull form using the Ship Tank at QinetiQ Haslar. In these tests, the towing arrangement was modified to include load cells that enabled the second order forces to be measured directly (described in next section) and, based on a recommendation by Driscoll and Musker, the forward tow post was moved further forward to provide greater stiffness in the lateral plane. However, the most significant difference in this current approach, compared to that used previously, was that the run plan included bichromatic waves. These types of tests provided the means, for the first time, to derive the second order transfer functions (or QTFs) of the vertical plane forces on a model of a fully appended submarine, with forward speed, in head waves; while Driscoll and Musker, [1988] only performed tests in regular waves and did not measure forces, and measured only heave and pitch motions.

3.2 Approach to testing for lightly restrained models

As mentioned, Musker et al [1988], included a set of lightly restrained tests on a submarine model as part of their validation studies; the experimental rig design, by Driscoll and Musker, [1988], is

shown in Figure 38. The rig is designed to enable the model to respond to the first order wave induced heave force and pitch moment, but response to the second order heave force and pitch moment is constrained by the use of a soft spring system; the model is fully constrained in the other degrees of freedom. Whilst there is the clear advantage of integrating the forward tow post within the bridge fin, as this would minimise interference effects due to the swords on the body itself, the reference recommended that this towing post should be moved forward to help make the model more directionally stable when in waves.

The model used by Musker et al, [1988] was neutrally buoyant at a keel to calm water surface depth of 1.07m. The motion of the model was determined from two Linear Variable Differential Transformers (LVDTs) measuring the linear displacement of each tow post. The spring assembly was designed to use two compression springs on each tow post to provide the restoring force in the vertical plane.

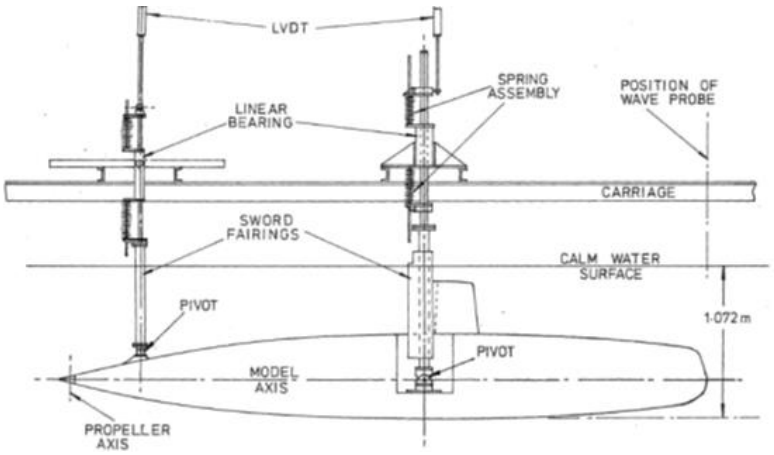

Figure 38: General arrangement of model and carriage, Driscoll and Musker, [1988].

There does not appear to be much readily available literature regarding lightly restrained model tests on submarines in waves so this work reviews the types of existing experimental methods used in both the offshore engineering and surface ship communities to measure second order forces.

Pinkster, [1980] analysed the mean and low frequency second order wave drift forces on stationary moored bodies subjected to waves by developing a three-dimensional linear potential theory; to validate the theory, a series of zero speed model tests were performed using a tanker, semi-submersible, a rectangular barge and a submerged horizontal cylinder in oblique regular waves. The requirement for these experiments was to measure the mean second order drift forces on a free-floating vessel where the mooring system must be such that the first order motions are not significantly influenced by the mooring system itself.

Whilst in the case of Pinkster, [1980], the experiment was designed to measure the horizontal drift force on the submerged cylinder, and not the vertical suction force, the approach in both cases is similar. For the horizontal loads, a soft spring mooring system was used, which, in regular waves , would apply a force on the model that has a constant component equivalent to the mean second order drift force and an oscillating component that is a function of the first order motions and the spring characteristics of the mooring system. Pinkster chose spring constants so that the natural frequency of the mooring system was approximately 5 times lower than the lowest frequencies of the waves to be tested to ensure that that the effect of the mooring system will have negligible effect on the first order motions and hence the mean second order forces.

Pinkster also discussed the choice of where to measure the force in the mooring system to obtain the correct value for the mean second order forces; three positions are possible:

1. A force transducer, fixed to the model, would measure the horizontal component of the mooring line force relative to the body axes,
2. A force transducer located in the mooring line would measure the tension in the line itself
3. A force transducer, fixed to the mooring point, would determine the horizontal drift force relative to an earth-fixed system of axes.

Pinkster chose the third method as the most appropriate means of obtaining the true horizontal drift force but also illustrated that measurements could be in error by only 0.5% if either of the other means of measuring the second order force were used (assuming the amplitude of the angular motions of the model are small < 0.1 rad or 6°).

Dev and Pinkster, [1995] conducted model tests on a semi-submersible that was lightly restrained by a soft mooring system in regular waves at zero speed and with forward velocity to simulate the effect of current; the impact on the test rig design of testing with forward speed appears to be minimal since a very low equivalent Froude number of 0.045 (based on length of model) was considered. The model was held by two horizontal springs located between the model and the force transducer; the force transducer provided the measurements of the second order forces

For experiments that include Froude numbers typical of a submarine operating at periscope depth, this review needs to focus on the surface ship community. A research initiative called Energy Efficient Safe SHip OPERAtions (SHOPERA) was aimed at creating guidelines that will allow ships to meet the Energy Efficiency Design Index (EEDI) requirements without compromising the installed power in the vessel, [SHOPERA website, 2016]. The SHOPERA project looked to develop numerical

and empirical methods for the second order wave induced forces and moments to inform on the simulation of a ship manoeuvring in waves. As part of the studies a number of experiments were conducted to provide validation data for any numerical prediction methods; three hull designs were used, by a number of member tanks, in tests to measure the drift forces in regular waves in deep and shallow water.

To be able to measure the mean drift forces in regular waves, the KVLCC2 model, a Very Large Crude Carrier (VLCC) tanker designed and developed by the Korean Institute of Ship & Ocean Engineering, was restrained using a soft mooring system consisting of four lines arranged in the shape of a diamond in the horizontal plane. The mooring arrangement was designed to ensure that the natural period of the spring/mass system was significantly above (greater than 6 times) the longest wave period. The design of this soft spring system constrained the second order motion, as a consequence of the drift forces, but allowed the model to respond to the first order wave forces in six degrees of freedom. The wave forces were measured by two six-component dynamometers at the attachment points on the mooring lines with additional load cells mounted to each of the mooring lines. Both dynamometers and the load cells can be combined separately to give two different measurements of the surge and sway forces and the yaw moment but this approach allowed for some redundancy in the experimental set-up. The motions were measured using an optical tracking system. This arrangement developed, by CEHIPAR (El Pardo, Spain), allowed the heading, relative to the waves, to be conveniently changed using the facility Planar Motion Mechanism (PMM).

Also as part of the SHOPERA project, a series of tests were performed at the SINTEF Ocean facility in Trondheim (previously MARINTEK) with the Duisburg Test Case (DTC) container vessel. The model was lightly restrained using diamond shaped soft spring arrangement; again the natural period of the spring/mass system was more than 6 times greater than the longest wave period considered in these tests. For these drift tests, the mooring lines were attached to the model and led though low friction pulleys to vertical springs mounted on a transverse beam across the facility carriage. This allowed the model to maintain position, allowing the model to be towed at a constant speed, and to minimise the yaw drift angle (kept within ±2°). A set of force transducers were installed in the aft and forward part of the model, where the mooring lines were attached, to measure the second order forces. The set-up constrained the model to second order surge, sway, and yaw motion whilst allowing it to be free to heave, roll, and pitch.

Lee et al, [2016] conducted model tests on a ship in regular beam waves to create a reliable experimental database for use in validation studies; a mooring system was constructed to measure

the 6 degrees of freedom motion responses of the ship model in both intact and damaged conditions. The mooring system was designed to minimise the effects of the first order responses on the measured results of second order. The connection between the model and springs was designed to allow the model to freely rotate in the horizontal plane.

The required spring constants for the mooring system were estimated by assuming that the surge added mass was 20% of the model mass while the sway added mass was assumed to be 80% of the model mass; the mooring system was designed to have a natural period approximately 5-6 times that of the longest wave period. The mooring forces and moments applied on the model were estimated from the measured tension in the springs; measurements of ship motions were also taken.

Clearly, the design of the towing rig that was used by Driscoll and Musker, 1988 was only suitable for tests in head and following waves (for both zero and modest forward speeds). The rig is suitable for constraining the model in the lateral plane when in head or following seas but is not able to withstand the lateral plane wave induced forces that would occur in oblique wave headings.

Therefore, to undertake lightly restrained tests in oblique seas, preferably with forward speed, would require a different rig design for the submerged case. To develop a solution for a lightly restrained towing rig, based on the use of soft springs, this work considered the features of the test rigs used from both the offshore and surface ship areas. Figure 42 shows an example concept for a test rig, developed, as an early concept, by the candidate and documented in [Morales, 2019], that may be used for measuring the second order forces on a lightly restrained submarine model.

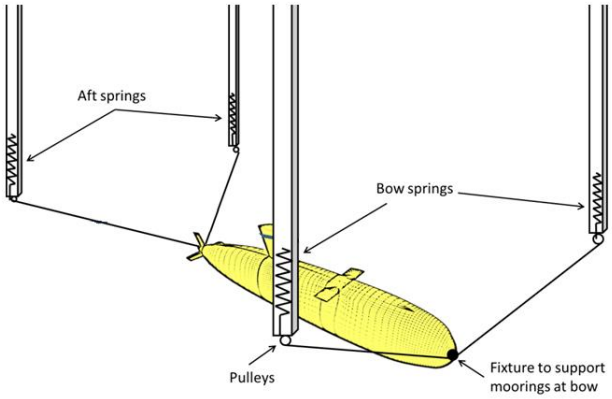

Figure 39: Concept rig for measuring second order forces on a submarine model, [Morales, 2019]

However, a limitation with this design, if the mooring lines are in the horizontal plane (which would be the most appropriate solution to remove any unrepresentative induced pitch moment due to surge motion), is that there would be little in the way of restoring force in the vertical plane due to the mooring lines. Thus, there are two conflicting requirements – a requirement to choose a spring stiffness that means the natural frequency of the spring mass system is at least 5 times less than the lowest wave frequency to be considered in the tests, against a requirement to have sufficient stiffness in the vertical plane to prevent the model from broaching the surface when in waves.

Bowker and Crossland, [2020] successfully employed a model ballast and trim system capability, as described by Crossland and Marchant, [2019], to provide the equivalent restoring force in the vertical plane. The paper by Crossland and Marchant, [2019] describes a ballast and trim system, integrated into a submarine free running model capability, that is able to actively control the weight of the model. This capability has been successful employed to emulate the recovery of a submarine when subjected to flooding. The ballast and trim system consists of two open ended cylinders where each contains an internal piston. The position of this piston is controlled by a stepper motor via a worm and wheel drive which changes the size of the 'dry' volume contained behind the piston. The maximum range of volume for each cylinder is 10.1 litres.

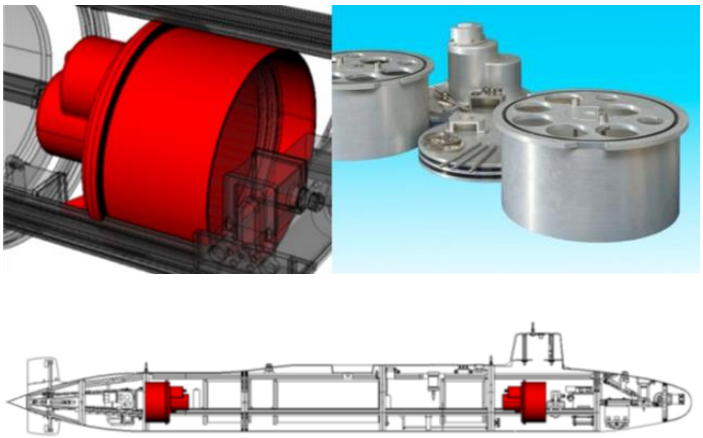

Figure 40: Ballast system components in SRMII, [Crossland and Marchant, 2019]

The innovative solution to minimising the capacity of the stepper motor required to hold or move position of the piston, the dry side (inside the cylinder) is pressurised with high pressure (HP) air to offset the hydrostatic pressure. The air is supplied from a one litre diver's air bottle inside the model that is charged to 200bar. A regulator on the air supply line to the ballast cylinder ensures that the pressure behind the piston is maintained only slightly higher than the ambient hydrostatic pressure. The ballast cylinders are located at either end of the model and can be operated as pair (or

independently) to provide a wide range of mass and moment changes in the free running model; the components, assembly and locations within the model are shown in Figure 40.

The trim and ballast system has the capacity, in terms of volume and rate of change of volume, to emulate a flood recovery in a submarine at model scale; this should be more than sufficient to provide a system that can offset the mean and slowly varying second order force.

Bowker and Crossland, [2020] used this ballast and trim capability to provide the restoring force in the vertical plane that emulated the equivalent force provided by a spring system. The position of the piston in each ballast can was controlled by an autopilot designed to maintain, depth, at the initial depth, and zero pitch angle during the run. The autopilot included a wave filter similar to that proposed in Crossland, [2017] designed to respond only to the second order motion and ignore the first order wave effects. The mean and low frequency movements of the ballast were used to determine the mean and slowly varying suction forces respectively. The advantage of this approach is that the spring systems providing the restoring forces to counter the second order forces in the horizontal plane and the vertical plane are uncoupled (to first order motion).

In this case, the test rig was designed specifically for the case of oblique seas at zero speed which was as consequence of the limitations in the Ocean Basin facility at Haslar – there is no XY carriage across the tank to tow the model. Whilst the design could also be considered feasible for modest forward speeds providing the facility has the means to tow the model in oblique waves, the purpose of the research described here was to understand the effects of forward speed on the hydrodynamic forces. Therefore, a modification of the test rig used by Driscoll and Musker, [1988] was considered for the lightly restrained tests in the Ship Tank at QinetiQ Haslar, and is described in the following section.

3.3 Lightly restrained tests with the Euclid 10.17 geometry

3.3.1 Design of towing arrangement

In this PhD study the lightly restrained tests were performed in the Ship Tank at QinetiQ Haslar using the Submarine Research Model (SRM), see Figure 42, configured as the EUCLID 10.17 geometry tested at MARINTEK by Martinussen, [2006] but at a larger scale; the details of the full-scale geometry are provided in Appendix D.

The SRM, a QinetiQ submarine model capability described by Bayliss *et al*, [2005], was lightly restrained using two towing swords that attached the model to the Ship Tank carriage. The SRM

displacement was 1225Kg and conditioned to be neutrally buoyant at an initial keel depth of 1.04m (1.75 times the hull diameter) with a BG (distance between centre of buoyancy and centre of gravity) of 26mm. The roll, pitch and yaw radii of gyration were 0.243, 1.23 and 1.208m respectively. The model was attached to the Ship Tank towing carriage by two tow swords via a pivot assembly that allowed the model to pitch and heave, Figure 41.

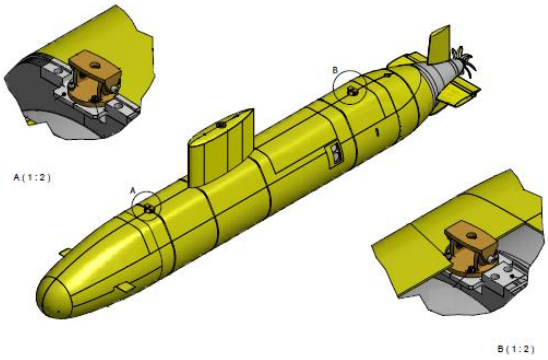

Figure 41: Tow sword attachment points to the SRM

The fairings around each of the towing swords had non zero volume that when submerged contributed to the buoyancy of the overall system configuration. Therefore, as the model would heave and pitch the extent of the submerged volume of the forward and aft towing swords would change – hence the buoyancy of that part of the system would change as the model oscillated around mean water level . This was accounted for in the subsequent analysis by making a correction for the change in buoyancy for each of the towing swords that was a linear function of the change in immersion around the measured datum (Calm water condition at zero speed), as follows:

delta_bouyancy_fwd = 0.1258*1000 N/m

delta_bouyancy_aft = 0.1119*1000 N/m

Now, the towing assembly was designed to fully restrain horizontal motion (surge only in the case of a Ship Tank experiment) and each towing sword was fitted with a similar spring system to that used by Driscoll and Musker, [1988] to lightly restrain the model in the vertical plane.

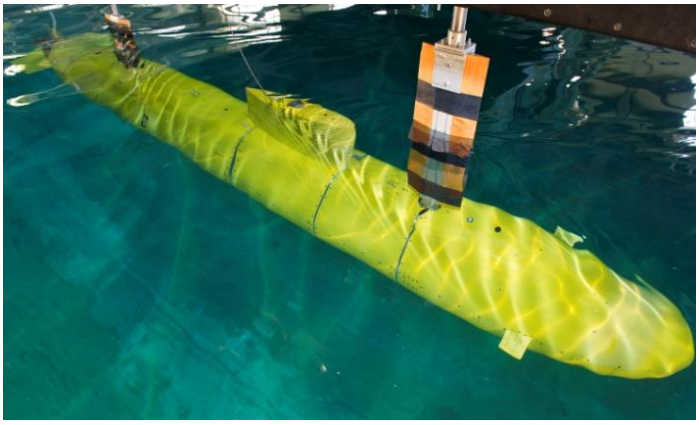

Figure 42: SRM on the carriage in the Ship Tank at QinetiQ Haslar

The towing arrangement that attached the swords to the Ship Tank carriage included two sets of compression springs, one set for each tow post to providing the stiffness in the vertical plane. Each tow post had two compression springs that had one end rigidly fixed to a load cell to measure the vertical force directly. In this configuration, only one spring on each tow post provided the restoring force (when that spring was under compression) – when one spring was under compression the other one would provide no force at all. Figure 43 shows the aft tow post spring assembly with the principal components marked. Whilst this was essentially the same spring assembly as that developed by Driscol and Musker, [1988], the design was modified, for these current tests, to include a load cell mounted to the end of the spring; as the spring compressed the load cell would measure the force and simple geometric calculations could then be performed using the load cell readings from the forward and aft spring assemblies to derive the mean heave force and pitch moment (which was not possible with the set-up used by Driscol and Musker, [1988]. .

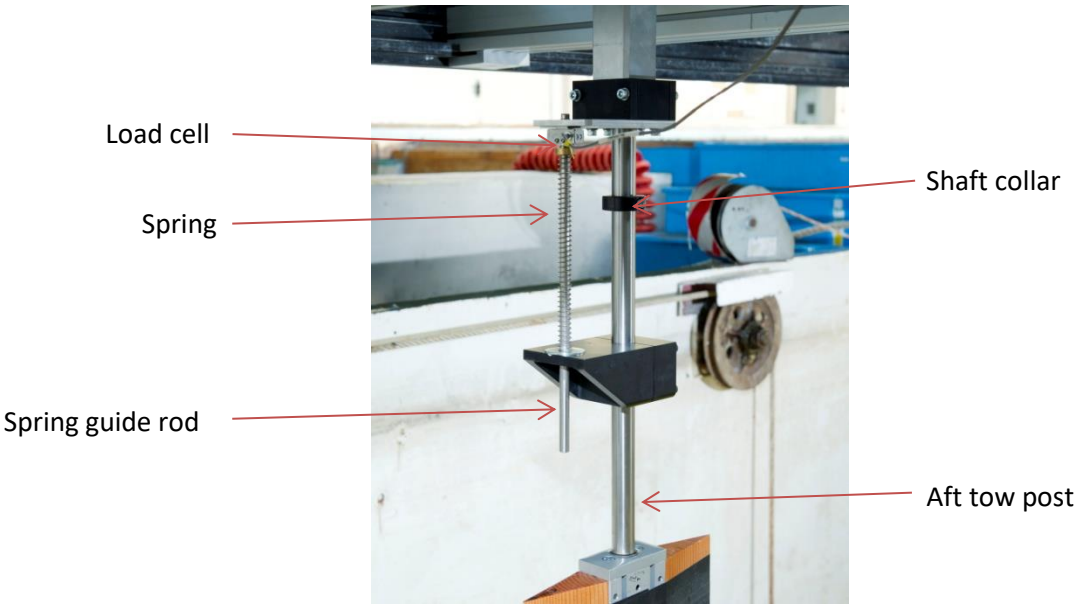

Figure 43: Aft tow post spring assembly

In this example, as the stern of the model rises in waves, the spring, shown in the figure, would compress to provide the restoring force; the compressed spring would impart a force on the load cell from which this component of the overall second order force can be determined. A shaft collar was included to prevent the movement of the tow post to an extent that the spring gets compressed beyond its elastic limit, potentially leading to overloading and damaging the load cell.

An LDVT was fitted to each tow post to measure its vertical motion from which the vertical plane rigid body motions of the model were derived.

As mentioned previously, in such tests the towing rig should be designed so that the natural frequency of the restraining system is significantly less than the lowest frequency to which the linear response of the model may be still noticeab; the lower the spring stiffness, the lower the natural frequency of this spring/mass system would be. So, the spring constants are chosen so that the natural frequencies of the vessel motions, as a consequence of the presence of the springs in the restraining system, are sufficiently far removed from the frequency range of the regular waves. In terms of avoiding resonant responses in structures, a typical guide seems to be avoiding main excitation frequencies being in range of $\frac{1}{\sqrt{2}}$ and $\sqrt{2}$ of the natural frequency; generally, from a hydrodynamic perspective, spring constants are chosen such that the natural frequencies of the restraining system are around 5 times lower than the frequencies of the waves, [Pinkster, 1980]. However, if the spring constants were too low then they would not have the capability to withstand the expected vertical plane forces due to the second order wave effects, and thus not being able to either prevent model from broaching or the springs reaching their compression limit. Three springs of varying stiffness were considered during the experimental design as shown in Table 2 (along with estimates of the natural frequency of the system).

Spring stiffness (N/mm)	Representative mass (Kg)	Natural frequency (rads/s)	Natural period (s)
0.130	1882.5	0.372	16.91
0.238	1882.5	0.503	12.50
0.870	1882.5	0.961	6.54

Table 2: Spring types and predicted natural frequency of system

For the purpose of these tests, the mid spring stiffness (0.238 N/mm) was chosen to reduce the natural frequency as much as practicable whilst limiting the vertical displacement due to springs responding to the second order waves force to prevent the bridge fin from emerging from the water.

The minimum wave encounter frequency that was tested was approximately 2 rads/s (or 0.65 Hz) and the natural frequency of the system was expected to be around 0.08Hz by using springs with a stiffness of 0.238 N/mm. The separation between the lowest expected wave frequency and the natural frequency of the system is not as large as that achieved by Aranha et al [2001] but lies within the range defined by Pinkster [1980].

3.3.2 Test conditions

Model tests were carried out in regular, bichromatic and irregular waves in head seas at zero and a forward speed (Fr = 0.14), the case of forward speed also included tests in calm water. The regular wave conditions (frequencies at model scale) are shown in Table 3; wave amplitudes for each frequency are also shown. Each of the frequencies, in Table 3, where paired to form the two frequency wave systems that were generated for the bichromatic wave tests (for the bichromatic tests, where two waves are paired, the amplitude of each wave is half of the amplitude in regular waves). Finally, a series of tests were performed in long crested irregular head waves, the details of the irregular waves are shown in Table 3; an ITTC two-parameter spectrum formulation was used for each of the irregular wave tests.

$\frac{\lambda}{L}$	Wave frequency (rads/s)	Wave amplitude (m)
0.75	4.07	0.033
0.88	3.77	0.034
1.00	3.53	0.030
1.25	3.16	0.027
1.50	2.88	0.029
1.75	2.67	0.031
2.00	2.50	0.028
2.25	2.35	0.031
2.50	2.23	0.032
3.00	2.04	0.033

Table 3: Wave conditions used in lightly restrained model tests

Sea State	Significant wave height (m)	Modal period (s)
Low 3	0.6	7.5
High 3	0.9	8.8

Table 4: Irregular wave tests (full-scale equivalent)

3.3.3 Characterisation of spring-mass system

Some decay tests in calm water were undertaken to ascertain the dynamic characteristics of the towing arrangement and the model. These decay tests consisted of raising the model, specifically the stern which would cause the upper spring on the aft tow post to compress, then released and the subsequent combined heave and pitch motion allowed to decay. The natural frequency of the towing arrangement and the model can be estimated by considering the simplified single degree of freedom equation of free heave decay $a\ddot{x} + b\dot{x} + cx = 0$, where x is the heave displacement, a is summation of the body mass and added mass, b is the damping, c is the stiffness. Figure 44 shows the time trace from a heave decay test at zero speed.

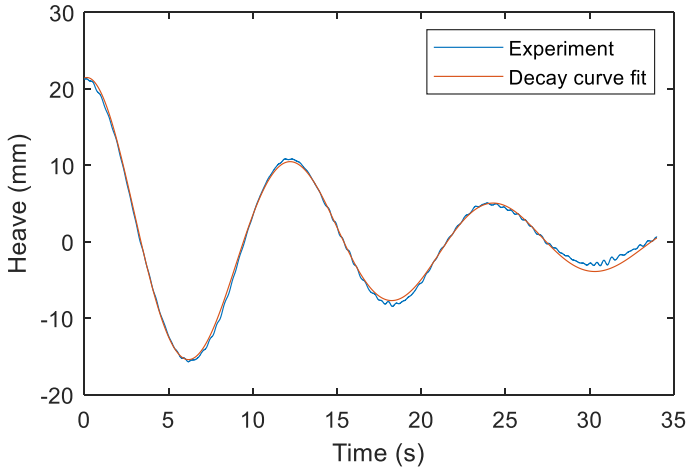

Figure 44: Calm water free heave decay test and decay curve fit

The curve fit has the form of $x = x_0 e^{\frac{-t}{\tau}} \cos(\omega_d t)$ where

$$\tau = \frac{2a}{b},\ \omega_d = \omega_* \sqrt{1-\eta^2},\ \eta = \frac{b}{2\sqrt{ca}} \text{ and } \omega_* = \sqrt{\frac{c}{a}}$$

which can be fitted to the decay time history, from the experiment, using non-linear regression techniques. From the solution to the curve fit, damped natural frequency ω_d at zero speed can be

determined and was found to be around 0.524 rads/s. This can be compared to an estimate undamped natural frequency of 0.503 rads/s obtained by assuming the added mass to be 50% of the actual mass of the body, as shown in Table 2 for the spring stiffness of 0.238 N/mm . Knowing the damped natural frequency and the non-dimensional decay coefficient ($\eta = 0.112$) which is also obtained from the solution to the regression fit to the decay curve, Eqn 35 can be used to quantify the amplitude response function of the measured force in ratio to the wave force for this spring-mass system.

Figure 45 shows the amplitude response of the measured force for this model submarine and the lightly restraining rig. From the figure, it can be seen that, at low frequencies of excitation, the measured force will be equals to the force due to the waves, whilst for frequencies higher than the natural frequency of the spring-mass system, the measured force becomes increasingly smaller in ratio to the wave induced forces. There is a region in between these low and high frequencies where dynamic magnification is evident.

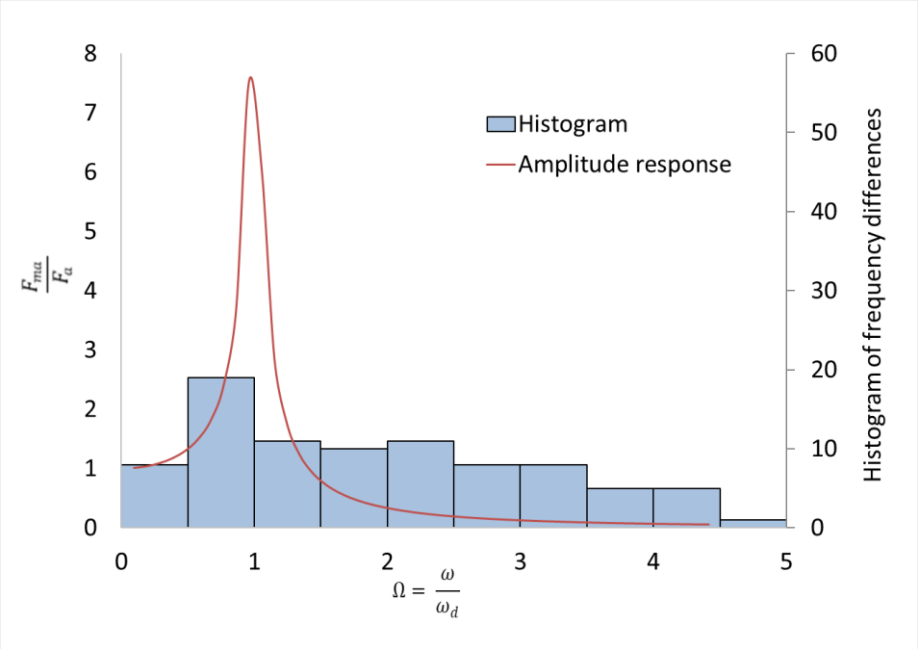

Figure 45: Amplitude response of measured force with histogram of differences frequency tested.

In the experiment designed by Pinkster [1980], the stiffness of the mooring system was chosen with the stiffness of the mooring to be sufficiently large so that the peak of the response function would lay between the expected frequencies of the second order forces and the wave frequencies considered during the experiment. In doing this, the dynamic magnification of the measured force can be small in the range of frequencies of the low frequency second order forces whilst the ratio

of measured mooring force to the wave force in the range of the first order motions and first order wave frequencies will be small.

The wave frequencies, considered during the test campaign, were deliberately chosen to ensure that the first order motions were unaffected by the restraining system. The wave amplitudes were chosen to ensure that the first order motions remained sufficiently low to prevent the springs going beyond their elastic limit and to prevent the tow rig from experiencing excessive second order loads.

So, by choosing the lowest wave frequency, considered in the tests described here, to be $\omega = 2.04$ rads/s, then $\Omega = 3.89$ so the influence of the restraining system on the first order motions can be considered to be insignificant. Likewise, the influence of the restraining system on the measured steady second order force (mean force) can be considered to be insignificant.

However, it is likely that there would be dynamic magnification of the slowly varying second order forces, due to the frequency difference in two regular wave trains. Superimposed on Figure 45 , is an histogram of the bichromatic tests, that were performed, from the permutations of sets of two regular waves taken from in Table 3. This shows that there were a number of bichromatic tests performed (probably around 11 or the 86 tests performed) where there would be significant dynamic magnification of the measured slowly varying second order force. This dynamic magnification of the slowly varying second order force would also be present in the irregular wave tests. This means that the effect of the towing arrangement needs to be modelled in any simulation that is to be used to compared directly with the output from the experiments.

The effect of the towing arrangement on the model needs to be represented, in the simulation, as a time varying external non-hydrodynamic vertical force applied at each of the tow post locations. The vertical force, due to each towing post, can be represented by a damped harmonic oscillator in the form:

$$F_{tow} = -cx_{tow} - b\frac{dx_{tow}}{dt}$$

where

x_{tow} is the vertical displacement of each of the tow posts about their datum (mean) positions.

b is the stiffness term accounting for the spring constant (in the towing arrangement, see Figure 43 for illustration of spring assembly) and the change in buoyancy due to the changing waterline of the sword section (due to vertical motion of the model relative to the wave at the tow locations).

b is a damping term derived by matching time histories of free decay tests in calm water performed in the experiments.

This approach to replicating the effect of the two posts is a first-order linear approximation to the forces applied by tow posts, due to the springs and the changing buoyancy of the posts, on the body. The approximation assumes that both the stiffness and mechanical damping of the towing arrangement, are constant across the test conditions. It is likely that the damping, in particular, will change with forward speed.

3.3.4 Regular waves

With regards to the analysis of the time histories, the 23rd International Towing Tank Conference Ocean Engineering Committee, [2002] developed a procedure for analysing typical regular wave tests on models in the offshore technology area. For an offshore structure, the response to waves can be non-linear, containing a number of harmonic responses which can be captured by assuming that the response takes the form of:

$$x(t) = \bar{x} + \sum_{j=1}^{m} A_j \sin(j\omega t + \varphi_j)$$

where

$\bar{x}$ is the mean of the time history

ω is the fundamental frequency (actual wave frequency with the model at zero forward speed and encounter frequency with the model at forward speed)

A_j is the amplitude of the jth harmonic

φ_j is the phase of the jth harmonic

m is the number of harmonic responses

According to the ITTC procedure, 7.5-02-07-03.2 Analysis Procedure for Model Tests in Regular Waves dated 2017, both spectral analysis of the time histories and a least squares fit of the harmonic response are considered as suitable methods for analysing data from regular wave tests. The least square method involves fitting a multi-harmonic theoretical signal, which consists of determining values of $\omega, \bar{x}, A_j, \varphi_j$ that minimises the following:

$$\varepsilon^2(\omega, \bar{x}, A_j, \varphi_j) = \frac{1}{N}\sum_{i=1}^{N}\left[x(t) - \bar{x} + \sum_{j=1}^{m} A_j \sin(j\omega t + \varphi_j)\right]^2$$

71

where N is the number of points in the time history.

ε is the error between the measured and fitted data).

According to the ITTC, the least squares fit is more accurate for short time history records. The length of a time history measured during an experiment is dependent upon the usable length of the facility, the speed of the model and the frequency content of the waves. The aim is to curtail any experimental test prior to the point where the effects of waves reflecting from any beach structure in the facility become significant.

The least squares regression is linear when the relationship between the dependent variable and the independent variables in the regression model (2nd term on the RHS of Eqn. 71) is assumed to be linear. It should be noted that the regression model in Eqn. 71 is non-linear because of the term involving ω . Now, ω is the fundamental frequency, equivalent to the actual wave frequency, for the model at zero speed, and the encounter frequency at forward speed. In either case, of zero speed or with forward speed, for this type of experiment, the actual wave frequency and speed of the model are known. Therefore, for known ω the regression model in Eqn. 71 is linear and so can be solved through linear regression analysis. However, due to experimental uncertainty, there may be small differences in the expected and achieved wave frequency obtained when generating waves that will mean that linear regression analysis may be problematic. It may be possible to obtain the actual achieved wave frequency from Fourier analysis of the encountered wave time history before performing the linear least squares regression. However, the approach adopted here was to use the non-linear fit function (*fitnlm*) that is part of the Statistics Toolbox in MATLAB®. This approach means that ω in the regression model in Eqn. 71 does not need to be known *aprior* but will be determined as part of the non-linear least square regression . The following is the MATLAB script used for the regular wave data analysis.

For this experiment, the lightly restrained model is able to respond to first order forces, where the restraining system is designed to have an insignificant influence on the first order motion, but the mean forces are countered by the spring system in the towing assembly. Therefore, for regular waves (single frequency), this first order regression analysis is of the measured heave and pitch response;

it is assumed that each response will have a non-zero mean and a response at the input frequency. The second order forces are extracted from the means of the heave force and pitch moment derived from the strain gauge measurements, accounting for the contribution from the buoyancy changes in the tow posts. Figure 46 gives an example that is typical of the measured heave and pitch motions and heave force and pitch moment and the result of the least squares fit to each of these measurements.

```
%
%Non-linear regression utility in MATLAB
%using Statistics Toolbox Version 8.3
%
% Define the expected function form for regular waves
%
% x(t) = x̄ + Asin(ωt + φ)
      reg_mdl_function = @(a,t) (a(1)*sin(a(2)*t+ a(3)));

% a(1) = amplitude, a(2)=frequency, a(3) = phase;
% Make an initial estimate of for the iterative process
      a0=[0.2 Input_frequency 0.5];
%
% Perform the regression
mdl_fit = fitnlm(t,motion,reg_mdl_function,a0);
%
% Generate fitted curve
      motion_regress = predict(mdl_fit,t) + motion_mean;
%
% Extract coefficients
      motion_hat = mdl_fit.Coefficients.Estimate(:,1);
```

Matlab script for regular wave analysis

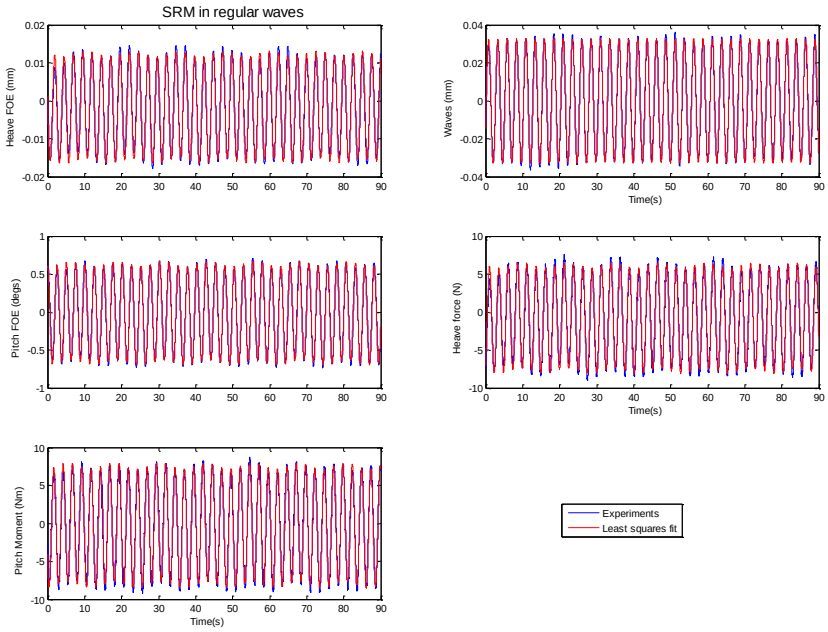

Figure 46: Model response in regular waves of 2.49 rads/s (zero speed)

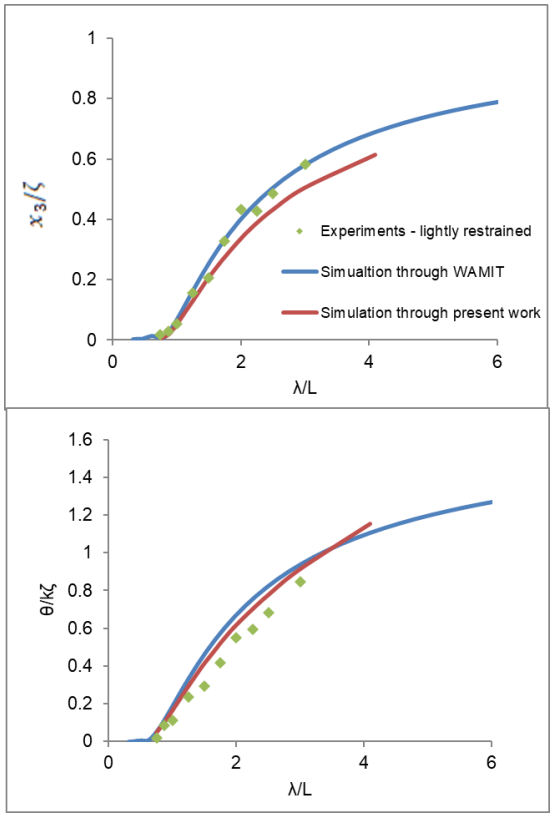

Figure 47: First order heave and pitch responses of the lightly restrained EUCLID model in regular head waves (zero speed)

For the lightly restrained (semi-captive) submarine model, the results of the computations (time domain simulation through the present work and frequency domain simulation using WAMIT) and measurements at zero speed with respect to the first order heave and pitch responses are shown in Figure 47. The results are presented as functions of non-dimensional wavelength; the heave motion is non-dimensionalised with respect to the wave amplitude and pitch with respect to the wave slope. Comparing the experimental data with the two predictions appears to provide confirmation that the rig, designed to lightly restrain the model against the second order forces, does not appear to be influencing the first order motions significantly. There are differences between the results from the experiments and both numerical simulations (through present work and WAMIT). This could be due to the numerical simulations neglecting some of the viscous related damping effects on pitch motion, particularly the damping due to the bow planes and stern planes.

Shown in Figure 48, is the non-dimensionalised mean heave force obtained from the fully restrained tests in regular waves, Martinussen, [2006], compared with the mean heave forces measured in the lightly restrained tests of the same geometry. In the first instance, the comparison of the experimental data from the restrained tests and the lightly restrained tests provides further confirmation that the mean heave forces, due to waves, on a restrained submerged body are greater than those measured on the same body (that is allowed to respond to first order motions). This could be due to the phase relationship between diffraction and radiation potentials for a body that is free to move in a fluid. This knowledge of the forces on a body provides clear guidance on the type of simulations and/or experimental tests that are required to provide a quantitative understanding of the capacity of compensation systems required to offset surface suction effects at early stages of submarine design.

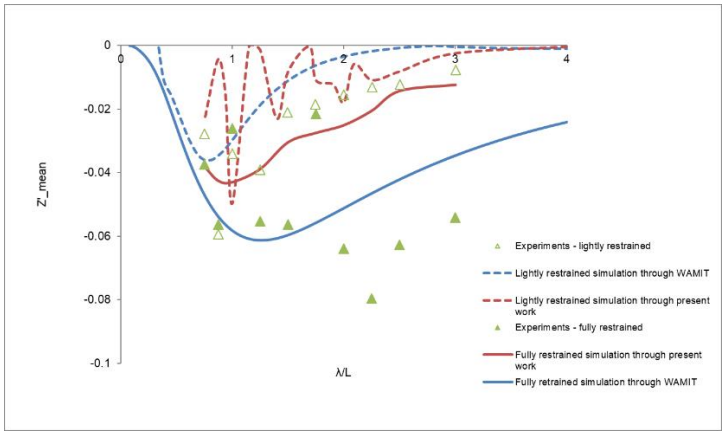

Figure 48: Mean heave force on the EUCLID model in regular head waves (zero speed)

Figure 48 shows the comparison of results from WAMIT (frequency domain analysis allowing first order responses) and the time domain simulation that emulated the effects of the towing rig spring system with experiments. This means that, in the latter, an additional external force is applied that is dependent upon the displacement of the submarine by emulating the compression effect of each pair of springs in the towing system and the associated spring constant. The heave force is non-dimensionalised as before and plotted as a function of non-dimensional wavelength.

Comparing the WAMIT and the time domain computations of the mean heave force, the overall magnitudes are comparable but the frequency at which the peak heave force occurs is different in the predictions when compared with the experiments. This difference is not as a consequence of the lightly restrained towing rig since the amplification factors of the measured mean force is one, see Figure 45 for zero frequency. Again, the differences could be due to viscous effects of the simplification of the free surface boundary condition.

Figure 49 shows the results of the computations (time domain simulation through the present study only since WAMIT is only zero speed) and measurements with the model travelling with forward speed (F_r=0.14). Presented are the first order heave and pitch responses as functions of the non-dimensional wavelength; the heave motion is non-dimensionalised with respect to the wave amplitude and pitch with respect to the wave slope. Comparisons show that the predicted first order motions agree with the experimental data.

Figure 50 shows the comparison of the mean heave forces obtained from the lightly restrained case for the model travelling with forward speed (F_r=0.14) with those obtained from the restrained model tests by Martinussen, [2006]; again, it is clear that the restrained case, gives larger suction forces than the lightly restrained case. Also, shown are the time domain computations that emulated the effects of the towing rig spring system. Comparing its results with the experimental data shows that these second order forces are under-predicted by the time domain method; the overall predicted magnitudes is smaller than that measured in experiments. In all cases, the component of vertical force due to the forward speed of the body in calm water has been removed from the presentation of the data; the mean heave force (Z') is the mean force due entirely to the presence of regular waves.

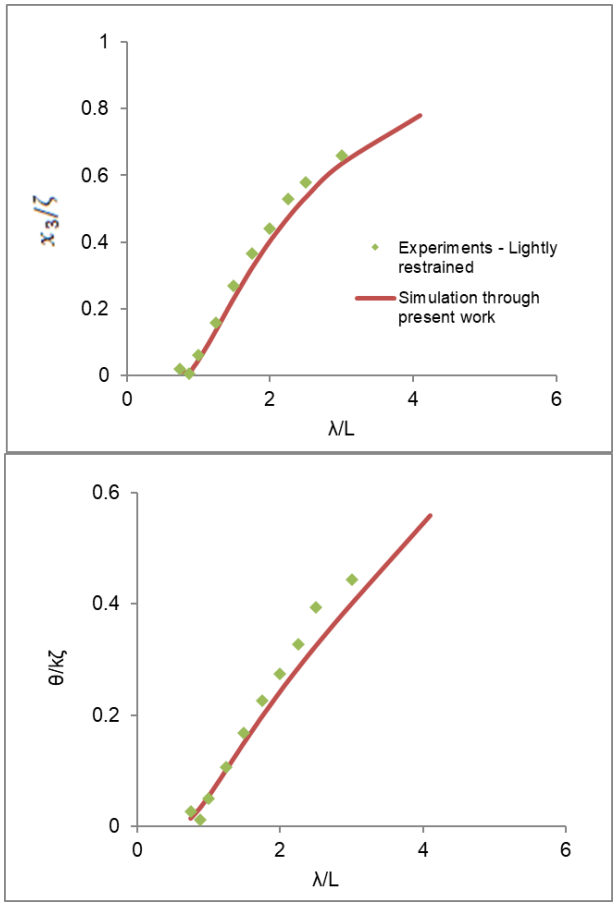

Figure 49: First order heave and pitch responses of the lightly restrained model in regular head waves (F_r =0.14)

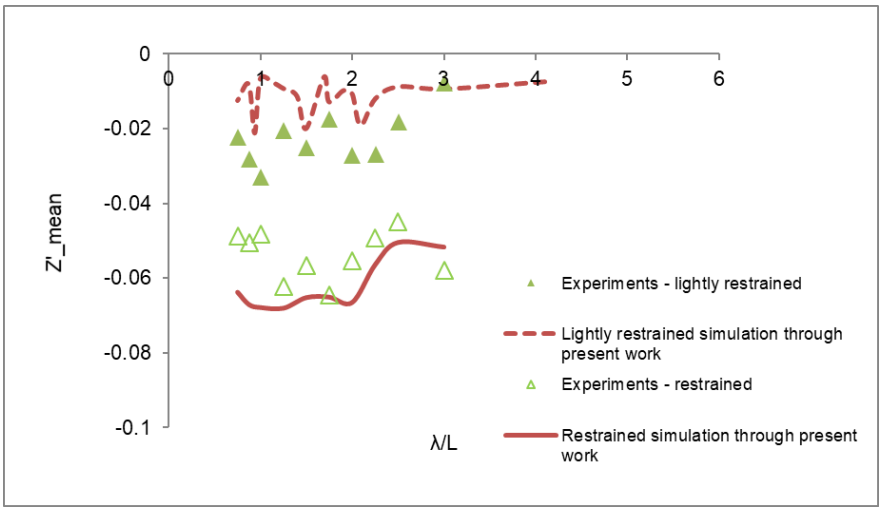

Figure 50: Mean heave force in regular head waves (F_r =0.14)

3.3.5 Bichromatic waves

As mentioned earlier, the lightly restrained tests undertaken in this study included, for the first time, bichromatic tests. By considering only terms up to second order, the approach to analysing data from the bichromatic test is somewhat similar to the output from the regular wave tests except that the motion and force responses will take the following extended form where ω_1, $\omega_2, A_1,..A_6$ and $\varphi_1 \ldots \varphi_6$ are obtained in the same way as those in Eqn. 71

$$x(t) = \bar{x} + A_1 \sin(\omega_1 t + \varphi_1) + A_2 \sin(\omega_2 t + \varphi_2) + A_3 \sin((\omega_2 - \omega_1)t + \varphi_3) + A_4 \sin(2\omega_1 t + \varphi_4) + A_5 \sin(2\omega_2 t + \varphi_5) + A_6 \sin((\omega_2 + \omega_1)t + \varphi_6)$$

72

which consists of a mean value, two components due to the individual regular waves and the remainder are the other second order components due to the two regular waves.

Figure 51 shows an example of a non-linear least squares regression fit to data (model scale) obtained from a bichromatic test in head waves at zero speed. This example provides an indication of the quality of the fit between the measured time history and the expected form of the regression model provided in Eqn. 72. From the regression fit, the mean force ($\bar{x}$) and the amplitude of the slowly varying force (A_3) can be obtained

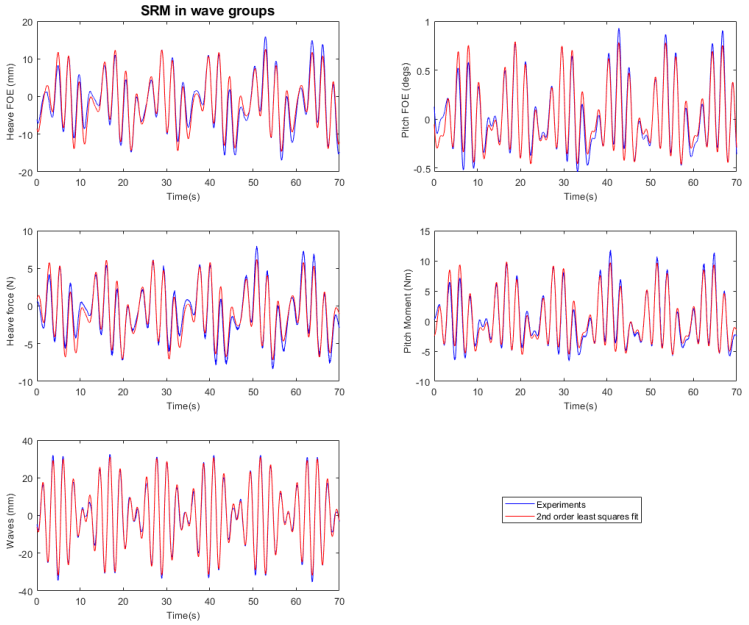

Wave frequencies 2.88 rads/s and 2.35 rads/s

Figure 51: Example of regression fit to a model test in a bichromatic wave (head seas and zero speed)

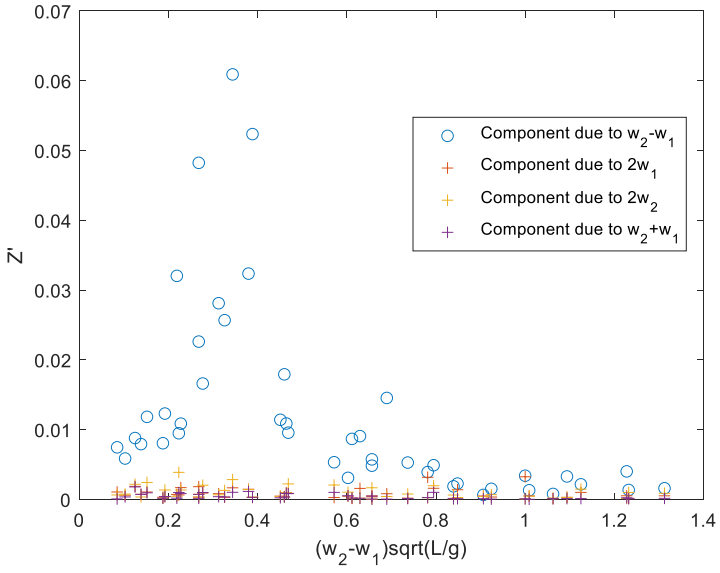

Figure 52: Relative magnitude of the components of the second order non-dimensional heave force in bichromatic waves (head seas and zero speed)

For zero speed in head waves, Figure 52 shows the relative magnitude of the frequency dependent second order components of the non-dimensional heave force as measured during the experiments in bichromatic waves; the second order components have been plotted on a common x-axis for ease of comparison. This figure shows that the frequency dependent second order heave force on a submarine under waves is dominated by the difference frequency component for non-dimensional frequency differences of less than 0.8.

Figure 53 shows the contour plot for the second order heave force obtained from the tests on a lightly restrained model at zero speed, and time domain and WAMIT simulations for the case of bichromatic waves. Also shown are the equivalent Cartesian plots showing the entire dataset plotted against wavelength (associated with the first frequency) and WAMIT predictions plotted against non-dimensional difference frequency. The Cartesian plot is essentially showing the 3D contour plot in two dimensions as multiple slices through the datasets perpendicular to the y=x axis. This accounts for the multiple data points for a single value of $(\omega_2 - \omega_1)$. The Cartesian plot of the entire data set provides a qualitative comparison between WAMIT and time domain predictions and experimental measurements. Generally, the data agree with the peak in the second order heave forces observed around non-dimensional wavelengths between 1 -2 model lengths. The contour plots show that there are differences between the three data sets. WAMIT and the time domain predictions show agreement for a range of values for $\frac{\lambda_2}{L}$ where $\frac{\lambda_1}{L} \approx 1$ (albeit there are more scatter in the time domain predictions); the experiments do not seem to demonstrate the same features.

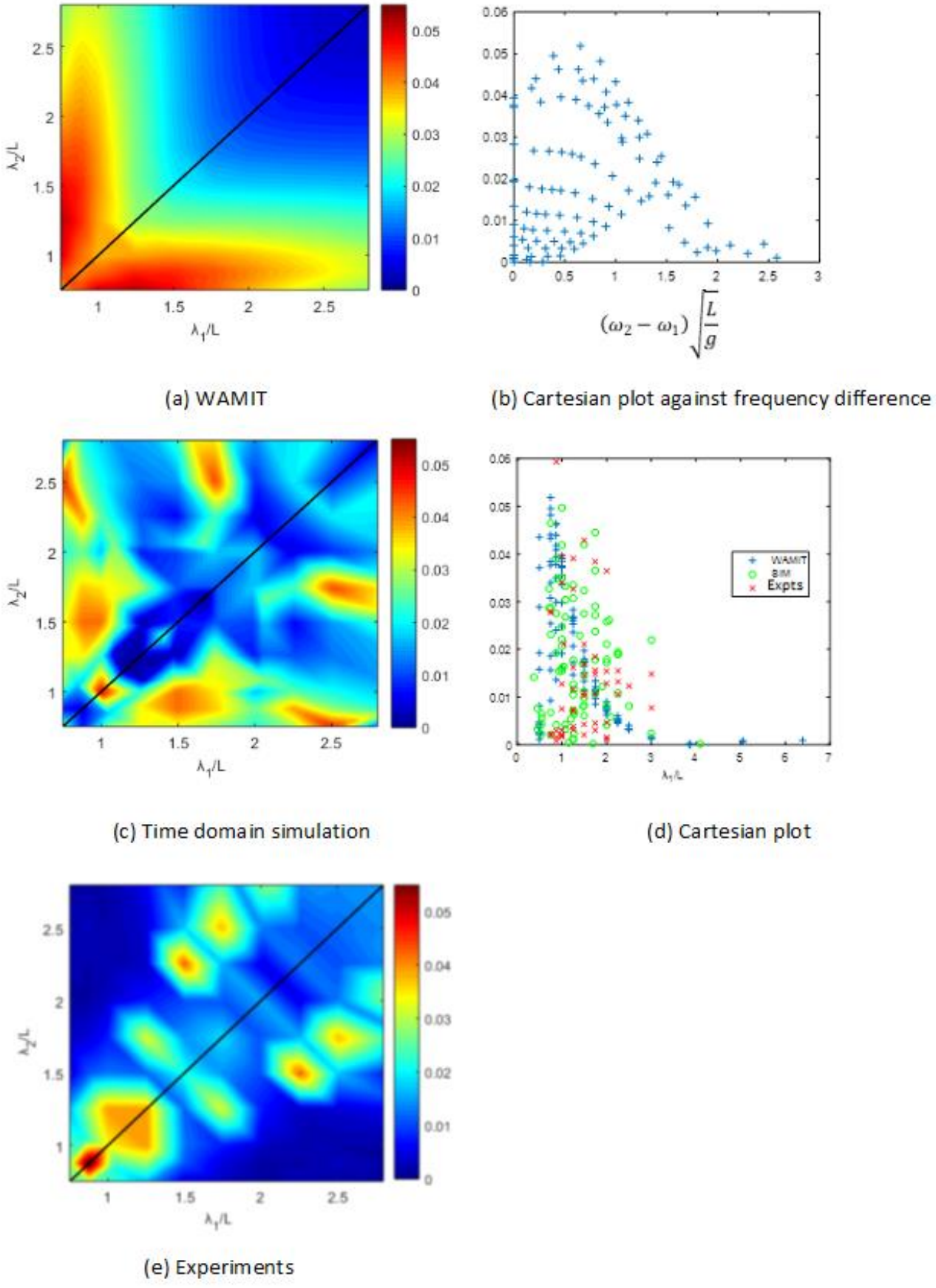

Figure 53: Non-dimensional heave force from lightly restrained model in bichromatic waves (head waves and zero speed)

The Cartesian plot of the WAMIT predictions plotted against the frequency difference shows that the maximum non-dimensional heave force Z' does not occur on the y-axis. Instead, the maximum occurs at $(\omega_2 - \omega_1)\sqrt{\frac{L}{g}} = 0.65$.This confirms the earlier observation, for predictions of the fully restrained submarine in bichromatic waves, that the Newman approximation would be inaccurate when there is a resonant response predicted at non-zero difference frequencies (or $\omega_1 \neq \omega_2$). As mentioned previously, the attraction of Newman's approximation is that to determine the QTFs of the submarine under waves, only experiments and/or predictions in regular waves are required. If this approach was adopted the implications, for submarine design, could be that if a submarine compensation system was designed to counter the mean suction force and the slowly varying force based on Newman's approximation, there is a possibility that the system will have insufficient capacity to counter the actual slowly varying suction force. Furthermore, as will be seen in Chapter 4, if these slowly varying effects are not accounted for accurately, in the design of the depthkeeping autopilot, the performance of the controller could be below optimum.

3.3.6 Irregular waves

The lightly restrained tests, undertaken in this study, also included a series of tests in irregular waves. These were performed in long crested irregular head waves. An ITTC two-parameter spectrum formulation was used as shown below.

$$S(\omega) = \frac{A}{\omega^5} e^{-\frac{B}{\omega^4}}$$

73

Where $A = \frac{487.3 H_{1/3}^2}{T_0^4}$ and $B = \frac{1949}{T_0^4}$

For an irregular wave with significant wave height $H_{1/3}$ and modal (or peak) period T_0 .The significant wave heights and modal periods used for the irregular wave tests are shown in Table 2.

For the generation of time histories from these spectra, there are a number of methods of synthesising time histories from spectra, see [Fryer, 1991] who developed a technique of filtering white noise that provided irregular time series with large repeat periods. The frequency domain synthesization methods that are perhaps most commonly used (in both a simulation environment and in an experimental facility) is to generate a time history based on the summation of sinewaves with amplitudes given by Eqn. 74 and a set of random phases.

$$a(\omega) = \sqrt{2S(\omega)\delta\omega}$$

where $\delta\omega$ is the frequency step used in the spectral formulation.

The frequencies in which the amplitudes are calculated can either be chosen by setting a constant $\delta\omega$ or randomly distributed over the range of interest ($\delta\omega$ is not constant). The former method is considered to be more convenient to implement, whilst it is suggested that latter is required to generate purely random realisations of the given spectrum, see, [Tucker *et. al*., 1984]. Different time history realisations of the same wave spectrum are chosen through random seed numbers used to derive the random phases (and the random frequencies).

The repeat period of the irregular time history is:

$$T_H = \frac{2\pi}{\delta\omega}$$

For random frequency steps, the denominator in the above equation is slightly modified to become $min(\delta\omega_i)$.

The wavemaker control system, for generating the irregular wave time histories in the experiments performed as part of this research, uses the approach by [Fryer, 1991], by applying an appropriate filter to white noise. This method provides an efficient signal generation technique for use in an experimental facility but also enables a higher number of frequencies to be considered in the generation of the wave time histories (resulting in a longer repeat period). Spurious free waves can be avoided in the facility by ensuring that any shallow water effects (where depth of water is less than the wavelength of the wave train) are kept to a minimum by choice of wavelengths to be tested.

During the experiments, the duration of each run was dictated by the requirement to prevent the wave reflections from the beach, at the opposite end of the tank to the wavemaker, significantly influencing the response of the model. For the case of zero speed, the model was located close to the wavemaker to maximise the run duration to about 100 seconds (any wave reflections from the side of the tank away from the natural frequencies of the tank were considered insignificant); for tests with forward speed, the run duration was reduced (due to the length of the facility) around 60 seconds. Furthermore, the tests were conducted in six different time history realisations of each spectrum; each of these six runs were then concatenated prior to analysis to extend the overall run length.

In total for the zero speed cases, each irregular wave test represented about 38 minutes of full scale testing (and 23 minutes for those tests including forward speed).

The ITTC, 2008b reported that, in irregular waves, the test duration should be sufficiently long to allow at least 100 wave encounters to ensure that the motion statistics are stable. For the tests in this thesis, 38 minutes run duration is equivalent to approximately 300 wave encounters for the longest wave period, which suggests that the run duration was sufficiently long for obtaining reliable results from these "random" tests

In the case of the simulation developed through this present work, an irregular wave time history is synthesized through the summation of a number of regular waves as follows:

$$\eta(t) = \sum_{i=1}^{N_W} a_i \sin(\omega_i t + \varepsilon_i)$$

Where $N_W = 100$ is the number of regular waves and the phases $\varepsilon_i \in [0, 2\pi)$ and $\omega_i \in \left[\frac{\omega_m}{2}, 3\omega_m\right]$ are randomly generated with

$$\omega_m = \frac{2\pi}{T_0}$$

The measured heave and pitch motion responses from the irregular wave tests were compared with the same responses predicted using the time domain simulation; an example of the time histories and spectra from the combined measurements and predictions, in a low sea state 3 at zero speed, are plotted at model scale in Figure 54. Figure 55 shows another example this time with forward speed. Table 5 and Table 6 provide the statistics from the experiments and simulations; presented at model scale.

All time histories have had their mean values removed prior to plotting. Whilst the wave spectrum used in the simulation is representative of the required ITTC spectra, the wave time histories generated in the Ship Tank are not the same as those generated in simulations. The means that direct comparison of the two sets of time histories is not possible However, Fourier analysis of the simulations and the measurements can be performed which does provide a means of comparing predictions with experiments. Qualitatively, it can be seen that the magnitudes of the responses are similar between simulations and measurements. There are some features in the measurements –

low frequency oscillations that are not obviously present in the simulations as seen in the spectral plots. This maybe as a consequence of the dynamic magnification due to the resonant frequency of the towing arrangement as seen in Figure 45. As described in section 3.3.3, the forces on the body due to the towing arrangement was modelled as a first-order linear approximation (linear in vertical motion of the model) of the forces on the model due to the spring compression and buoyancy effects of the tow posts themselves. It maybe that there are other effects from the tow post, such as friction in bearing arrangements or hydrodynamic interference effects from the posts on the model that are not modelled in simulation that may account for the differences between the measured and predicted motions at the lower frequencies. However, the spectral plots of the experimental data are showing clear second order heave and pitch effects at frequencies lower than those measured in the wave spectrum. This confirms the assertion in this thesis, that it is important to include the first order motions when modelling the second order forces for the problem of the submarine under waves.

Variable	Mean		RMS	
	Expts	Sim	Expts	Sim
Waves (m)	-	-	0.01	0.01
Heave (m)	1.04	1.04	0.002	0.003
Pitch (degs)	0.02	0.00	0.10	0.07

Table 5: Statistics Irregular wave responses in a low sea state 3 (head waves and F_r=0)

Variable	Mean		RMS	
	Expts	Sim	Expts	Sim
Waves (m)	-	-	0.01	0.01
Heave (m)	1.04	1.03	0.002	0.002
Pitch (degs)	-0.49	-0.09	0.08	0.04

Table 6: Statistics Irregular wave responses in a low sea state 3 (head waves and F_r=0.14)

Whilst, the spectral plots show some quite significant differences in the frequency content of the predicted heave and pitch motion compared to that measured during the tests, part of the difference frequencies particularly at the lower frequencies. This is due to the dynamic amplification

of the measured slowly varying second order force at difference frequencies close to the natural frequency of the towing rig, see Figure 45.

The statistics (mean and RMS values) show closer agreement between the experiments and simulation. However, sea state 3 is considered to be a benign wave condition in the context of submarines at periscope depth. As mentioned earlier the wave heights in these tests were deliberately kept low to prevent over-loading the capacity of the tow rig. Armed with the benefit of experience from these tests, future tests could look to improve the design of the rig to consider higher sea states. Furthermore, it would be prudent to include the dynamics of the towing rig in any simulation if wishing to compare directly with the results from these experiments.

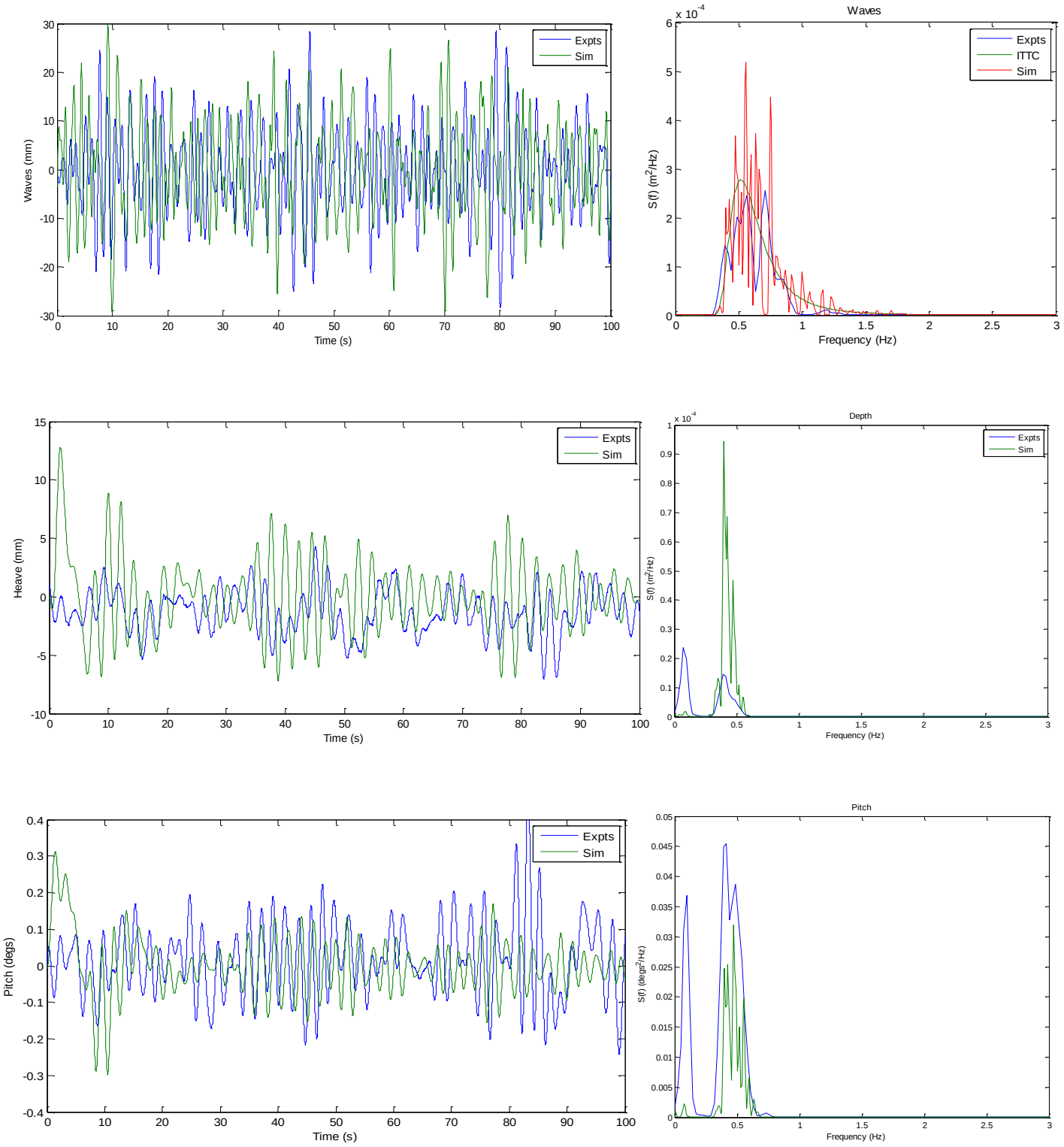

Figure 54: Irregular wave responses in a low sea state 3 (head waves and F_r=0)

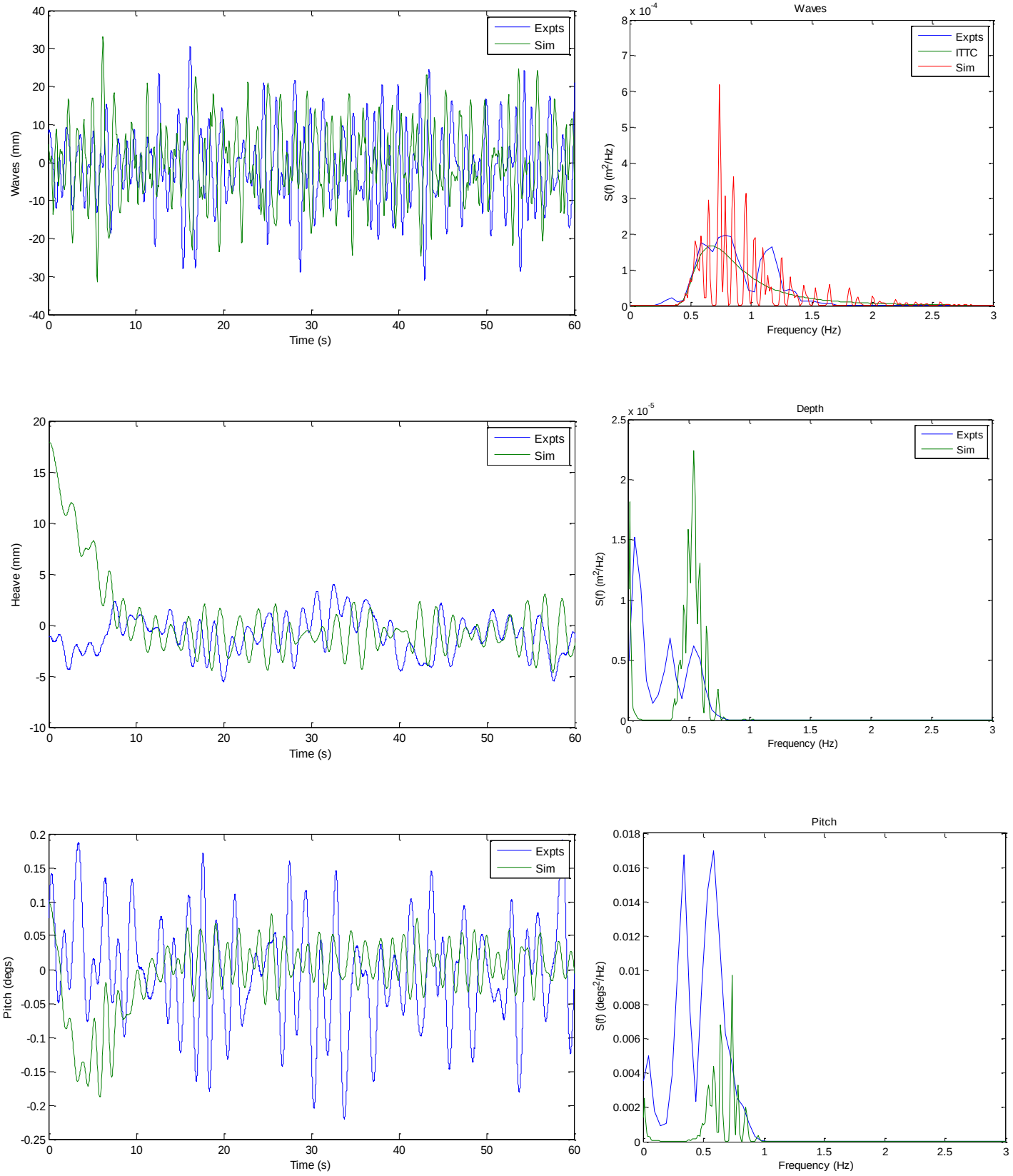

Figure 55: Irregular wave responses in a low sea state 3 (head waves and F_r=0.14)

3.4 Chapter summary

This chapter has described a series of tests, undertaken during this PhD study, using a fully appended submarine, which was lightly restrained in the vertical plane (allowing the model to heave and pitch, whilst being constrained in the other degrees of freedom), in regular, bichromatic and irregular head waves at zero and forward speed. The results of the experiments have been compared with predictions made using the time domain simulation developed in this present study and with the commercially available software WAMIT.

The main themes of this chapter provided:

1) detailed case studies by which the physical phenomena associated with the behaviour of a submarine under waves were extensively investigated.
2) full description of the experiment methodology that will enable others to recreate the tests both experimentally and numerically for comparison.
3) comparison between experiments and numerical simulation.

As part of the contribution to the field, the work described in this chapter has shown that using data from experiments where the submarine is not free to move in response to the waves may result in over-estimating the expected second order mean forces against which a compensation system would be designed to counter the surface suction effects due to waves. The mean second order heave force obtained for the case where the submarine is free to respond to first order motion provides a more representative means of determining likely forces that can be used in design; this result has also been confirmed through simulation.

The experiments have shown that the frequency dependent second order forces on a submarine are dominated by the force due to the frequency difference for non-dimensional frequency differences of less than 0.8.

The experiments have also confirmed, earlier observations from predictions for the fully restrained submarine in bichromatic waves, that the Newman approximation would be inaccurate when there is a resonant response predicted at non-zero difference frequencies (or $\omega_1 \neq \omega_2$). Use of the Newman approximation for this problem could result in under predicting the slowly varying suction force.

The experiment methodology has been described in sufficient detail, coupled with the geometry description in Appendix C, to provide the means to replicate both experimentally and numerically in the future. The results of these experiments provide the validation data for numerical methods or, more directly, can be used to understand the impact of suction effects on the design of compensation systems in submarines.

Comparisons are shown between the experimental results and the results from predictions using the time domain code and WAMIT. The predictions of the first order motions compared very well with those measured during the experiments, which suggests that the experimental rig design is appropriate for measuring first order motion and second order forces. Both simulation approaches confirm the results from the experiments in that the mean second order heave force for a lightly restrained body is less than that for a fully restrained body.

The time domain and WAMIT predictions of the slowly varying second order force at zero speed appear to agree with the measured data with the peak in the second order heave forces observed around non-dimensional wavelengths between 1 -2 model lengths. However, there are some differences between the three data sets. WAMIT and the time domain predictions show agreement for a range of values for $\frac{\lambda_2}{L}$ where $\frac{\lambda_1}{L} \approx 1$ (albeit there are more scatter in the time domain predictions); the experiments do not seem to demonstrate the same features.

Comparisons of the measured and predicted responses in irregular waves, show that mean and rms responses appear to be predicted well; further investigation of the response spectra shows some differences, especially in the second order low frequency responses.

In the following chapter, a case study is presented showing how a better understanding of the second order forces on a submarine under waves can be used to improve the ability of a submarine to maintain depth through the design of the depthkeeping autopilot. The time domain approach developed in this present study is used to evaluate the performance of the autopilot as a coupled simulation that includes the wave induced forces and the manoeuvring forces on the Euclid geometry.

4 DEPTH CONTROL OF A SUBMARINE AT PERISCOPE DEPTH

4.1 Introduction

So far, this thesis has focused on the development of a time domain simulation to predict the wave induced forces on a submarine under the influence of surface waves. Chapter 3 described a set of experiments that helped understand the physics of the problem but also provided a means to compare results from these tests with the time domain simulations from the present study. This chapter links the work that has been presented earlier to a particular case study. The particular problem under consideration here is related to the design and evaluation of a control system that is suitable as a depthkeeping autopilot in a submarine operating under the influence of surface waves. In the first instance, the time domain method, developed as part of this research, is used to evaluate the depth control performance of the EUCLID submarine in waves for a series of control approaches that culminates in the use of quadratic transfer functions (predicted using the same time domain method) that are used as shaping functions for controller design.

The design of an algorithm for controlling the depth of a submarine in deep water, away from the influence of surface waves, is considered to be straightforward but when the submarine is at periscope depth, and under the influence of surface waves, the controller design becomes more complex, [Liceaga-Castro and Van Der Molen, 1995]. The main concern to the designer is to understand how best to accommodate the effects of the suction force (present when a submarine operates near the free surface), which could mean that if the hydroplanes and compensation systems are poorly designed they may be unable to control the submarine in certain wave conditions. Also, whether, the designer adopts an approach based on hydrodynamic or hydrostatic control is based, to some extent, on the operational requirements for the platform.

At very low speeds with the submarine operating near the free surface including waves, the suction force due to the steady forward speed of the submarine may be small in which case the primary suction force on the submarine will be due to the second order steady heave force due to the waves only. However, any control surface may also become ineffective, at these low speeds, since the forces that can be generated by these lifting surfaces are speed dependent the control surfaces maybe insufficient to counter the second order wave induced forces. In this case, the designer would need to consider hydrostatic control by means of an active compensation system such as that described, for example, by [Crossland, 2017] and [Font and Garcia-Pelaez, 2013]. Alternatively, if depth control is required for operational speeds, and submergence depths, typical of those when using the periscope or snorting then it is likely that the hydroplanes would be the best means of

control as they can produce sufficient force. Indeed, it may be necessary for the designer to develop a system that utilises a hybrid of hydrodynamic and hydrostatic control. Whichever approach is used, the integration of a control system, especially one that utilises an active compensation system, into a submarine design would be complex and therefore such trade-off design studies should be performed early in the design process.

This chapter provides a detailed case study utilising the time domain simulation developed in this present work to investigate the design of a depthkeeping control autopilot for a submarine under the influence of surface waves when cognisant of a better understanding of the second order wave induced forces on the body gained form this research. The case study describes particular techniques for the hydrostatic and hydrodynamic control of a submarine under waves that are, then, evaluated using the time domain computational tool developed as part of this research; this approach of utilising linearization techniques to develop controllers but analysing the performance of said controllers using non-linear techniques is unusual. More traditional control system design approaches would use the same techniques to design the controller as used to evaluate its performance. The chapter begins by developing a suitable depth-autopilot, based on the H_∞ controller by [Postlethwaite, 1991b], for the full-scale equivalent (Full-scale length is 74.25mm or 15 times the length of the model) of the Euclid hull form considered in earlier chapters. This depth-autopilot utilises a linearised model of the Euclid design based on the approach by [Marshfield, 1991]. H_∞ was chosen, as an example, for this study because it is considered to be a robust control strategy that can be designed to be insensitive to variations in the so called plant model. Furthermore, H_∞ is also a suitable control strategy for what is considered to be a MIMO (Multi-Input,Multi-Output) system (described further later in this chapter). The benefit of a time domain approach develop here is, of course, that a wide range of alternative autopilot design strategies can be assessed. However, the focus of this chapter is in demonstrating the benefits that may be gained from a well-designed depth-autopilot; different H_∞ loop-shaping techniques are considered and evaluated. The benefits of utilising filters that can reduce the response of the control surfaces to frequencies that are typical of the wave environment are shown. In particular, the benefits of considering the combined effects of the steady and slowly varying second order suction forces in the design of a depth-autopilot to control a submarine at periscope depth under the influence of waves are demonstrated.

4.2 H_∞ controller

Figure 4 shows a schematic of a control system in a submarine; the model describing the submarine dynamics and the external disturbances (in the case of the submarine, the wave induced forces and moments for example) have been described in Chapter 2; the knowledge and understanding of these are now used to design an autopilot based on H_∞ loop-shaping techniques. There are a number of alternative approaches to control system design, see [Fossen, 1995] for example. This case study, presents a possible solution to the depth control of a submarine at PD.

The design of any control system requires, in the first instance, an understanding on how the submarine behaves or so called "plant model"; this is usually quantified using mathematical models. In most cases, these mathematical models will have been developed for detailed performance assessment at the design stage of a submarine and usually require simplification for use in control design, [Fossen, 1995].

In the example here, autopilot design is focussed on the control of depth and heading of the submarine; under standard control design conditions, control in the horizontal plane (heading) and vertical plane (depth) are assumed to be decoupled, [Solberg,1992] which means that the control algorithms for vertical and horizontal plane control can be designed in isolation of each other. The separation of the vertical and horizontal control is largely due to the convenience of the control surface configuration. The traditional cruciform appendage configuration for a submarine consists of a pair of bow planes (or sailplanes) and a pair of stern hydroplanes to control depth and an upper and lower rudder, usually mechanically linked, to control heading. It is this orthogonal arrangement of the aft appendages that allows the vertical and horizontal plane control to be considered as separate problems. For alternative aft control surface arrangements like X-planes, the horizontal and vertical control system design is more closely coupled.

When a submarine is at an oblique heading to the surface waves, say 135 degrees bow seas then there will be second order body forces in the horizontal plane that are similar, in their frequency content and maybe even magnitude, to those in the vertical plane. These forces will manifest themselves as a mean and slowly varying drift force on the submarine which will require a rudder response to maintain heading. However, the depth controller is considered to be the more important part of the submarine control system, [Grimble et al, 1993]. This is largely from a perspective of safety and the requirement to operate within tight constraints such as the avoidance of large unexpected depth excursions (overshoot) as a result of an autopilot-controlled depth change.

In our control design, it is assumed that the bow planes and stern planes are not mechanically linked thus allowing separate control of those control surfaces; in this case, the actuation system within the submarines allows for independent control of the bow and stern planes, [Grimble *et al,* 1993], providing the ability to control both depth and pitch. Independent control of the bow and stern planes (2 inputs) for controlling depth and pitch (2 outputs) is considered to be a multivariate system (referred to as a MIMIO, Multiple-Input-Multiple-Output, system) with more advanced control requirements, [Grimble *et al,* 1993] who used the example of submarine depth and pitch to explore the design of an H_∞ controller.

H_∞ methods are used to synthesize controllers to achieve stabilization with guaranteed performance and are suitable for multivariate systems, (Postlethwaite, 1991). However, H_∞ techniques require a higher level of mathematical understanding to apply them successfully and the need for a reasonably good model of the system to be controlled.

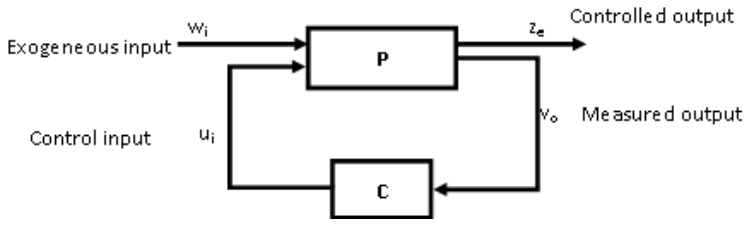

Figure 56: Standard compensation configuration (Postlethwaite, 1991)

A control system can be represented by the configuration shown in Figure 56. The plant *P* (or system dynamics) has two inputs, the external input w_i, that includes the reference signal and disturbances (ordered depth and wave disturbances, respectively, in the case of a submarine under waves), and the manipulated variables u_i (bow planes and stern planes in the case of a traditional cruciform stern arrangement). There are two outputs, the error signals z_e (depth and pitch error) that need to be minimized, and the measured variables v_o (measured depth and pitch), that are used for input into the controller *C*; v_m is used in *C* to calculate the manipulated variables u_i. The system in Figure 56 can be represented as:

$$\begin{bmatrix} z_e \\ v_o \end{bmatrix} = P(s) \begin{bmatrix} w_i \\ u_i \end{bmatrix} = \begin{bmatrix} P_{11}(s) & P_{12}(s) \\ P_{21}(s) & P_{22}(s) \end{bmatrix} \begin{bmatrix} w_i \\ u_i \end{bmatrix}$$

$$u_i = C(s) v_i$$

The dependency of z_e on w_i can be written as:

$$z_e = F_l(P, C)w_i$$

where

$$F_l(P, C) = P_{11} + P_{12}C(I - P_{22}C)^{-1}P_{21}$$

75

The objective of H∞ control design is to find a controller C such that $F_l(P, C)$ is minimized according to the H∞ norm. The H∞ norm is defined as:

$$\|F_l(P, C)\|_\infty = \sup_{w_i} \varkappa(F_l(P, C)(jw_i))$$

76

where $\varkappa$ is the maximum singular value of the matrix $F_l(P, C)(jw_i)$ over all w_i; "sup" is the mathematical term for supremum and $j = \sqrt{-1}$.

According to [Postlethwaite, 1991b], to deal with a constrained optimisation problem to obtain the "best" possible performance under hard physical constraints such as actuator saturation and limitations on feedback due to plant uncertainty, the closed loop transfer function $F_l(P, C)$ can be partitioned into sub-matrices S and CS, where S is the sensitivity function ($S(j\omega) = \frac{1}{1+P(j\omega)C(j\omega)}$) and C is the controller as;

$$\|F_l(P, C)\|_\infty \equiv \left\| \begin{matrix} S \\ CS \end{matrix} \right\|_\infty$$

77

where the function on the RHS is the infinity norm such that for an arbitrary set of values x_i :

$$\|x\|_\infty \equiv \max_i |x_i|$$

The weights, in the optimisation process, are then selected so that S dominates the cost function at low frequencies and CS dominates the cost function at high frequencies. The means that the aim of the optimisation process is to improve performance at low frequencies whilst providing enhanced robust stability at high frequencies.

The above approach to optimisation requires that the system is essentially linear or that linearisation of a non-linear system can be considered to be a suitable representation of the system dynamics. Furthermore, the models in the system tend to be represented by polynomials, for example, the dynamics of the submarine are characterised by simple second order low pass filters, [Grimble *et al,* 1993]. Using these simplified approaches, the design of a control system for a deeply submerged is considered to be straightforward, [Liceaga-Castro and Van Der Molen, 1995], but the approach to design becomes more complex when the submarine is operating at periscope depths. In this case, the wave disturbances need to be also characterised and considered as part of the control system design.

The first step in control system design, is to decide to what extent should the effect of the external disturbances (waves) be controlled. In submarines, the design of the appendages and actuators is for the primary purpose of controlling for heading and depth whilst deeply submerged. This usually means the actuator rates are quite low, typically, around 5degs/s; space limitations in the design of a submarine would usually preclude actuators with more significant power.

In terms of control, it is desirable to maintain the submarine at a constant depth relative to the calm surface with a zero mean pitch angle, [Marshfield, 1991]. The wave frequencies, around 0.1 Hz, are outside the control bandwidth of the vessel, in that these are considered to be frequencies that the submarine will not respond to, but they are inside the bandwidth of the hydroplane servos. Therefore, a poorly designed control system will make the planes respond to these frequency components. This is usually due to the depth measurement that is used to determine the depth error input signal into the controller is usually derived from pressure transducers. This means that is it likely that the depth signal would be contaminated by noise at the wave frequencies. According to [Marshfield, 1991], the gain of most autopilots is quite high at the wave frequencies so that, in the case of submarine depthkeeping, this signal noise on the inputs can cause considerable plane motions which serve no useful purpose in controlling the submarine. Furthermore, using the planes in this manner could lead to excessive wear and tear on the actuator because of the increase in duty cycle and potentially causing the autopilot to become unstable.

H_∞ method with loop-shaping, [Grimble *et al,* 1993], is an approach to control design theory that uses the infinity norm optimization techniques to achieve controllers whose stability and performance properties hold despite uncertainties in the mathematical models representing the behaviour of the submarine, in this case. The control system design approach is to describe the desired responsiveness and noise-suppression properties by weighting the plant transfer function

in the frequency domain; these weighting functions are themselves described by transfer functions (polynomials in the frequency domain). Williams and Marshfield [1990] applied H_∞ techniques to submarine control as a means of demonstrating the potential application of such techniques in designing depth control autopilots for use at periscope depth. It has been found that designing a controller using H_∞ loop-shaping means that the controllers are not unduly sensitive to changes in characteristics of the wave disturbance and measurement noise providing the general characteristics are representative, [Grimble *et al,* 1993].

[Liceaga-Castro and Van Der Molen, 1995] developed a procedure for H_∞ loop-shaping design. In this case, transfer functions represented by polynomials allowed the wave disturbances to be included in the controller design. These wave disturbance models, which consisted of the first-order wave frequency components and the second order drift components, were considered crucial in the design procedure. The first order wave force model adopted by Liceaga-Castro and Van Der Molen, [1995] was a fourth order filter of white noise to represent the shape of a Pierson-Moskowitz wave spectrum; the second order effects were assumed to only consist of a non-zero mean force and moment. The objectives of submarine depthkeeping control in this case was to minimise depth excursions due to the second order wave effects yet reduce unnecessary plane activity due to the first order wave frequency effects. In terms of a feedback system, this means that the second order effects are treated as the input disturbances to be countered whilst the first order wave effects and measurement noise are represented as output disturbances and therefore ignored by the controller, [Grimble *et al,* 1993]. .

4.3 Submarine model

As discussed in Chapter 2, simulating motion of a manoeuvring submarine is typically by using the six-degrees-of-freedom non-linear hydrodynamic coefficient based model, such as that by [Gertler and Hagen, 1967]. Whilst such a non-linear simulation is used to evaluate the performance of a control system design, [Marshfield, 1991], the depth-autopilot is usually designed by linearising these non-linear six degrees of freedom equations of motion; the design problem is naturally limited to just the vertical plane .

The approach used by [Marshfield, 1991] to design a depth-autopilot, the non-linear six degrees of freedom equations of motion were linearised and limited to just the vertical plane (depth and pitch together with the body axis motions w and q). [Marshfield, 1991] described the equations as a system of matrices in the following way for a traditional cruciform submarine:

$$E\dot{x}_s = Fx_s + Gu_i$$

where $x_s = (w, q, z, \theta)^T$, E is the inertia, matrix, F is the force derivative matrix and G is the input matrix to the control system

$$E = \begin{pmatrix} m - Z_{\dot{w}} & -Z_{\dot{q}} & 0 & 0 \\ -M_{\dot{q}} & I_y - M_{\dot{q}} & 0 & 0 \\ 0 & 0 & 1 & 0 \\ 0 & 0 & 0 & 1 \end{pmatrix}$$

$$F = \begin{pmatrix} UZ_{uw} & U(m + Z_{uq}) & 0 & 0 \\ UM_{uw} & UM_{uq} & 0 & -mgBG \\ 1 & 0 & 1 & -U \\ 0 & 1 & 0 & 0 \end{pmatrix}$$

$$G = U^2 \begin{pmatrix} Z_{uu\delta B} & Z_{uu\delta S} \\ M_{uu\delta B} & M_{uu\delta s} \end{pmatrix}$$

where U is the forward speed of the submarine and BG is the distance between the centre of buoyancy and the centre of gravity. The variables in the matrices are the speed independent linearised derivatives obtained from the non-linear model. These linearised system matrices for the full-scale Euclid geometry at 12 knots are defined in Appendix C.

For the autopilot design studies, [Marshfield, 1991] converted the above set of 4 equations to the following state space form.

$$\dot{x_s} = Ax_s + Bu_i$$

$$y_o = Cx_s + Du_i$$

where D = 0 but is retained here for generality . The input vector $u_i = (\delta B, \delta S)^T$, state variables $x_s = (w, q, z, \theta)^T$ and the output vector $y_o = (z, \theta)^T$.

Then the system can be expressed in the frequency domain as:

$$Y(s) = C(sI - A)^{-1}BU(s)$$

where $s = i\omega$ is the variable of Laplace transform with respect to time t, $Y(s)$ and $U(s)$ are the Laplace transforms of y_o and u_i respectively. The above was represented as the following structure from [Liceaga-Castro and van der Molen, 1995], by including the loop shaping functions for the input and output disturbances.

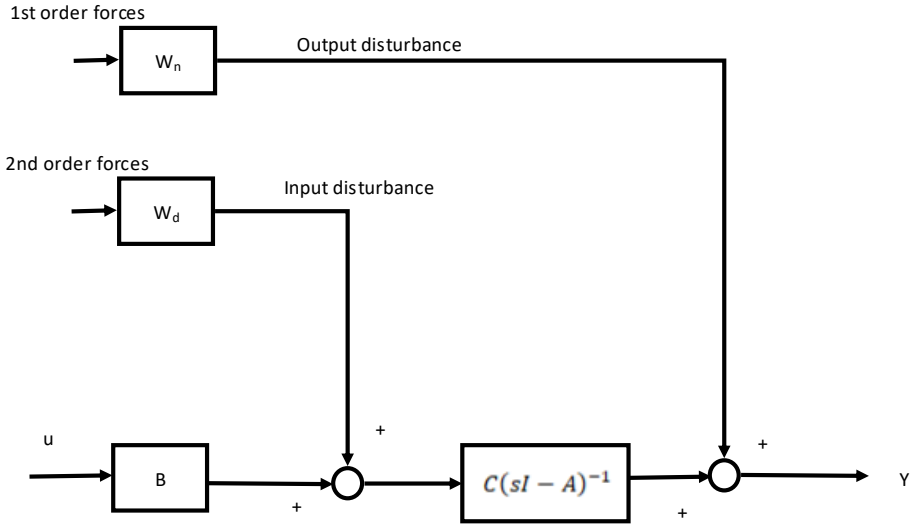

Figure 57: Control design structure [Liceaga-Castro and van der Molen, 1995]

In this case W_d and W_n describe the responsiveness and suppression properties of the input and output disturbances respectively; they are effectively amplifiers or filters. Figure 58 provides the system response, in the form of Bode plots, of the Euclid hull form. The plot provides the depth (or the first element in $|Y(s)|$) (around the mean submergence depth of 20m) and pitch (or the second element in $|Y(s)|$) response to either the bow planes or stern planes oscillating at a single frequency. The Bode magnitude plot shows a graph of $|Y(s)|$ where the y-axis is logarithmic where the magnitude is given in decibels, i.e., a value for $|Y(s)|$ is plotted on the axis as $20\ log_{10}|Y|$.

The figure shows the response characteristics of the linearised mathematical model of the full-scale equivalent Euclid hull form to the control surface inputs at three speeds (6, 12 and 18 knots, full-scale equivalent). The figure illustrates how the ability of the control surfaces to induce a depth and pitch response reduces significantly with frequency; the figure also shows how the effectiveness of the control surfaces increases with forward speed (as would be expected with a lifting surface) as seen by the increase in gain for a given frequency.

Figure 59 shows a time series response of this linearised system to oscillating the bow planes, the stern planes and both sets of control surfaces, with a sinusoidal motion of frequency 0.05Hz and amplitude of 10 degrees. These time series are compared with the same forced oscillations using the full non-linear time domain simulation described by Eqn 3, where the hydrodynamic forces on the submarine are obtained from the derivatives described in Eqns 7 – 10, and the wave induced forces are set to zero. The derivatives have been taken from [Kimber and Thompson, 2007] and listed in Appendix C.

The comparison is shown in Figure 59 for a single speed of 12 knots. In general, the linear response appears to be a good estimation of the predictions made using the full non-linear equations for most of the responses shown in Figure 59 except the linearised model over estimates the depth excursion due to the stern planes when compared with the non-linear model. This is because of the increased depth rate induced on the submarine, as a consequence of oscillating the stern planes (or the stern planes and bow planes) compared to the rate induced by oscillating the bow planes only, means that higher order effects become more significant.

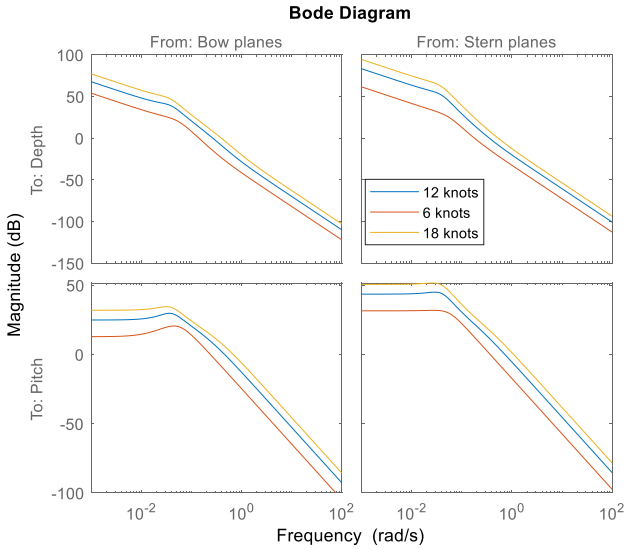

Figure 58: System response of the Euclid submarine at three speeds

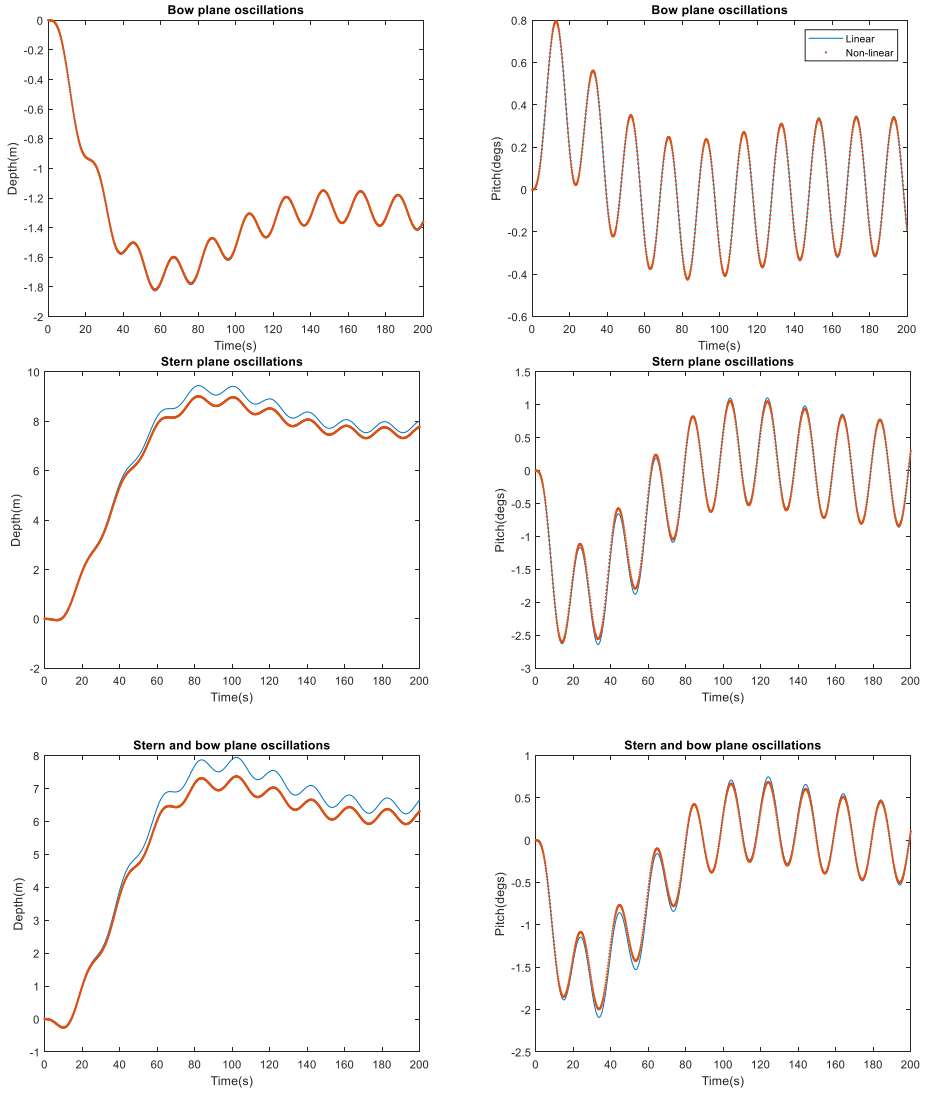

Figure 59: Euclid response to open loop force oscillations using the hydroplanes (Frequency of 0.05 Hz and amplitude of 10 degrees)

4.4 Hydrodynamic control

There are a number of design configurations of control surface arrangement for a submarine, and this chapter considers the more traditional cruciform stern arrangement with forward hydroplanes mounted at the bow. Whilst the approaches described here are valid for alternative configurations, such as an X-plane stern arrangement or a design with hydroplanes mounted on the bridge fin (so called sailplanes), the details of these configurations are not discussed here.

As discussed previously, for a traditional cruciform arrangement, with bow planes, the depth control of a submarine is undertaken using a combination of bow planes and stern planes. At speeds and submergence depths typical of periscope depthkeeping, the problem of control is considered to be a 2-input, 2-ouput design problem (inputs are bow planes and stern planes, outputs are depth and

pitch) requiring MIMO (Multi-Input,Multi-Output) techniques to derive a suitable control algorithm, [Marshfield, 1991]. In the case of a submarine under waves at periscope depth, the control requirement is to maintain depth relative to the calm water surface with a zero mean pitch angle. As discussed in section 3.1, the effect of the first order wave forces on the submarine is too large to be controlled by the hydroplanes; it is the smaller second order wave forces and moments that must be counteracted by the depthkeeping autopilot. At the moderate speeds which are typical at periscope depthkeeping operations, both bow planes and stern planes are required to provide an effective means of controlling depth; bow planes are most effective in controlling depth and stern planes controlling pitch, [Marshfield, 1991]. As an aside, this change in relative effectiveness of the two sets of control surfaces is a consequence of the position of the critical point on the submarine. The critical point is a virtual point on the submarine where a vertical external force applied to the submarine would cause a steady pitch angle but no change in depth, [Renilson, 2015]. This virtual position, which varies with speed, is close to the stern at low speed, for typical submarine designs, and moves forward with increased speed. At low speeds, the stern planes which are close to the critical point can control pitch while not affecting the depth noticeably. At high speeds the stern planes which are now away from the critical point can control depth and pitch effectively, [Marshfield, 1991].

In order to include filters into the controller design, [Postlethwaite, 1991b] extended the portioned form of the H∞ norm in Eqn 77 to design a controller C that minimised the following infinity norm:

$$\min_{C} \left\| \begin{matrix} W_1 S W_i \\ W_2 C S W_i \end{matrix} \right\|_\infty \qquad 78$$

where

W_1 is a loop shaping function (amplifier) applied to the input disturbance.

W_2 is a loop shaping function (filter) applied to the output.

W_i is a loop shaping function that can be used to weight some inputs more heavily than others; [Postlethwaite, 1991b] assumed this to be unity without loss of generality.

S is the sensitivity function defined as $S(j\omega) = \frac{1}{1+P(j\omega)C(j\omega)}$ where $P(j\omega)$ and $C(j\omega)$ denote the plant and the controller transfer functions, respectively, in a closed loop system.

The solution to the cost function in Eqn.78 was determined, in this thesis, for the Euclid design, for the case with no loop shaping, ($W_1 = 1 = W_2$) following the approach in [McFarlane and Glover, 1992] which has been implemented as a function in the MATLAB® Robust Control Toolbox; the subsequent H∞ controller was applied to the problem of submarine periscope depthkeeping.

To investigate the effect of control design on the performance of a submarine operating at periscope depth under the influence of surface waves a Simulink© implementation of the non-linear time domain theory was developed. This time-domain theory is described by Eqn. 3, where the manoeuvring forces on the submarine are obtained using the set of hydrodynamic derivatives described in Eqns. 7 – 10 (taken from Kimber and Thompson, [2007] and repeated in Appendix C), coupled with the wave induced forces that are obtained from the theory described in Chapter 2. The following presents a discussion of the results from this time domain simulation for a number of different approaches to control design. All data are presented as full-scale equivalent values with a model to full-scale dimension ratio of 15 for the Euclid geometry.

The following is a number of examples showing how the time domain simulation can be used to evaluate control system performance that can support the overall design of the submarine.

In the first example, depth and pitch are controlled using the H∞ controller described earlier, however, there are no loop shaping functions included in the controller design (and no notch filter to remove the first order wave effects). Figure 60 shows the predicted responses of the Euclid submarine whilst depthkeeping at a nominal depth of 20 m and a speed of 12 knots in head seas, sea state 5 (ITTC spectrum with $H_{1/3} = 2.5\ m$ and $T_0 = 9.7\ s$).To confirm that the wave conditions are simulated correctly, Figure 61 shows the wave spectrum plotted from a frequency analysis of the simulated wave time history and compared with the required ITTC spectrum (theoretical) ; both spectra are plotted as a function of the encounter frequency.

In simulation, as part of the management of the trim condition of the submarine and in order to prevent the control surfaces from becoming angle limited, the mean (steady) suction force has been compensated for by taking on a fixed amount water ballast, equivalent to 2 tonnes; it appears that the submarine is capable of holding depth in this sea state using the control surfaces. However, in the absence of any filter in the control algorithm to remove the high frequency first order effects, the bow planes are regularly rate-limiting (set to be 5 degs/s for both sets of planes).

This would have the potential effect of reducing the depthkeeping performance of the submarine but, moreover, would lead to rapid deterioration of the bearing arrangements on the control surface actuator systems (unless the system was specifically designed for these types of duty cycles). However, actuation systems that are designed to deal with these increased duty cycles would probably be larger and heavier than an actuator designed to meet the requirements of a duty cycle typical of a deeply submerged submarine.

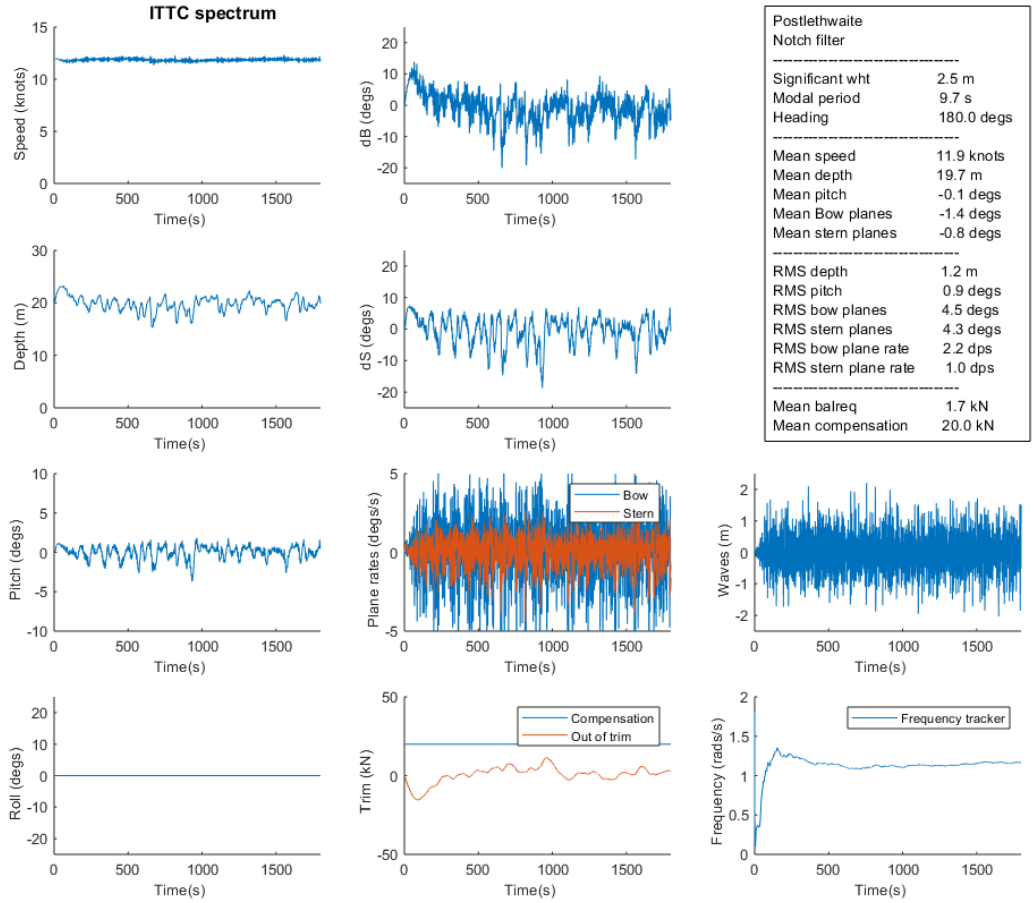

Figure 60: Euclid submarine periscope depthkeeping at 12 knots with an H_∞ controller (no notch filter or loop shaping)

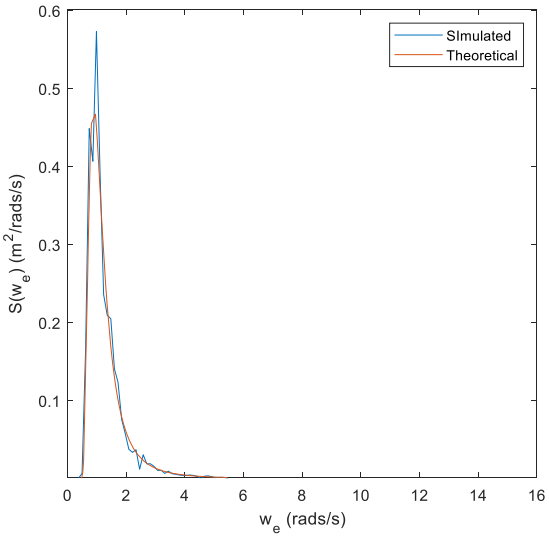

Figure 61: Theoretical and simulated wave spectra

The absence of the filter means that the demands from the depth-autopilot include the depth excursions due to the first order wave effects. In order to understand, fully, the potential of control system improvements due to knowledge that we now have of the second order mean and slowly varying forces on the submarine, it is necessary to include a filter designed to reduce this excessive control surface activity.

[Marshfield, 1991] developed a notch filter with a filter frequency, that may vary with each time step, derived from the time varying principal frequency component within the pitch response. Even though the notch filter is not used in the simulations shown in Figure 60, the time varying output from the frequency tracker is plotted. The output shows that, once passed the initial transient, the frequency settles at approximately 1.1 rads/s.

The frequency tracker is described by [Marshfield, 1991] but is based on the assumption that the input u (in this case pitch) can be approximated by a sinusoid form. In the same way as Marshfield, [1991], the practical implementation of the frequency tracker, in this thesis, is to apply high pass and low pass filters to the pitch input. The frequency ω_n that is subsequently output at each time step used in the notch filter is taken as the time averaged output from the equations defined by [Marshfield, 1991]. In the same way as Marshfield the output frequency is limited to between 0.4 rad/s and 1.8 rads/s. These limits are considered practicable, for this application, since the limits correspond to the bandwidth of a typical wave spectrum.

The output from the frequency tracker can then be used in the notch filter that can then be applied to the pitch signal.

A notch filter is a filter that eliminates a narrow band of frequencies from an input signal yet allows the transmission of all the frequencies above and below this band to the output signal. Therefore, a notch filter has unit gain at low and high frequencies (relative to the notch frequency) with signal attenuation around the notch frequency, as seen in Figure 62.

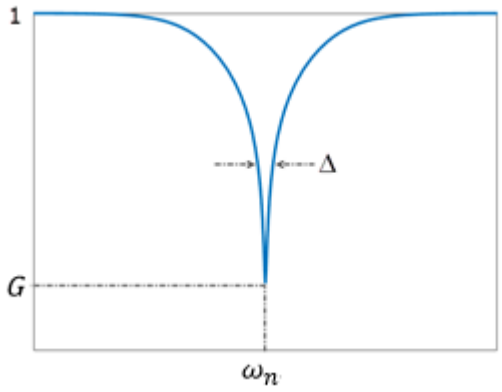

Figure 62: Characteristics of a notch filter (Matlab©)

The transfer function of a typical 2nd order notch filter takes the following form, see [Schei, 1995] for example.

$$N(s) = \frac{s^2 + 2G\eta\omega_n s + \omega_n^2}{s^2 + 2\eta\omega_n s + \omega_n^2} \qquad 79$$

where

s is the Laplace transform variable, ω_n is the notch frequency

G is the minimum gain which controls the depth of the notch in the filter

η is the damping ratio which controls the width of the notch; larger the damping ratio means larger Δ

The Simulink representation of the notch filter is shown in Figure 63. In this case, Simulink provides the ability to vary the notch frequency, minimum gain and damping ratio with each time step. In the case of this study, the characteristics of the notch filter will change at each time step depending upon the frequency $\omega_n$only; the minimum gain, G, was fixed at 10^{-15} and the damping ratio set at 0.75.

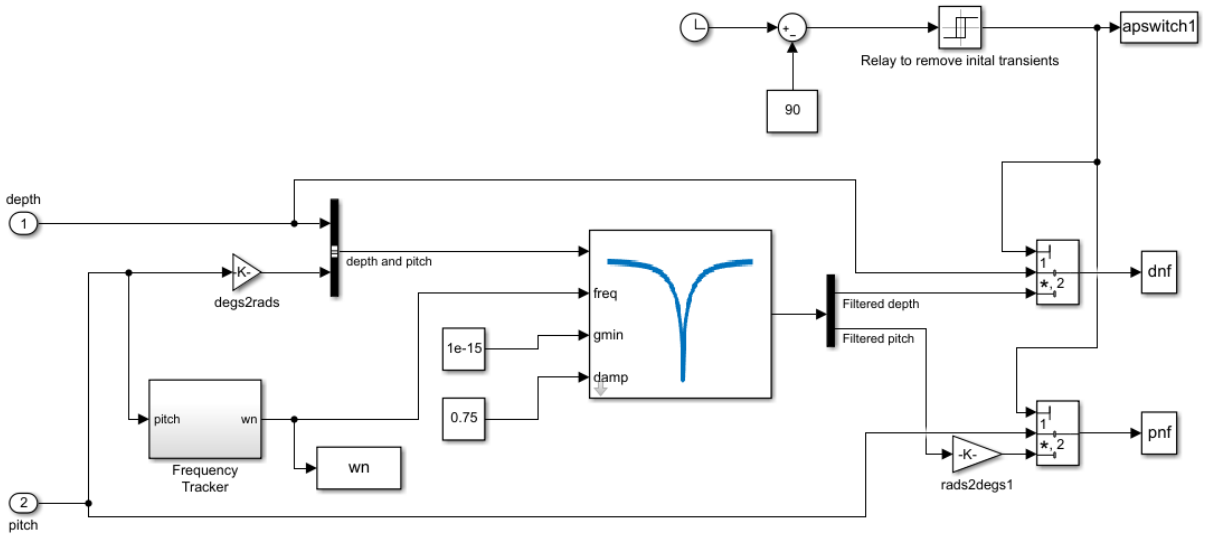

Figure 63: Simulink representation of the notch filter

By means of providing a practical application of the notch filter, in order to remove transients in the filtered depth and pitch responses, due to establishing a stable notch frequency early in the time series, the unfiltered depth and pitch responses are used for the first 90 seconds. These transients are due to the stability of the frequency tracker algorithm at the start of the simulation, not due to transients in the simulation itself.

The effect of the notch filter can be seen in Figure 64 by determining the transfer function between the filtered and unfiltered pitch response obtained from a simulation.

$$H(f) = \frac{G_{xy}(f)}{G_{xx}(f)}$$

where

$G_{xy}(f)$ is the cross spectral density between the unfiltered pitch angle (x) and the pitch angle filtered by the notch filter (y).

$G_{xx}(f)$ is the autospectral density of the unfiltered pitch response.

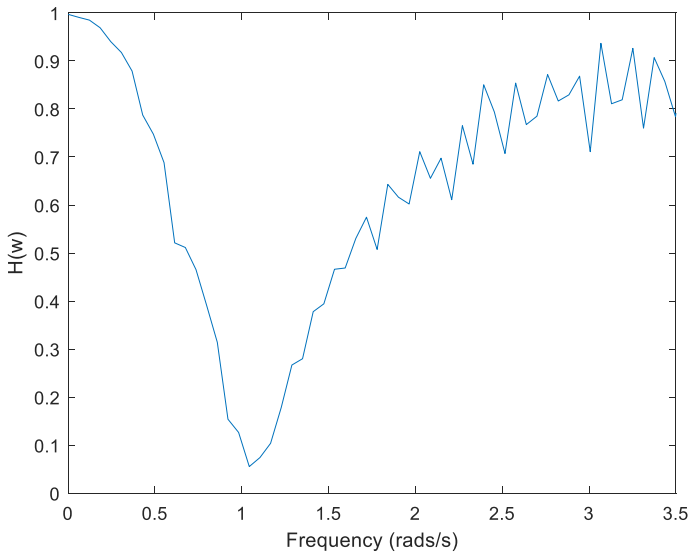

Figure 64: Effect of notch filter on pitch response

For this particular example, the frequency of the notch is at 1.1 rads/s, the minimum gain at this frequency is $1e10^{-15}$ and the damping ratio of the notch was chosen to be 0.75. The notch frequency compares with the frequency of the peak in the wave encounter spectrum or is around 0.9 rads/s.

Figure 65 shows further simulations of the Euclid submarine, in the same wave time history as previously, but the notch filter has been included to reduce the effect of the first order wave frequencies on the controller demands. As found by [Marshfield, 1991] including a notch filter into the controller reduced the first order wave frequency demands on the control surfaces. The mean responses are no different compared to the case without the notch filter. The RMS depth and pitch are similar but there is a reduction or 13% in the demanded bow planes angles and an 8.5% increase in stern plane demands. However, there is a 59% reduction in demanded bow plane rates and 40% reduction in demanded stern plane rates showing that the controls surfaces are working significantly less hard in the case with the notch filter included. Whilst there is overall no impact on the depthkeeping performance by introducing a notch filter, this significant reduction in the plane rates, as a consequence of including a notch filter, will result in reducing the wear and tear on the bearings in a control surface actuator. The depth-autopilot used in the simulations in Figure 65 does not include any attempt to optimise the controller by using loop-shaping functions such as those used by [Postlethwaite, 1991b]. In the next example, loop-shaping filters are included in the controller design. The form of these filters (W_1 and W_2), based on those developed by [Postlethwaite, 1991b] have been updated in this thesis to be more applicable to the problem of periscope depthkeeping.

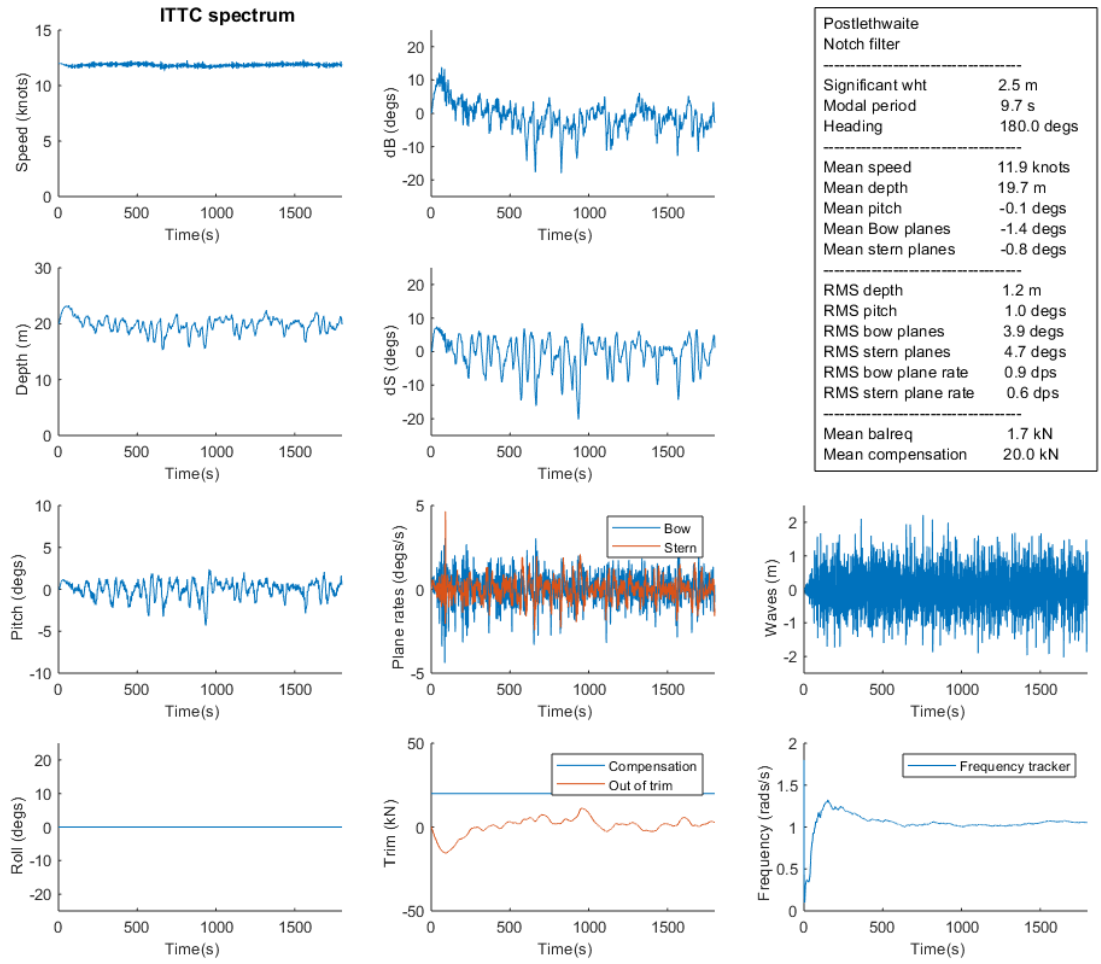

Figure 65: Euclid submarine periscope depthkeeping at 12 knots with an H∞ controller (notch filter but no loop shaping).

As discussed, previously, the typical approach to the design of the input disturbance filter, W_1 is to focus on ensuring the autopilot is correcting the effects of the steady heave force by providing good performance in the form of a steady state depth and pitch disturbance error of 2% (or $|W_1(0)| = 50$) for example. However, we have seen in Chapter 3, that second order slowly varying heave forces are also present when a submarine is operating in irregular waves. Therefore, the next set of simulations includes a modified input disturbance filter, W_1 that is designed to account for not only the steady heave force but also the slowly varying heave force. The filter is designed for performance at low frequency using the Quadratic Transfer Functions of the second order heave force for this design. For a submergence depth of 20 m and zero speed, the QTFs, generated using WAMIT, for the Euclid hull form is shown in Figure 66.

The approach discussed here is perhaps an example of how this problem can be approached but is based on achieving a balance between designing a controller for performance at low frequency (not just zero frequency) and ensuring the control system is not significantly rate limited as a consequence of first order wave effects.

The approach, firstly, considers a line $w_2 - w_1 = c_1$ plotted through the peak of the heave force QTF, in Figure 66, (which of course is parallel to $w_2 - w_1 = 0$ or the steady heave force). The value of c_1 represents a frequency bandwidth, that is chosen to accommodate the slowly varying heave forces that have a significant effect on the submarine. The basis of the filter is taken as a 2D slice through the QTF on a second line, $w_2 + w_1 = c_2$, which is perpendicular to $w_2 - w_1 = c_1$ and intersects at the peak in the QTF ; w_1 and w_2 are the first and second frequency components in the bichromatic waves (plotted in Figure 66 at full-scale frequencies).

An input disturbance filter based the directly on the characteristics of this 2D slice includes increasing gains at frequencies that are typical of first order wave frequencies which means that a controller designed in this way would likely lead to the control surfaces saturating leading to the potential for the autopilot to become unstable. To reduce this impact of the first order wave frequencies on the controller demands a weighting was applied to the QTF 2D slice based on $\frac{|w_2 - w_1|_{min}}{(w_2 - w_1)^{0.85}}$ with $w_2 > w_1$.

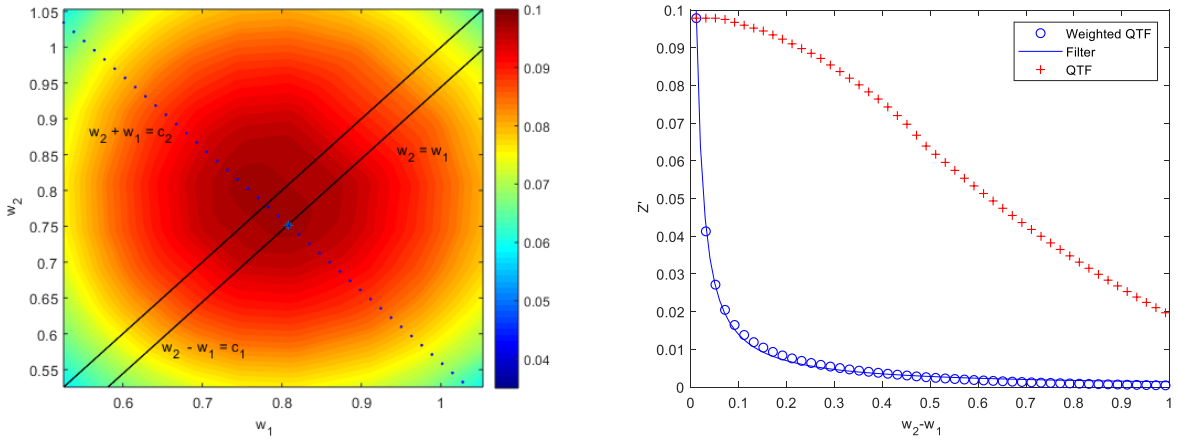

(a) Contour of QTF

(b) 2D slice at $w_2 + w_1 = c_2$

Figure 66: Derivation of input disturbance filter from QTF.

This weighted curve, shown in Figure 66, was used to design of the input disturbance filter, W_1 of the form:

$$W_1 = G_1\left(\frac{a_1 + a_2\Delta\omega}{b_1 + b_2\Delta\omega}\right)$$

where $\Delta\omega = w_2 - w_1$

The output filter W_2 included in this autopilot design was a first order polynomial that further reduced the effect the first order waves would have on the controller demands; also included was the notch filter designed by [Marshfield, 1991].

The benefit of the work described in this thesis is that, armed with an increased knowledge of the second order mean and slowly varying forces on a submarine, alternative approaches to controller design can be easily evaluated using the non-linear time domain simulation to better understand the impact on submarine performance early in the design stage.

Figure 67 shows simulations of the depthkeeping response of the Euclid submarine in head seas using an ITTC spectrum with $H_{1/3} = 2.5\ m$ and $T_0 = 9.7\ s$ (same wave time history as previously; the theoretical and simulated wave spectra are shown in Figure 61). In this case, the controller has been optimised using the input disturbance filter, W_1, derived from the weighted QTF 2D slice and the output disturbance filter W_2. The modified controller leads to a marginal improvement, of approximately 8.3% reduction, in RMS depth at a marginal cost of increased plane activity (7.7% and 4.3% increase in RMS bow plane and stern plane demands respectively).

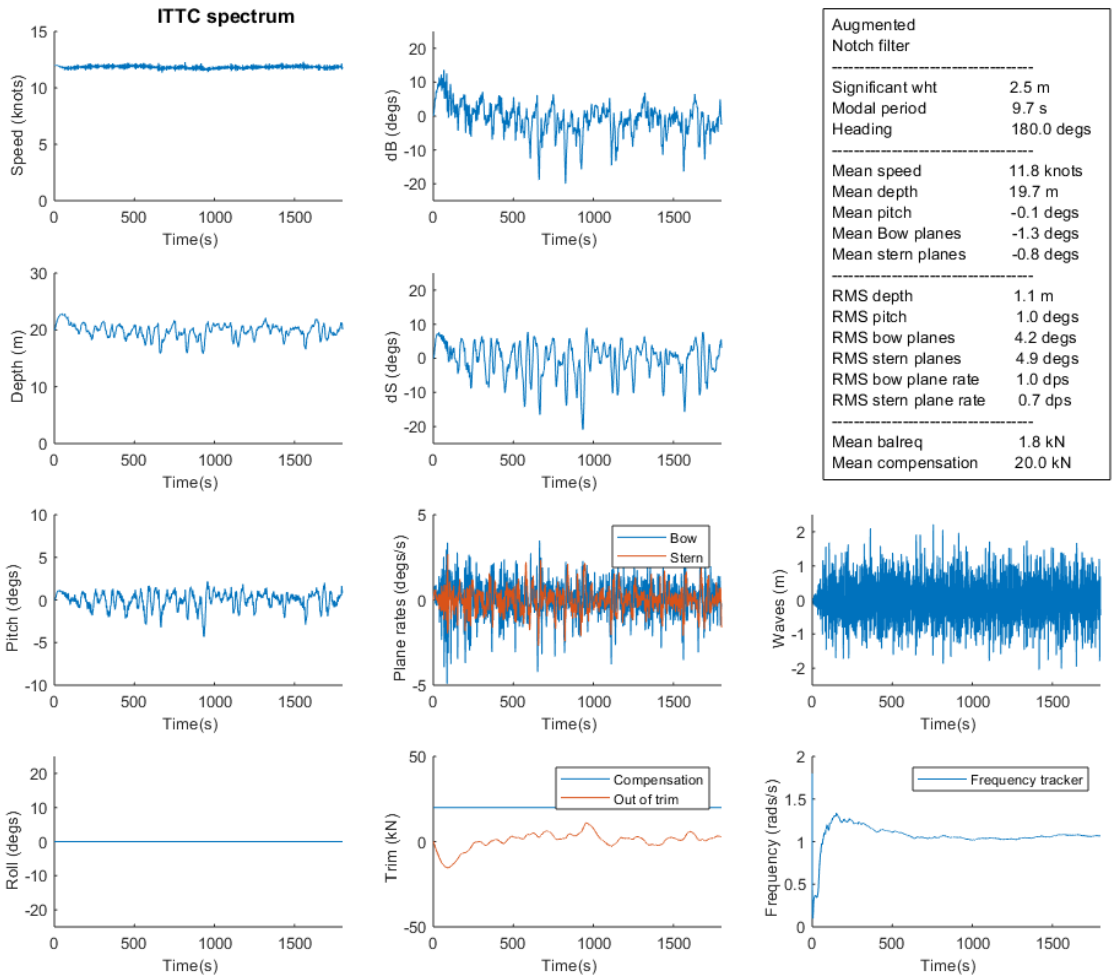

Figure 67: Euclid submarine periscope depthkeeping at 12 knots with a loop shaped controller (with notch filter).

To understand the potential performance gains with this new depth-autopilot at different heading, simulations were performed for the Euclid submarine in beam seas. Figure 68 shows simulations of the depthkeeping response in beam seas using the same depth-autopilot that includes the loop-shaping filters. It should be noted that the amount of seawater ballast required to compensate the mean (steady) second order suction force had to be reduced (compared to the 2 tonnes used for head seas) to reflect the reduction in the force due to the change in heading. To understand why this is the case, we need to refer back to the breakdown of the terms in the integral equation of the second order force on offshore floating structures provided by Pinkster [1980] and discussed on Section 2.5.2. Pinkster showed that the different contributions to the total force on a horizontal cylinder vary significantly with heading. In head waves, the contribution to the force from the pressure reduction due the first order velocity is dominant and contributions from the pressure due

to product of gradient of first order pressure and first order motion and from the products of first order angular motions and inertia forces have only a minor effect. In beam seas, contributions from the pressure due to product of gradient of first order pressure and first order motion and from the products of first order angular motions and inertia are of the same order but opposite in sign, which leads to a reduction in the overall second order force in beam seas.

Actually, in this case, seawater ballast had to be removed from the compensation tanks since, in this case, the direction of the steady vertical force changes with heading, no longer drawing the submarine to the surface but actually trying to push it deeper . Interestingly, this presents another challenge for the design of compensations systems; particularly, the rate at which the pumps can fill and empty the compensation tanks. In the example of the Euclid submarine, the submarine would have approximately 2 tonnes of seawater taken on to counter the mean suction forces in head seas. If the submarine then requires a turn to beam seas, the capacity of the pumps in the compensation system would need to be sufficient to remove 2 tonnes of seawater ballast, and a further 0.55 tonnes from other tanks, to ensure that the submarine is in a good trim once it gets to beam seas. If the pump capacity is insufficient and the submarine turns to beam seas whilst still compensating for the suction forces in head seas, the submarine could be severely out-of-trim in beam seas. During the turn from head seas to beam seas, the total heave force on the submarine due to net effects of the, now varying (due to the change in heading), steady wave induced suction force and the out-of-trim due to the seawater ballast will need to be countered by the control surfaces, until the compensation system can correct the out-of-trim. This may cause the hydroplanes to become angle limited for periods of time during the turn leading to a reduction in depth control performance.

However, once the submarine is again in-trim for beam seas, as is the case in Figure 68, the depth-autopilot appears to be able to maintain depth in this wave condition. It is interesting to note that, compared to the head seas case, the RMS pitch response is greater. This could be as a consequence of the increase in roll motion creating a cross coupling effect in the vertical plane that manifests itself as a increase in the RMS pitch.

Further simulations were performed to understand the effects of forward speed on depth keeping performance. Figure 69 shows simulations of the depthkeeping response, in head seas, at 16 knots using the same loop-shaping filters; in this case, once again the compensation had to be changed to reflect the change in the mean suction force at the higher speed of 16 knots compared to the 12 knots case. As expected, at these higher speeds, the ability of the control surfaces to maintain depth

improves as seen by the reduction in demands on the actuation systems. This is due to the increase in the amount of lift, for a given angle of attack, that can be generated by the control surfaces, as the lift is proportional to the square of the forward speed.

Conversely, in the example of the Euclid submarine design, once the forward speed reduces below 10 knots the ability of the control surfaces to maintain depth in sea state 5 (head seas) is severely limited. Figure 70 shows an example of this, where at 9 knots the submarine is unable to maintain depth and eventually broaches resulting in the simulation terminating at 680 s as a consequence. Prior to broaching the submarine experiences significant depth excursions highlighting the difficulties with maintaining depth at this speed when using hydrodynamic control.

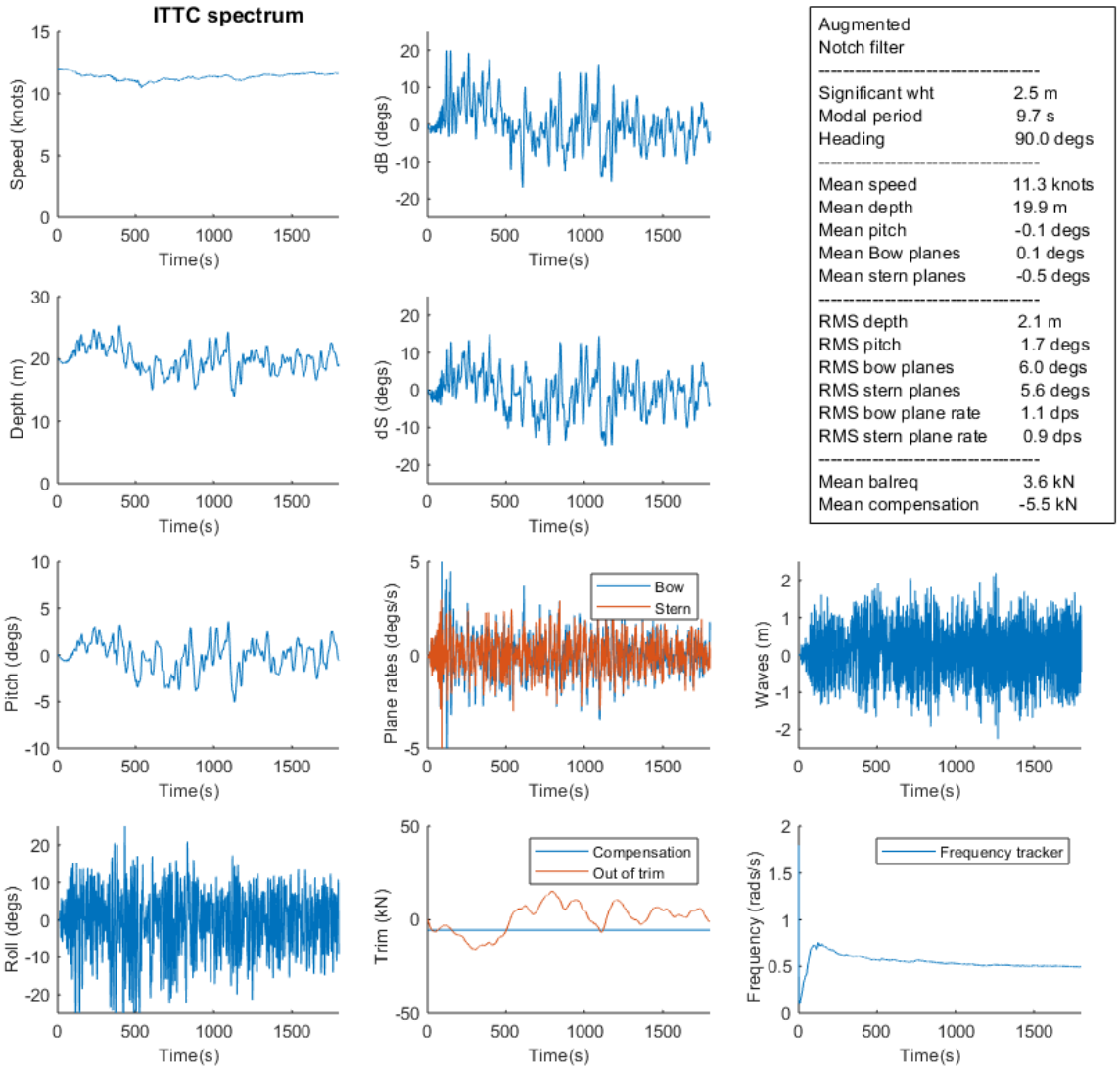

Figure 68: Euclid submarine periscope depthkeeping at 12 knots with a loop shaped controller (with

notch filter) in beam seas.

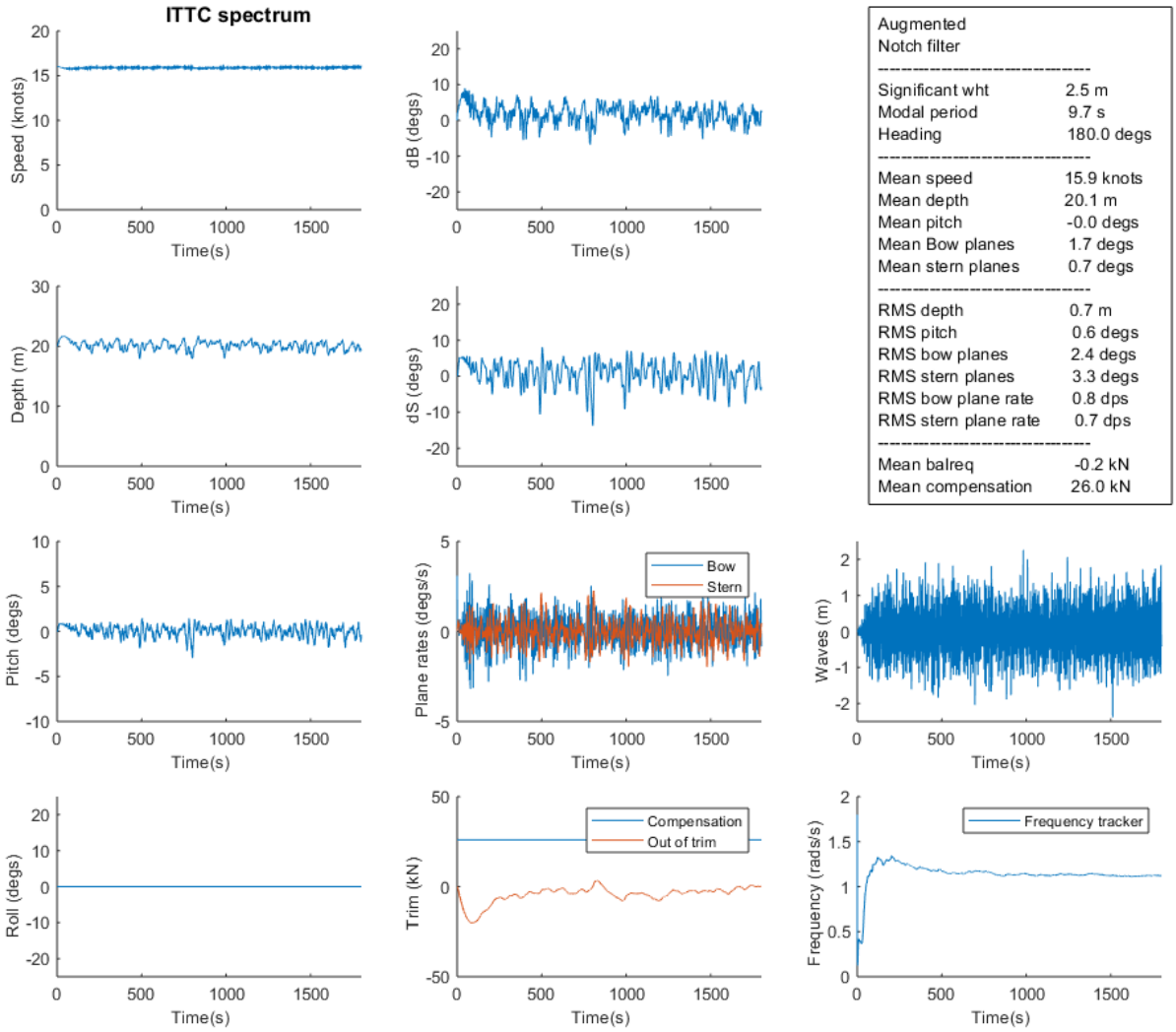

Figure 69: Euclid submarine periscope depthkeeping at 16 knots with a loop shaped controller (with notch filter).

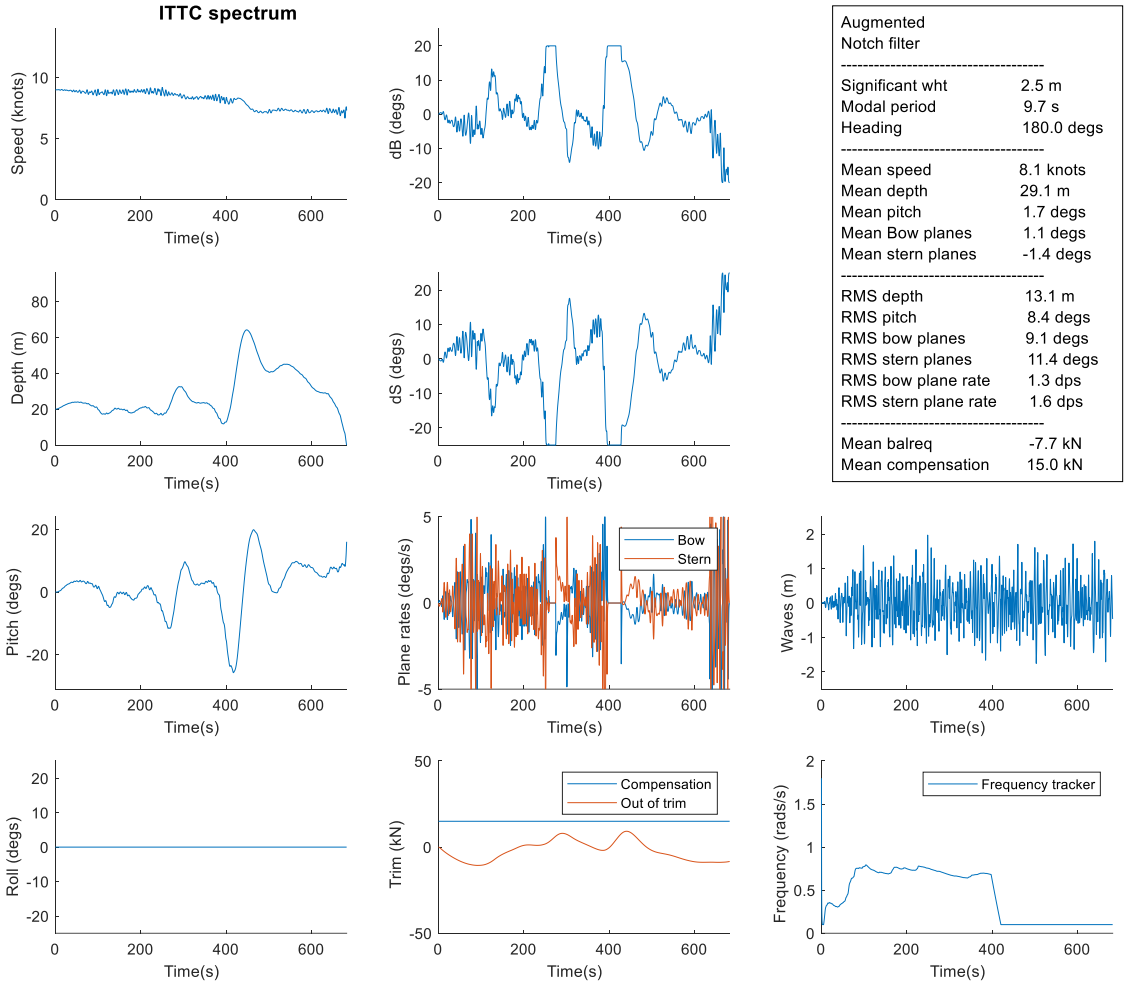

Figure 70: Euclid submarine periscope depthkeeping at initial speed of 9 knots with a loop shaped controller (with notch filter).

4.4 Hydrostatic control.

As mentioned, as the speed of the submarine reduces the effectiveness of the control surfaces reduce; Hirom [1974] reported that typical submarine hydroplanes can generate about 2 kN/(knot)^2 which severely limits the ability of the hydroplanes at slow speeds. As seen previously, through simulation, the control surfaces of the EUCLID are not able to maintain depth below 10 knots in a sea state 5. Therefore, an alternative method of depth control is considered in the form of active compensation tanks. This section describes the results of a number of simulations that show the slow speed depth keeping performance of the EUCLID submarine fitted with an active compensation system. Figure 71 shows the system used in the EUCLID simulations; this is a single compensation tank where the pump valve, controlling the pumping and flooding out of or into the tank, is controlled by a PID controller responding to depth error, [Crossland,2017]. In this example, the flow rate through the pumps is limited to 0.5 m^3/s and the single compensation, located at the LCG of the submarine, and tank has a capacity of 15 tonnes (i.e., +/- 7.5 tonnes).

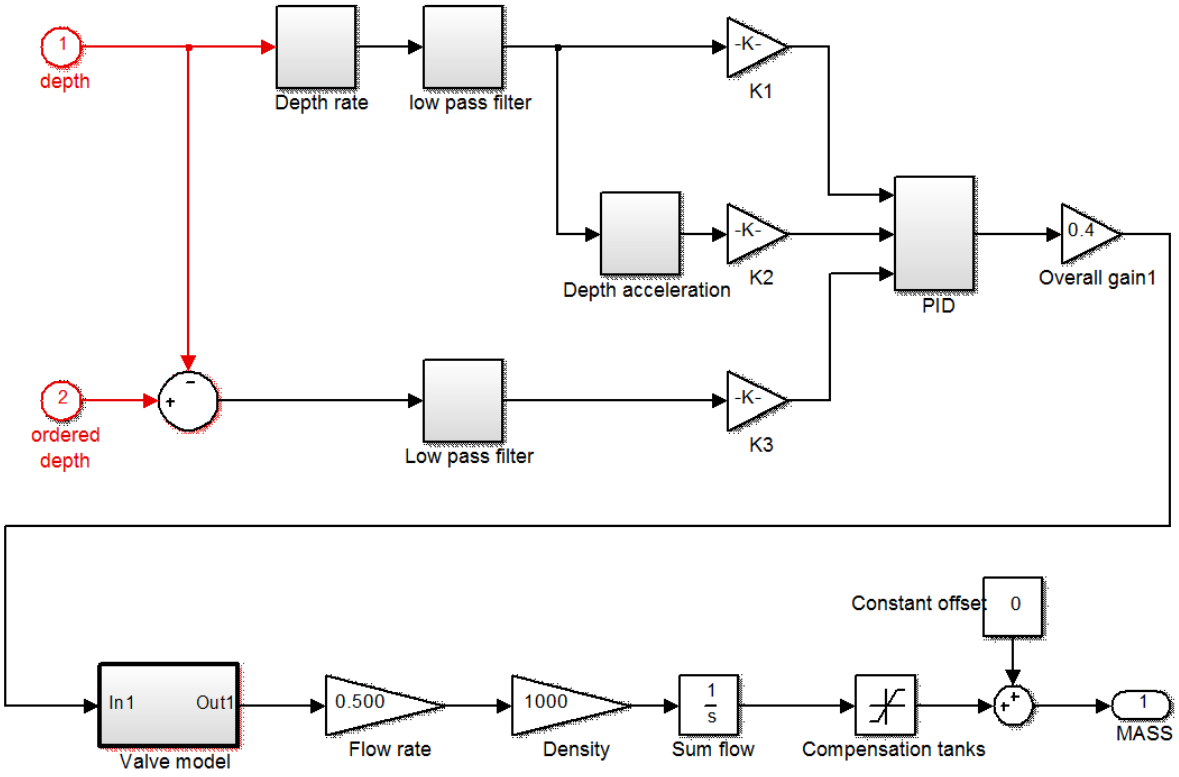

Figure 71: PID controller for an active compensation system (Crossland, 2017).

Figure 72 shows a time history of a depth change, of the EUCLID submarine in calm water (no surface waves), from PD to 150 m at an initial speed of 0.5 knots using the active compensation system. The increase in forward speed is due to the depth change itself, the forward speed (and rate of change

of depth, w' in body axes) causes the pitch angle rather than this single compensation tank system (which since located at the LCG won't generate a moment). Once the submarine is close to the desired depth and the rate of change depth is reduced, forward speed begins to reduce to the initial speed and pitch reduces to around zero.

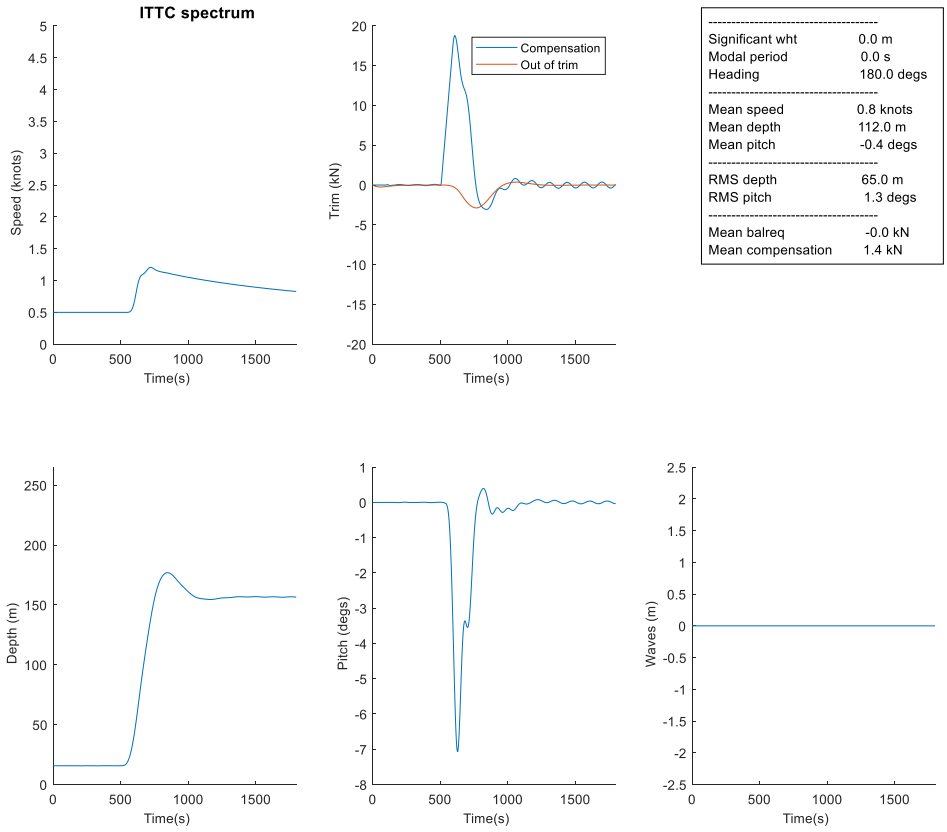

Figure 72: Depth change at 0.5 knots using the active compensation system.

Figure 73 shows an example of the EUCLID submarine at 0.5 knots at depth of 20 m in a sea state 3. The example shows a case where there is active compensation for depth control with no hydroplane actuation at all. Without this ballast system, the submarine would have broached almost immediately. However, whilst this single compensation tank, located around the centre of gravity of the submarine, is able to maintain depth to some extent, the compensation tank is unable to control pitch directly. To control pitch, in addition to depth, would require at least two compensation tanks, ideally both, situated away from the centre of gravity of the submarine. Figure 74 gives an example of including pitch control by using two compensation tanks. In this case, the approach is simplistic in that the control algorithm is essentially the same as the previous depth controller. However, in the case of depth and pitch control, the measured pitch motion is used to derive a required moment to correct the non-zero pitch angle – the demand from the depth

controller is then shared between the two compensation tanks to generate an appropriate pitch restoring moment. As a consequence of introducing the additional pitch control, the RMS pitch and RMS depth are reduced compared to the same responses from the case of a single compensation tank.

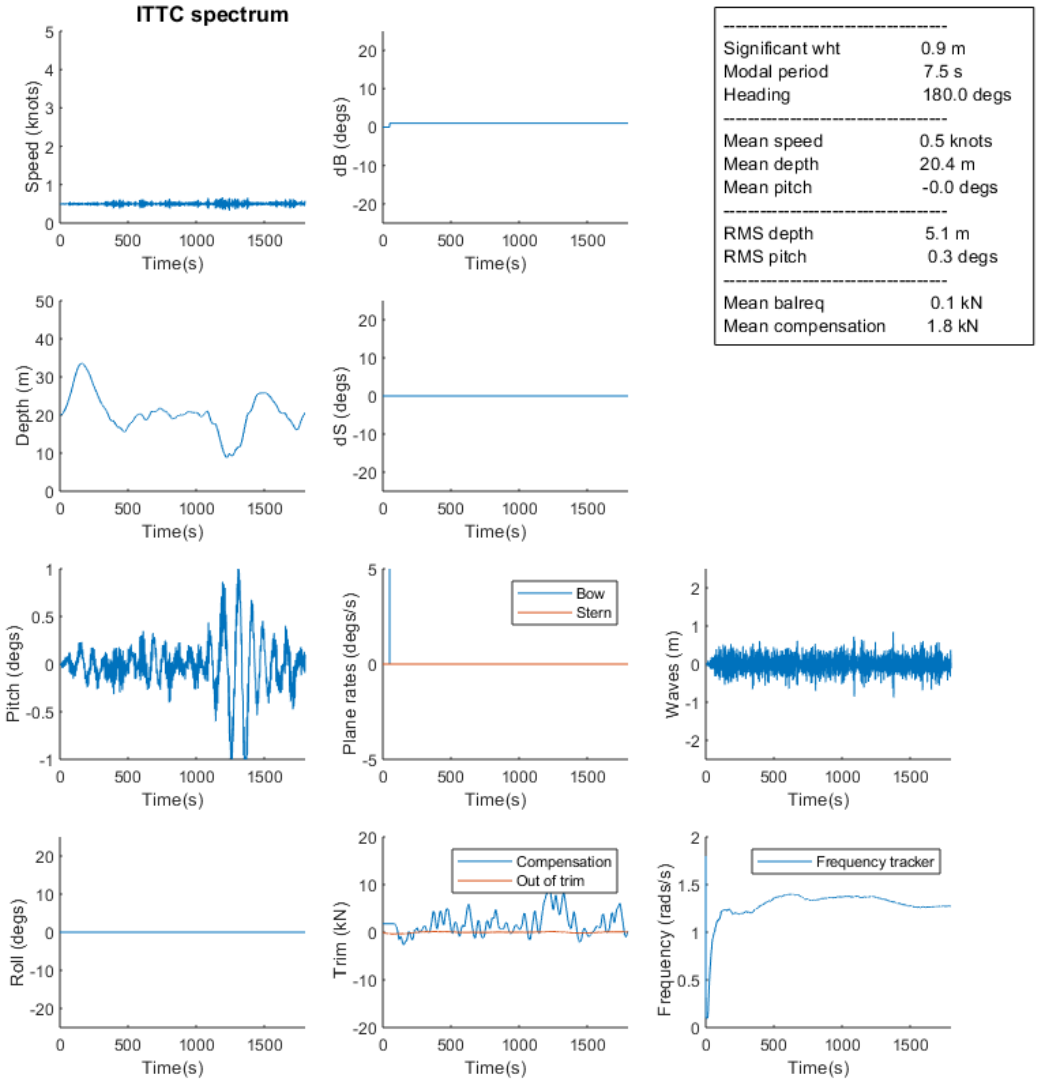

Figure 73: Slow speed depth control in sea state 3. (with a single tank)

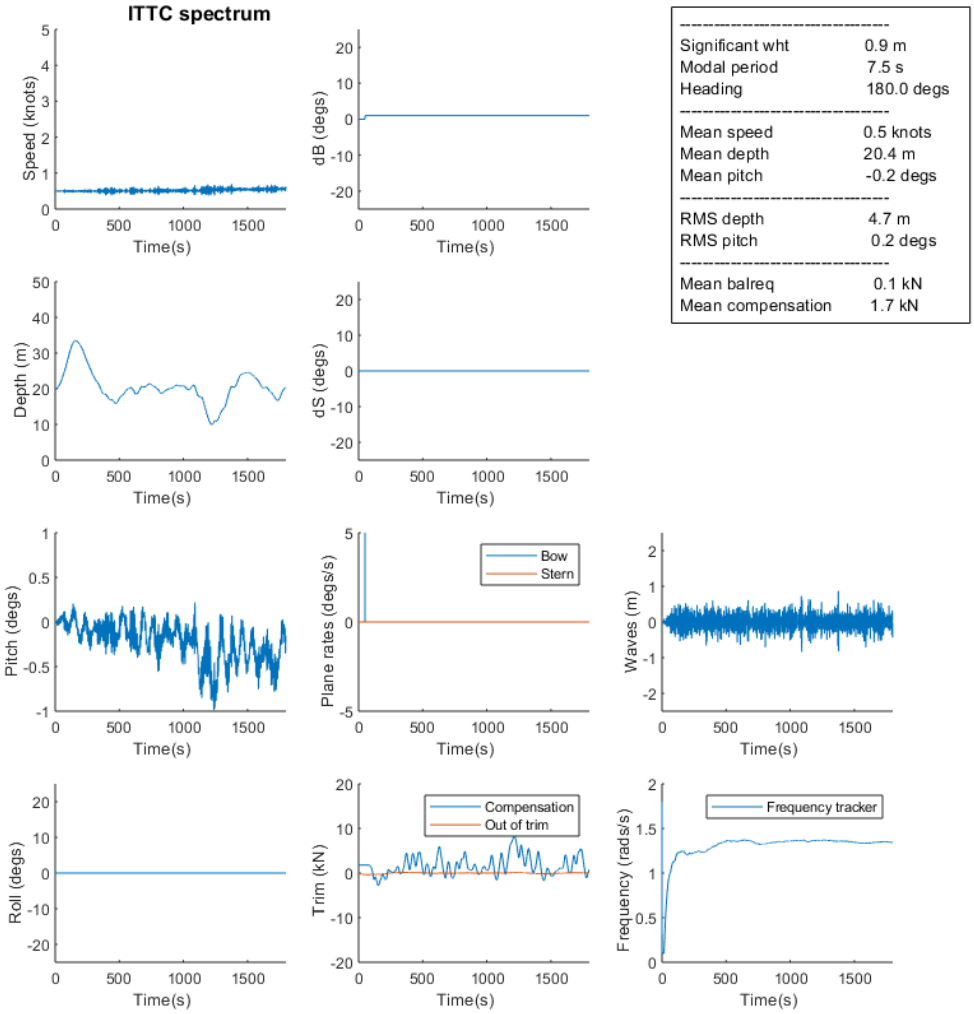

Figure 74: Slow speed depth and pitch control in sea state 3 (with two tanks)

4.5 Chapter summary

This chapter has presented a number of case studies, that bring together the tools and the techniques that have been developed as part of this thesis, to support the designer in understanding how best to accommodate/counter the effects of the suction force (present when a submarine operates near the free surface) from a hydrodynamic and hydrostatic control perspective. The chapter has illustrated, through a number of case studies using the EUCLID geometry, how, based on the knowledge of the second order transfer functions, improvements in depth keeping performance can be obtained through control algorithm design thus reducing the risk of producing poorly designed solutions for submarine depth control in certain wave conditions. Also, presented in this chapter are some examples of hydrodynamic or hydrostatic control simulations performed using the time domain method developed as part of this thesis. The time domain method has been used to evaluate the depthkeeping performance of a submarine for the case where the control

design is increased in complexity to include wave filters and loop shaping functions that are able to account for the effects of the mean forces on the submarine and then further improved to include the effects of the slowly varying second order forces.

The methodology outlined in earlier chapters and demonstrated, by examples, in this chapter, has the potential to allow the integration of both hydrodynamic and hydrostatic control systems earlier into submarine design. Thereby, leading to a reduction in the detailed design, and implementation, of unsuitable solutions, and improving submarine safety.

5 CONCLUSIONS AND FUTURE WORK

An analysis of the hydrodynamics and the control of a submarine, at submergence depths and forward speeds that are typical of the periscope depthkeeping problem, in the presence of incoming waves, is presented. The detailed findings for each section is described at the end of the appropriate chapter. In this chapter, some of the key conclusions are drawn from the research and some suggestions for future work are presented.

5.1 Conclusions from completed work

It is clear from the review of previous work, in Chapter 2, that most of the research has been targeted to solving the problem of the deeply submerged submarine; methods of solving the particular problem of a submarine operating under the influence of surface waves relies on empirical based methods that require a number of simplifying assumptions to be made. The numerical and experimental techniques developed in the ocean engineering community are exclusively for the case of a floating body at zero speed (in some cases incorporating the effects of current).

This research has been shown that, for the zero speed case, frequency domain predictions using the commercial-off-the-shelf software WAMIT have demonstrated that consideration of the second order potential when solving the body boundary condition is significant in the determination of the Quadratic Tranfer Functions of the vertical plane second order force and moment. However, comparisons of WAMIT predictions that includes the second order boundary condition for the free surface with the simplified approach of solving only the first order boundary condition shows that solving the second order problem at the free surface is not necessary for determining the QTFs for the problem of the submarine at periscope depth. As part of the contribution to the field, it has been shown that the wave-induced forces on a submarine are dominated by the combined Froude-Krylov and diffraction forces; the added mass and damping forces are already included as the frequency independent contributions in the hydrodynamics derivatives.

Whilst submarines may operate at zero speed, it is more likely that operations, in close proximity to the sea surface, will be undertaken with forward speeds that are greater than those typical of speeds due currents. Analysis methods are developed in Chapter 2, through adopting and extending existing approaches to include forward speed, particularly for the case of experimental techniques. A non-linear time domain method for determining the wave induced forces and moments on a submarine is developed that is based on the extension and refinement of a rational combination of

existing theoretical methods. This hybrid approach provides a prediction capability, somewhat akin to those used to solve the problem of a surface ship manoeuvring in waves, which can be readily interfaced with the traditional hydrodynamic coefficient based manoeuvring model.

In chapter 3, the knowledge is extended by including the analysis of a series of tests performed on a lightly restrained submarine model in head waves both with and without including forward speed. The experimental data confirm that the physical phenomena that contribute to the second order vertical forces on a submarine, so called suction forces, are the same as those that create the horizontal drift forces in large offshore floating structures. As a consequence, the mean and slowly varying forces on a submarine can be quantified by quadratic transfer functions (QTFs). As part of the contribution to the field, the thesis has confirmed that using data from experiments or predictions where the submarine is not free to move in response to the waves may result in over-estimating the expected forces against which a compensation system would be designed to counter the surface suction effects due to waves. Second order force data obtained for the case where the submarine is free to respond to first order motion provides a more representative means of determining likely forces that can be used in design. For the case considered in this thesis, Newman's approximation does not replicate the peaks in the QTFs for large frequency differences (away from mean values where the frequency difference is zero); The approximation may be sufficient for use in early system design studies in establishing sizes of compensation tanks and pump capacities for example. However, there is a possibility using such an approach could lead to such systems having insufficient capability to deal with the combined effects of the slowly varying and the mean forces.

Finally, the experimental data are presented in such a way that they can be used by others for their validation studies.

Chapter 4 brings together the tools and the techniques that have been developed as part of this thesis to provide a series of cases studies to help the designer in understanding how best to accommodate the effects of the suction force (present when a submarine operates near the free surface) from a hydrodynamic and hydrostatic control perspective. The chapter reflects on submarine control using both hydrodynamic and hydrostatic methods using control surfaces or compensation tanks respectively. The different approaches used for designing and evaluating the performance of a control system to reduce the effects of surface waves on the submarine are reviewed some technical shortfalls are highlighted. The more advanced control techniques look to remove the first order effects of the waves by introducing filters into the control system design. However, whilst the use of a non-zero mean heave force and pitch moment on a submarine is readily

recognised in control system design, it is assumed that the second order effects consist only of these non-zero mean components. This approach means that the slowly varying second order forces, that are quantified by QTFs, have not been routinely incorporated into the control system design. This thesis demonstrates the potential benefits from including QTFs in the control system design process.

5.2 Suggestion for future work

The approach described in this thesis requires a method of describing the dynamic behaviour of a submarine under the influence of surface whilst operating at speeds and depths typical of periscope depthkeeping operations. The computational tool developed as part of this thesis may not be considered the most advanced computational capability. The choice of approach was based on a balance between fidelity and computational time, or a balance between computational sophistication and practicable applications, since the data required to inform on control system design is quite extensive and can be time consuming to generate. The contribution to the field in this thesis is a practicable method for quantifying the second order suction forces on a fully appended submarine that can be readily interfaced with an empirical manoeuvring model for use in design studies.

In the context of the more modern computational techniques, clearly, unsteady CFD will develop further, which when coupled with the ever increase in computing capability, will provide a different outlook to the balance between fidelity and computational time in the future. Nevertheless, these techniques will require validation, ideally for a range of headings rather than the specific problem of head seas largely described here. Therefore, the approach used for performing semi-captive model tests in oblique seas and including forward speed should be investigated further.

As discussed by Perez, [2003], methods for performance assessment bring important insights into control system design, because these allow control system specifications to be established that commensurate with the performance assessment methods themselves. The methods developed as part of this thesis can be used to establish specifications that will support future submarine design studies. The proposed approach, described here, provides a systematic method for control system design based on an increased understanding of the second order effects; this approach should be considered for future control system design which may allow for tailoring in the future.

REFERENCES

23rd International Towing Tank Conference Ocean Engineering Committee. Analysis procedure for model tests in regular waves. No, 7.5 – 02 07 - 03.2, 2002.

24th International Towing Tank Conference, The Manoeuvring Committee report. Proceedings, Vol I, Edinburgh, UK, September 2005.

25th International Towing Tank Conference, The Seakeeping Committee report. Proceedings, Vol I, Fukuoka, Japan, September 2008a.

25th International Towing Tank Conference Seakeeping Committee. Procedure on Seakeeping Experiments, Procedure No. 7.5-02-07-02.1, September 2008b.

28th International Towing Tank Conference, The Resistance Committee report. Proceedings, Vol I, Wuxi, China, September 2017.

Abbot, IA., Von Doenhoff, AE., Theory of wing sections including a sumary of airfoil data. Dover Publications, Standard Book Number 486-60586-8, 1949

Bailey, PA., Price, WG., and Temarel P., A unified mathematical model describing the manoeuvring of a ship travelling in a seaway. Trans RINA, W6, 1997.

Bayliss, JA, Kimber, NI, Marchant, P, Bryars J. Submarine trials and experimentation – dealing with real-life data. RINA Warship 2005: Naval Submarines 8, London, June 2005.

Bertram, V., Practical ship hydrodynamics. Published by Butterworth-Heinemann, ISBN 0 7506 4851 1, 2000.

Bishop, RED., Parkinson, AG., Directional stability and control of marine vehicles. Department of Mechanical Engineering, University College London, Nav. Arch. Rep. 3/70, 1970a.

Bishop, RED., Parkinson, AG., On the planar motion mechanism used in ship model testing. Phil Trans (A), Volume 226, pp35-61, 1970b.

Bishop, RED., Parkinson, AG., Price, WG., The equations of motion of a submarine near the surface. Admiralty Marine Technology Establishment Technical Memorandum, Haslar, AMTE(H) TM78025, June 1978.

Bowker, J., Crossland, P., Morales, R., Forces and moments acting on a semi-constrained submarine model under waves. Internal QinetiQ report, October 2020.

Bretschneider, CL. Wave variability and wave spectra for wind generated gravity waves. Beach Erosion Board Tech. Memo. No.113, US Army Corps of Engineers, 1959.

Burcher, RK., Rydill, LT. Concepts in submarine design, Cambridge University Press, 1994. ISBN 0 521 41681 7.

Byström, L., Adaptive control of a submarine in a snorting condition in waves. RINA Warship'88: Conventional Naval Submarines, London, 1988.

Chatjigeorgiou, IK., Hydrodynamic exciting forces on a submerged oblate spheroid in regular waves. Computers & Fluids, Vol 57, pp151–162, 2012.

Chatjigeorgiou, IK., Miloh, T., Hydrodynamics of submerged prolate spheroids advancing under waves: Wave diffraction with forward speed. Journal of Fluids and Structures, Vol 49, pp202–222, 2014.

Chen, B., Lu, L., Greated, CA., Kang, H., Investigation of wave forces on partially submerged horizontal cylinders by numerical simulation. Ocean Engineering. Vol 107, pp23–31, 2015.

Comstock, JP., Principles of Naval Architecture, Vol III, SNAME, 1967.

Cooley, JW., Tukey JW., An algorithm for the machine computation of the complex fourier series, Mathematics of Computation, Vol. 19, April 1965.

Cooper, G.J., EUCLID 10.17, Submarine motions in confined waters – final report. QinetiQ/07/02834, December 2007, QinetiQ Proprietary.

Crepel JL., Bovis AG., New trends in the design of steering and diving control systems. RINA Warship'91: Naval Submarines 3, London, May 1991.

Crossland P, Internal QinetiQ report, March 2005.

Crossland P., Profiles of Excess Mass for a Generic Submarine Operating Under Waves, Pacific 2013: International Maritime Conference, Sydney, October 2013.

Crossland P., Marchant P., Thompson N., Evaluating the Manoeuvring Performance of an X-Plane Submarine. Warship 2011: Naval Submarines and UUVs, 29 – 30 June, 2011, Bath, UK

Crossland P., Kimber NI., Thompson N., Understanding the Manoeuvring Performance of an X- plane Submarine in Deep Water and Near the Free Surface. Pacific 2012: International Maritime Conference, Sydney, January 2012.

Dev, AK., Pinkster, JA., Viscous Mean Drift Forces on Moored Semi-Submersibles. Proceedings of the Fifth International Offshore and Polar Engineering Conference, The Hague, The Netherlands, 1995.

Doctors LJ., Beck RF., Numerical aspects of the Neumann–Kelvin problem. Journal of Ship Research. 31 198

Faltinsen OM., Wave and current induced motions of floating production systems. Applied Ocean Research, Vol 15, pp351-370, 1994

Faltinsen OM., Løken AE., Slow drift oscillations of a ship in irregular waves, Applied Ocean Research, Vol 15, No.1, 1979

Feldmann, JP., Method of predicting captive-model experiments to predict the stability and control characteristics of submarines. Carderock Division, Naval Surface Warfare Center Bethesda, USA, CRDKNSWC-HD-0393-25 June 1995

Fossen, TI., Guidance and control of ocean vehicles. John Wiley and Sons Ltd, 1994, ISBN 0 471 94113 1

Fryer DK., The application of random signals to models for evaluating the performance of ships. PhD thesis, Portsmouth Polytechnic, 1991

Gabler, U., Submarine design. Bernard& Graefe Verlag, Koblenz, 1986, ISBN 3-7637-0124-9

Gertler, M., Hagen GR., Standard equations of motion for submarine simulation. Naval Ship Research and Development Center Report No. 2510, June 1967, David Taylor Model Basin, Carderock, MD, USA.

Glauert, H., The elements of aerofoil and airscrew theory, Cambridge University Press, 1947.

Griffin, MJ., Numerical prediction of the maneuvring characteristics of submarine operating near the free surface. PhD thesis, Department of Ocean Engineering, Massachusetts Institute of Technology, 2002.

Grimble MJ., Katebi MR., Zhang Y., . H_∞ - based ship fin-rudder roll stabilisation design. 10th Ship Control Systems Symposium, October 1993, Ottawa.

Grimble. MJ., Patton, RJ., Wise, DA., Use of Kalman filtering techniques in dynamic ship positioning systems, IEE proceedings, Vol. 127, Pt. D, No. 3.

He, S., Seddighi, M., Turbulence in transient channel flow. Journal of Fluid Mechanics, Vol 715, pp60-102, 2013.

Hervey, J., Submarines. Volume 7 of Brassey's Sea Power: Naval vessels, Weapons Systems and Technology Series. 1994, ISBN 0 08 040970 9.

Hess JL., Smith AMO., Calculation of non-lifting potential flow about arbitrary three-dimensional bodies. Douglas Aircraft Division Report No. E.S. 40622, March 1962.

Hirano, M., Takashina, J., Takeshi, K., Saruta, T., Ship turning trajectory in regular waves. Published in the West Japan Society of Naval Architecture, 1980.

Hirom, CPJ., A review of forces on a submarine near the surface. Admiralty Experiment Works Internal publication, AEW Report 16/74, Haslar, May 1974.

Hirom, CPJ., The mathematical analysis of submarine motion near the free surface. Admiralty Experiment Works Internal publication, AEW TR 77015, Haslar, March 1977.

Hsu, FH., Blenkarn, KA., Analysis of peak mooring forces caused by slow drift oscillations in random seas. Offshore Technology Conference, Houston, 1970

Hutchison, BL., Seakeeping studies: a status report. Trans. Society of Naval Architects and Marine Engineers, Vol.98, pp263-317, 1990.

Katz, J., Plotkin, A., Low speed aerodynamics – second edition. Cambridge University Press, 2001, ISBN 0 521 66219 2.

Kim, M-H., Yue, DKP., The complete second-order diffraction solution for an axisymmetric body Part 1. Monochromatic incident waves. Journal of Fluid Mechanics, vol. 200, pp 235-264, 1989.

Kim, M-H., Yue, DKP., The complete second-order diffraction solution for an axisymmetric body Part 2. Bichromatic incident waves and body motions. Journal of Fluid Mechanics, vol. 211, pp 557-2593, 1990.

Kim, S., Wilson PA., Chen, ZM., Large-eddy simulation of the turbulent near wake behind a circular cylinder: Reynolds number effect. Applied Ocean Research, Vol 49, pp1-8, 2015.

Kimber, NI., Crossland, P., Advances in experimental techniques for understanding the manoeuvring performance of submarines. RINA Warship 2008: Naval Submarines 9, Glasgow, June 2008.

Kimber, NI., Thompson, N., Submarine motions in confined waters, EUCLID RTP 10.17. Analysis of captive model experiments and manoeuvring simulations, QinetiQ/07/01163, April 2007, QinetiQ Proprietary.

Klose, GJ., Acosta,AJ., Unsteady force measurements on fully wetted hydrofoils in heaving motion. Journal of Ship Research, Vol. 12 No 1, March 1968.

Kormilitsin, YN., Khalizev, OA., Theory of submarine design. Published by Riviera Maritime Media, 2001, ISBN 0-9541446-0-0.

Lewis, EV., Principles of Naval Architecture, Vol III, Motions in waves and controllability, SNAME, 1989.

Lewis, FM., The inertia of water surrounding a vibrating ship. Trans SNAME, 1929.

Lloyd, ARJM., Progress towards a rational method of predicting submarine manoeuvres, RINA symposium on Naval Submarines, London, 1983.

Lloyd, ARJM., Seakeeping: ship behaviour in rough weather. Ellis Horwood Series in Marine Technology, ISBN 0-7458-0230-3. 1989a.

Lloyd, ARJM, A theory for submarine manoeuvring SUBSIM (Issue 3). Admiralty Research Establishment Internal Publication, Gosport, 1989b.

Mackay M, Conway, JT,. Modelling the crossflow body separation on a submarine using a panel method. Warship'91: RINA International Symposium on Naval Submarines 3, May 1991, London.

Mackay M., The standard submarine model: A survey of static hydrodynamic experiments and semi-empirical predictions. TR 2003—079, Technical Report DRDC Atlantic, Dartmouth, Nova Scotia, June 2003.

Mandzuka S, Mathematical model of a submarine dynamics at the periscope depth. Brodogradnja 46, (1998), 2, pp129-138.

Marthinsen, T., Calculation of slowly varying drift forces. Applied Ocean Research, Vol. 5, No. 3, 1983.

Martinussen K., Submarine motions in confined waters – tests in the Ocean Basin Labatory close to the surface in oblique waves. EUCLID/RTP 10.17/MARINTEK/WE-2.5/TR/1/1, Marintek Report 810009.00.01, March 2006.

Mofidi, A., Carrica, P.M., Simulations of zigzag maneuvers for a container ship with direct moving rudder and propeller. Computational Fluid 96, 191–203, 2014.

Murphy, JC., A novel approach to turbulence stimulation for ship-model testing. Technical Report US Naval Academy No. 390, 2010

Musker, AJ., Loader, PR., Butcher, MC., Simulation of a submarine under waves. International Shipbuilding Progress, 35, No. 404, 1998, pp 389-410.

Musker, AJ., Prediction of wave forces and moments on a near-surface submarine. Shipbuilding: Marine Technology Monthly, Volume 31, January 1984.

Newmann, JN., Second order slowly varying forces on vessels in irregular waves. International Symposium on Dynamics of Marine Vehicles and Structures, London, 1974.

Nikushchenko, D., Zubova, A., Hydrodynamic Interaction Phenomena Investigations during the Ship Overtaking Maneuver for Marine Related Simulators with the Use of CFD Methods. MARSIM 2015, Newcastle, UK.

Odabasi, AY., Hearn, GE., Seakeeping theories: what is the choice? Trans. North East Coast Institution of Engineers and Shipbuilders. Vol 94, pp53-84, 1977.

Ogilvie TF., First- and second- order forces on a cylinder submerged under a free surface. Journal of Fluid Mechanics, Vol.16, pp451-472, 1963.

Perez T., Performance analysis and constrained control of fin and rudder-based roll stabilizers for ships. Phd thesis, University of Newcastle, Australia, July 2003.

Pinkster, JA., Mean and low frequency wave drifting forces on floating structures. Ocean Engineering, Vol 6, pp593-615, 1979.

Prandtl, L., Über Flüssigkeitsbewegung bei sehr kleiner Reibung. Verhandlungen des III. Internationalen Mathematiker Kongresses, Heidelberg, 1904, pp. 484–491, Teubner, Leizig.

Ray, A, Seshadri V, Singh SN, Sen D, Manoeuvring studies of underwater vehicles – a review. International Journal of Maritime Engineering, 2008.

Sahin, I., Crane, JW., Watson, KP., Application of a panel method to hydrodynamics of underwater vehicles. Ocean Engineering, Vol.24, No. 6, pp501-512, 1997.

Sahin, I., Hyman, MC., Nguyan, TC., Three dimensional flow around a submerged body in finite-depth water. Applied Mathematics Modelling, 1994, Vol.18.

Salvesen, N., Tuck, EO., Faltinsen, O. Ship motions and sea loads. Trans Society of Naval Architects and Marine Engineers, Vol 78, pp 250-287, 1970.

Schei, TS., Wave disturbance filtering in dynamic positioning systems. IFAC Proceedings, Volume 28, Issue 2, May 1995, pp 27-34.

Shao, YL., Numerical potential-flow studies on weakly-nonlinear wave-body interactions with/without small forward speeds. Doctoral theses at Norwegian University of Science and Technology, 2010:215.

SNAME (1950). Nomenclature for treating the motion of a submerged body through a fluid. Technical Report Bulletin 1-5. Society of Naval Architects and Marine Engineers, New York, USA.

Stokes, GG., On the theory of oscillatory waves, Transactions, Cambridge Philosophical Society 8, 1847.

Sutulo, S., Guedes Soares, G., A unified nonlinear mathematical model for simulating ship manoeuvring and seakeeping in regular waves. International Conference On Marine Simulation And Ship Manoeuvrability, Terschelling, The Netherlands, 2006

Tucker, MJ., Challenor, PG., Carter, DJT., Numerical simulation of a random sea: a common error and its effect upon wave group statistics , Applied Ocean Research, Vol. 6, pp. 118-122, 1984.

Ursell, F., On the wave motion near a submerged sphere between parallel walls: I Multipole Potentials. Quarterly Journal Mechanics and Applied Mathematics, Vol 52(4), 585-604, 1999

Ursell, F., On the heaving motion of a circular cylinder on the surface of a fluid. Quarterly Journal Mechanics and Applied Mathematics, Vol 2, 218-231, 1949

Veillon A., Aillard JM., Brunet, P. Submarine depth control under waves: an experimental approach. RINA Warship '96: naval Submarines 5 – the total weapon system, London, 1996.

Wang, S., Motions of a spherical submarine in waves. Ocean Engineering, Vol.13, No.3, pp 249-281, 1986.

Westlake, PC., Wilson, PA., A new conformal mapping techniques for ship sections. International Shipbuilding Progress, Vol 47, No. 449, pp5-22, 2000.

Whicker, LF., Fehlner, LF., Free stream characteristics of a faily of low aspect ratio all moveable control surfaces for application to ship design. David Taylor Model Basin Report 933, 1958, Carderock, MD, USA.

Wu, GX. and Eatock Taylor, R., Radiation and diffraction of water waves by a submerged sphere at forward speed, Proceedings of the. Royal Society London, Vol.A417, pp.433-461.1988

Wu, GX. and Eatock Taylor, R., Second order diffraction forces on horizontal cylinders in finite water depth, Applied Ocean Research, Vol.12, pp.106-111. 1990

Wu, GX. and Eatock Taylor, R., The exciting force on a submerged spheroid in regular waves, Journal of Fluid Mechanics Vol.182 pp.411-426.1987

Wu, GX., Witz, JA., Ma, Q. Brown DT., Analysis of wave induced drift forces acting on a submerged sphere in finite water depth. Applied Ocean Research, Vol. 16, pp 353-361, 1994.

Wu, GX., Second-order wave radiation by a submerged horizontal circular Cylinder. Applied Ocean Research, Vol. 15, pp 293-303, 1993.

Wu, TM., Hydrodynamic loadings acting on submerged bodies advancing in waves an assessment of accuracy. Engineering Analysis with Boundary Elements Vol. 13, pp 21-33, 1994.

APPENDIX A FORCES AND MOMENTS ON A SUBMARINE

A1 IMPLEMENTATION OF HESS AND SMITH

Hess and Smith [1962] presented a method for calculating the velocity potential around the surface of an arbitrary body S that is deeply submerged with the steady free stream flow represented by the velocity vector $\bar{V}_\infty = (U_\infty, V_\infty, W_\infty)$.

The fluid velocity at a point is expressed as the negative gradient of the potential ϕ_B, where ϕ_B satisfies the following boundary conditions:

$$\nabla^2 \phi_B = 0 \text{ in fluid region R}$$

$$\frac{\partial \phi_B}{\partial n} = -\bar{V}_\infty . \bar{n} \text{ on the body surface S}$$

where in this case $\bar{n}$ is the unit outward normal and

$$\phi_b \to 0 \; for \; x^2 + y^2 + z^2 \to \infty$$

The body surface is covered with a surface source distribution σ and the potential ϕ_b is written as:

$$\phi_b(x', y', z') = \iint_S \frac{\sigma(q)}{r(p,q)} ds$$

where $r(p,q)$is the distance from the integration point q on the surface to the field point p (x', y', z') (see Figure A1 from Hess and Smith [1962]).

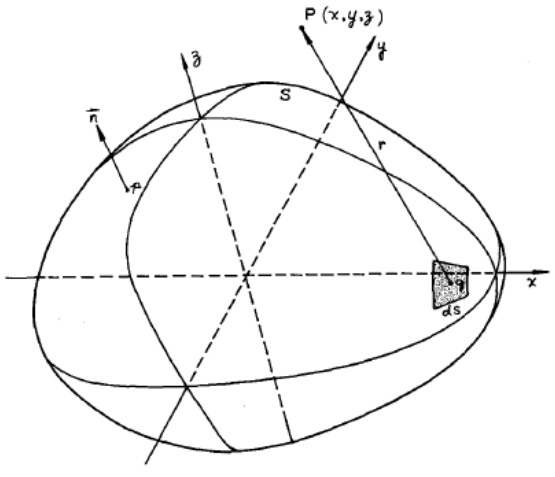

Figure A1: *The potential due to a surface source density distribution [Hess and Smith, 1962].*

The form of ϕ_b in the above equation satisfies the boundary conditions; the function σ, which is the source distribution, must be determined to satisfy the body boundary condition that requires the evaluation of the normal derivative of the integral equation at a point p on the surface S. However, this is singular at points on the surface and so Hess and Smith, [1964] approached the problem by extracting a principal value corresponding to the contribution of the local source to the local normal velocity and the contribution of the source to the remainder of the surface.

The principal value was taken to be $2\pi\sigma(p)$ (only at the null point, it is 2π) and the normal derivative of $\phi_b$on the body surface is:

$$\left.\frac{\partial \phi_b}{\partial n}\right|_s = 2\pi\sigma(p) - \iint_S \frac{\partial}{\partial n}\left(\frac{1}{r(p,q)}\right)\sigma(q)ds$$

which gives the integral equation:

$$2\pi\sigma(p) - \iint_S \frac{\partial}{\partial n}\left(\frac{1}{r(p,q)}\right)\sigma(q)ds = -V_\infty.\bar{n}(p)$$

In this case the flow velocity is opposite to the direction of the x-axis. Once this equation is solved for σ, the disturbance potential ϕ_b (and hence the velocities) can be found. This method is valid for arbitrary bodies, the only requirement is that the unit normal $\bar{n}$ is continuous across the body surface, [Hess and Smith, 1964] – what this means for practical purposes is that the body should not have sharp corners i.e., infinite curvature. This is not expected to be an issue for typical submarine hull forms where sharp corners tend to be avoided.

The numerical integration of the above equation requires a representation of the body surface by approximating the body surface from a series of surface data points, [Hess and Smith, 1962]. Hess and Smith [1962] method used planar elements with a constant-strength source distribution over each panel bounded by four straight lines; a first order approximation panel and zeroth order approximation of the source to determine the potential flow around arbitrary 3D non-lifting bodies.

There have been many advances in discretization techniques for potential flow methods, see Chan [1990] as an example of a review of these techniques; techniques such as higher order panel methods. However, the fundamentals of many of these methods are based on the work of Hess and Smith [1962]. Therefore, a discretization method based upon the approach by (Hess and Smith, 1962) except with triangular elements was used in this research. As mentioned earlier Hess and

Smith [1962] chose to use quadrilateral elements for convenient data handling. However, utilities that come with more modern commercial software packages allow for more sophisticated data handling processes.

Body discretization.

Consider a plane triangular source element lying in the(x', y') plane as shown in Figure A2. Without loss of the generality, the element is assumed to be on z'=0 plane. The surface source element of strength σ is constant across the element of area A. The coordinates defining the three corners of the element are (x_1, y_1), (x_2, y_2) and (x_3, y_3).

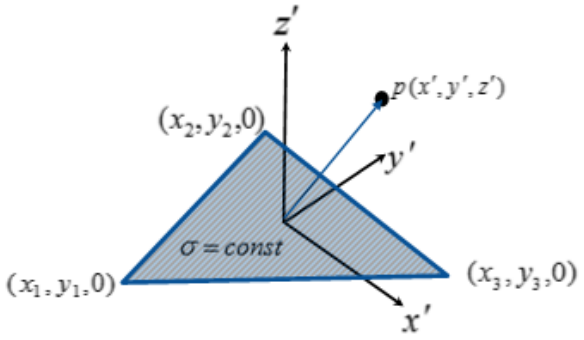

Figure A2: *A plane triangular source element.*

The velocity components induced by this source element are required at some point; the potential at *p (x'y',z')* is given by:

$$\phi_p(x', y', z') = \frac{\sigma}{4\pi}\int_A \frac{1}{r}dA = \frac{\sigma}{4\pi}\int_A \frac{1}{\sqrt{(x'-x_0)^2 + (y'-y_0)^2 + z'^2}}dA$$

The velocity components at *p* are:

$$(u, v, w) = \left(-\frac{\partial\phi_p}{\partial x}, -\frac{\partial\phi_p}{\partial y}, -\frac{\partial\phi_p}{\partial z}\right)$$

Hess and Smith [1962] reduced the problem of finding the velocities induced by a triangular element to the problem of determining velocities induced by the pair of semi-infinite strips associated with one side of the element to derive the following for the potential and for the components for velocities (although shown here for triangular elements rather than quadrilaterals).

$$\phi_p(x,y,z) = -\frac{\sigma}{4\pi}\left[\frac{(x-x_1)(y_2-y_1)-(y-y_1)(x_2-x_1)}{d_{12}} ln\frac{r_1+r_2+d_{12}}{r_1+r_2-d_{12}}\right.$$
$$+\frac{(x-x_2)(y_3-y_2)-(y-y_2)(x_3-x_2)}{d_{23}} ln\frac{r_2+r_3+d_{23}}{r_2+r_3-d_{23}}$$
$$+\frac{(x-x_3)(y_1-y_3)-(y-y_3)(x_1-x_3)}{d_{31}} ln\frac{r_3+r_1+d_{31}}{r_3+r_1-d_{31}}$$
$$-|z|\left\{tan^{-1}\left(\frac{m_{12}e_1-h_1}{zr_1}\right)-tan^{-1}\left(\frac{m_{12}e_2-h_2}{zr_2}\right)+tan^{-1}\left(\frac{m_{23}e_2-h_2}{zr_2}\right)\right.$$
$$\left.\left.-tan^{-1}\left(\frac{m_{23}e_3-h_3}{zr_3}\right)+tan^{-1}\left(\frac{m_{31}e_3-h_3}{zr_3}\right)-tan^{-1}\left(\frac{m_{31}e_1-h_1}{zr_1}\right)\right\}\right]$$

$$u = \frac{\sigma}{4\pi}\left[\frac{(y_2-y_1)}{d_{12}} ln\frac{r_1+r_2+d_{12}}{r_1+r_2-d_{12}}+\frac{(y_3-y_2)}{d_{23}} ln\frac{r_2+r_3+d_{23}}{r_2+r_3-d_{23}}+\frac{(y_1-y_3)}{d_{31}} ln\frac{r_3+r_1+d_{31}}{r_3+r_1-d_{31}}\right]$$

$$v = \frac{\sigma}{4\pi}\left[\frac{(x_2-x_1)}{d_{12}} ln\frac{r_1+r_2+d_{12}}{r_1+r_2-d_{12}}+\frac{(x_3-x_2)}{d_{23}} l\frac{r_2+r_3+d_{23}}{r_2+r_3-d_{23}}+\frac{(x_1-x_3)}{d_{31}} ln\frac{r_3+r_1+d_{31}}{r_3+r_1-d_{31}}\right]$$

$$w = \frac{\sigma}{4\pi}\left[tan^{-1}\left(\frac{m_{12}e_1-h_1}{zr_1}\right)-tan^{-1}\left(\frac{m_{12}e_2-h_2}{zr_2}\right)+tan^{-1}\left(\frac{m_{23}e_2-h_2}{zr_2}\right)\right.$$
$$\left.-tan^{-1}\left(\frac{m_{23}e_3-h_3}{zr_3}\right)+tan^{-1}\left(\frac{m_{31}e_3-h_3}{zr_3}\right)-tan^{-1}\left(\frac{m_{31}e_1-h_1}{zr_1}\right)\right]$$

where

$$d_{12} = \sqrt{(x_2-x_1)^2+(y_2-y_1)^2}$$

$$d_{23} = \sqrt{(x_3-x_2)^2+(y_3-y_2)^2}$$

$$d_{31} = \sqrt{(x_1-x_3)^2+(y_1-y_3)^2}$$

and

$$m_{12} = \frac{(y_2-y_1)}{(x_2-x_1)}, m_{23} = \frac{(y_3-y_2)}{(x_3-x_2)}, m_{31} = \frac{(y_1-y_3)}{(x_1-x_3)}$$

$r_k = \sqrt{(x' - x_k)^2 + (y' - y_k)^2 + z'^2}$, $e_k = (x' - x_k)^2 + z'^2$, $h_k = (x' - x_k)(y' - y_k)$ for $k = 1,2,3$

The velocity components u and v are defined everywhere, but at the edges of the triangular element they become infinite. In practice, the influence of the element on itself is determined near the centroid (so called null point) where these velocity components approach 0; the normal velocity component as $z' \to 0$ inside the element is given by:

$w(z' = 0 \pm) = \frac{\pm\sigma}{2}$ where, adopting the notation used by Katz and Plotkin, [2001], $w(z' = 0 \pm)$ is the value of the normal velocity when approaching $z' = 0$ from above the z'-axis w^+ and approaching from below the z'-axis w^-.

To confirm that the discretization methods were implemented correctly, the Hess and Smith formulation for a quadrilateral was repeated here and compared with open source showing the induced velocity. Figure A3 shows the velocity induced by a rectangular source element along a diagonal survey line (*y=0)* at $\frac{z}{a} = 0.75$ above the element surface.

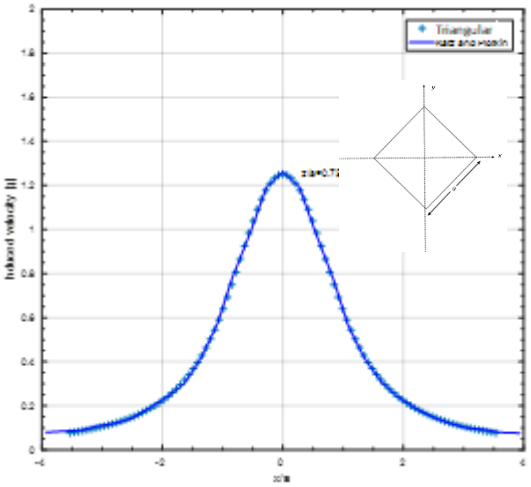

Figure A3: Velocity induced by two triangular source elements compared to a rectangular source element along a diagonal survey line in Katz and Plotkin, [2001].

Figure A4 shows contours of the velocity induced by a triangular source element defined by 4 points and again by 3 points. The contours are taken at a plane $\frac{z}{a} = 0.75$ above the element surface. The contours are identical suggesting that the conversion from a four point quadrilateral to a three point triangular element is consistent.

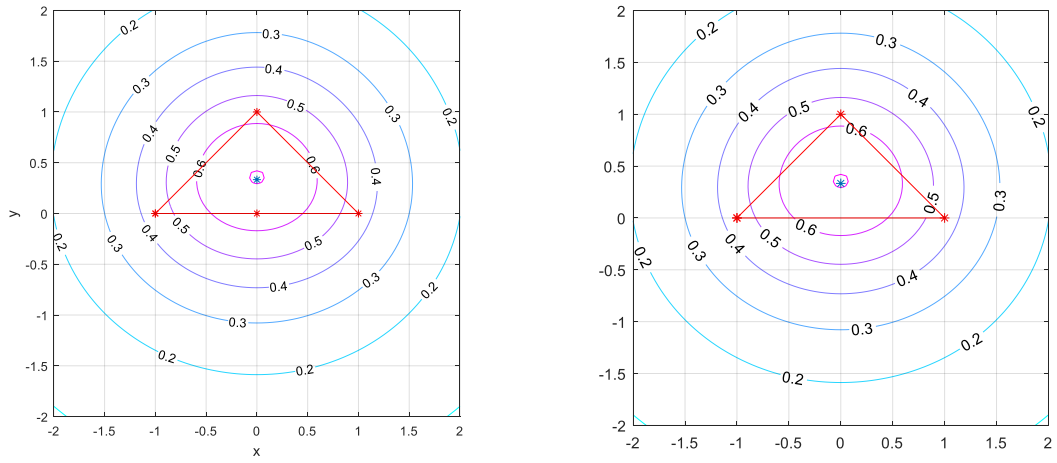

(a)element defined by 4 points *(b) element defined by three points*

Figure A4: *Velocity induced by a triangular source element defined by 4 and 3 points*

Formulation of the plane triangular surface element coordinate system

The plane surface element is formed from three points identified as $\{(m,n),(m+1,n),(m,n+1)\}$ or points 1,2,3. These points are number consecutively around the element in the clockwise direction as shown in Figure A5

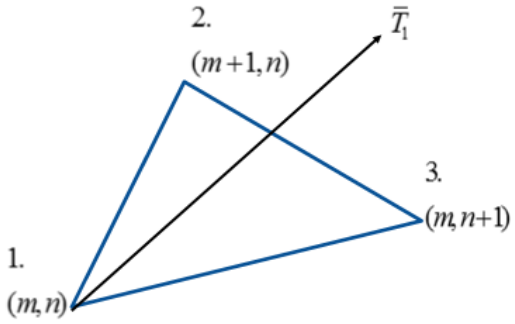

Figure A5: *Convention for plane triangular element.*

So, the i[th] element will have input coordinates in the reference frame as:

$$1: x_1^i, y_1^i, z_1^i$$

$$2: x_2^i, y_2^i, z_2^i$$

$$3: x_3^i, y_3^i, z_3^i$$

The element coordinate system is defined using the unit normal (n_{31}, n_{32}, n_{33}) as one of the orthogonal axes; another one is given by:

$$\overline{T_1} = (T_{11}, T_{12}, T_{13}) = \left(\frac{x_3 + x_2}{2} - x_1, \frac{y_3 + y_2}{2} - y_1, \frac{z_3 + z_2}{2} - z_1 \right)$$

i.e. $\overline{T_1}$ is the vector from vertex 1 through the middle point between vertices 2 and 3. The remaining orthogonal axis (T_{21}, T_{22}, T_{23}) is the cross product of the unit normal and $\overline{T_1}$. Therefore, define a transformation matrix for each element:

$$\overline{T_{ij}} = \begin{bmatrix} T_{11} & T_{12} & T_{13} \\ T_{21} & T_{22} & T_{23} \\ n_{31} & n_{32} & n_{33} \end{bmatrix}$$

with origin at $(\bar{x}, \bar{y}, \bar{z})$ given by:

$$\bar{x} = \frac{1}{3}\left(x_1^i + x_2^i + x_3^i\right), \bar{y} = \frac{1}{3}\left(y_1^i + y_2^i + y_3^i\right), \bar{z} = \frac{1}{3}\left(z_1^i + z_2^i + z_3^i\right)$$

These input points are transformed into the *xy*-plane in the element coordinate system, (x'y',z') as shown in Figure A2.

$$\begin{bmatrix} \xi_j^i \\ \eta_j^i \\ \zeta_j^i \end{bmatrix} = \overline{T_{ij}} \cdot \begin{bmatrix} x_j^i - \bar{x} \\ y_j^i - \bar{y} \\ z_j^i - \bar{z} \end{bmatrix} \text{ for } j=1,2,3$$

Since the axis lies in the plane of the element $\zeta_j^i \equiv 0$ on the surface of the element.

Determination of the null point

The null point is the point on the triangular element where the induced tangential velocities are to be computed; it is the point where the element itself induces no velocities in its own plane, Hess and Smith [1962]. The (x, y) coordinates of the null point are obtained from the solution to $u(x, y) = 0$ and $v(x, y) = 0$ at *z=0*.

Hess and Smith (1962) solved the equations using an iterative procedure based on analytic expressions for the partial derivatives of *u* and *v* shown as:

$$\frac{\partial u}{\partial x}=\frac{\eta_2-\eta_1}{D_{12}}\frac{\partial(r_1+r_2)}{\partial x}+\frac{\eta_3-\eta_2}{D_{23}}\frac{\partial(r_2+r_3)}{\partial x}+\frac{\eta_1-\eta_3}{D_{31}}\frac{\partial(r_3+r_1)}{\partial x}$$

$$\frac{\partial u}{\partial y}=\frac{\eta_2-\eta_1}{D_{12}}\frac{\partial(r_1+r_2)}{\partial y}+\frac{\eta_3-\eta_2}{D_{23}}\frac{\partial(r_2+r_3)}{\partial y}+\frac{\eta_1-\eta_3}{D_{31}}\frac{\partial(r_3+r_1)}{\partial y}$$

$$\frac{\partial v}{\partial x}=\frac{\xi_2-\xi_1}{D_{12}}\frac{\partial(r_1+r_2)}{\partial x}+\frac{\xi_3-\xi_2}{D_{23}}\frac{\partial(r_2+r_3)}{\partial x}+\frac{\xi_1-\xi_3}{D_{31}}\frac{\partial(r_3+r_1)}{\partial x}$$

$$\frac{\partial v}{\partial y}=\frac{\xi_2-\xi_1}{D_{12}}\frac{\partial(r_1+r_2)}{\partial y}+\frac{\xi_3-\xi_2}{D_{23}}\frac{\partial(r_2+r_3)}{\partial y}+\frac{\xi_1-\xi_3}{D_{31}}\frac{\partial(r_3+r_1)}{\partial y}$$

where

$$\frac{\partial(r_1+r_2)}{\partial x}=\frac{x-\xi_1}{r_1}+\frac{x-\xi_2}{r_2};\ \frac{\partial(r_2+r_3)}{\partial x}=\frac{x-\xi_2}{r_2}+\frac{x-\xi_3}{r_3};\ \frac{\partial(r_3+r_1)}{\partial x}=\frac{x-\xi_3}{r_3}+\frac{x-\xi_1}{r_1};$$

$$\frac{\partial(r_1+r_2)}{\partial y}=\frac{x-\xi_1}{r_1}+\frac{x-\xi_2}{r_2};\ \frac{\partial(r_2+r_3)}{\partial y}=\frac{x-\xi_2}{r_2}+\frac{x-\xi_3}{r_3};\ \frac{\partial(r_3+r_1)}{\partial y}=\frac{x-\xi_3}{r_3}+\frac{x-\xi_1}{r_1};$$

$$D_{12}=\frac{1}{2}\left[(r_1+r_2)^2-d_{12}^2\right];\ D_{23}=\frac{1}{2}\left[(r_2+r_3)^2-d_{23}^2\right];\ D_{31}=\frac{1}{2}\left[(r_3+r_1)^2-d_{31}^2\right];$$

The iterative procedure was defined by taking (x_p, y_p) as the *p^th^* approximation of the coordinates of the null point, then the *(p+1)^th^* approximation is obtained by solving

$$\left[\frac{\partial u}{\partial x}\right]^{(p)}(x_{p+1}-x_p)+\left[\frac{\partial u}{\partial y}\right]^{(p)}(y_{p+1}-y_p)=-[u]^{(p)}$$

$$\left[\frac{\partial v}{\partial x}\right]^{(p)}(x_{p+1}-x_p)+\left[\frac{\partial v}{\partial y}\right]^{(p)}(y_{p+1}-y_p)=-[v]^{(p)}$$

using the centroid of the triangular element as the first iteration and where $[\ ]^{(p)}$ means to evaluate the function within the brackets at point (x_p, y_p). The null point is then transformed from the element coordinate system to the reference frame.

To obtain a discretised numerical solution to flow around a body, the body boundary condition needs to be applied to the control points of all the panels on the body surface. The choice of the null point

of each element as the control point in contrast to the element centroid is arbitrary, to some extent. Hess and Smith [1962] used the null point as the control point for each element but they subsequently found that using the centroid of the area of the quadrilateral element to be just as valid choice; Chan, [1990], did not consider using the null point. For low aspect ratio quadrilaterals, the difference between the null points and the centroid will not be significant. For this present study, the null points were chosen as the control points, because of the potential for high aspect ratio elements to be included in the mesh based upon triangular elements.

Formation of the matrix of influence coefficients – the induced velocities on body surface

Once the null points have been derived for all the elements, the velocities induced by each triangular element at each other's null point is required. Thus, for each element the following information is used:

$\left(x'_{np}, y'_{np}, z'_{np}\right)$ is the null point in the reference frame

(x'_0, y'_0, z'_0) is the centroid in the reference frame

$\bar{T}_{ij}$ is the transformation matrix

(ξ_1, η_1), (ξ_2, η_2), (ξ_3, η_3) are the input points in the element coordinate system

A is the area of each element

d is a characteristic length for each element defined as:

$$d_1 = \sqrt{\left(\frac{x_3 + x_2}{2} - x_1\right)^2 + \left(\frac{y_3 + y_2}{2} - y_1\right)^2 + \left(\frac{z_3 + z_2}{2} - z_1\right)^2}$$

$$d_2 = \sqrt{\left(\frac{x_2 + x_1}{2} - x_3\right)^2 + \left(\frac{y_2 + y_1}{2} - y_3\right)^2 + \left(\frac{z_2 + z_1}{2} - z_3\right)^2}$$

$$d = \max(d_1, d_2)$$

The distance between the null point of the i^{th} element and the centroid of the j^{th} element is calculated in the reference frame as:

$$r_0 = \sqrt{\left(x'_{np} - x_0\right)^2 + \left(y'_{np} - y_0\right)^2 + \left(z'_{np} - z_0\right)^2}$$

with $\left(x'_{np}, y'_{np}, z'_{np}\right)$ the coordinate of the *i*th null point and (x_0, y_0, z_0) is the coordinate of the *j*th centroid. Hess and Smith used the notation $\left(X_{ij}, Y_{ij}, Z_{ij}\right)$to represent the velocities (u, v, w) induced at the *i*th null point by the *j*th element; a vector $\bar{V}_{ij} = \left(X_{ij}, Y_{ij}, Z_{ij}\right)$ was also defined.

Then the normal velocity induced at the null point of the *i*th element by unit source density on the *j*th element is given as $A_{ij} = \bar{n}_i.\bar{V}_{ij}$, where $\bar{n}_i$ is the unit normal vector of the *i*th element.

Formulation of the body boundary condition for steady flow

The source density is assumed constant on each of the triangular elements, which means there are N unknown values of source density and N equations from the elements.

To maintain the body boundary condition for a steady onset flow $\bar{V}_\infty = (U_\infty, V_\infty, W_\infty)$ results in the following set of N equations:

$$\sum_{j=1}^{N} A_{ij}\sigma_i = -\bar{n}_i.\bar{V}_\infty$$

where the unknown source strengths σ_i are found following inverting the matrix of influence coefficients A_{ij}. The above equation is imposed at each of the null points of the body surface elements.

Steady state verification

In addition to the verification studies reported in the main body of this thesis, a number of representative steady state calculations were performed with the Hess and Smith method using triangular elements and compared against analytic solutions and the original implementation of Hess and Smith [1962] with quadrilateral elements. Figure A6 shows the calculations for the flow over a sphere in a steady onset flow. These early studies were performed to verify the correct implementation of the basic Hess and Smith method.

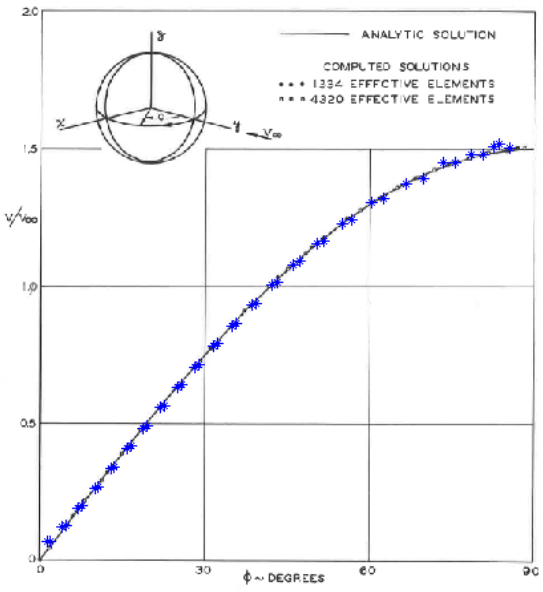

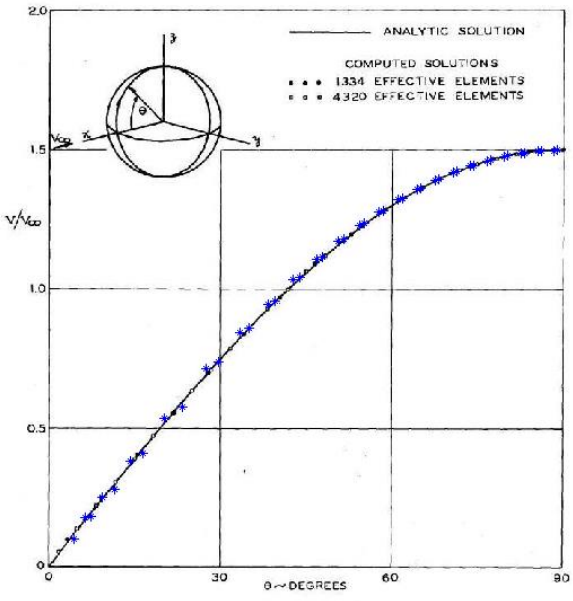

(a) Onset flow parallel to x-axis *(b) Onset flow parallel to y-axis*

FigureA6: *Comparison of analytic and calculated velocity distributions on a sphere (Hess and Smith, 1962) (symbols in blue added– triangular method).*

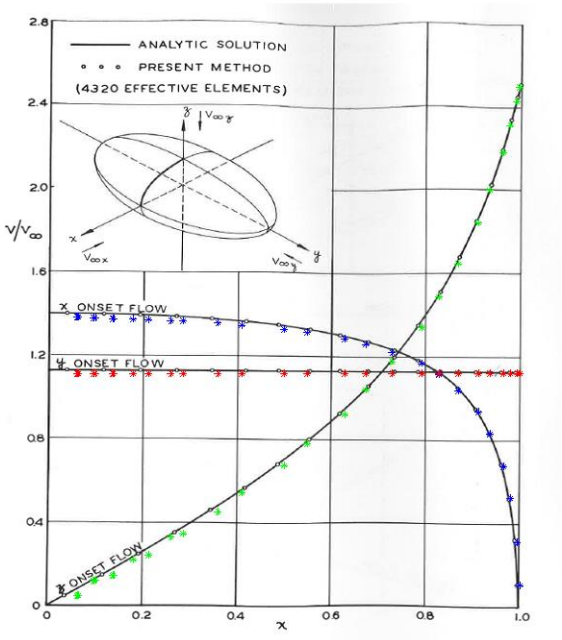

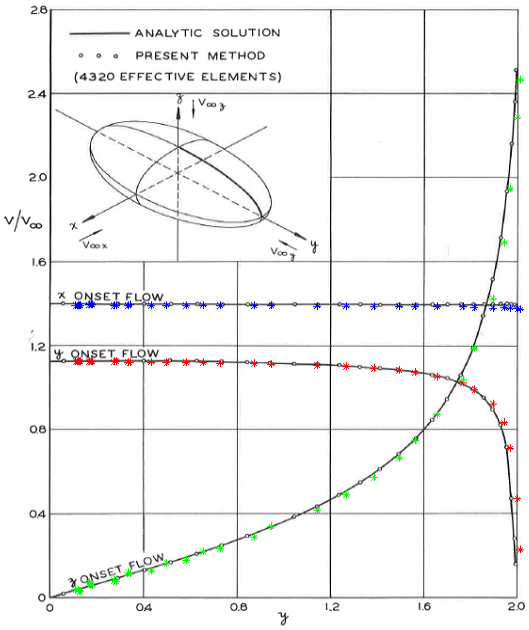

(a) Velocities in xz-plane *(b) Velocities in yz-plane*

Figure A7: *Comparison of analytic and calculated velocity distributions on an ellipsoid with axes ratios 1:2:0.5 (Hess and Smith, 1962) (symbols in colour added– triangular method).*

Faceting

Matlab© contains in-built functions for performing triangulation; the function "delaunayTriangulation" creates a 3D triangulation from a set of input points, S, that represents the body. Figure A8 shows an example of a Delaunay triangulation on the surface of a sphere. A Delaunay triangulation for a set input point S, is a triangulation such that no point in S is inside the circumscribed circle of any triangle. In the example of the sphere, the volume of the facetted object has a volume to within 1.26% of the sphere itself.

However, in some case, see Figure A9, for example where the stern of the SUBOFF geometry is concave; the Delaunay triangulation is limited in that the 3D body must be convex to produce an adequate set of facets. In the case, the author developed an interface between an ICEM surface mesh software package and the required inputs into MATLAB to handle the triangular facets. The ICEM software produces a ".stl" which is then read into the MATLAB. Figure A10 shows the results of an ICEM triangulation of the same DARPA hull form, in this case the concave nature of the aft part of the hull is captured correctly; furthermore, the grid resolution is distributed in a way that is conducive to capture flow features, e.g. concentrations located at points of high curvature.

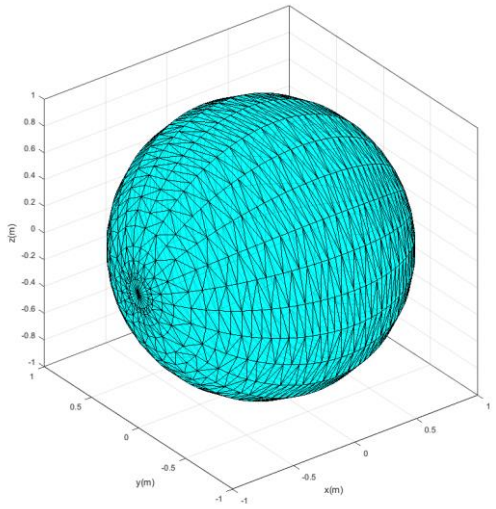

Figure A8: Triangulation of the surface of a sphere.

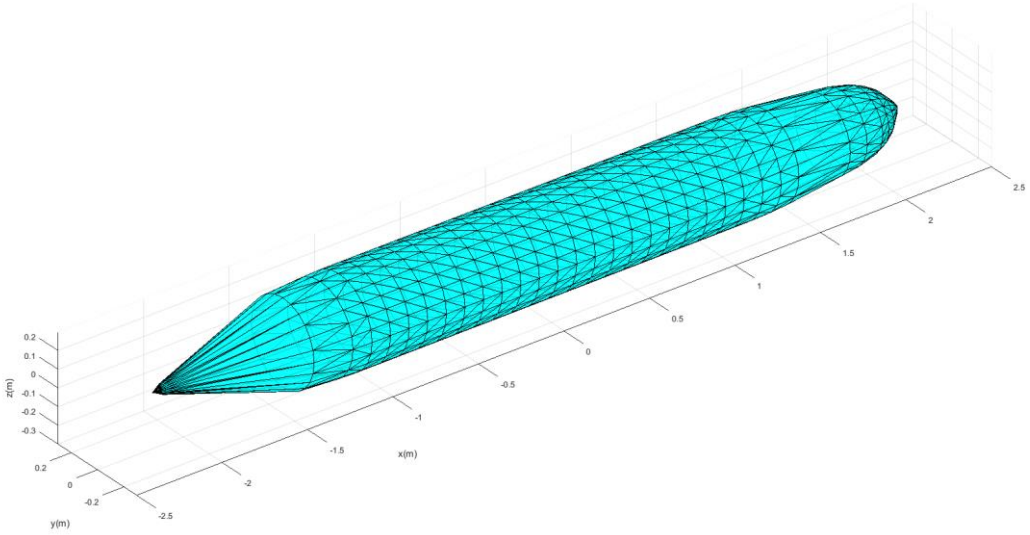

Figure A9: Delaunay triangulation of the DARPA SUBOFF hull form.

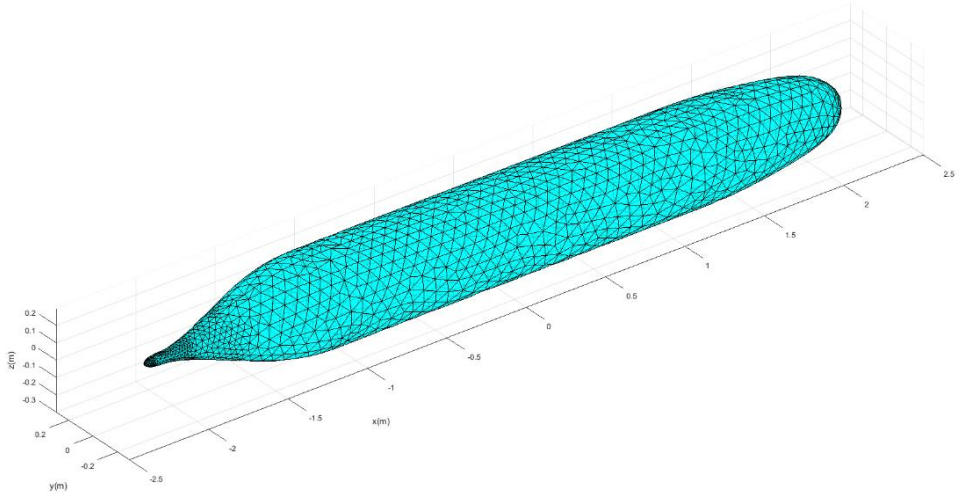

Figure A10: ICEM triangulation of the DARPA SUBOFF hull form.

Free surface

The effect of the free surface is treated through a flat plane which is equivalent by using an image of the body about the free surface, as shown in Figure A11. For example, in the case of sphere with radius r with an origin at (0,0,0), if the body is at a depth *d* then the image has an origin at (0,0,2d) when z is located undisturbed the free surface.

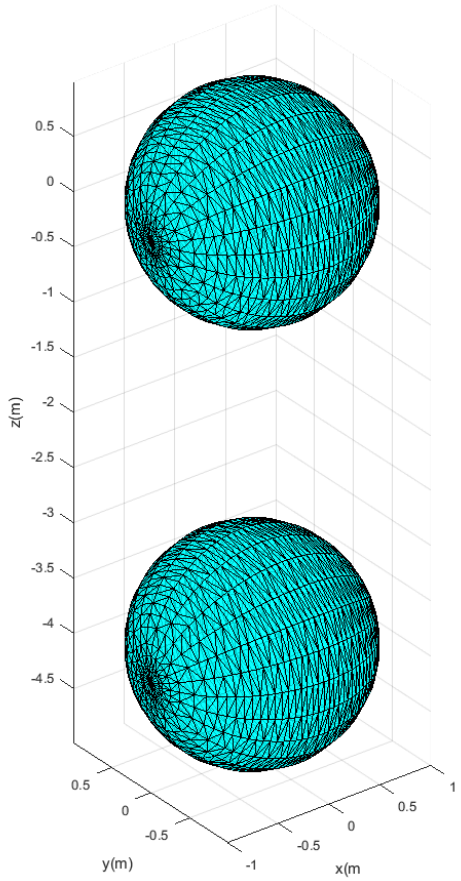

Figure A11: Image of body.

A2 FLOW SEPARATION AND BODY VORTICES

The approach adopted in the present study follows that developed by [Lloyd, 1989]; this method represented separated flow around a deeply submerged submarine by 12 discrete vortices located along a curved arc around of the body, see Figure A12. The position and strength of these vortices are determined through empirical relationships derived from experimental data and effectively become part of the system of equations used to solve for the Kinematic body boundary condition in Eqn 47 [Lloyd, 1989] arranged 12 vortices symmetrically about the plane of the incident flow at the stern of the hull. The longitudinal location of each of these vortices are projected from the plane that defines the incident angle downstream of the body. The vortices are assumed to have a viscous core, with strength and core radius determined empirically, which rotates as a solid body downstream of the submarine.

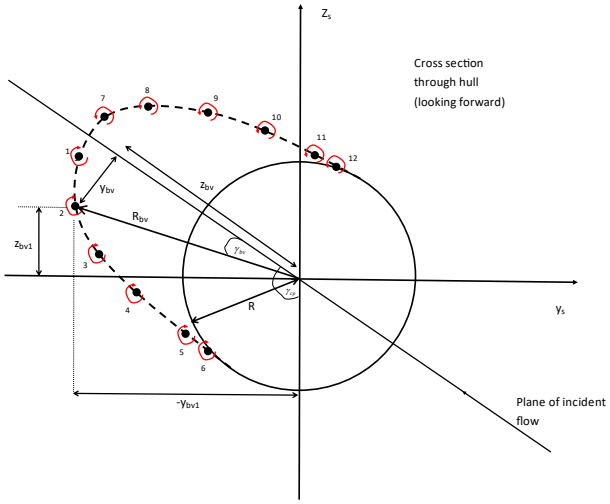

Figure A12: Location of body vortices, [Lloyd,1989].

In a Cartesian coordinate system aligned with the plane of the incident flow vortices 1-6 are located at (y_{BV}, z_{BV}) which in body axes vortices1-6 are located at (y_{BV1}, z_{BV1}) and vortices 7-12 are located at (y_{BV2}, z_{BV2})

A3 APPENDAGE LIFT FORCES

For a lifting, thin, finite aerofoil moving at a constant velocity with the free stream velocity vector $\bar{V}_{\infty}$ at a small angle of attack relative to a coordinate system attached to the aerofoil, the velocity field for the potential flow problem is obtained by solving the potential $\nabla^2\phi = 0$ subject to the boundary condition. This body boundary condition requires no relative flow normal to the solid boundary surface of the appendage (approximated as a thin plate by z=0).

$$\frac{\partial \phi}{\partial z}(x, y, \pm 0) = \bar{V}_{\infty}\left(\frac{\partial \varsigma}{\partial x} - \alpha\right)$$

80

where

$\bar{V}_{\infty} = (U_{\infty}, V_{\infty}, W_{\infty})$ is the free stream velocity.

$\varsigma = \varsigma(x, y)$ is the camber surface.

α is the angle of attack.

The notation ± 0 in this context means the evaluation of the function as z approaches z=0 from above and as z approaches z=0 from below.

The simplest means of solving this 3D problem is to assume that the chordwise circulation, at any spanwise station, is replaced by a single concentrated vortex with circulation

$$\Gamma = \Gamma(\mathrm{y})$$

placed along a single spanwise line, [Katz and Plotkin, 2001] which is usually along the quarter chord and solved using the lifting line theory developed by Prandtl [1929]. A solution to the spanwise circulation
$\Gamma = \Gamma(\mathrm{y})$ can be obtained by describing the unknown distribution in terms of a trigonometric expansion. In the context of appendages on submarine Lloyd [1989] used a spanwise coordinate $_{\theta_A}$, from which following Fourier expansion was used.

$$\Gamma(\theta_A) = 4b_e U_\infty \sum_{n=1}^{\infty} A_n \sin(n\theta_A)$$

81

where

θ_A is the spanwise coordinate given by:

$$\varsigma = \frac{y_A - (b - b_e)}{b_e} = -cos\Theta_A$$

82

y_A is the distance from the hull surface to the geometric centre of the appendage.

For appendages that are typical of those used for submarines, Lloyd [1989] used an approximation $c(\theta)$ such that:

$$c(\theta) = c_r(1 - cos\theta_A(1 - e))$$

83

with

$e = \frac{c_t}{c_r}$ as the taper ratio

c_r the root chord

c_t the tip chord

By re-arranging Eqn.*81* and including Eqn.83, Lloyd, [1989] reduced the problem to determining the unknown coefficients A_n by solving the simulation equations.

$$\sum_{n=1}^{\infty} A_n \sin(n\theta_A)\,(n\mu + sin\theta_A) = \mu\beta_L sin\theta_A$$

84

where

$$\mu = \frac{\pi}{4b_e} c_r(1 - cos\theta_A(1 - e))$$

85

Lloyd [1989b] considered only the odd powers of the Fourier expansion, as a result of an assumption that submarine appendages would have symmetric chordwise cross sections, and reduced Eqn. 84 to a finite set of nine equations to determine the coefficients $A_1, A_3, A_5, \ldots, A_{17}$. The lift generated by the whole appendage is the spanwise integration of the section lift. To account for the effect of the hull on the appendage Lloyd [1989] used an empirical function, k_{BL}, that reduced the circulation close to the hull itself.

The expression used by Lloyd, [1989], was modified in the present study to take account of the presence of the hull in the following way:

$$L_c = b_e \rho \int_{\theta_m}^{\pi} k_{BL} \Gamma(\theta_A) U_A sin\theta_A d\theta_A$$

86

U_A is the spanwise velocity (in the axial direction) obtain from the off-body velocities derived from Hess and Smith.

It should be noted that the above means of accounting for the reduction in circulation, due to the presence of the hull (Eqn. 86), is empirical in nature. Therefore their use should be restricted the applicability to only those configurations of body and lifting surfaces that are typical of submarines, that is, are similar to those used to derive the empirical data.

In determining the contribution of the appendages to the total force on the submarine, the unsteady lift and drag forces on each appendage, as a consequence of the unsteady flow velocities due to the waves, are extracted. The forces imparted by the appendages due to a steady velocity, as a consequence of forward speed, for example, are already accounted for in the appendage terms in Eqns. 8 to 13.

Whilst at periscope depth under the effects of surface waves, the control surfaces of a submarine will be continually changing to counter the effects of the waves, i.e. there is not just an angle of attack on the appendage but also an angle rate. [Klose and Acosta, 1968] derived an empirical formula to account for the effect of rate of change of angle of incidence $\dot{\alpha}$

$$C_{LC} = \frac{dC_L}{d\alpha}\left(\alpha + \frac{\bar{c}}{2\bar{U}}\dot{\alpha}\right)$$

87

where $\bar{c}$ is the mean chord of the appendage and $\bar{U}$ is the mean forward speed.

APPENDIX B HARMONIC ANALYSIS

The 23rd ITTC Ocean Engineering Committee, [ITTC, 2002] recommended a procedure for analysing typical regular waves tests on models in the offshore technology area. For an offshore structure, the response to waves can be non-linear, containing a number of harmonic responses,[ITTC 2002], which can be captured by assuming the response takes the form of:

$$x(t) = \bar{x} + \sum_{j=1}^{m} A_j \sin(j\omega_e t + \phi_j) \qquad \text{...B1}$$

Where

$\bar{x}$ is the mean of the time history

ω_e is the fundamental frequency

A_j is the amplitude of the jth harmonic

ϕ_j is the phase of the jth harmonic

m is the number of harmonic responses

The reference recommends several approaches to analysing such time histories with a view to extracting the amplitude and phase of all the harmonics. One such approach is a non-linear least square fitting of this multi-harmonic theoretical signal, which consists of minimising the error in:

$$\varepsilon^2\left(\omega_e, \bar{x}, A_j, \phi_j\right) = \frac{1}{N}\sum_{i=1}^{N}\left[x(t) - \bar{x} + \sum_{j=1}^{m} A_j \sin(j\omega_e t + \phi_j) \right]^2 \qquad \text{...B2}$$

where N is the number of points in the time history

This function is non-linear only in ω_e for which a good estimate is known; so for known ω_e the problem reduces to linear least squares regression analysis.

Furthermore, in the case of submarines under waves further assumptions can be made regarding the number of harmonics in the response time histories. As a result of the non-linear pressure around the body, each of the forces and moments will have a non-zero mean and first and second

harmonics (indeed there may even by higher order components also). Thus, for a sinusoidal input (the wave) (in fact, the wave itself also has second order harmonics) each force or moment time history can be approximated by the following general form:

$$R = R_1 \sin(\omega t + \varepsilon_1) + R_2 \sin(2\omega t + \varepsilon_2) \quad \text{...B3}$$

where *R* is the time history or the measured response; the values to be determined are the mean and first and second order response amplitudes R_1 and, R_2 their respective phases ε_1 and ε_2, (in rads), ω is the fundamental frequency of the oscillation in rads/s and 2ω is the second harmonic frequency, and $\overline{R}$ is the non-zero mean. The units of these terms are dependent upon the units of the time history.

The equation can be re-written as

$$R = R_1 \sin \omega t cos\varepsilon_1 + R_1 \cos \omega t sin\varepsilon_1 + R_2 \sin 2\omega t cos\varepsilon_2 + R_2 \cos 2\omega t sin\varepsilon_2 + \overline{R} \quad \text{...B4}$$

The phase determined from this least square method is meaningless unless it is made relative to something; in this the basis for the phases are obtained from the phases derived from the least square calculation on the wave itself.

An alternative approach to evaluating harmonic responses such as this is to use the Fourier analysis by [Cooley and Tukey, 1965]. The key to this method of Fourier analysis is ensuring there is sufficient frequency resolution in the FFT to capture the frequencies at which the peaks occur and the amplitude and phase of such peaks.

To demonstrate this, these two methods of analysis were compared using an idealised time history of 200 seconds sampled at 10Hz. The fft function in Matlab® was used for this exercise and compared with the least square method. The idealised time history containing upto the 3rd Harmonic was chosen to be:

$$R = 1.0 * \sin(\omega t + 0.1) + 0.5 * \sin(2\omega t + 0.2) + 0.3 * \sin(3\omega t + 0.3) + 0.5$$

With $\omega = 1.866\, rads/s$

A Matlab® script was written to systematically increase the number of frequencies in the FFT analysis, ranging from 2^4 to 2^{21}. The standard practice is to use the next power of 2 higher than the number of points in the time history which in the case of 200 seconds at 10 Hz is 2^{11}.

Figure B1 shows how the identification of the frequencies at which the peaks in the FFT appear and the subsequent amplitude and phase of those peaks varying with the number of frequencies used in the FFT analysis.

Each line represents one of the harmonics and the red asterisks represents the results from the 2^{11} analysis.

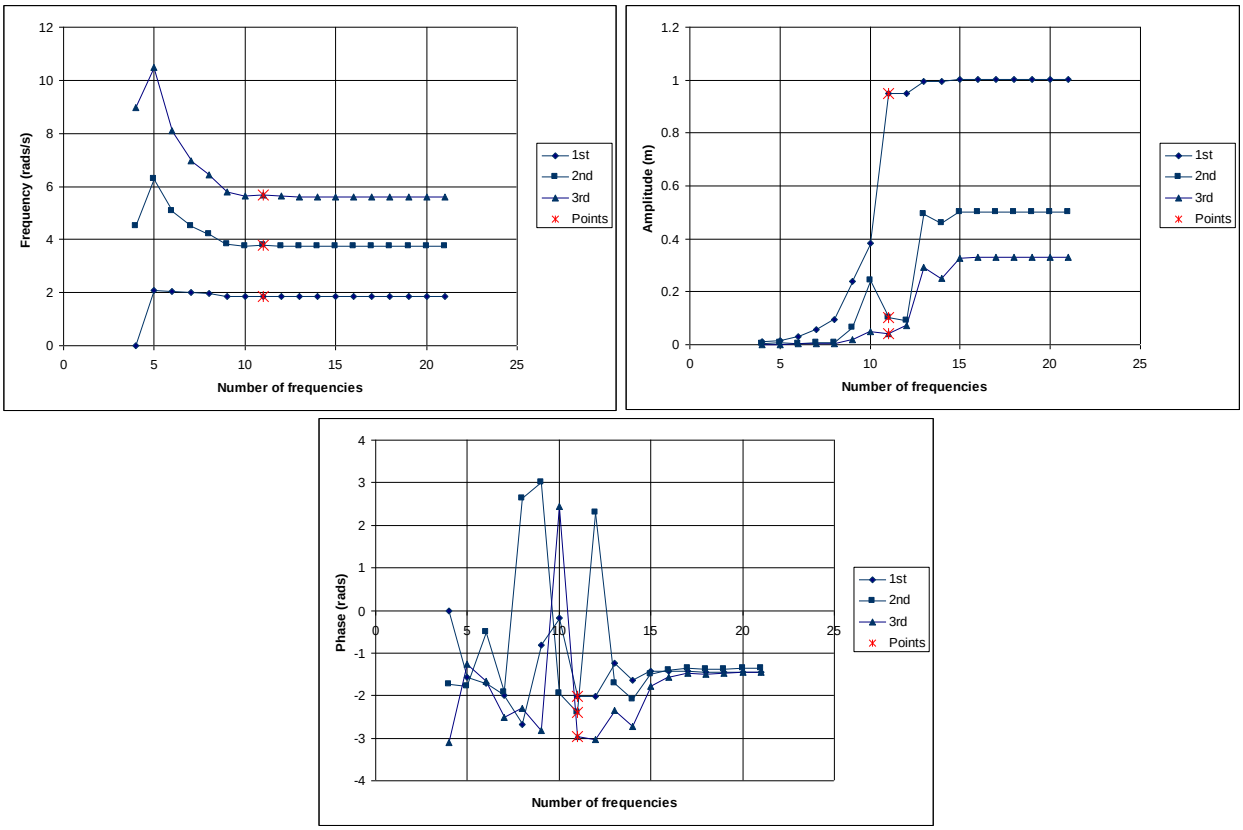

Figure B1: Variation in signal characteristics with number of frequencies in the FFT

In the case of this idealised time history, it appears that the FFT technique does not adequately capture the characteristics of the time history unless they are around 2^{17} frequencies in the analysis; the other point to note is that the phases from the FFT are offset by $\frac{\pi}{2}$.

Geometry input definition for PERISIM

This excel file can be used to enter information on the submarine geometry prior to exporting as a text file for GENCOF and PERISIM

input data is required in the shaded grey boxes only

Symmetry is assumed port and starboard
0 degrees is the keel

Submarine Length	4.6060	m
Scale Factor	1.0000	

drawing measurements made in mm, result divided by 1000 to give scaled result in m

BRXCP	BRYCP	BRZCP	BRTHICK	BRAREA	BRASP	BRANG
7.010E-01	0.000E+00	-4.670E-01	1.800E-01	5.910E-01	9.900E-01	0.000E+00
BPXCP	BPYCP	BPZCP	BPTHICK	BPAREA	BPASP	BPANG
0.000E+00	0.000E+00	0.000E+00	1.000E-02	2.040E-04	9.900E-01	-9.000E+01
SPXCP	SPYCP	SPZCP	SPTHICK	SPAREA	SPASP	SPANG
-1.810E+00	-2.240E-01	0.000E+00	1.110E-01	1.310E-01	1.750E+00	-9.000E+01
RUXCP	RUYCP	RUZCP	RUTHICK	RUAREA	RUASP	RUANG
-1.810E+00	0.000E+00	-2.240E-01	1.110E-01	1.310E-01	1.750E+00	0.000E+00
RLXCP	RLYCP	RLZCP	RLTHICK	RLAREA	RLASP	RLANG
-1.810E+00	0.000E+00	2.240E-01	1.110E-01	1.310E-01	1.750E+00	1.800E+02

Additional information for GENCOF file

x co-ordinate of C's relative to C'	0.0000	m
y co-ordinate of C's relative to C'	0.0000	m
z co-ordinate of C's relative to C'	0.0000	m
Number of bodypoints for potential flow	43.0000	

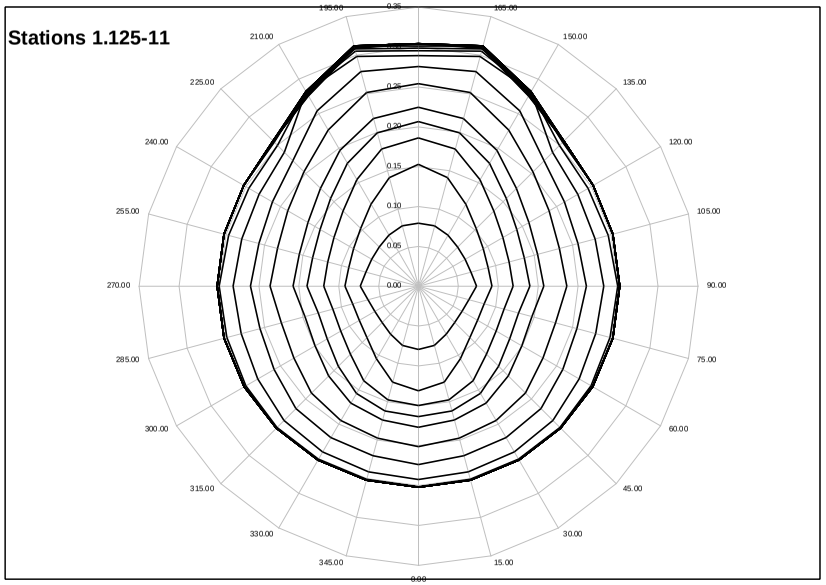

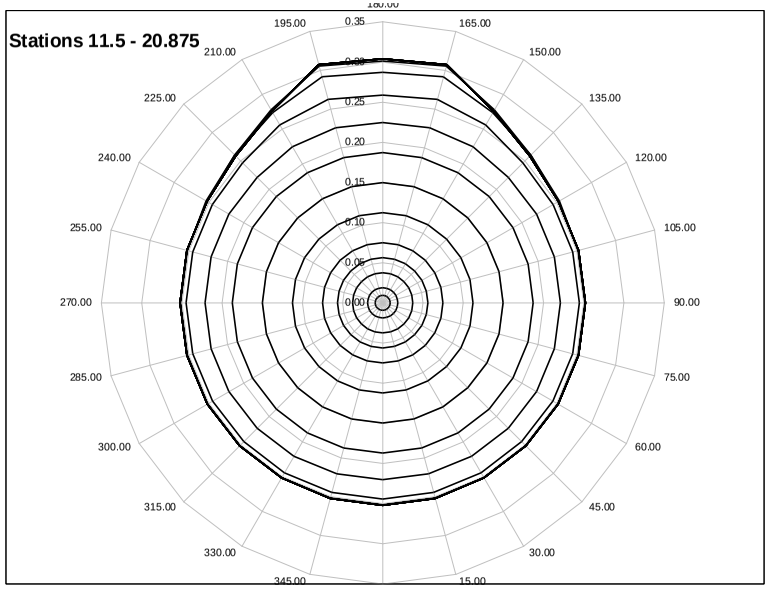

C2 HYDRODYNAMIC MODEL [Kimber and Thompson, 2007]

C2.1 Hull parameters

Parameter	Value	Units
Form Volume	4235	M^3
Mass	4352	Tonnes
Length	74.25	M
I_{xx}	54194	TonnesM
I_{yy}	1442813	TonnesM
I_{zz}	389656	TonnesM
I_{xy}, I_{yz}, I_{zx}	0	
Centre of gravity	(0, 0, -0.1050)	M from origin
Centre of buoyancy	(0, 0, -0.4920)	M from origin
Maximum rudder angle	35	Degs
Maximum bow plane angle	20	Degs
Maximum stern plane angle	25	Degs
Maximum control surface rate	5	Deg/s

C2.2 Non-linear hydrodynamic derivatives

Surge force

Term	Non-dimensional factor	Value
X'_{uu}	$\frac{1}{2}\rho U^2 l^2$	-1.600E-03
X'_{vv}	$\frac{1}{2}\rho U^2 l^2$	2.758E-02
X'_{ww}	$\frac{1}{2}\rho U^2 l^2$	0.000E-03
$X'_{\dot{u}}$	$\frac{1}{2}\rho U^2 l^3$	-6.599E-04
X'_{vr}	$\frac{1}{2}\rho U^2 l^3$	2.556E-02
X'_{wq}	$\frac{1}{2}\rho U^2 l^3$	0.000E-03
X'_{qq}	$\frac{1}{2}\rho U^2 l^4$	0.000E-03
X'_{rr}	$\frac{1}{2}\rho U^2 l^4$	-1.605E-03
X'_{rp}	$\frac{1}{2}\rho U^2 l^4$	0.000E-03
$X'_{uu\delta b\delta b}$	$\frac{1}{2}\rho U^2 l^2$	-2.922E-03
$X'_{uu\delta s\delta s}$	$\frac{1}{2}\rho U^2 l^2$	-2.255E-03
$X'_{uu\delta r\delta r}$	$\frac{1}{2}\rho U^2 l^2$	-6.703E-03
$X'_{vvn'}$	$\frac{1}{2}\rho U^2 l^2$	0.000E-03
$X'_{wwn'}$	$\frac{1}{2}\rho U^2 l^2$	0.000E-03
$X'_{uu\delta s\delta sn'}$	$\frac{1}{2}\rho U^2 l^2$	0.0000-03
$X'_{uu\delta r\delta rn'}$	$\frac{1}{2}\rho U^2 l^2$	-4.961E-03

Propulsion force (thrust model)

$$X'_{n'} = \frac{X_{n'}}{\frac{1}{2}\rho U|U|l^2} = \begin{cases} b'_1 + b'_2\eta + b'_3\eta^2 \; if \; \infty > \eta \geq 1 \\ b'_4 + b'_5\eta + b'_6\eta^2 \; if \; 1 > \eta \geq 0 \\ b'_7 + b'_8\eta + b'_9\eta^2 \; if \; 0 > \eta > -\infty \end{cases}$$

$n' = \frac{u_c}{U}$ where u_c is the command speed (steady state ahead speed component for a given propeller rpm) when the submarine is in steady level flight

Coefficient	Value	Coefficient	Value	Coefficient	Value
b'_1	-3.18E-03	b'_4	0.05417E-03	b'_7	-0.7132E-03
b'_2	3.32E-03	b'_5	0.383E-03	b'_8	2.034E-03
b'_3	1.46E-03	b'_6	1.618E-03	b'_9	1.45E-03

Sway force

Term	Non-dimensional factor	Value
Y'_{uu}	$\frac{1}{2}\rho U^2 l^2$	0.000E-03
Y'_{uv}	$\frac{1}{2}\rho U^2 l^2$	-5.778E-02
Y'_{vw}	$\frac{1}{2}\rho U^2 l^2$	-110.1E-03
Y'_{vv}	$\frac{1}{2}\rho U^2 l^2$	-86.87E-03
$Y'_{\dot{v}}$	$\frac{1}{2}\rho U^2 l^3$	-2.274E-02
Y'_{up}	$\frac{1}{2}\rho U^2 l^3$	-2.770E-03
Y'_{ur}	$\frac{1}{2}\rho U^2 l^3$	7.099E-03
Y'_{vq}	$\frac{1}{2}\rho U^2 l^3$	0.000E-03
Y'_{wp}	$\frac{1}{2}\rho U^2 l^3$	1.866E-02
Y'_{wr}	$\frac{1}{2}\rho U^2 l^3$	-8.273E-03
$Y'_{vv\left\|\frac{r}{v}\right\|}$	$\frac{1}{2}\rho U^2 l^3$	-8.273E-03
$Y'_{\mathrm{u\|r\|\delta r}}$	$\frac{1}{2}\rho U^2 l^3$	2.491E-03
$Y'_{\dot{p}}$	$\frac{1}{2}\rho U^2 l^4$	-0.3024E-03
$Y'_{\dot{r}}$	$\frac{1}{2}\rho U^2 l^4$	0.3061E-04
$Y'_{p\|p\|}$	$\frac{1}{2}\rho U^2 l^4$	0.000E-03
Y'_{pq}	$\frac{1}{2}\rho U^2 l^4$	0.000E-03
Y'_{qr}	$\frac{1}{2}\rho U^2 l^4$	0.000E-03
$Y'_{\mathrm{uu\delta r}}$	$\frac{1}{2}\rho U^2 l^2$	1.398E-02
$Y'_{\mathrm{ur}n'}$	$\frac{1}{2}\rho U^2 l^3$	0.000E-03
$Y'_{uvn'}$	$\frac{1}{2}\rho U^2 l^2$	0.000E-03
$Y'_{v\|v\|n'}$	$\frac{1}{2}\rho U^2 l^2$	0.0000-03
$Y'_{\mathrm{uu\delta r}n'}$	$\frac{1}{2}\rho U^2 l^2$	1.9973E-03

Heave force

Term	Non-dimensional factor	Value
Z'_{uu}	$\frac{1}{2}\rho U^2 l^2$	-0.017E-03
Z'_{uw}	$\frac{1}{2}\rho U^2 l^2$	-28.06E-03
Z'_{uv}	$\frac{1}{2}\rho U^2 l^2$	0.000E-03
Z'_{vv}	$\frac{1}{2}\rho U^2 l^2$	7.397E-02
$Z'_{\mathrm{uu\delta b}}$	$\frac{1}{2}\rho U^2 l^2$	-2.332E-03
$Z'_{\mathrm{uu\delta s}}$	$\frac{1}{2}\rho U^2 l^2$	-7.483E-03
Z'_{wv}	$\frac{1}{2}\rho U^2 l^2$	-69.064E-03
$Z'_{u\lvert w\rvert}$	$\frac{1}{2}\rho U^2 l^2$	0.000E-03
$Z'_{\lvert wv\rvert}$	$\frac{1}{2}\rho U^2 l^2$	0.000E-03
$Z'_{\dot{w}}$	$\frac{1}{2}\rho U^2 l^3$	-1.8665E-02
Z'_{uq}	$\frac{1}{2}\rho U^2 l^3$	-9.470E-03
Z'_{vp}	$\frac{1}{2}\rho U^2 l^3$	-2.275E-02
Z'_{vr}	$\frac{1}{2}\rho U^2 l^3$	-2.962E-02
$Z'_{wv\lvert\frac{q}{w}\rvert}$	$\frac{1}{2}\rho U^2 l^3$	0.000E-03
$Z'_{\mathrm{u}\lvert q\rvert\delta\mathrm{s}}$	$\frac{1}{2}\rho U^2 l^3$	0.000E-03
$Z'_{\dot{q}}\dot{q}'$	$\frac{1}{2}\rho U^2 l^4$	-0.2329E-03
Z'_{pp}	$\frac{1}{2}\rho U^2 l^4$	0.000E+00
Z'_{rr}	$\frac{1}{2}\rho U^2 l^4$	-2.7691E-03
Z'_{rp}	$\frac{1}{2}\rho U^2 l^4$	0.000E-03
$Z'_{uwn'}$	$\frac{1}{2}\rho U^2 l^2$	0.000E-03
$Z'_{uqn'}$	$\frac{1}{2}\rho U^2 l^3$	0.000E-03
$Z'_{w\lvert w\rvert n'}$	$\frac{1}{2}\rho U^2 l^2$	0.000E-03
$Z'_{\mathrm{uu\delta}sn'}$	$\frac{1}{2}\rho U^2 l^2$	0.0000-03

Roll moment

Term	Non-dimensional factor	Value
K'_{uu}	$\frac{1}{2}\rho U^2 l^3$	0.000E-03
K'_{uv}	$\frac{1}{2}\rho U^2 l^3$	-2.122E-03
K'_{vw}	$\frac{1}{2}\rho U^2 l^3$	4.142E-03
K'_{vv}	$\frac{1}{2}\rho U^2 l^3$	-3.432E-03
$K'_{uu\delta r}$	$\frac{1}{2}\rho U^2 l^3$	0.226E-03
$K'_{\dot{v}}\dot{v}'$	$\frac{1}{2}\rho U^2 l^4$	-0.302E-03
K'_{up}	$\frac{1}{2}\rho U^2 l^4$	-0.315E-03
K'_{ur}	$\frac{1}{2}\rho U^2 l^4$	-0.024E-03
K'_{vq}	$\frac{1}{2}\rho U^2 l^4$	0.000E+00
K'_{wp}	$\frac{1}{2}\rho U^2 l^4$	0.000E-03
K'_{wr}	$\frac{1}{2}\rho U^2 l^4$	0.812E-03
$K'_{\dot{p}}$	$\frac{1}{2}\rho U^2 l^5$	-0.023E-03
$K'_{\dot{r}}$	$\frac{1}{2}\rho U^2 l^5$	-0.009E-03
$K'_{p\|p\|}$	$\frac{1}{2}\rho U^2 l^5$	-0.090E-03
K'_{pq}	$\frac{1}{2}\rho U^2 l^5$	0.000E-03
K'_{qr}	$\frac{1}{2}\rho U^2 l^5$	-0.066E-03
$K'_{n'}$	$\frac{1}{2}\rho U^2 l^3$	0.000E-03

Pitch moment

Term	Non-dimensional factor	Value
M'_{uu}	$\frac{1}{2}\rho U^2 l^3$	0.039E-03
M'_{uw}	$\frac{1}{2}\rho U^2 l^3$	8.475E-03
M'_{vv}	$\frac{1}{2}\rho U^2 l^3$	13.346E-03
$M'_{\mathrm{uu\delta b}}$	$\frac{1}{2}\rho U^2 l^3$	1.341E-03
$M'_{\mathrm{uu\delta s}}$	$\frac{1}{2}\rho U^2 l^3$	-3.202E-03
M'_{wv}	$\frac{1}{2}\rho U^2 l^3$	17.019E-03
$M'_{u\lvert w\rvert}$	$\frac{1}{2}\rho U^2 l^3$	0.000E-03
$M'_{\lvert wv\rvert}$	$\frac{1}{2}\rho U^2 l^3$	0.000E-03
$M'_{\dot{w}}\dot{w}'$	$\frac{1}{2}\rho U^2 l^4$	-0.2329E-03
M'_{uq}	$\frac{1}{2}\rho U^2 l^4$	-5.7300E-03
M'_{vp}	$\frac{1}{2}\rho U^2 l^4$	0.000E+00
M'_{vr}	$\frac{1}{2}\rho U^2 l^4$	-8.6221E-03
M'_{qv}	$\frac{1}{2}\rho U^2 l^4$	0.000E-03
$M'_{\mathrm{u}\lvert q\rvert\delta \mathrm{s}}$	$\frac{1}{2}\rho U^2 l^4$	0.000E-03
$M'_{\dot{q}}\dot{q}'$	$\frac{1}{2}\rho U^2 l^5$	-1.068E-03
M'_{pp}	$\frac{1}{2}\rho U^2 l^5$	0.000E-03
M'_{rr}	$\frac{1}{2}\rho U^2 l^5$	0.068E-03
M'_{rp}	$\frac{1}{2}\rho U^2 l^5$	1.111E-03
$M'_{q\lvert q\rvert}$	$\frac{1}{2}\rho U^2 l^5$	0.000E-03
$M'_{\mathrm{uqn}'}$	$\frac{1}{2}\rho U^2 l^4$	0.000E-03
$M'_{uwn'}$	$\frac{1}{2}\rho U^2 l^3$	0.000E-03
$M'_{\lvert wv\rvert n'}$	$\frac{1}{2}\rho U^2 l^3$	0.000E-03
$M'_{\mathrm{uu\delta s}n'}$	$\frac{1}{2}\rho U^2 l^3$	0.000E-03

Yaw moment

Term	Non-dimensional factor	Value
N'_{uu}	$\frac{1}{2}\rho U^2 l^3$	0.000E+00
N'_{uv}	$\frac{1}{2}\rho U^2 l^3$	-14.412E-03
N'_{vw}	$\frac{1}{2}\rho U^2 l^3$	22.492E-03
N'_{vv}	$\frac{1}{2}\rho U^2 l^3$	13.658E-03
$N'_{\mathrm{uu\delta r}}$	$\frac{1}{2}\rho U^2 l^3$	-6.021E-03
$N'_{\dot{v}}\dot{v}'$	$\frac{1}{2}\rho U^2 l^4$	0.036E-03
N'_{up}	$\frac{1}{2}\rho U^2 l^4$	-1.100E-03
N'_{ur}	$\frac{1}{2}\rho U^2 l^4$	-5.260E-03
N'_{vq}	$\frac{1}{2}\rho U^2 l^4$	0.000E-03
N'_{wp}	$\frac{1}{2}\rho U^2 l^4$	0.000E-03
N'_{wr}	$\frac{1}{2}\rho U^2 l^4$	1.767E-03
N'_{rv}	$\frac{1}{2}\rho U^2 l^4$	-1.068E-03
$N'_{\mathrm{u\|r\|\delta r}}$	$\frac{1}{2}\rho U^2 l^4$	0.331E-03
$N'_{\dot{p}}$	$\frac{1}{2}\rho U^2 l^5$	-0.0091E-03
$N'_{\dot{r}}$	$\frac{1}{2}\rho U^2 l^5$	-1.1335E-03
$N'_{r\|r\|}$	$\frac{1}{2}\rho U^2 l^5$	0.000E-03
N'_{pq}	$\frac{1}{2}\rho U^2 l^5$	0.5499E-03
N'_{qr}	$\frac{1}{2}\rho U^2 l^5$	0.000E-03
$N'_{\mathrm{urn'}}$	$\frac{1}{2}\rho U^2 l^3$	0.000E-03
$N'_{uvn'}$	$\frac{1}{2}\rho U^2 l^4$	0.000E-03
$N'_{vvn'}$	$\frac{1}{2}\rho U^2 l^3$	0.000E-03
$N'_{\mathrm{uu\delta rn'}}$	$\frac{1}{2}\rho U^2 l^3$	-1.4988E-03

C3 LINEARIZED SYSTEM MATRICES FOR EUCLID AT 12 KNOTS

States: **w q h theta**

Inputs: **fore aft;** Outputs: **depth pitch**

A =	**w**	**q**	**h**	**theta**
w	-0.06035	1.90835	0	0.00270
q	0.00413	-0.20572	0	-0.00623
h	1	0	0	-6.17724
theta	0	1	0	0

B =	**Fore**	**Aft**
w	-0.03180	-0.09241
q	0.00400	-0.00932
h	0	0
theta	0	0

C =	**w**	**q**	**h**	**theta**
depth	0	0	1	0
pitch	0	0	0	57.29578

D =	**Fore**	**Aft**
depth	0	0
pitch	0	0